Generalizations of H-Infinity Optimization / Control of Rotating Stall

Thesis by
Raffaello D'Andrea

In Partial Fulfillment of the Requirements
for the Degree of
Doctor of Philosophy

California Institute of Technology
Pasadena, California
1997
Submitted May 31, 1996

To Maria Grazia and Giuseppe D'Andrea

Acknowledgements

My deepest gratitude goes to my advisor, John Doyle. In my pre-graduate school days, I had what by any standards would be considered unrealistic and naive expectations of what the role of an advisor should be: a mentor who would push me to my limits and bring out the best in me, a colleague who I could work with and share the excitement of discovery, and finally, someone who I could confide in, share a joke with, and count as one of my friends. Now that I'm a little bit older and wiser, I feel very fortunate in having had these expectations met.

I am also greatly indebted to Richard Murray for making me part of the compressor team and for providing an environment which allowed me to develop many invaluable skills. His incredible energy and excitement for research have been a positive influence throughout these years which I will carry with me in my future endeavors.

My thanks also to the rest of my committee, Jerry Marsden, Pietro Perona, and Roy Smith. I would also like to thank Jan Willems and the rest of the gang at the University of Groningen for the many stimulating discussions and for being such great hosts during my two month stay in the System Theory Group.

My experience at Caltech was made memorable by the other truly outstanding people I have had the privilege to interact with. I owe much to Fernando Paganini for being a great friend, colleague, and office mate; we shared many exciting and unforgettable experiences together, and his presence greatly accelerated my development as a researcher. I am very thankful for having had the chance to work closely with Bob Behnken on the Caltech compressor; I learned a great deal from Bob during our experimental work together, and we shared many laughs which made the countless hours of taking data in the compressor lab bearable, if not enjoyable. I would like to thank my lab mates for their great help and friendship, in particular Geir Dullerud, Matt Newlin, and Sven Khatri; the rest of the people associated with the Caltech compressor, in particular Asif Khalak, Simon Yeung, and Dave Richard, for their contribution to my research; the lads on the Caltech soccer team for keeping me sane; and finally, John Josephson for being the greatest of friends, my house mates for putting up with me, and the rest of my friends at Caltech, especially Will Law, Bob M'Closkey, and Nicole Peill, for being there.

This dissertation could not have been possible without the courage, sacrifices, hopes, and dreams of my mother Maria Grazia and my late father Giuseppe. I thank them for instilling in me the lust for knowledge and the sense of wonder which got me this far.

And finally, my fiancée and *raison d'être* Leanna Caron, who stood by me through the rough and turbulent times, for which I am eternally grateful.

Abstract

Arguably one of the most significant contributions to the field of optimal control has been the formulation and eventual solution of the $\mathcal{H}_\infty$ design problem. Armed with this mathematical tool, designs which are robust to plant uncertainty and insensitive to plant parameters can be performed in a systematic and rigorous fashion.

The $\mathcal{H}_\infty$ methodology, however, typically leads to conservative designs. The reasons are twofold. The first is that the plant uncertainty can only be accounted for in an approximate manner, with the result that designs are performed for a set of allowable systems which is larger than what is being modeled; thus the resulting control strategy is forced to guard against non-realizable situations, potentially sacrificing system performance. The second has to do with the physical interpretation of $\mathcal{H}_\infty$ optimization: the minimization of a system's power to power gain. Thus it is implicitly assumed in the design process that the worst case disturbance is allowed to be an arbitrary power signal, such as a sinusoid. This is clearly a poor modeling choice for many types of physical disturbances, such as sensor or thermal noise, wind gusts, and impulsive forces.

The main contribution of this dissertation is the extension of $\mathcal{H}_\infty$ optimization to allow for general closed loop design objectives which address the two limitations outlined above. In particular, non-conservative, computationally tractable, linear matrix inequality based methods for control design are developed for a certain class of physically motivated uncertain systems. In addition, these new techniques can accommodate constraints on the allowable disturbances, excluding unrealistic disturbances from the design process.

Another contribution of this dissertation is an attempt to view control in the broader context of system design. Typically, a control algorithm is only sought after the system to be controlled has already been designed, and the type and location of the actuators and sensors has been determined. For most applications, however, the level of performance which can be attained by any control strategy is dictated by the dynamics of the plant. Thus from a system level, the above methodology is not optimal, since the control design process is decoupled from the design of the rest of the system. By adopting the *behavioral framework* for systems, an optimization problem where the given system is not treated as an input-output operator, a natural assumption when considering first principles models, is formulated and solved. The interpretation of the above extension of $\mathcal{H}_\infty$ optimization is that of designing optimal

systems.

In contrast to the general purpose tools developed in the first part of the dissertation and summarized above, the second part deals with an actual experimental problem, that of controlling rotating stall using pulsed air injection in a low-speed, axial flow compressor. By modeling the injection of air as an unsteady shift in the compressor characteristic, the viability of various air injection orientations are established. A control strategy is developed which controls the pulsing of air in front of the rotor face based on unsteady pressure measurements near the rotor face. Experimental results show that this technique eliminates the hysteresis loop normally associated with rotating stall. A parametric study is used to determine the optimal control parameters for suppression of stall. The resulting control strategy is also shown to suppress surge when a plenum is present. Using a high fidelity model, the main features of the experimental results are duplicated via simulations. The main contributions of this part of the dissertation are a simple control scheme which has the potential of greatly increasing the operability of compressors, and a low-order modeling mechanism which captures the essential features of air injection, facilitating subsequent analyses and control designs which make use of air injectors.

Table of Contents

Acknowledgements iv

Abstract v

1 Introduction 1
1.1 Organization of Dissertation 2

I Generalizations of $\mathcal{H}_\infty$ Optimization 4

2 Preliminaries 5
2.1 Background and Notation 5
2.2 Robust Control 11
2.3 Behavioral Systems 20

3 Generalized l_2 Synthesis 24
3.1 Problem Formulation 25
3.2 Properties of Sets $\mathfrak{D}$, $\mathfrak{E}$, $\mathcal{D}$, and $\mathcal{E}$ 27
3.3 Analysis Condition 31
3.4 Synthesis Condition 39
3.5 Concluding Remarks 42

4 Applications of Generalized l_2 Synthesis 43
4.1 Square $\mathcal{H}_\infty$ 43
4.2 Robust Stability 46
4.3 Robust Performance 49
4.4 Robust Gain Scheduling 52

5 Extension to Deterministic Noise Disturbances 66
5.1 Problem Formulation 67
5.2 Image Representation for $\mathcal{W}_N^m$ 68
5.3 Converting to Generalized l_2 Synthesis Setup 71
5.4 Computation 74

5.5 Mixed $\mathcal{H}_2 - \mathcal{H}_\infty$ Synthesis 74
5.6 Synthesis for Robust $\mathcal{H}_2$ Performance 76
5.7 Numerical Example 77
5.8 Robust $\mathcal{H}_2$ Synthesis 79

6 State-Space Manipulations for Behavioral Representations 82
6.1 Output Nulling Representations 82
6.2 I/O Maps 85
6.3 Stability 85
6.4 Interconnection 86
6.5 Latent Variable Elimination 88
6.6 Example 91
6.7 Extension to Uncertain Systems 94

7 $\mathcal{H}_\infty$ Optimal Interconnections 100
7.1 Introduction 100
7.2 Problem Formulation 101
7.3 Example 103
7.4 Dual Representations 104
7.5 Problem Conversion 106
7.6 $\mathcal{H}_\infty$ Solution 111
7.7 Example Revisited 117
7.8 Full Information and Full Control in a Behavioral Context 118
7.9 Another Example 125
7.10 Concluding Remarks 126

II Rotating Stall Control of an Axial Flow Compressor using Pulsed Air Injection 128

8 Preliminaries 129
8.1 Introduction and Motivation 130
8.2 Previous Work 133
8.3 Experimental Setup 134
8.4 Moore-Greitzer Three-State Model 138

9 Control of Rotating Stall 141
9.1 Characteristic Shifting 141
9.2 Experimental Results Using Pulsed Air Injection 143
9.3 Simulations 156
9.4 Conclusions and Future Work 160

10 Conclusions **163**
10.1 Summary 163
10.2 Future Research Directions 164

Bibliography **165**

Chapter 1

Introduction

Recent years have seen the emergence of sophisticated mathematical techniques for the design and analysis of control systems. There are several factors which have contributed to this phenomenon. The first is the ever increasing demand for high performance systems, which has driven research into correspondingly high performance mathematics. A second is the emergence of technologically advanced sensors and actuators, which have greatly increased the applicability of active control methods and have allowed control theory to be applied to more complex systems. A third is the enormous increase in computing power, which has pushed research into areas which until recently would have been dismissed as impractical.

The initial contribution of these advanced mathematical techniques was limited to the analysis portion of the control design. The main reason for this is that many designs require the use of unwritten engineering know-how and rules of thumb, and rely on past experience, which are hard to formalize. Thus the design process has typically entailed tuning various parameters and then verifying that the resulting design meets certain performance specifications.

There are several obvious limitations to this approach. The first is that a control design can only be performed by a select few with many years of practical experience. A second is that trial and error design is a losing proposition for large and complex systems. This has driven research into formal synthesis methods.

A desirable property of any useful synthesis methodology is that the design process should be automated as much as possible while still allow room for engineering know-how to enter the design process. For example, $\mathcal{H}_\infty$ and $\mathcal{H}_2$ design methods are popular in the control community because the stability of the closed loop system is ensured while weights may be chosen by the design engineer to tailor the design to the particular application at hand. The engineering know-how is thus reflected on the choice of weights. The "mundane" task of ensuring stability is thus automatically taken care of, and the designer is left to worry about issues of performance and sensitivity to modeling errors.

The main contribution of this dissertation is the development of formal synthesis methods which lead to designs that are robust to modeling errors. Tools are developed which automate the design process and allow the incorporation of as much a priori information as possible without becoming computationally intractable.

By their very nature, however, the above techniques have limited scope. Because of the maturity of optimal control in the context of general purpose design methods, these techniques are only justified when a modest increase in performance is an acceptable objective. Another contribution of this dissertation is an attempt to view control in the broader context of system design. Thus while the gains to be made by designing better controllers appears to be marginal for most applications and be subject to diminishing returns, a mathematical framework for designing better systems has the potential of being widely applicable and of being a significant contribution.

In contrast to the general purpose tools developed in the first part of the dissertation and summarized above, the second part deals with an actual experimental problem, that of controlling rotating stall using pulsed air injection in a low-speed, axial flow compressor. By modeling the injection of air as an unsteady shift in the compressor characteristic, the viability of various air injection orientations are established. Based on unsteady pressure measurements near the rotor face, pulses of air are injected in front of the rotor face. Experimental results show that this technique eliminates the hysteresis loop normally associated with rotating stall. A parametric study is used to determine the optimal control parameters for suppression of stall. The resulting control strategy is also shown to suppress surge when a plenum is present. Using a high fidelity model, the main features of the experimental results are duplicated via simulations. The main contributions of this part of the dissertation are a simple control scheme which has the potential of greatly increasing the operability of compressors, and a low-order modeling mechanism which captures the essential features of air injection, facilitating subsequent analyses and control designs which make use of air injectors.

1.1 Organization of Dissertation

The dissertation is divided into two parts. The first part, which consists of Chapters 2 through 7, deals with various extensions of $\mathcal{H}_\infty$ control and their applications. This first part can itself be divided into two relatively non-overlapping components; Chapters 3 through 5 deal with input-output systems, while Chapters 6 and 7 are concerned with systems described as sets of allowable trajectories; Chapter 2 serves as the common thread between these two topics. The second part, Chapters 8 and 9, contains results on the control of rotating stall using pulsed air injection in an axial flow compressor.

1.1.1 Generalizations of $\mathcal{H}_\infty$ Optimization

Chapter 2 contains the background material relevant to the first part of the dissertation. The notation is introduced, and the various problems which are encountered in this part of the dissertation are motivated.

In Chapter 3, a framework for optimal controller design with generalized l_2 objectives is presented. This framework is used to solve various open problems in robust

and optimal control in Chapter 4. These include synthesis for independently norm bounded disturbances, robust stability with "element by element" bounded structured uncertainty, and certain classes of robust performance problems. In addition, recent results on the design of gain scheduled controllers are extended to the above cases.

In Chapter 5, the results in the previous chapter are extended to allow for deterministic noise disturbances. This extension is also used to provide a solution to the so-called Mixed $\mathcal{H}_2 - \mathcal{H}_\infty$ problem, and allows one to extend the iterative schemes developed for robust controller synthesis to the case of white noise disturbances.

Chapters 6 and 7 contain results in the area of behavioral systems. State-space descriptions of behavioral systems are introduced in Chapter 6, and are extended to include uncertainty. An optimal control problem for continuous time, linear time invariant systems described by behavioral equations is formulated and solved in Chapter 7. This general formulation, which includes standard $\mathcal{H}_\infty$ optimization as a special case, provides added freedom in the design of sub-optimal compensators, and can in fact be viewed as a means of designing optimal systems. In particular, the formulation presented allows for singular interconnections, which naturally occur when interconnecting first principles models.

1.1.2 Control of Rotating Stall in an Axial Flow Compressor

Chapter 8 contains the background material relevant to this part of the dissertation. The issue of rotating stall in compressors is addressed, and the objective of rotating stall suppression is motivated. The main experimental and theoretical results are found in Chapter 9.

Part I

Generalizations of $\mathcal{H}_\infty$ Optimization

Chapter 2
Preliminaries

This chapter contains the essential background material for the first part of the dissertation. The notation is introduced, and the motivation for the various problems which will be addressed in this first part is provided.

2.1 Background and Notation

The set of integers is denoted $\mathbb{Z}$, the set of real numbers is denoted $\mathbb{R}$; $\mathbb{Z}^+$ and $\mathbb{R}^+$ denote the respective non-negative subsets. The set of complex numbers is denoted $\mathbb{C}$; the subset consisting of those elements with non-negative real component is denoted $\mathbb{C}^+$, while $\mathbb{C}^-$ is used to denote the subset whose elements have negative real component. The space of $m \times m$ symmetric matrices is denoted $\mathbb{R}_{\mathbf{S}}^{m\times m}$; $\mathbb{R}_{\mathbf{P}}^{m\times m}$ denotes the space of positive semi-definite symmetric matrices.

Given a real valued function $f(\epsilon)$, $f(\epsilon) \leq \mathrm{O}(\epsilon)$ denotes $f(\epsilon) \leq C\epsilon$ for some $C \in \mathbb{R}^+$ and for all $\epsilon \geq 0$.

Given two sets V and W, where $W \subset V$, the complement of W in V is denoted $V-W$, and is defined as

$$V-W := \{v \in V : v \notin W\}. \tag{2.1}$$

When V is clear from context, $V-W$ is denoted $-W$.

The maximum singular value of matrix A is denoted $\overline{\sigma}(A)$, the minimum singular value is denoted $\underline{\sigma}(A)$.

An affine matrix inequality (AMI), often referred to in the literature as a linear matrix inequality (LMI), is a matrix inequality of the form

$$\sum_k x_k A_k + A_0 < 0, \tag{2.2}$$

where the A_k are constant matrices of fixed dimension and the x_k are the scalar decision variables. Many problems in this dissertation will be converted to solving an AMI for the decision variables, which is a convex feasibility problem [Boyd et al., 1994, Nesterov and Nemirovsky, 1994].

2.1.1 Discrete Time Signals and Operators

A signal is a vector valued sequence which may be represented in either column form

$$v = \begin{bmatrix} v_1 \\ \vdots \\ v_n \end{bmatrix}, \tag{2.3}$$

or in n-tuple form

$$v = (v_1, \cdots, v_n), \tag{2.4}$$

i.e., each v_i is a scalar valued sequence. Both will be used interchangeably.

The Hilbert space of square summable n-valued sequences over $\mathbb{Z}$ is denoted l_2^n, with inner product

$$\langle u, v \rangle := \sum_{t=-\infty}^{\infty} u^*(t)v(t), \tag{2.5}$$

where $*$ denotes conjugate transpose. When the spatial structure is either clear from context or not crucial to the argument being presented, l_2^n will also be referred to as l_2. The norm of a signal $v \in l_2$ is denoted $\|v\|$:

$$\|v\| := \sqrt{\langle v, v \rangle}. \tag{2.6}$$

The outer product of $u, v \in l_2^n$ is defined as

$$\Lambda(u, v) := \sum_{t=-\infty}^{\infty} u(t)v^*(t) \in \mathbb{R}_{\mathrm{S}}^{n \times n}. \tag{2.7}$$

Abbreviation $\Lambda(v)$ is used to denote $\Lambda(v, v)$.

Given two subsets of l_2, S_1 and S_2, the maximum distance between S_1 and S_2 is defined as

$$\mathrm{d}\left(S_1, S_2\right) := \max\left(\sup_{s_1 \in S_1} \inf_{s_2 \in S_2} \|s_1 - s_2\|, \sup_{s_2 \in S_2} \inf_{s_1 \in S_1} \|s_2 - s_1\|\right). \tag{2.8}$$

For $T \in \mathbb{Z}$, the truncation operator $\boldsymbol{P_T}$ is defined as

$$\boldsymbol{P_T}(v) = \begin{cases} v(t) & t \leq T \\ 0 & t > T \end{cases}. \tag{2.9}$$

Operators on l_2 are maps from l_2 to l_2. An operator $\mathbf{H}$ on l_2 is causal if $\boldsymbol{P_T}\mathbf{H}\boldsymbol{P_T} = \boldsymbol{P_T}\mathbf{H}$ for all T; operator $\mathbf{H}$ is bounded if there exists a finite γ such that $\|\mathbf{H}v\| \leq \gamma \|v\|$ for all $v \in l_2$; operator $\mathbf{H}$ is linear if $\mathbf{H}(\alpha u + \beta v) = \alpha \mathbf{H}u + \beta \mathbf{H}v$ for all $\alpha, \beta \in \mathbb{R}$, $u, v \in l_2$.

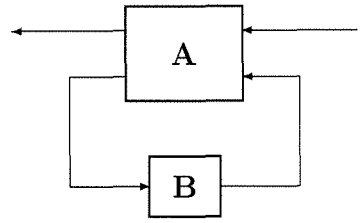

Figure 2.1: Lower LFT

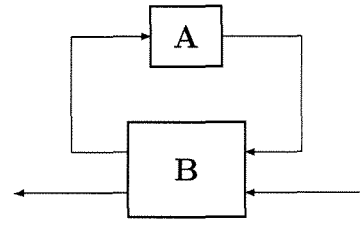

Figure 2.2: Upper LFT

The lower linear fractional transformation (LFT) of two operators $\mathbf{A}$ and $\mathbf{B}$ is denoted $\mathbf{A} \star \mathbf{B}$, and is defined as:

$$\mathbf{A} \star \mathbf{B} := \mathbf{A}_{11} + \mathbf{A}_{12}\mathbf{B}(\mathbf{I} - \mathbf{A}_{22}\mathbf{B})^{-1}\mathbf{A}_{21}, \tag{2.10}$$

where

$$\mathbf{A} = \begin{bmatrix} \mathbf{A}_{11} & \mathbf{A}_{12} \\ \mathbf{A}_{21} & \mathbf{A}_{22} \end{bmatrix},$$

when the inverse of $(\mathbf{I} - \mathbf{A}_{22}\mathbf{B})$ is well defined. It corresponds to the feedback interconnection of Figure 2.1.

The upper LFT of two operators $\mathbf{A}$ and $\mathbf{B}$ is also denoted $\mathbf{A} \star \mathbf{B}$, and is defined as:

$$\mathbf{A} \star \mathbf{B} := \mathbf{B}_{22} + \mathbf{B}_{21}\mathbf{A}(\mathbf{I} - \mathbf{B}_{11}\mathbf{A})^{-1}\mathbf{B}_{12}, \tag{2.11}$$

where

$$\mathbf{B} = \begin{bmatrix} \mathbf{B}_{11} & \mathbf{B}_{12} \\ \mathbf{B}_{21} & \mathbf{B}_{22} \end{bmatrix},$$

when the inverse of $(\mathbf{I} - \mathbf{B}_{11}\mathbf{A})$ is well defined. It can be captured by the feedback interconnection of Figure 2.2. Note that the same notation is used for the lower and upper LFT, since it will be clear from context which operation is being performed (i.e., it can be determined solely on the relative sizes of $\mathbf{A}$ and $\mathbf{B}$).

The set of linear, bounded operators $\mathbf{H} : l_2^m \to l_2^p$ is denoted $\mathcal{L}(l_2^m, l_2^p)$, or $\mathcal{L}(l_2)$. The l_2-induced norm of $\mathbf{H} \in \mathcal{L}(l_2)$ is denoted

$$\|\mathbf{H}\| := \sup_{\|v\| \neq 0} \frac{\|\mathbf{H}v\|}{\|v\|}. \tag{2.12}$$

Given $\mathbf{H} \in \mathcal{L}(l_2)$, $\mathbf{H} > 0$ (≥ 0) if

$$\langle v, \mathbf{H}v \rangle > 0 \ (\geq 0) \tag{2.13}$$

for all $v \in l_2, \|v\| \neq 0$. The adjoint of operator $\mathbf{H} \in \mathcal{L}(l_2)$ is denoted $\mathbf{H}^*$ and is the unique operator in $\mathcal{L}(l_2)$ which satisfies

$$\langle u, \mathbf{H}v \rangle = \langle \mathbf{H}^* u, v \rangle \tag{2.14}$$

for all $u, v \in l_2$.

An operator $\mathbf{H}$ is linear, time invariant (LTI) if $\mathbf{H}\boldsymbol{\lambda} = \boldsymbol{\lambda}\mathbf{H}$, where $\boldsymbol{\lambda}$ is the unit delay operator:

$$(\boldsymbol{\lambda} v)(t) = v(t-1). \tag{2.15}$$

An LTI operator can equivalently be described by a convolution kernel $h(t)$ [Kailath, 1980]:

$$(\mathbf{H}v)(t) = \sum_{\tau=-\infty}^{\infty} h(t-\tau)v(\tau). \tag{2.16}$$

2.1.2 Continuous Time Definitions

Although most of the notation previously introduced can trivially be extended to the continuous time case by replacing summations with integrals, most of the results in this dissertation which make use of the previously defined concepts are for the discrete time case. In continuous time, signals are taken to be vector valued functions. The space of square integrable functions over $\mathbb{R}$ is denoted $\mathcal{L}_2$; $\mathcal{L}_2^+$ is the subset of $\mathcal{L}_2$ functions over $\mathbb{R}^+$. $\mathcal{L}_1^{loc}$ is defined to be the space of vector valued, locally absolutely integrable functions over $\mathbb{R}$, and C^∞ the space of vector valued, infinitely differentiable functions over $\mathbb{R}$.

2.1.3 Input-Output Systems and Performance

An input-output (I/O) system is simply taken to be an operator between signals, as described in Section 2.1.1. Thus a system maps one set of signals, referred to as the input, to another set of signals, referred to as the output. A bounded system will be referred to as a stable system. A finite dimensional LTI system $\mathbf{G}$ is one that can be expressed in the following state-space form:

$$\begin{aligned} (\boldsymbol{\sigma} x)(t) &= Ax(t) + Bu(t) \\ y(t) &= Cx(t) + Du(t) \end{aligned} \tag{2.17}$$

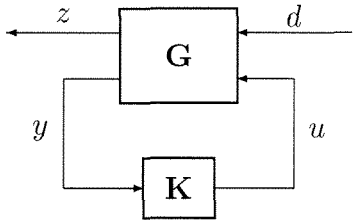

Figure 2.3: General Plant-Controller feedback interconnection

where A, B, C, D are constant matrices, u is the input, y is the output, x is the internal state, and $\boldsymbol{\sigma}$ is the unit advance operator $\boldsymbol{\lambda}^{-1}$ in discrete time and the differentiation operator $\frac{d}{dt}$ in continuous time; the notation

$$\mathbf{G} := \left[\begin{array}{c|c} A & B \\ \hline C & D \end{array}\right] \tag{2.18}$$

is used to define system $\mathbf{G}$ as per equation (2.17). In this section, only finite dimensional LTI systems are considered.

Consider the interconnection of systems $\mathbf{G}$ and $\mathbf{K}$ in Figure 2.3. Denote the closed loop map from d to z by $\mathbf{M} := \mathbf{G} \star \mathbf{K}$. $\mathbf{K}$ is referred to as a stabilizing controller if the closed loop map of Figure 3.1 is internally stable [Zhou et al., 1995]; this corresponds to requiring that the map from d, and signals injected anywhere in the loop, to z, y, and u exists, is bounded, and causal.

Many control problems can be cast in the framework of Figure 2.3. It is usually required that system $\mathbf{K}$ stabilize system $\mathbf{G}$, and in addition, that the closed loop system $\mathbf{M}$ have certain desired properties, often termed performance requirements. Two widely used performance criteria are that the $\mathcal{H}_\infty$ or the $\mathcal{H}_2$ norm of the closed loop system $\mathbf{M}$ be made as small as possible. While these are frequency domain concepts, it will be useful to consider their time domain interpretation, since they naturally extend to the time varying case. We will concentrate on the discrete time definitions; the continuous time counterparts can be defined analogously (most of the definitions apply directly by simply replacing l_2 with $\mathcal{L}_2$).

The $\mathcal{H}_\infty$ norm of $\mathbf{M}$ is simply the l_2 induced norm, $\|\mathbf{M}\|$, and thus gives the design problem a simple interpretation: it is required to minimize the energy (or power) gain of system $\mathbf{M}$. The $\mathcal{H}_2$ norm can be defined as follows:

$$\|\mathbf{M}\|_2 := \left(\sum_{-\infty}^{\infty} \mathbf{trace}\left(m^*(t) m(t)\right) \right)^{\frac{1}{2}} \tag{2.19}$$

where $m(t)$ is the convolution kernel representation for $\mathbf{M}$. The $\mathcal{H}_2$ design problem has typically been given a stochastic interpretation; minimizing the $\mathcal{H}_2$ norm is equivalent to minimizing the variance of z when the input d is stochastic white

noise [Anderson and Moore, 1990]. An alternate interpretation has been explored in [Paganini, 1995b], which will be used in Chapter 5 and outlined in Section 2.2.3. Computationally attractive solutions to the $\mathcal{H}_\infty$ and $\mathcal{H}_2$ design problems may be found in [Doyle et al., 1989].

In many instances, minimizing the $\mathcal{H}_2$ system norm is a much more sensible design objective than $\mathcal{H}_\infty$ optimization. This is essentially due to the gain interpretation; it is often better to model disturbances as white noise signals than as arbitrary bounded power signals. This is the case for many types of disturbances, such as thermal noise. Many other types of disturbances, such as wind gusts, are typically modeled as a filtered white noise signal. By absorbing these filters, or weights, into system $\mathbf{G}$, one can consider the case of purely white noise disturbances.

2.1.4 Polynomial Matrices

Polynomial matrices, matrices whose elements are polynomials in some indeterminate, are used extensively when describing the behavior of a system in Chapters 6 and 7. What follows are some definitions and results pertaining to polynomial matrices used throughout these two chapters; the reader is referred to [Kailath, 1980] for details.

A square polynomial matrix $R(s)$ is said to be *nonsingular* if $\det(R(s)) \neq 0$. A nonsingular polynomial matrix whose determinant is not a function of s is called *unimodular*; equivalently, $R(s)$ is unimodular if and only if $R^{-1}(s)$ is a polynomial matrix.

$R(s)$ is said to have *full normal row rank* if $R(s)$ is full row rank for almost all $s \in \mathbb{C}$. Similarly, $R(s)$ is said to have *full normal column rank* if $R(s)$ is full column rank for almost all $s \in \mathbb{C}$.

$R(s)$ is said to be *right invertible* if there exists a polynomial matrix $M(s)$ such that $R(s)M(s) = I$; equivalently, $R(s)$ is right invertible if and only if $R(s)$ is full row rank for all $s \in \mathbb{C}$. $R(s)$ is said to be *left invertible* if there exists a polynomial matrix $M(s)$ such that $M(s)R(s) = I$; equivalently, $R(s)$ is left invertible if and only if $R(s)$ is full column rank for all $s \in \mathbb{C}$. If $R(s)$ is right invertible, there exists a polynomial matrix $N(s)$ such that

$$\begin{bmatrix} R(s) \\ N(s) \end{bmatrix}$$

is unimodular. If $R(s)$ is left invertible, there exists a polynomial matrix $N(s)$ such that $\begin{bmatrix} R(s) & N(s) \end{bmatrix}$ is unimodular.

Any polynomial matrix $R(s)$ can be *Smith* decomposed as

$$R(s) = U(s) \begin{bmatrix} \Delta(s) & 0 \\ 0 & 0 \end{bmatrix} V(s), \tag{2.20}$$

where $U(s)$ and $V(s)$ are unimodular and $\Delta(s)$ is square and nonsingular.

2.2 Robust Control

When attempting to capture the behavior of a physical system by a mathematical model, there will invariably be some mismatch between the true behavior of the system and that predicted by the model. There are two major sources of this mismatch. The first is that the parameters which make up a model can never be determined exactly; this is due to incomplete knowledge of the system, or variations of physical properties over time. The second, and more compelling source, is due to the fact that for a mathematical model to be useful, it must be tractable. Thus the goal of the modeling process is to extract the salient features of a physical system in as concise a manner as possible. Experimental validation is then used to justify the simplifications and assumptions which took place in the modeling stage. For example, treating a fluid as incompressible and inviscid leads to some very elegant and simple equations which govern its behavior, but leads to models which can only be applied in a restricted set of circumstances [Shames, 1992]. Dropping the compressibility assumption, and more importantly, adding viscosity to the problem, leads to more complicated models which have a wider applicability.

The essence of the robust control paradigm is the concept of explicitly bounding the mismatch between a mathematical model and the behavior of the system it is trying to capture. This mismatch is commonly referred to as system uncertainty. This approach, by necessity, is conservative, since the uncertainty must account for complex, yet hopefully not crucial, behavior. There is thus an inherent tradeoff in the modeling of a system between model fidelity and model complexity.

In the traditional robust control framework, the approach taken is to model a physical system as the interconnection of a finite dimensional LTI system and a bounded, but unknown, operator (which accounts for the mismatch). This will be formalized shortly. This framework has been very successful, if judged by the amount of research activity it has generated and the significant number of applications which it has serviced. The main reason for this success is that the robust control framework seems to provide the right mix of fidelity and model tractability. It is rich enough to capture complex systems, yet at the same time remains a tractable paradigm. Extensions of this framework to encompass non-linear and time varying systems have been made, with promising results [Tierno, 1995, Packard, 1994]; the price paid, of course, is computational complexity, which is increased substantially.

Just like any tool, however, the applicability of the robust control framework is not all-encompassing. By that it is meant that even though the idea at the root of robust control is applicable to most systems, the theory at its present state can only be applied to a modest (yet significant) number of physical systems. For example, robust control methods have extensively and successfully been used in flight control applications, but are not amenable to applications where the behavior is dominated by non-linearities.

The need for incorporating model mismatch in the design process is best illustrated by a simple example. Consider the diagram of Figure 2.4. It is required to find a control law which stabilizes a cylindrical spinning satellite about its minor principal

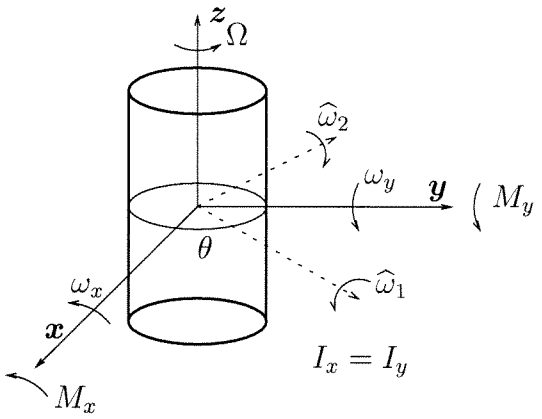

Figure 2.4: Spinning satellite stabilization

axis. The satellite is modeled as a rigid body. The equations of motion are described using a body-fixed co-ordinate system, which is co-incident with the principle axes and is rotating relative to an inertial frame of reference with angular velocity $\omega = (\omega_x, \omega_y, \omega_z)$. The moment of inertia matrix I is diagonal, where $I_x = I_y > I_z$. Torques M_x and M_y are available for control purposes. Angular rates w_x and w_y are measured in a rotated co-ordinate system relative to the x/y plane:

$$\begin{bmatrix} \widehat{\omega}_1 \\ \widehat{\omega}_2 \end{bmatrix} = \begin{bmatrix} \cos\theta & \sin\theta \\ -\sin\theta & \cos\theta \end{bmatrix} \begin{bmatrix} w_x \\ w_y \end{bmatrix}. \tag{2.21}$$

Assuming no dissipative mechanisms, equating moments results in the following:

$$\begin{bmatrix} \dot{\omega}_x \\ \dot{\omega}_y \end{bmatrix} = \begin{bmatrix} 0 & a \\ -a & 0 \end{bmatrix} \begin{bmatrix} \omega_x \\ \omega_y \end{bmatrix} + \frac{1}{I_x} \begin{bmatrix} M_x \\ M_y \end{bmatrix}, \tag{2.22}$$

$$a := \Omega\left(1 - \frac{I_z}{I_x}\right), \tag{2.23}$$

where Ω denotes the constant value of angular rotation about the z axis, ω_z. Due to the energy conservation assumption, the system is marginally open-loop stable. Since the satellite is prolate, however, any energy dissipation will result in the satellite eventually spinning along an axis on the x/y plane. The goal is thus to apply torques M_x and M_y based on measurements $\widehat{\omega}_1$ and $\widehat{\omega}_2$ and stabilize the satellite about angular velocity $\omega = (0, 0, \Omega)$.

To simplify the argument, assume that $a \gg 1$ and that $\tan\theta = a$. Applying control law

$$\begin{bmatrix} M_x \\ M_y \end{bmatrix} = -\frac{I_x}{\cos\theta} \begin{bmatrix} \widehat{\omega}_1 \\ \widehat{\omega}_2 \end{bmatrix} \tag{2.24}$$

results in the following closed loop system:

$$\begin{bmatrix} \dot{\omega}_x \\ \dot{\omega}_y \end{bmatrix} = \begin{bmatrix} -1 & 0 \\ 0 & -1 \end{bmatrix} \begin{bmatrix} \omega_x \\ \omega_y \end{bmatrix}, \tag{2.25}$$

which is exponentially stable. Note, however, that when θ is perturbed by a small amount, $\theta = \theta_0 + \bar{\theta}$, the closed loop system takes the following form:

$$\begin{bmatrix} \dot{\omega}_x \\ \dot{\omega}_y \end{bmatrix} \approx \begin{bmatrix} -1 + a\bar{\theta} & \bar{\theta} \\ -\bar{\theta} & -1 + a\bar{\theta} \end{bmatrix} \begin{bmatrix} \omega_x \\ \omega_y \end{bmatrix}, \tag{2.26}$$

which is unstable for small positive values of $\bar{\theta}$. Thus the control design is extremely sensitive to modeling errors, and does not inspire much confidence in its successful implementation.

2.2.1 Linear Fractional Transformations and Structured Uncertainty

Referring back to the diagram of Figure 2.3, many standard control design problems are of the following form:

Control Synthesis

Given system $\mathbf{G}$, *find system* $\mathbf{K}$ *such that*

- *The closed loop system is internally stable.*
- *The closed loop map from d to z satisfies the given performance requirements.*

The above is a reasonable problem formulation; it is required to stabilize the given system (or equally important, to ensure that $\mathbf{K}$ does not de-stabilize an otherwise stable system), and to achieve a certain level of performance. This performance requirement is typically to ensure that the map from d to z be small in some sense. This is natural when addressing disturbance rejection problems, tracking problems by setting z to be the difference between a reference signal and the process output, or a combination thereof.

As previously discussed, however, it is important to ensure that a design is not sensitive to model mismatch and uncertainty. In the robust control framework, the standard control design problem is replaced by the following:

Robust Control Synthesis

Given a set of possible plants $\mathcal{G}$, *find system* $\mathbf{K}$ *such that*

- *For all* $\widetilde{\mathbf{G}} \in \mathcal{G}$, *the closed loop system is internally stable.*
- *For all* $\widetilde{\mathbf{G}} \in \mathcal{G}$, *the closed loop map from d to z satisfies the given performance requirements.*

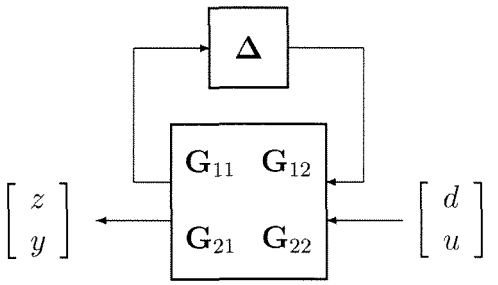

Figure 2.5: LFTs and plant sets

In the spinning satellite, for example, the set of plants $\mathcal{G}$ could be those parameterized by values of θ in a given interval (note that there is no performance requirement in this example, since there are no exogenous disturbances).

Linear fractional transformations provide a natural and convenient means to parametrize plant sets $\mathcal{G}$. Referring to the diagram of Figure 2.5, $\mathbf{G}$ is a finite dimensional LTI system and $\boldsymbol{\Delta}$ is a bounded operator which will serve as the means to parametrize $\mathcal{G}$. For a fixed $\boldsymbol{\Delta}$, plant $\widetilde{\mathbf{G}}$ is of the form

$$\widetilde{\mathbf{G}}(\boldsymbol{\Delta}) = \boldsymbol{\Delta} \star \mathbf{G} = \mathbf{G}_{22} + \mathbf{G}_{21}\boldsymbol{\Delta}(\mathbf{I} - \mathbf{G}_{11}\boldsymbol{\Delta})^{-1}\mathbf{G}_{12}, \tag{2.27}$$

where $\mathbf{G}_{22}$ is the nominal system ($\boldsymbol{\Delta} = \mathbf{0}$). Operator $\boldsymbol{\Delta}$ is assumed to have the following spatial structure:

$$\boldsymbol{\Delta} = \mathbf{diag}\left[\ \delta_1 I,\ \cdots,\ \delta_L I,\ \boldsymbol{\Delta}_{L+1},\ \cdots,\ \boldsymbol{\Delta}_{L+F}\ \right], \tag{2.28}$$

i.e., $\boldsymbol{\Delta}$ is a block diagonal operator. Two types of uncertainty blocks appear in equation (2.28). The first are the repeated scalar blocks $\delta_i I$, where each identity is of fixed, but arbitrary, dimension; if $x = (\delta_i I)w$, then $x_j = \delta_i w_j$. The second type consists of full blocks $\boldsymbol{\Delta}_{L+i}$, which are general multi-variable operators.

There are two main reasons for considering this structure for $\boldsymbol{\Delta}$. The first is that many types of plant uncertainty can be captured in this form; this is intimately related to the fact that LFT systems with the above spatial structure for the uncertainty are invariant under addition, cascade, and interconnection, three common system manipulations. By this it is meant that the addition, cascade, or interconnection of two or more LFT systems with the uncertainty structure of equation (2.28) can always be written as an LFT system with the uncertainty structure of equation (2.28) (of possibly different dimension). The reader is referred to [Zhou et al., 1995] for an in-depth treatment of these issues. The second is that the LFT interconnection of Figure 2.5 is in fact the natural generalization of state-space descriptions; for example, by setting $\boldsymbol{\Delta} = \delta_1 = \boldsymbol{\lambda}$ and

$$\mathbf{G} = \begin{bmatrix} A & B \\ C & D \end{bmatrix},$$

one recovers the state-space description of equation (2.17). This is further explored in [Beck, 1995], along with issues of model reduction for these more general types of systems.

In addition to the spatial structure of equation (2.28), each component of $\boldsymbol{\Delta}$ is typically restricted to be one of the following types of operators:

- real parameter;
- LTI operator;
- arbitrary linear operator, or equivalently, linear time varying (LTV) operator;
- static non-linearity.

A further restriction is that the operators be causal (this is clearly not an issue for real parameters and static non-linearities). This is an important restriction, in light of the definition of internal stability. The issue of causality will be further explored in later chapters when various robustness problems are encountered.

Let the spatial structure of $\boldsymbol{\Delta}$ and the type of each operator in $\boldsymbol{\Delta}$ be given (LTI, LTV, etc.), and denote this class of allowable uncertainty as $\mathbf{\Delta}$. In order to complete the parameterization of $\mathcal{G}$, a norm bound is imposed on all allowable $\boldsymbol{\Delta}$ as follows:

$$\mathbf{B\Delta} := \left\{ \boldsymbol{\Delta} \in \mathbf{\Delta} : \|\boldsymbol{\Delta}\| \leq 1 \right\}. \tag{2.29}$$

For a given system $\mathbf{G}$, set $\mathcal{G}$ is then parameterized as follows:

$$\mathcal{G} := \left\{ \widetilde{\mathbf{G}} : \widetilde{\mathbf{G}} = \boldsymbol{\Delta} \star \mathbf{G}, \boldsymbol{\Delta} \in \mathbf{B\Delta} \right\}. \tag{2.30}$$

Note that when imposing a size constraint on $\boldsymbol{\Delta}$, it is natural to do so as a condition on the induced gain. The l_2 induced gain is used, but other measures such as the l_∞ induced gain [Dahleh and Diaz-Bobillo, 1995] can be employed as well.

2.2.2 Synthesis for Robust l_2 Performance

We are now in a position to formulate the standard l_2 robust synthesis problem:

Robust l_2 Synthesis

Given system $\mathbf{G}$ *and uncertainty class* $\mathbf{\Delta}$, *find system* $\mathbf{K}$ *such that*

- $\boldsymbol{\Delta} \star \mathbf{G} \star \mathbf{K}$ *is internally stable for all* $\boldsymbol{\Delta} \in \mathbf{B\Delta}$.
- $\|\boldsymbol{\Delta} \star \mathbf{G} \star \mathbf{K}\| < 1$ *for all* $\boldsymbol{\Delta} \in \mathbf{B\Delta}$.

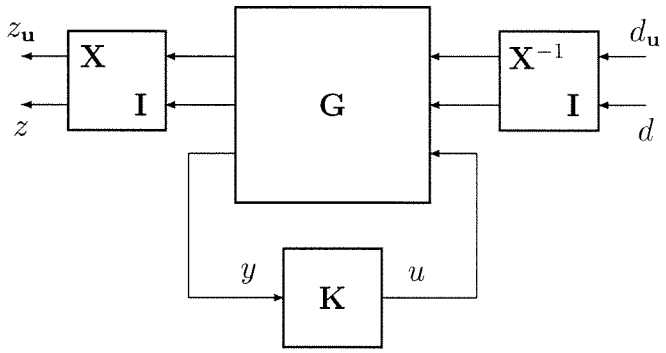

Figure 2.6: Iterative Robust $\mathcal{H}_\infty$ Synthesis design

Thus the performance measure is to minimize the l_2 to l_2 gain for all allowable uncertainty. Note that the term Robust $\mathcal{H}_\infty$ Synthesis is typically used instead for the above design problem (strictly speaking, the two are equivalent for LTI uncertainty, but the term $\mathcal{H}_\infty$ is a misnomer for LTV uncertainty). It turns out that this problem, in its full generality, is a very difficult one to solve. The following facts support this statement:

- The analysis problem alone, i.e., just determining whether the closed loop system satisfies the stability and performance requirement for all $\mathbf{\Delta} \in \mathbf{B\Delta}$ has been shown to be NP-Hard in the number of diagonal blocks of $\mathbf{\Delta}$ when the $\boldsymbol{\delta}_i$ and $\mathbf{\Delta}_i$ are real parameters or LTI operators [Braatz et al., 1994], [Toker and Ozbay, 1995b]. The implication of this result is that in the worst case, the analysis question for structured real or LTI uncertainty (or any mix thereof) cannot be computed exactly without exponential growth in computational cost with problem size [Garey and Johnson, 1979].

- The easiest analysis problem to solve, in that it displays the lowest growth in computational complexity as a function of problem size, is the case of LTV uncertainty. For this case, the computational cost growth is polynomial in the number of diagonal blocks, and can in fact be converted to an AMI. The synthesis problem in this case can be converted to a bilinear matrix inequality (BMI) [Safonov et al., 1994], which is, in general, an NP-Hard problem [Toker and Ozbay, 1995a].

Various techniques such as branch and bound [Newlin, 1996] and power algorithms [Packard and Doyle, 1993] combined with various upper bounds [Fan et al., 1991], [Young, 1993] have been shown to yield acceptable growth rates for the analysis question for typical problems (although as previously mentioned, the worst case growth is still exponential). These techniques cannot, however, be applied directly to the synthesis problem.

The state of the art in synthesis is to iterate between an analysis step and a scaled $\mathcal{H}_\infty$ synthesis step, as proposed in [Stein and Doyle, 1991]. This is depicted

in Figure 2.6. Scales $\mathbf{X}$ are systems such that $\mathbf{X}^{-1}\Delta\mathbf{X} \in \mathbf{\Delta}$ for all $\Delta \in \mathbf{\Delta}$; for LTV uncertainty, for example, the $\mathbf{X}$ are constant matrices (of appropriate spatial structure), while for LTI uncertainty, the $\mathbf{X}$ can themselves be LTI systems (again of appropriate spatial structure). By a simple application of the small gain theorem [Zames, 1966], it can be shown that if an internally stabilizing controller $\mathbf{K}$ and scales $\mathbf{X}$ can be found such that the closed loop $\mathcal{H}_\infty$ norm of the system with input $(d_\mathbf{u}, d)$ and output $(z_\mathbf{u}, z)$ is less than one, then $\mathbf{K}$ solves the Robust l_2 Synthesis problem. The reader is referred to [Packard and Doyle, 1993] for a thorough explanation of these issues. The above motivates the following iteration:

Synthesis: For fixed scale $\mathbf{X}$, find $\mathbf{K}$ which minimizes the closed loop $\mathcal{H}_\infty$ norm of the system with input $(d_\mathbf{u}, d)$ and output $(z_\mathbf{u}, z)$. This is a computationally tractable problem [Doyle et al., 1989].

Analysis: For fixed $\mathbf{K}$, obtain new scales which minimize the closed loop $\mathcal{H}_\infty$ norm of the system with input $(d_\mathbf{u}, d)$ and output $(z_\mathbf{u}, z)$. This problem can be either converted to an AMI (for LTV uncertainty), or can be approximated by an AMI (for LTI and parametric uncertainty) [Balakrishnan et al., 1994]. As previously mentioned, this step is in fact a sufficient condition for the analysis problem; if scales can be found such that the closed loop $\mathcal{H}_\infty$ norm is less than one, then the system is robustly stable and the worst case l_2 induced gain is less than one. It can be shown that it is also a necessary condition for LTV uncertainty [Shamma, 1994].

Thus one would iterate between these two steps until the resulting $\mathcal{H}_\infty$ norm, at either step, is less than one. If this cannot be accomplished, the performance requirement will have to be relaxed or the size of the uncertainty will have to be reduced (or both). It should be stressed that the above iterative scheme is not guaranteed to converge to the global minimum. Furthermore, even if the global minimum is achieved and is greater than one, the existence of a controller $\mathbf{K}$ which solves the robust synthesis problem is not precluded (except for the LTV case; but as previously mentioned, it is likely that finding the global minimum for the LTV case is an NP-Hard problem).

In order to obtain exact solutions to the Robust l_2 Synthesis problem, either a restricted class for the uncertainty or systems $\mathbf{G}$ with a special structure must be considered; this is addressed in Chapter 4.

2.2.3 Deterministic Noise Sets

In this section, the notions introduced in [Paganini, 1995a] to capture white noise in sets are reviewed. Given a signal $n \in l_2^m$, its autocorrelation function is defined as

$$R_n(\tau) := \Lambda(n, \boldsymbol{\lambda}^\tau n). \tag{2.31}$$

Note that there is no time averaging in the above definition, as would be used for power signals, since we are dealing with finite energy signals. Given positive integer N and positive number γ, we define the following set of autocorrelation functions:

$$\mathcal{R}_{N,\gamma}^{m} := \left\{ R(\tau) : \mathbb{Z} \to \mathbb{R}^{m\times m} \;\middle|\; \begin{array}{l} R(-\tau) = R^{*}(\tau) \\ \max_{i,j} |(R(0) - I)_{i,j}| \leq \gamma \\ \max_{i,j} |R(\tau)_{i,j}| \leq \gamma, \;\; 1 \leq \tau \leq N \end{array} \right\}, \tag{2.32}$$

and corresponding signal set

$$\mathcal{W}_{N,\gamma}^{m} := \left\{ n \in l_2^m : R_n(\tau) \in \mathcal{R}_{N,\gamma}^{m} \right\}. \tag{2.33}$$

For $\gamma = 0$, define

$$\mathcal{W}_{N}^{m} := \mathcal{W}_{N,0}^{m}. \tag{2.34}$$

The motivation for the above definitions is that sets $\mathcal{W}_{N,\gamma}^{m}$ capture "typical" instances of white noise. For example, when deciding whether a measured signal is a sample of white noise, one would perform a hypothesis test in terms of some statistic. The sample correlogram [Ljung, 1987] is such a test; it is required that the sampled signal be in set $\mathcal{W}_{N,\gamma}^{m}$ (after normalization) for a sufficiently large N and sufficiently small γ.

Let $\mathbf{H}$ be a LTI system. Define the following induced norm:

$$\|\mathbf{H}\|_{\mathcal{W}_N^m} := \sup \left\{ \|\mathbf{H}n\| : n \in \mathcal{W}_N^m \right\}. \tag{2.35}$$

The following result is from [Paganini, 1995b]:

Lemma 2.1

$$0 \leq \left(\|\mathbf{H}\|_{\mathcal{W}_N^m} - \|\mathbf{H}\|_2 \right) \overset{N\longrightarrow\infty}{\longrightarrow} 0. \tag{2.36}$$

Furthermore, the convergence rate is exponential in N.

Thus one may induce the $\mathcal{H}_2$ norm of a system by considering the worst case norm resulting from signals in $\mathcal{W}_N^m$, as N approaches infinity.

Note that bounded energy, not bounded power signals are considered. While this may seem a strange and unnatural way to describe noise (i.e., requiring noise signals to decay to zero as time goes to infinity) it is argued quite convincingly in [Paganini, 1995b] that for the study of disturbance rejection problems, the theory is best developed in l_2. This is analogous to $\mathcal{H}_\infty$ theory; it is more convenient mathematically to consider the $\mathcal{H}_\infty$ norm as induced from l_2 to l_2, although it also has the perhaps more natural interpretation as the worst case power to power gain. Irrespective of which interpretation is given (energy to energy or power to power), the resulting design is the same. One should thus use the interpretation which facilitates the theoretical development, which in our case is l_2.

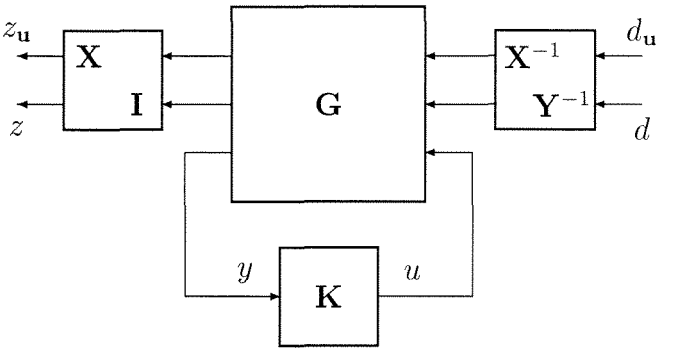

Figure 2.7: Iterative Robust $\mathcal{H}_2$ Synthesis design

2.2.4 Synthesis for Robust $\mathcal{H}_2$ Performance

As previously argued, in the absence of uncertainty the $\mathcal{H}_2$ design problem is typically more physically motivated than the $\mathcal{H}_\infty$ design problem; most disturbances are much better modeled as white noise signals rather than arbitrary bounded power signals (such as sinusoids, for example). The reason that $\mathcal{H}_\infty$ performance has dominated the robust control literature is simply that until recently, there was no natural way to incorporate a system's uncertainty (naturally captured by $\mathcal{H}_\infty$ type bounds) with $\mathcal{H}_2$ performance (which has typically been given a stochastic interpretation).

Armed with the previous definitions for deterministic noise, we are now in a position to formulate the robust $\mathcal{H}_2$ synthesis problem:

Robust $\mathcal{H}_2$ Synthesis

Given system $\mathbf{G}$ *and uncertainty class* $\mathbf{\Delta}$*, find system* $\mathbf{K}$ *such that*

- $\mathbf{\Delta} \star \mathbf{G} \star \mathbf{K}$ *is internally stable for all* $\mathbf{\Delta} \in \mathbf{B\Delta}$.
- $\lim_{N\to\infty} \|\mathbf{\Delta} \star \mathbf{G} \star \mathbf{K}\|_{\mathcal{W}_N^m} < 1$ *for all* $\mathbf{\Delta} \in \mathbf{B\Delta}$.

Note that for LTI uncertainty, the limit may be replaced by the system $\mathcal{H}_2$ norm, by Lemma 2.1. As in the Robust $\mathcal{H}_\infty$ Synthesis problem, this is generally a very difficult problem to solve. Recent results [Paganini et al., 1994, Paganini, 1995b], however, have shown that the Robust $\mathcal{H}_2$ Synthesis problem as formulated above may be converted to a Robust $\mathcal{H}_\infty$ Synthesis problem; in particular, it has been shown in [Paganini, 1995b] that the Robust $\mathcal{H}_\infty$ Synthesis problem may be augmented to achieve Robust $\mathcal{H}_2$ performance by introducing an extra scaling system $\mathbf{Y}$, as shown in Figure 2.7. This yields the following iterative scheme:

Synthesis: For fixed scales $\mathbf{X}$ and $\mathbf{Y}$, find $\mathbf{K}$ which minimizes the closed loop $\mathcal{H}_\infty$ norm of the system with input $(d_{\mathbf{u}}, d)$ and output $(z_{\mathbf{u}}, z)$.

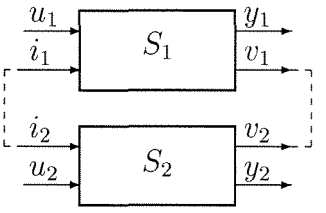

Figure 2.8: Interconnection of two networks

Analysis: For fixed $\mathbf{K}$, obtain new scales $\mathbf{X}$ and $\mathbf{Y}$ which minimize the closed loop $\mathcal{H}_\infty$ norm of the system with input $(d_\mathbf{u}, d)$ and output $(z_\mathbf{u}, z)$. This problem may be approximated by an AMI [Paganini, 1995b].

The above iterative scheme has two shortcomings:

1. There is now an extra scale to search over, $\mathbf{Y}$. This could potentially introduce more local minima in the iteration.

2. The resulting $\mathbf{Y}$ in the analysis step needs to be approximated by a finite dimensional system in order for the synthesis step to be applied. This can be avoided by choosing basis functions [Balakrishnan et al., 1994] to parametrize $\mathbf{Y}$, which is in effect equivalent to fixing the maximum size of N in the Robust $\mathcal{H}_2$ Synthesis problem formulation. Furthermore, increasing the number of basis functions which parametrize $\mathbf{Y}$ increases the computation time and the order of the resulting controller.

In Chapter 5, the Robust $\mathcal{H}_2$ Synthesis problem is solved for a restricted class of uncertainty. In addition, a method is proposed which eliminates the search for scale $\mathbf{Y}$ in the above iterative scheme for problems with general uncertainty structure.

2.3 Behavioral Systems

The behavioral framework, as proposed in [Willems, 1991], is essentially a mathematical formalism for dynamical systems which makes no distinction between inputs and outputs. The predominant reason for not describing systems as I/O operators is that in practice it is often not clear which of the variables should be regarded as inputs and which as outputs. Examples of this are situations in which the system is an interconnection of several subsystems. Such an interconnection may induce constraints such that variables which could have been considered as inputs or as outputs in a subsystem can no longer be labeled as such in the interconnected system. Thus it would seem that imposing an I/O structure to a system, or component, would require an a priori knowledge of how that component will be used.

As a simple example, consider the two electrical networks of Figure 2.8, described as I/O operators. It is desired to connect a node together, i.e., to set $v_1 = v_2$ and

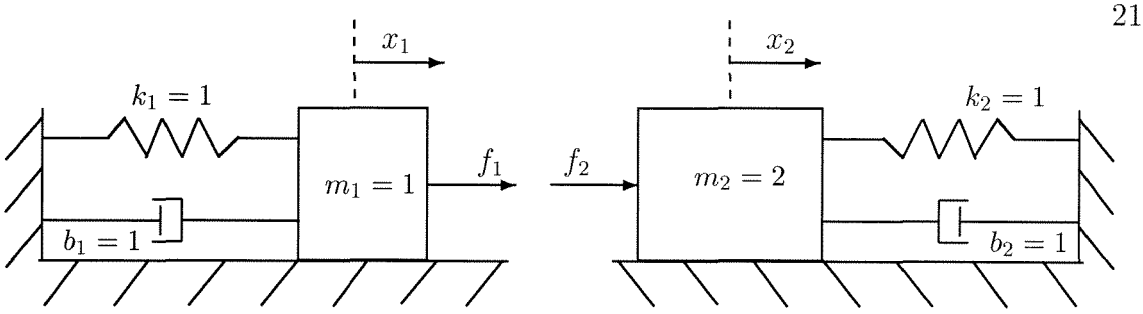

Figure 2.9: Mass-spring-damper systems

$i_1 = i_2$. If the two networks are defined as in Figure 2.8, where i_1 and i_2 are inputs, and v_1 and v_2 are outputs, there is no clear way to represent this interconnection. The problem is, of course, with the choice of inputs and outputs. If system 2 were represented with v_2 an input and i_2 an output, a simple expression for the above interconnection could then be derived.

It might also be the case that an I/O structure is not required: should a resistor in an electrical circuit be considered a voltage to current operator, or a current to voltage operator? As long as the relation $v - Ri = 0$ is satisfied, the answer to this question is irrelevant. It would thus seem that the effort undertaken by the design engineer to provide I/O system representations might not be warranted.

In addition, equations where no distinction is made between inputs and outputs arise naturally when modeling physical systems from first principles; it is almost always the case that components are modeled in terms of mass, momentum, or energy balances, or physical laws, which are inherently of the form $f(w) = 0$, where f is an operator, and w a vector of variables.

Another reason for adopting the behavioral paradigm is that this approach unifies first principles modeling and interconnection. Both are mathematically equivalent, since both consist of combining constraint equations. Tools developed for interconnection can then be used for modeling purposes, and vice-versa.

The above discussion may seem elementary to anyone who has ever constructed a model from first principles. In terms of the control community, however, there has been a bias towards describing systems as I/O operators. There are good reasons for this bias; I/O methods have been extremely successful at dealing with conventional control applications, where the I/O relation describing a given plant is impervious to the system with which it is connected to. In fact, sensors and actuators are physically designed with this in mind, as are many electronic devices (for example, the operational amplifier). Furthermore, no one would argue that a cause-effect (or I/O) relationship exists when a controller is implemented by a digital computer, where sensor signals are sampled and processed to produce the control signals.

The buffering assumption, however, is not an inherent property of all systems to be controlled. This assumption, in fact, limits the applicability of control methods. Consider, for example, the mechanical systems of Figure 2.9, where each mass is

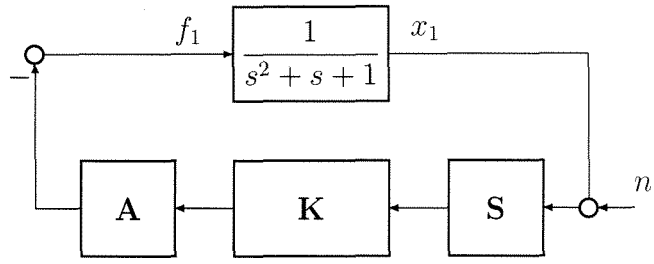

Figure 2.10: Conventional control design. **A** corresponds to the actuator, **S** corresponds to the sensor.

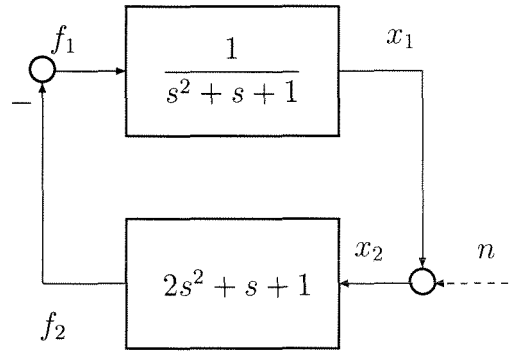

Figure 2.11: "Undesirable" control design

attached to a spring and a damper sliding on a frictionless surface. Consider system one, on the left-hand side of the figure. It is required to construct a control system for it. From the standard control viewpoint, position x_1 will be measured by a sensor, and force f_1 will be applied by an actuator. This is described by the block diagram of Figure 2.10, where n is sensor noise. Thus the problem is to find suitable actuators and sensors and design controller **K** to achieve certain design objectives. Now consider the block diagram of Figure 2.11. There are three major problems with this feedback interconnection from the traditional control view point:

1. There are no actuators and sensors.

2. There is differentiation in the feedback loop (in fact, double differentiation), an undesirable property for a controller and one which can only be approximated over a limited frequency range.

3. Any noise at n will result in infinite (in practice large) values of f_1 and f_2.

In fact, the block diagram of Figure 2.11 simply captures the interconnection of system two with system one, as depicted in Figure 2.12. The three previously raised objections do not seem to apply to this interconnection:

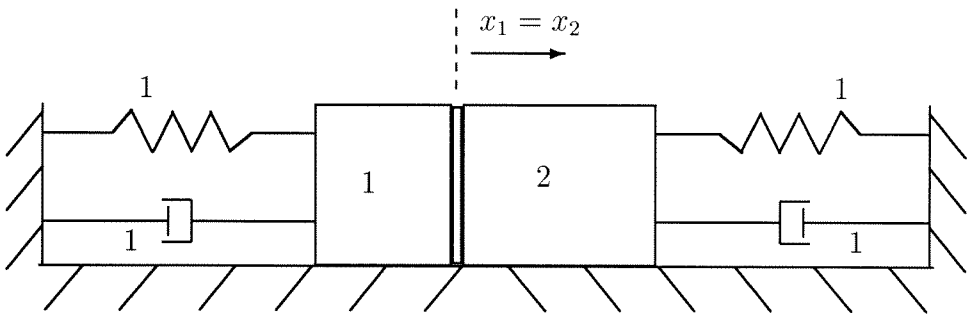

Figure 2.12: Interconnection of systems one and two

1. No actuators or sensors are needed.
2. There is no differentiation; differentiation is an artifice of writing the governing equations in I/O form.
3. There is no noise at the x_1/x_2 junction, and the system is well behaved.

It thus appears that the I/O framework is not natural, and is in fact a hindrance, when the role of control is expanded to include non-buffered interconnections.

2.3.1 Continuous Time System Representations

Systems for which the allowable trajectories are the solution set of the following set of differential equations will be considered:

$$R_L \frac{d^L w}{dt^L} + \cdots + R_0 w = 0 \tag{2.37}$$

where $R_0, \cdots, R_L$ are constant matrices. Defining

$$R(s) := R_L s^L + \cdots + R_0 \tag{2.38}$$

results in the shorthand notation $R(\frac{d}{dt})w = 0$ for equation (2.37). The above is referred to as an autoregressive (AR) representation.

Using the notation in [Willems, 1991], a system will be denoted $\Sigma := \{\mathbb{R}, \mathbb{R}^q, \mathcal{B}\}$, where $\mathbb{R}$ and $\mathbb{R}^q$ correspond to $\mathbb{R}^q$ valued, bi-infinite, continuous time, trajectories, and $\mathcal{B}$ is the behavior, or the allowable trajectories:

$$\mathcal{B} := \left\{ w \in \mathcal{L}_1^{loc} : R(\frac{d}{dt})w = 0 \right\}. \tag{2.39}$$

According to the dynamical model Σ, time signals in $\mathcal{B}$ can in principle occur, while those outside $\mathcal{B}$ cannot.

Chapter 3
Generalized l_2 Synthesis

In the standard $\mathcal{H}_\infty$ paradigm, the allowable disturbance class consists of arbitrary unit l_2 norm signals, while the design objective is to ensure that all output errors have l_2 norm less than one. In this chapter, the allowable disturbance class and the design objectives are generalized to encompass a wide class of optimization problems. The underlying signal space is still taken to be l_2; as opposed to standard $\mathcal{H}_\infty$ synthesis, however, the allowable disturbance set and performance objective are general functions of the various inner products of the input and output variables. For example, denoting d as the exogenous disturbance and z as the output error, a specific choice is

$$\sum \langle d_k, d_k \rangle \leq 1, \quad \sum \langle z_l, z_l \rangle < 1, \tag{3.1}$$

which leads to $\mathcal{H}_\infty$ optimization. Using the tools developed in this chapter, other criteria such as

$$\langle d_k, d_k \rangle \leq 1 \; \forall k, \tag{3.2}$$

$$\begin{bmatrix} \langle d_1, d_1 \rangle & \langle d_1, d_2 \rangle \\ \langle d_2, d_1 \rangle & \langle d_2, d_2 \rangle \end{bmatrix} - I \leq 0 \tag{3.3}$$

$$\sum_l \sqrt{\langle z_l, z_l \rangle} < 1, \tag{3.4}$$

and many others may be utilized. The motivation for considering these more general sets are twofold. From a practical point of view, many interesting problems may be cast in this framework; in Chapters 4 and 5, various open problems are solved using the framework developed in this chapter. From a purely theoretical standpoint, these results extend the boundary for which optimization in the l_2 framework results in computationally tractable solutions.

The chapter is organized as follows: The problem formulation is outlined in Section 3.1. In Section 3.2, various properties of the allowable disturbance classes and cost criteria are explored. In Section 3.3, an analysis condition is derived, which takes the form of an operator inequality. Using this condition, a method for constructing controllers which meet the performance objectives is presented in Section 3.4, which takes the form of an AMI.

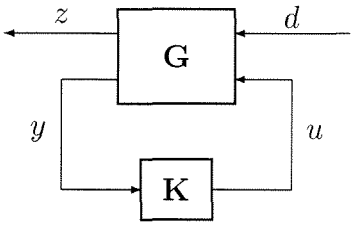

Figure 3.1: Synthesis formulation

3.1 Problem Formulation

Consider the feedback interconnection of finite dimensional LTI systems (simply referred to as *systems* in this and the next two chapters) $\mathbf{G}$ and $\mathbf{K}$ in Figure 3.1, and denote the closed loop system by $\mathbf{M} := \mathbf{G} \star \mathbf{K}$. If sets $\mathcal{D}$ and $\mathcal{E}$ are defined as

$$\mathcal{D} = \left\{ d \in l_2^m : \|d\|^2 \leq 1 \right\}, \quad \mathcal{E} = \left\{ e \in l_2^p : \|e\|^2 \leq 1 \right\}, \tag{3.5}$$

then it can readily be verified that $\|\mathbf{M}\| < 1$ if and only if

$$\sup_{e \in \mathcal{E}} \sup_{d \in \mathcal{D}} \langle e, \mathbf{M}d \rangle < 1. \tag{3.6}$$

Thus $\mathcal{H}_\infty$ optimization can be formulated as finding a controller $\mathbf{K}$ such that equation (3.6) is satisfied for a particular choice of $\mathcal{D}$ and $\mathcal{E}$.

In this chapter, optimization problems where sets $\mathcal{D}$ and $\mathcal{E}$ are not restricted to be balls in l_2 are considered. In particular, the following class of sets will be considered:

$$\mathcal{D} := \left\{ d \in l_2^m : f_k\left(\Lambda(d)\right) - M_k \leq 0, \;\; 0 \leq k \leq C_{\mathbf{d}} \right\}, \tag{3.7}$$

$$\mathcal{E} := \left\{ e \in l_2^p : g_l\left(\Lambda(e)\right) - P_l \leq 0, \;\; 0 \leq l \leq C_{\mathbf{e}} \right\}, \tag{3.8}$$

where the f_k and g_l are matrix valued linear functions, the M_k and P_l are matrices of compatible dimension, $\Lambda(\cdot)$ is the outer product operator defined in equation (2.7), and $C_{\mathbf{d}}$ and $C_{\mathbf{e}}$ dictate the number of constraints which $\Lambda(d)$ and $\Lambda(e)$ must satisfy. For example, setting $C_{\mathbf{d}} = C_{\mathbf{e}} = 0$, $M_0 = P_0 = 1$, and $f_0 = g_0 = \mathbf{trace}(\cdot)$ yields the sets of equation (3.5) and results in $\mathcal{H}_\infty$ optimization.

In order to formalize the construction of sets $\mathcal{D}$ and $\mathcal{E}$, some definitions need to be introduced. For matrices $A \in \mathbb{R}^{pm \times pm}$ and $B \in \mathbb{R}^{m \times m}$, the *trace product* $C \in \mathbb{R}^{p \times p}$ of A and B is defined as

$$C =: A \textcircled{T} B, \tag{3.9}$$

$$C_{[i,j]} := \mathbf{trace}\left(A^{i,j} B\right), \tag{3.10}$$

$$A =: \begin{bmatrix} A^{1,1} & \cdots & A^{1,p} \\ & \vdots & \\ A^{p,1} & \cdots & A^{p,p} \end{bmatrix}, \tag{3.11}$$

where $A^{i,j} \in \mathbb{R}^{m\times m}$, and $C_{[i,j]}$ is the i,j element of matrix C. Thus C is a square matrix, each of whose elements is a linear combination of the elements of B. The trace product allows us to conveniently define the matrix valued linear functions f_k and g_l in terms of constant matrices D_k and E_l, as shown below.

Define the following sets for all $\epsilon \geq 0$:

$$\mathfrak{D}^\epsilon := \left\{\Psi \in \mathbb{R}_{\mathbf{P}}^{m\times m} : D_k \textcircled{T} \Psi - M_k \leq \epsilon I,\ 0 \leq k \leq C_{\mathbf{d}}\right\}, \tag{3.12}$$

$$\mathfrak{E}^\epsilon := \left\{\Psi \in \mathbb{R}_{\mathbf{P}}^{p\times p} : E_l \textcircled{T} \Psi - P_l \leq \epsilon I,\ 0 \leq l \leq C_{\mathbf{e}}\right\}, \tag{3.13}$$

$$\mathcal{D}^\epsilon := \left\{d \in l_2^m : \Lambda(d) \in \mathfrak{D}^\epsilon\right\}, \tag{3.14}$$

$$\mathcal{E}^\epsilon := \left\{e \in l_2^p : \Lambda(e) \in \mathfrak{E}^\epsilon\right\}, \tag{3.15}$$

where $M_k \in \mathbb{R}_{\mathbf{S}}^{m_k\times m_k}$, $P_l \in \mathbb{R}_{\mathbf{S}}^{p_l\times p_l}$, $m_k, p_l \in \mathbb{Z}^+$, and $D_k \in \mathbb{R}^{m_k m\times m_k m}$, $E_l \in \mathbb{R}^{p_l p\times p_l p}$. Denote $\mathfrak{D} := \mathfrak{D}^0$, $\mathfrak{E} := \mathfrak{E}^0$, $\mathcal{D} := \mathcal{D}^0$, $\mathcal{E} := \mathcal{E}^0$. It will be assumed that $0 < M_0, P_0 \in \mathbb{R}$, with $D_0 = I \in \mathbb{R}^{m\times m}$ and $E_0 = I \in \mathbb{R}^{p\times p}$ (which in fact implement the **trace** function). This imposes constraints $\|d\|^2 \leq M_0$, $\|e\|^2 \leq P_0$, and ensures that sets $\mathcal{D}$ and $\mathcal{E}$ are bounded. It will also be assumed that $\mathfrak{D}$ and $\mathfrak{E}$ are not empty sets; using similar arguments to those of Lemma 3.3, it can be shown that this implies that $\mathcal{D}$ and $\mathcal{E}$ are not empty as well. In Section 3.2, various properties of sets $\mathfrak{D}$, $\mathfrak{E}$, $\mathcal{D}$, and $\mathcal{E}$ will be explored.

Remarks: Since only the symmetric portions of $D_k \textcircled{T} \Psi$ and $E_k \textcircled{T} \Psi$ are required in constraints (3.12) and (3.13), it can be assumed that $D_k^{i,j} = D_k^{j,i}$, $E_l^{i,j} = E_l^{j,i}$. Furthermore, since $\Lambda(d)$ and $\Lambda(e)$ are symmetric, $D_k^{i,j}$ and $E_l^{i,j}$ can be assumed to be symmetric as well.

The problem formulation may now be stated:

Generalized l_2 Synthesis:

Given system $\mathbf{G}$ *and sets* $\mathcal{D}$ *and* $\mathcal{E}$*, find a stabilizing controller* $\mathbf{K}$ *such that*

$$\sup_{e\in\mathcal{E}} \sup_{d\in\mathcal{D}} \langle e, \mathbf{M}d\rangle < 1. \tag{3.16}$$

The term *Generalized l_2 Synthesis* stems from the fact that sets $\mathcal{D}$ and $\mathcal{E}$ which define the allowable disturbances and the cost criterion are not restricted to be balls in l_2. Sets $\mathfrak{D}$ and $\mathfrak{E}$ are, in general, convex sets which can be used to constrain $\Lambda(d)$ and $\Lambda(e)$, respectively. In particular, each constraint in equations (3.12) and (3.13) is an AMI in the elements of $\Lambda(d)$ and $\Lambda(e)$ of variable dimension. As an illustrative example, consider the following sets in l_2^2

$$\mathcal{D}_1 := \left\{d \in l_2^2 : \Lambda(d) \leq I\right\}, \tag{3.17}$$

$$\mathcal{D}_2 := \left\{d \in l_2^2 : \|d_1\|^2 \leq 1,\ \|d_2\|^2 \leq 1\right\}, \tag{3.18}$$

which can readily be captured in the format of equations (3.14) and (3.12). $\mathcal{D}_1 \subset \mathcal{D}_2$ since $\mathcal{D}_1$ possesses an additional constraint on $\langle d_1, d_2\rangle$. This is depicted in Figure 3.2.

Thus for $\mathcal{D}_1$, signals which have unit energy content must be orthogonal to each other; adding constraint $\langle d_1, d_2 \rangle = 0$ to $\mathcal{D}_2$ imposes an orthogonality constraint irrespective of the signal energy.

Matrix valued constraints, such as the one used to describe $\mathcal{D}_1$, appear naturally when dealing with certain types of uncertainty, and are encountered in Chapter 4.

Remarks:

- In general, any compact, convex set may be approximated to any desired accuracy with the constraints of equation (3.12). This can, in fact, be achieved with only scalar valued constraints; the matrix valued constraints offer flexibility, and extend the class of convex sets which may be described without error ($\Psi \leq I$, for example).
- Note that 0 does not have to be an element of $\mathfrak{D}$ or of $\mathfrak{E}$, and consequently of $\mathcal{D}$ or $\mathcal{E}$; equivalently, matrices M_k and P_l are not restricted to be positive semi-definite. This allows us to consider very general convex sets, at the expense of complicating some of the proofs which follow.
- The constraints used to define $\mathcal{D}$ and $\mathcal{E}$ are very closely related to Integral Quadratic Constraints (IQCs) [Yakubovich, 1971], [Megretski and Treil, 1993] :

$$\langle d, \mathbf{\Pi} d \rangle \geq 0, \tag{3.19}$$

where $\mathbf{\Pi}$ is an LTI, self adjoint operator in $\mathcal{L}(l_2)$. If $\mathbf{\Pi}$ is a constant matrix, then the constraint of equation (3.19) can readily be captured by the constraints in $\mathfrak{D}$ ($\langle d, \mathbf{\Pi} d \rangle$ is a linear combination of the elements of $\Lambda(d)$); generalizations which will allow $\mathbf{\Pi}$ to be an LTI system are discussed in Section 3.5. On the other hand, IQCs cannot, in general, capture the constraints in $\mathfrak{D}$ since the latter can be matrix valued and affine in $\Lambda(d)$.

3.2 Properties of Sets $\mathfrak{D}$, $\mathfrak{E}$, $\mathcal{D}$, and $\mathcal{E}$

As previously mentioned, sets $\mathfrak{D}$ and $\mathfrak{E}$ are bounded, convex sets which live in a finite dimensional real vector space. In this section, other properties of sets $\mathfrak{D}$, $\mathfrak{E}$, $\mathcal{D}$, and $\mathcal{E}$ are explored. This is done for technical reasons (some of the proofs which follow rely on the results in this section), and to provide insight into the Generalized l_2 Synthesis optimization problem.

3.2.1 Continuity of Sets $\mathcal{D}^\epsilon$ and $\mathcal{E}^\epsilon$

The following theorem states that sets $\mathcal{D}^\epsilon$ and $\mathcal{E}^\epsilon$ are in some sense continuous as a function of ϵ:

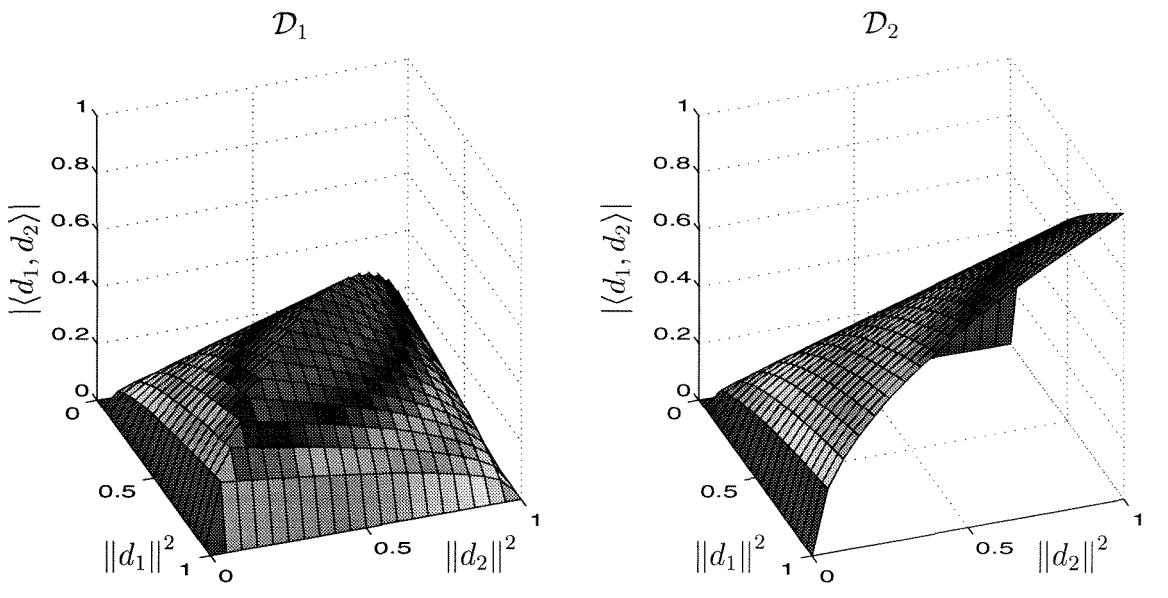

Figure 3.2: $\mathcal{D}_1$ and $\mathcal{D}_2$. Only the surface of each set is shown; all points below the surface are allowable.

Theorem 3.1

$$\mathrm{d}\left(\mathcal{D}^\epsilon, \mathcal{D}\right) \overset{\epsilon \to 0^+}{\longrightarrow} 0, \quad \mathrm{d}\left(\mathcal{E}^\epsilon, \mathcal{E}\right) \overset{\epsilon \to 0^+}{\longrightarrow} 0, \tag{3.20}$$

where the maximum distance function $\mathrm{d}(\cdot,\cdot)$ *is defined in equation (2.8).*

Before proving the above theorem, two preliminary lemmas need to be introduced. The following lemma states that $\mathfrak{D}^\epsilon$ (similarly $\mathfrak{E}^\epsilon$) is continuous in ϵ:

Lemma 3.2

$$\sup_{\Psi_\epsilon \in \mathfrak{D}^\epsilon} \inf_{\Psi \in \mathfrak{D}} \overline{\sigma}\left(\Psi - \Psi_\epsilon\right) \overset{\epsilon \to 0^+}{\longrightarrow} 0. \tag{3.21}$$

Proof of Lemma 3.2: Assume that equation (3.21) is not satisfied. There exists, therefore, a number $\delta > 0$ and a sequence $\left\{\Psi^k\right\}$ with $\Psi^k \in \mathfrak{D}^{\frac{1}{k}}$ such that

$$\inf_{\Psi \in \mathfrak{D}} \overline{\sigma}\left(\Psi - \Psi^k\right) > \delta \ \ \forall k. \tag{3.22}$$

Since $\mathfrak{D}^1$ is compact, there exists a subsequence of $\left\{\Psi^k\right\}$ converging in $\mathfrak{D}^1$. Denote this limit by Ψ_0. Since the trace product is a linear function of its argument (and is thus bounded), $\Psi_0 \in \mathfrak{D}$. Substituting Ψ_0 in equation (3.22) leads to a contradiction. ■

The following lemma states that if $\tilde{\Psi} \in \mathbb{R}_{\mathbf{P}}^{m \times m}$ is sufficiently close to $\Lambda(d) \in \mathbb{R}_{\mathbf{P}}^{m \times m}$, one can find $\tilde{d} \in l_2^m$ close to d such that $\Lambda(\tilde{d}) = \tilde{\Psi}$:

Lemma 3.3 *Let $C_1 \geq 0$ be given. There exists $C_0 \geq 0$ such that $\forall d \in l_2$ of compact support and $0 \leq \tilde{\Psi} \in \mathbb{R}_{\mathbf{P}}^{m\times m} \leq C_1 I$ satisfying $\overline{\sigma}\left(\tilde{\Psi} - \Lambda(d)\right) \leq \delta^2 \leq 1/2$, there exists $\tilde{d} \in l_2$ such that $\Lambda(\tilde{d}) = \tilde{\Psi}$ and $\|d - \tilde{d}\|^2 \leq C_0\delta$.*

Proof of Lemma 3.3: Fix d and $\tilde{\Psi}$. Let $\Sigma = \begin{bmatrix} \Sigma_1 & 0 \\ 0 & \Sigma_2 \end{bmatrix} := T^*\tilde{\Psi}T$, where T is unitary, $\overline{\sigma}(\Sigma_2) \leq \delta$, $\underline{\sigma}(\Sigma_1) > \delta$. Define

$$V := T^*\Lambda(d)T \quad , \quad E := \Sigma - V = T^*\left(\tilde{\Psi} - \Lambda(d)\right)T, \tag{3.23}$$
$$\bar{V} := \begin{bmatrix} (1-\delta)V_{11} & 0 \\ 0 & 0 \end{bmatrix} \quad , \quad \bar{E} := \Sigma - \bar{V} = \begin{bmatrix} (1-\delta)E_{11} + \delta\Sigma_1 & 0 \\ 0 & \Sigma_2 \end{bmatrix},$$

where the partitions of V, E and $\bar{E}$ are consistent with Σ. Since T is unitary, $\overline{\sigma}(E_{11}) \leq \delta^2$, and thus $0 \leq \bar{E} \leq \delta(C_1 + 1)$. Define $\bar{d} := T\begin{bmatrix} \sqrt{1-\delta}I & 0 \\ 0 & 0 \end{bmatrix}T^*d$. It follows that $\Lambda(\bar{d}) = T\bar{V}T^*$, and

$$\begin{aligned} \mathbf{trace}\left(\Lambda(d - \bar{d})\right) &= \left(1 - \sqrt{1-\delta}\right)^2 \mathbf{trace}\left(\Sigma_1 - E_{11}\right) + \mathbf{trace}\left(\Sigma_2 - E_{22}\right) \\ &\leq \left(1 - \sqrt{1-\delta}\right)^2 \left(m\left(\overline{\sigma}(\Sigma_1) + \delta^2\right)\right) + m\left(\overline{\sigma}(\Sigma_2) + \delta^2\right) \quad (3.24) \\ &\leq \delta m\left(C_1 + 3\right). \end{aligned}$$

Since $\bar{E} \geq 0$, there exists $Q \in \mathbb{R}_{\mathbf{P}}^{m\times m}$ such that $Q^2 = T\bar{E}T^*$. Define $\hat{d} \in l_2^m$ as follows:

$$\begin{aligned} \begin{bmatrix} \hat{d}(1) & \cdots & \hat{d}(m) \end{bmatrix} &:= \begin{bmatrix} Q_1 & \cdots & Q_m \end{bmatrix}, \quad (3.25) \\ \hat{d}(t) &:= 0 \text{ otherwise.} \end{aligned}$$

It thus follows that $\Lambda(\hat{d}) = T\bar{E}T^*$. Finally, define $\tilde{d} := \bar{d} + \boldsymbol{\lambda}^\tau \hat{d}$, where τ is any integer larger than the support of d. This yields $\Lambda(\tilde{d}) = \tilde{\Psi}$. Furthermore,

$$\begin{aligned} \|d - \tilde{d}\|^2 &= \|d - \bar{d}\|^2 + \|\hat{d}\|^2 \quad (3.26) \\ &\leq \delta m\left(C_1 + 3\right) + \delta m\left(C_1 + 1\right). \end{aligned}$$

Defining $C_0 := m\left(2C_1 + 4\right)$ completes the proof. ∎

We are now in a position to prove Theorem 3.1:

Proof of Theorem 3.1: Since $\mathfrak{D}$ is bounded, there exists $C_1 \geq 0$ such that $\tilde{\Psi} \leq C_1 I \ \forall \ \tilde{\Psi} \in \mathfrak{D}$. Fix $0 < \delta < 1/2$. By Lemma 3.2, there exists $\epsilon > 0$ such that $\forall d_\epsilon \in \mathcal{D}^\epsilon$, there exists $\tilde{\Psi} \in \mathfrak{D}$ such that $\overline{\sigma}\left(\tilde{\Psi} - \Lambda(d_\epsilon)\right) \leq \delta^2/2$. Furthermore, there exists $T \in \mathbb{Z}^+$ sufficiently large such that $\|d_\epsilon - \boldsymbol{P_T} d_\epsilon\|^2 \leq \delta$ and $\overline{\sigma}\left(\tilde{\Psi} - \Lambda(\boldsymbol{P_T} d_\epsilon)\right) \leq \delta^2$.

By Lemma 3.3, there exists $\tilde{d}$ such that $\Lambda(\tilde{d}) = \tilde{\Psi}$, implying that $\tilde{d} \in \mathcal{D}$, and furthermore

$$\|d_\epsilon - \tilde{d}\|^2 \leq \Big(\|d_\epsilon - \boldsymbol{P_T} d_\epsilon\| + \|\boldsymbol{P_T} d_\epsilon - \tilde{d}\|\Big)^2 \leq 2C_0\delta. \tag{3.27}$$

Since δ is arbitrary, this implies that $\mathrm{d}(\mathcal{D}^\epsilon, \mathcal{D}) \stackrel{\epsilon\to 0}{\longrightarrow} 0$, as required. Similarly, $\mathrm{d}(\mathcal{E}^\epsilon, \mathcal{E}) \stackrel{\epsilon\to 0}{\longrightarrow} 0$. ■

The following corollary follows immediately:

Corollary 3.4 *Given bounded* $\mathbf{M}$, *there exists* $\epsilon > 0$ *such that*

$$\sup_{e\in\mathcal{E}} \sup_{d\in\mathcal{D}} \langle e, \mathbf{M}d\rangle < 1 \;\Rightarrow \sup_{e\in\mathcal{E}^\epsilon} \sup_{d\in\mathcal{D}^\epsilon} \langle e, \mathbf{M}d\rangle < 1. \tag{3.28}$$

Thus for small enough ϵ, sets $\mathcal{D}$ and $\mathcal{E}$ are interchangeable with $\mathcal{D}^\epsilon$ and $\mathcal{E}^\epsilon$. This fact is crucial in proving the main result of Section 3.3.

3.2.2 Convexity Properties

The allowable disturbances are directly specified by $\mathcal{D}$. The cost criterion, however, is only indirectly specified by $\mathcal{E}$. Define the following sets:

$$\mathcal{Z} := \left\{ z \in l_2^p : \sup_{e\in\mathcal{E}} \langle e, z\rangle < 1 \right\}, \tag{3.29}$$

$$\mathfrak{Z} := \left\{ \Psi \in \mathbb{R}_{\mathrm{P}}^{p\times p} : \Psi = \Lambda(z),\ z \in \mathcal{Z} \right\}. \tag{3.30}$$

It is clear that sets $\mathfrak{D}$ and $\mathfrak{E}$ are convex. Set $\mathfrak{Z}$ is not convex, but its complement is:

Theorem 3.5 $-\mathfrak{Z}$, *the complement of* $\mathfrak{Z}$ *in* $\mathbb{R}_{\mathrm{P}}^{p\times p}$, *is closed and convex.*

Proof: By using techniques similar to those in the proof of Theorem 3.1, it can be shown that $\mathfrak{Z}$ is open, thus $-\mathfrak{Z}$ is closed. To prove convexity, let $0 \leq \alpha \leq 1$ be given, and let $\Psi_1, \Psi_2 \in -\mathfrak{Z}$. Define $\Psi_0 := \alpha\Psi_1 + (1-\alpha)\Psi_2$. Let $\{z_1^k\}, \{z_2^k\} \in -\mathcal{Z}$ be sequences such that $\Lambda(z_i^k) \stackrel{k\to\infty}{\longrightarrow} \Psi_i$. Note that for all $e_1, e_2 \in l_2$, and fixed k,

$$\begin{aligned} \langle\sqrt{\alpha}e_1 + \sqrt{1-\alpha}\boldsymbol{\lambda}^\tau e_2, \sqrt{\alpha}z_1^k + \sqrt{1-\alpha}\boldsymbol{\lambda}^\tau z_2^k\rangle &\stackrel{\tau\to\infty}{\longrightarrow} \alpha\langle e_1, z_1^k\rangle + (1-\alpha)\langle e_2, z_2^k\rangle, \\ \Lambda\left(\sqrt{\alpha}e_1 + \sqrt{1-\alpha}\boldsymbol{\lambda}^\tau e_2\right) &\stackrel{\tau\to\infty}{\longrightarrow} \alpha\Lambda(e_1) + (1-\alpha)\Lambda(e_2). \end{aligned} \tag{3.31}$$

Thus by the continuity property of $\mathcal{E}$ established in Theorem 3.1 and the convexity of $\mathfrak{E}$, for fixed k,

$$\sup_{e\in\mathcal{E}} \langle e, \sqrt{\alpha}z_1^k + \sqrt{1-\alpha}\boldsymbol{\lambda}^\tau z_2^k\rangle - \left(\alpha \sup_{e\in\mathcal{E}} \langle e, z_1^k\rangle + (1-\alpha) \sup_{e\in\mathcal{E}} \langle e, z_2^k\rangle\right) \stackrel{\tau\to\infty}{\longrightarrow} [0, \infty). \tag{3.32}$$

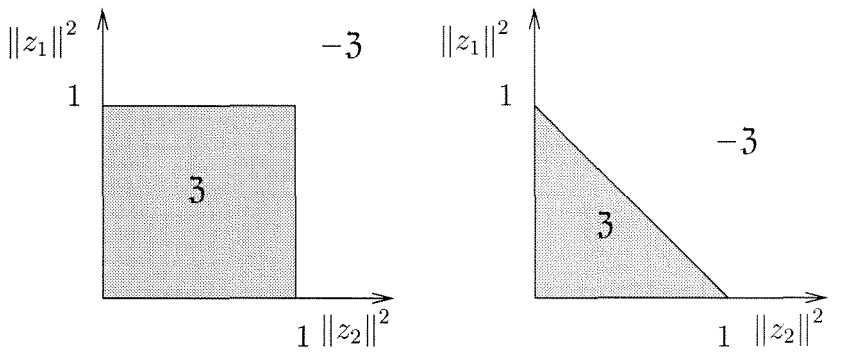

Figure 3.3: Cost criterion $\|z_1\|^2 < 1$, $\|z_2\|^2 < 1$ is incompatible, cost criterion $\|z\|^2 < 1$ is not incompatible.

Thus there exists τ_k sufficiently large such that

$$z_k := (1+1/k)(\sqrt{\alpha}z_1^k + \sqrt{1-\alpha}\boldsymbol{\lambda}^{\tau_k}z_2^k) \in -\mathcal{Z}, \tag{3.33}$$

$$\overline{\sigma}\left(\Lambda(z_k) - \Psi_0\right) \leq \frac{1}{k}\overline{\sigma}\left(\Psi_0\right) + 2\overline{\sigma}\left(\Psi_1 - \Lambda(z_1^k)\right) + 2\overline{\sigma}\left(\Psi_2 - \Lambda(z_2^k)\right), \tag{3.34}$$

which implies that $\Psi_0 \in -\mathfrak{Z}$, as required. ■

The above result establishes a necessary condition for a given cost criterion to be compatible with the Generalized l_2 Synthesis formulation. For example, cost criterion $\left\{z \in l_2^2 : \|z_1\|^2 < 1, \|z_2\|^2 < 1\right\}$ is incompatible, since the set

$$\{\Lambda(z) : \|z_1\|^2 \geq 1\} \cup \{\Lambda(z) : \|z_2\|^2 \geq 1\}$$

is not convex, as shown in Figure 3.3. Cost criterion $\left\{z \in l_2^2 : \|z\|^2 < 1\right\}$ is not incompatible since $\left\{\Lambda(z) : \|z\|^2 \geq 1\right\}$ is a convex set (and can in fact be implemented by setting $\mathcal{E} = \{e \in l_2 : \|e\|^2 \leq 1\}$).

With this insight, a natural way to describe the optimization of equation (3.16) is in terms of a game, with the adversary's task of finding d, with $\Lambda(d)$ in convex set $\mathfrak{D}$, such that $\Lambda(z) = \Lambda(\mathbf{M}d)$ is in convex set $-\mathfrak{Z}$ (modulo supremum arguments).

Remarks: Note that the result of Theorem 3.5 only establishes a necessary condition for a given cost criterion to be compatible with the Generalized l_2 Synthesis formulation. For example, cost criterion $\left\{z \in l_2^2 : \|z_1\|^2 < 1 \text{ or } \|z_2\|^2 < 1\right\}$ satisfies the condition in Theorem 3.5, but cannot be implemented with set $\mathcal{E}$.

3.3 Analysis Condition

The first step in providing a solution to the Generalized l_2 Synthesis problem is to obtain an analysis condition for the closed loop system, $\mathbf{M} = \mathbf{G} \star \mathbf{K}$. The main idea

is the so called *S-procedure* [Yakubovich, 1971], the process of transforming a problem to one involving multipliers; similar to the results in [Megretski and Treil, 1993, Paganini, 1995b], it can be shown that the S-procedure applied to our problem formulation is lossless, or non-conservative. In order to state the analysis condition, the following notation needs to be introduced. Let $A \in \mathbb{R}^{pm \times pm}$ be given, with p and m fixed. The *trace transpose* $\grave{A} \in \mathbb{R}^{mp \times mp}$ of A is defined as

$$\grave{A} := \begin{bmatrix} \grave{A}^{1,1} & \cdots & \grave{A}^{1,m} \\ & \vdots & \\ \grave{A}^{m,1} & \cdots & \grave{A}^{m,m} \end{bmatrix}, \tag{3.35}$$

$$\grave{A}^{k,l}_{[i,j]} := A^{i,j}_{[k,l]}. \tag{3.36}$$

Theorem 3.6 *Given linear, time invariant, bounded operator* $\mathbf{M}$ *and sets* $\mathcal{D}$ *and* $\mathcal{E}$*, the following are equivalent:*

I. *The following supremum is satisfied:*

$$\sup_{e \in \mathcal{E}} \sup_{d \in \mathcal{D}} \langle e, \mathbf{M}d \rangle < 1. \tag{3.37}$$

II. *There exist* $0 < X_k \in \mathbb{R}_{\mathbf{P}}^{m_k \times m_k}, 0 \leq k \leq C_{\mathbf{d}}$ *and* $0 < Y_l \in \mathbb{R}_{\mathbf{P}}^{p_l \times p_l}, 0 \leq l \leq C_{\mathbf{e}}$ *such that*

$$\left\| Y^{-\frac{1}{2}} \mathbf{M} X^{-\frac{1}{2}} \right\| < 1, \tag{3.38}$$

$$X := \sum_{k=0}^{C_{\mathbf{d}}} \grave{D}_k \textcircled{T} X_k > 0, \tag{3.39}$$

$$Y := \sum_{l=0}^{C_{\mathbf{e}}} \grave{E}_l \textcircled{T} Y_l > 0, \tag{3.40}$$

$$T_x := \sum_{k=0}^{C_{\mathbf{d}}} \mathbf{trace}\,(M_k X_k) < 1, \tag{3.41}$$

$$T_y := \sum_{l=0}^{C_{\mathbf{e}}} \mathbf{trace}\,(P_l Y_l) < 1. \tag{3.42}$$

The diagram in Figure 3.4 can provide insight into the above condition. Convex set $\mathfrak{D}$ captures the allowable disturbances, while set $\mathfrak{Z}$ (whose complement is convex) captures the cost criterion. Theorem 3.6 states that all disturbances inside $\mathfrak{D}$ result in outputs which are inside $\mathfrak{Z}$ (statement **I**) if and only if one can find convex region $\mathfrak{D}_0$, defined by a hyperplane and containing $\mathfrak{D}$, and convex region $\mathfrak{Z}_0$, also defined by a hyperplane and contained in $\mathfrak{Z}$, such that all disturbances inside $\mathfrak{D}_0$ result in outputs which are inside $\mathfrak{Z}_0$ (statement **II**). It is clear that the latter part of the above statement implies the former, making the proof that **II** implies **I** straightforward. S-Losslessness type arguments are used to prove that **I** implies **II**.

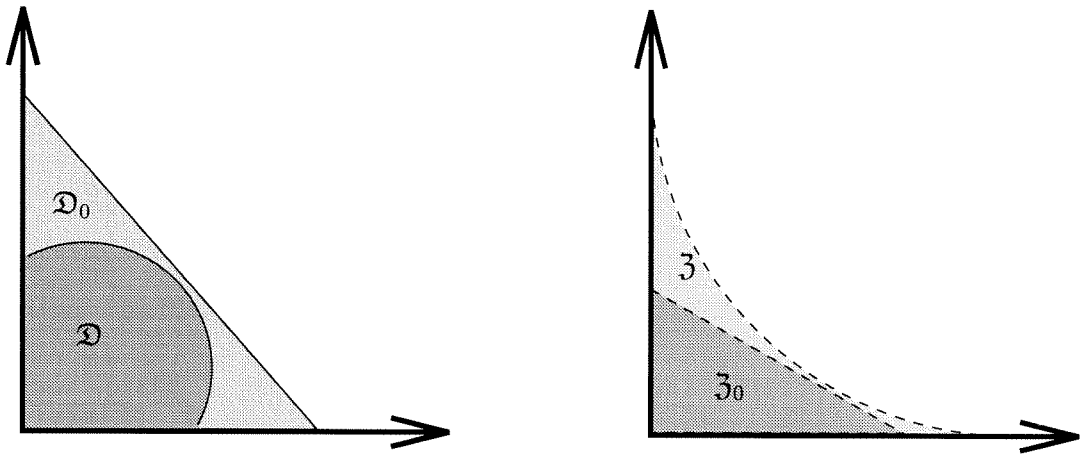

Figure 3.4: Insight into Theorem 3.6. Convex set $\mathfrak{D}$ captures the allowable disturbances, while set $\mathfrak{Z}$ (whose complement is convex) captures the cost criterion. Theorem 3.6 states that all disturbances inside $\mathfrak{D}$ result in outputs which are inside $\mathfrak{Z}$ if and only if one can find convex region $\mathfrak{D}_0$, defined by a hyperplane and containing $\mathfrak{D}$, and convex region $\mathfrak{Z}_0$, also defined by a hyperplane and contained in $\mathfrak{Z}$, such that all disturbances inside $\mathfrak{D}_0$ result in outputs which are inside $\mathfrak{Z}_0$.

Before proving the above theorem, the following preliminary results need to be established.

Proposition 3.7 *Let $A \in \mathbb{R}^{pm \times pm}$, $B \in \mathbb{R}^{m \times m}$, and $X \in \mathbb{R}^{p \times p}$ be given. Then*

$$\textbf{trace}\,((A \textcircled{T} B)X) = \textbf{trace}\left((\grave{A} \textcircled{T} X)B\right). \tag{3.43}$$

Proof of Proposition 3.7:

$$\textbf{trace}\,((A \textcircled{T} B)X) = \sum_{i,j=1}^{p} (A \textcircled{T} B)_{[i,j]} X_{[j,i]} = \sum_{i,j=1}^{p} X_{[j,i]} \sum_{k,l=1}^{m} A^{i,j}_{[k,l]} B_{[l,k]}, \tag{3.44}$$

$$\textbf{trace}\left((\grave{A} \textcircled{T} X)B\right) = \sum_{k,l=1}^{m} (\grave{A} \textcircled{T} X)_{[k,l]} B_{[l,k]} = \sum_{k,l=1}^{m} B_{[l,k]} \sum_{i,j=1}^{p} \grave{A}^{k,l}_{[i,j]} X_{[j,i]}. \tag{3.45}$$

■

The following lemma is a standard result in convex analysis (see [Rockafellar, 1970] for example):

Lemma 3.8 *Let $\mathcal{K}_1$, $\mathcal{K}_2$ be disjoint, convex sets in $\mathbb{R}^d$, where $\mathcal{K}_1$ is compact and $\mathcal{K}_2$ is closed. Then there exists vector $x \in \mathbb{R}^d$ and $\alpha, \beta \in \mathbb{R}$ such that*

$$\langle x, k_1 \rangle \leq \alpha < \beta \leq \langle x, k_2 \rangle \;\; \forall k_1 \in \mathcal{K}_1, k_2 \in \mathcal{K}_2. \tag{3.46}$$

Proof of Theorem 3.6:
II $\Rightarrow$ **I** : By Proposition 3.7 and equation (3.14), for all $d \in \mathcal{D}$,

$$\langle d, Xd\rangle = \langle d, \left(\sum_{k=0}^{C_{\mathbf{d}}} \dot{D}_k \textcircled{T} X_k\right) d\rangle = \mathbf{trace}\left(\sum_{k=0}^{C_{\mathbf{d}}} \left(\dot{D}_k \textcircled{T} X_k\right) \Lambda(d)\right) \tag{3.47}$$

$$= \sum_{k=0}^{C_{\mathbf{d}}} \mathbf{trace}\left(\left(D_k \textcircled{T} \Lambda(d)\right) X_k\right) \tag{3.48}$$

$$\leq \sum_{k=0}^{C_{\mathbf{d}}} \mathbf{trace}\left(M_k X_k\right) < 1. \tag{3.49}$$

Similarly, $\langle e, Ye\rangle < 1$ for all $e \in \mathcal{E}$. It thus follows that

$$1 > \left\| Y^{-\frac{1}{2}} \mathbf{M} X^{-\frac{1}{2}} \right\| \tag{3.50}$$

$$= \sup_{\|\overline{e}\|^2 \leq 1} \sup_{\|\overline{d}\|^2 \leq 1} \langle Y^{-\frac{1}{2}}\overline{e}, \mathbf{M} X^{-\frac{1}{2}}\overline{d}\rangle = \sup_{\langle e, Ye\rangle \leq 1} \sup_{\langle d, Xd\rangle \leq 1} \langle e, \mathbf{M}d\rangle$$

$$\geq \sup_{e \in \mathcal{E}} \sup_{d \in \mathcal{D}} \langle e, \mathbf{M}d\rangle. \tag{3.51}$$

I $\Rightarrow$ **II** : The proof of this claim is long and technical. The proof essentially consists of three parts. The first is to use use the separating plane argument of Lemma 3.8 to construct scaling matrices. In the second part, various arguments are employed to construct a scale, Y, which satisfies the constraints of equations (3.40) and (3.42). In the third part, the problem data is manipulated so that the first two parts can be utilized to construct a scale, X, which satisfies the constraints of equations (3.39) and (3.41), and yields the condition of equation (3.38). It will be assumed throughout the proof that $\mathbf{M} \neq \mathbf{0}$; if $\mathbf{M} = \mathbf{0}$, the proof is trivial.

Step 1: Separating Plane Argument

By the boundedness of $\mathcal{E}$ and Corollary 3.4, there exists $0 < \beta < \min(P_0^{-1}, 1/4)$ and $\epsilon > 0$ such that

$$\sup_{e \in \mathcal{E}^\epsilon} \sup_{d \in \mathcal{D}^\epsilon} \langle e, \mathbf{M}d\rangle + \beta + \beta^2 \|e\|^2 < 1. \tag{3.52}$$

Define the following matrix valued functions on l_2:

$$\sigma(d, e) := \langle e, \mathbf{M}d\rangle + \beta + \beta^2\|e\|^2 - 1, \tag{3.53}$$

$$\Sigma_k^{\mathcal{D}}(d, e) := M_k\langle e, \mathbf{M}d\rangle - D_k \textcircled{T} \Lambda(d), \quad 0 \leq k \leq C_{\mathbf{d}}, \tag{3.54}$$

$$\Sigma_l^{\mathcal{E}}(e) := P_l - E_l \textcircled{T} \Lambda(e), \quad 0 \leq l \leq C_{\mathbf{e}}, \tag{3.55}$$

the following constants,

$$B_{\mathbf{e}} := \max\left(\frac{1}{\beta^2}, \frac{P_0}{\beta^2}\right), \quad B_{\mathbf{d}} := 2M_0 \sup_{\|d\|^2 \leq M_0} \sup_{\|e\|^2 \leq B_{\mathbf{e}}} |\langle e, \mathbf{M}d\rangle|^2, \tag{3.56}$$

and corresponding bounded set:

$$\nabla := \left\{ \Upsilon(d,e) = \left(\sigma(d,e), \Sigma_k^{\mathcal{D}}(d,e), \Sigma_l^{\mathcal{E}}(e) \right) : \|e\|^2 \leq B_{\mathbf{e}}, \ \ \|d\|^2 \leq B_{\mathbf{d}} \right\}. \tag{3.57}$$

Define the following closed, convex set:

$$\mathbf{Z} := \left\{ Z = \left(z, Z_k^{\mathcal{D}}, Z_l^{\mathcal{E}} \right) : z \in \mathbb{R}^+, Z_k^{\mathcal{D}} \in \mathbb{R}_{\mathbf{P}}^{m_k \times m_k}, Z_l^{\mathcal{E}} \in \mathbb{R}_{\mathbf{P}}^{p_l \times p_l} \right\}. \tag{3.58}$$

Thus ∇ and $\mathbf{Z}$ live in the same finite dimensional real vector space. Equip this space with the following inner product:

$$\langle Z, \hat{Z} \rangle := z\hat{z} + \sum_{k=0}^{C_{\mathbf{d}}} \mathbf{trace} \left(Z_k^{\mathcal{D}} \hat{Z}_k^{\mathcal{D}} \right) + \sum_{l=0}^{C_{\mathbf{e}}} \mathbf{trace} \left(Z_l^{\mathcal{E}} \hat{Z}_l^{\mathcal{E}} \right). \tag{3.59}$$

Lemma 3.9 *$\nabla \bigcap \mathbf{Z}$ is the empty set.*

Proof of Lemma 3.9: Assume that there exists d, e such that equations (3.53), (3.54), (3.55) are all positive semi-definite. The constraints of equation (3.55) imply that $e \in \mathcal{E}$, and in particular, that $\|e\|^2 \leq P_0$. Furthermore, by the upper bound on β, $\gamma := \langle e, \mathbf{M}d \rangle > 1/2$. Define $\bar{d} := \gamma^{-\frac{1}{2}} d$; constraint $k = 0$ in equation (3.54) implies that $\|\bar{d}\|^2 \leq M_0$, ensuring that $\Upsilon(\bar{d}, e) \in \nabla$. By similar substitution, $\gamma M_k - \gamma D_k \textcircled{T} \Lambda(\bar{d}) \geq 0$, implying that $\bar{d} \in \mathcal{D}$, and $\langle e, \mathbf{M}\bar{d} \rangle = \sqrt{\gamma}$. If $\gamma \geq 1$, equation (3.52) is not satisfied. If $\gamma < 1$, $\sqrt{\gamma} > \gamma$, and equation (3.52) is not satisfied as well. ■

Proposition 3.10 *Let $\overline{\nabla}$ denote the closure of ∇. $\overline{\nabla} \cap \mathbf{Z}$ is the empty set.*

Proof of Proposition 3.10: Assume that $\overline{\nabla} \cap \mathbf{Z}$ is not the empty set. Thus for all $\epsilon > 0$, from the proof of Lemma 3.9,

$$\sup_{e \in \mathcal{E}^\epsilon} \sup_{d \in \mathcal{D}^\epsilon} \langle e, \mathbf{M}d \rangle + \beta + \beta^2 \|e\|^2 + \epsilon \geq 1 \tag{3.60}$$

which contradicts equation (3.52). ■

Lemma 3.11 *$\overline{\nabla}$ is convex and compact.*

Proof of Lemma 3.11: The proof uses arguments similar to those found in [Paganini, 1995b]. Let $\Upsilon_0 \in \mathrm{co}\,(\nabla)$, the convex hull of ∇. Thus

$$\Upsilon_0 = \sum_{k=0}^{N-1} \alpha_k \Upsilon\left(d_k, e_k\right), \alpha_k \geq 0, \sum_{k=0}^{N-1} \alpha_k = 1. \tag{3.61}$$

Define

$$f^\tau := \sum_{k=0}^{N-1} \sqrt{\alpha_k} \boldsymbol{\lambda}^{k\tau} d_k, \quad g^\tau := \sum_{k=0}^{N-1} \sqrt{\alpha_k} \boldsymbol{\lambda}^{k\tau} e_k, \tag{3.62}$$

$$S_d := \sum_{k=0}^{N-1} \alpha_k \|d_k\|^2 \leq B_{\mathbf{d}}, \quad S_e := \sum_{k=0}^{N-1} \alpha_k \|e_k\|^2 \leq B_{\mathbf{e}}, \tag{3.63}$$

$$d^\tau := \begin{cases} \frac{S_d}{\|f^\tau\|} f^\tau & \text{for } S_d > 0, \|f^\tau\| > 0 \\ 0 & \text{for } S_d \|f^\tau\| = 0 \end{cases}, \tag{3.64}$$

$$e^\tau := \begin{cases} \frac{S_e}{\|g^\tau\|} g^\tau & \text{for } S_e > 0, \|g^\tau\| > 0 \\ 0 & \text{for } S_e \|g^\tau\| = 0 \end{cases}. \tag{3.65}$$

Thus $\Upsilon(d^\tau, e^\tau) \in \nabla \ \forall \tau$. Since $\mathbf{M}$ is LTI and $\Upsilon(\cdot)$ is quadratic in d and e, it follows that

$$\Upsilon(d^\tau, e^\tau) \stackrel{\tau \to \infty}{\longrightarrow} \sum_{k=0}^{N} \Upsilon(\sqrt{\alpha_k} d_k, \sqrt{\alpha_k} e_k) = \Upsilon_0. \tag{3.66}$$

The above argument demonstrates that $\Upsilon_0 \in \overline{\nabla}$. Thus $\mathrm{co}(\nabla) \subset \overline{\nabla}$, and $\mathrm{co}\left(\overline{\nabla}\right) \subset \overline{\mathrm{co}(\nabla)} \subset \overline{\nabla}$, so $\overline{\nabla}$ is convex. ∎

We are now in a position to invoke Lemma 3.8:

Proposition 3.12 *There exists $\hat{Z} \in \mathbf{Z}$, with $\hat{z} > 0$, $\hat{Z}_k^{\mathcal{D}} > 0$, $\hat{Z}_l^{\mathcal{E}} > 0$ such that for all $\Upsilon \in \overline{\nabla}$, $Z \in \mathbf{Z}$,*

$$\langle \hat{Z}, \Upsilon \rangle < 0 \leq \langle \hat{Z}, Z \rangle. \tag{3.67}$$

Proof of Proposition 3.12: By Lemma 3.8, and by embedding $\overline{\nabla}$ and $\mathbf{Z}$ in $\mathbb{R}^d$, it follows that there exists α, β, and $\bar{Z}$ (not necessarily in $\mathbf{Z}$), such that for all $\Upsilon \in \overline{\nabla}$, $Z \in \mathbf{Z}$,

$$\langle \bar{Z}, \Upsilon \rangle \leq \alpha < \beta \leq \langle \bar{Z}, Z \rangle. \tag{3.68}$$

Setting $Z = 0$ yields $\beta \leq 0$. Since $\mathbf{Z}$ is unbounded and $\overline{\nabla}$ is compact, however, $\beta = 0$, and each (matrix) element of $\bar{Z} \geq 0$. Since $\alpha < 0$ and $\overline{\nabla}$ is compact, a sufficiently small positive element can be added to each element of $\bar{Z}$, thus defining $\hat{Z}$ and yielding the required result. ∎

Step 2: Constructing Y

Since $\hat{z}$ is positive, it can be assumed, without loss of generality, that $\hat{z} = 1$. Set $X_k := \hat{Z}_k^{\mathcal{D}}$, $Y_l := \hat{Z}_l^{\mathcal{E}}$. Denote pair (d, e) as *allowable* if $\|d\|^2 \leq B_{\mathbf{d}}$, $\|e\|^2 \leq B_{\mathbf{e}}$. Thus

for all allowable (d, e):

$$\begin{aligned}\langle e, \mathbf{M}d\rangle \leq \quad & 1-\beta-\beta^2\|e\|^2 + X_0\|d\|^2 + Y_0\|e\|^2 + \langle d, \bar{X}d\rangle + \langle e, \bar{Y}e\rangle \\ & - \left(\bar{T}_x + X_0 M_0\right)\langle e, \mathbf{M}d\rangle - \left(\bar{T}_y + Y_0 P_0\right), \qquad (3.69)\end{aligned}$$

$$\bar{X} := \sum_{k=1}^{C_\mathbf{d}} \grave{D}_k \textcircled{T} X_k, \quad \bar{Y} := \sum_{l=1}^{C_\mathbf{e}} \grave{E}_l \textcircled{T} Y_l, \qquad (3.70)$$

$$\bar{T}_x := \sum_{k=1}^{C_\mathbf{d}} \mathbf{trace}\,(M_k X_k), \quad \bar{T}_y := \sum_{l=1}^{C_\mathbf{e}} \mathbf{trace}\,(P_l Y_l). \qquad (3.71)$$

Note that $\bar{T}_x$ and $\bar{T}_y$ do not necessarily have to be positive, since M_k and P_l are assumed to be arbitrary, symmetric matrices. Define

$$\hat{x} := \sup\{X_0 : \text{ equation (3.69) satisfied for some } Y_0 > 0\}, \qquad (3.72)$$

$$\hat{y} := \sup\{Y_0 : \text{ equation (3.69) satisfied with } X_0 = \hat{x}\}. \qquad (3.73)$$

Since Y_0 is uniformly bounded for all X_0 by considering $d = 0$, $e = 0$, the second supremum is finite. Since one can always find allowable d and e such that $\|d\|^2 - M_0\langle e, Md\rangle$ is negative, and Y_0 is bounded, the first supremum is finite as well. From the above construction, X_0 cannot be larger than $\hat{x}$ (with all other scales except Y_0 fixed), and Y_0 cannot be larger than $\hat{y}$ with all scales fixed and $X_0 = \hat{x}$. This leads to the following proposition:

Proposition 3.13 *Let $X_0 = \hat{x}$, $Y_0 = \hat{y}$, denote the left-hand side of equation (3.69) by LHS, the right-hand side by RHS. Then*

$$\sup_{\|e\|^2 \leq P_0} \sup_{\|d\|^2 \leq B_\mathbf{d}} LHS(d,e) - RHS(d,e) = 0, \qquad (3.74)$$

$$\sup_{\|e\|^2 \leq B_\mathbf{e}} \sup_{\|d\|^2 \leq B_\mathbf{d}/2} LHS(d,e) - RHS(d,e) = 0. \qquad (3.75)$$

Proof of Proposition 3.13: By the construction of $\hat{x}$ and $\hat{y}$, the above suprema must be less than or equal to 0. If the first supremum is negative, Y_0 can be increased and still satisfy equation (3.69), a contradiction. By the definition of $B_\mathbf{d}$ in equation (3.56),

$$\sup_{\|d\|^2 \leq B_\mathbf{d}} \sup_{\|e\|^2 \leq B_\mathbf{e}} M_0\langle e, \mathbf{M}d\rangle \leq \frac{B_\mathbf{d}}{\sqrt{2}}. \qquad (3.76)$$

Thus for all $B_\mathbf{d}/2 \leq \|d\|^2 \leq B_\mathbf{d}$ and $\|e\|^2 \leq B_\mathbf{e}$, $\|d\|^2 - M_0\langle e, \mathbf{M}d\rangle \geq 0$. It thus follows that if the supremum in equation (3.75) is negative, X_0 can be increased and still satisfy equation (3.69), a contradiction as well. ∎

Lemma 3.14

$$T_y := \bar{T}_y + \hat{y}P_0 = 1 - \beta. \qquad (3.77)$$

Proof of Lemma 3.14: Let $X_0 = \hat{x}$, $Y_0 = \hat{y}$. There exists an allowable sequence (d_k, e_k) such that

$$LHS(d_k, e_k) - RHS(d_k, e_k) \stackrel{k\to\infty}{\longrightarrow} 0. \tag{3.78}$$

By Proposition 3.13, $\|d_k\|^2$ can uniformly be taken to be strictly less than $B_{\mathbf{d}}$, or $\|e_k\|^2$ can uniformly be taken to be strictly less than $B_{\mathbf{e}}$. Similar to the proof of Lemma 3.11, however, by appropriately shifting signals in time these two cases can be combined to construct a sequence (d_k, e_k) satisfying equation (3.78) such that both $\|d_k\|^2$ and $\|e_k\|^2$ are strictly, uniformly bounded by $B_{\mathbf{d}}$ and $B_{\mathbf{e}}$, respectively. It thus follows that there exists $\epsilon > 0$ such that $(1+\epsilon)(d_k, e_k)$ is allowable. Then

$$LHS\left((1+\epsilon)(d_k, e_k)\right) - RHS\left((1+\epsilon)(d_k, e_k)\right) \stackrel{k_i\to\infty}{\longrightarrow} \epsilon^2(1 - \beta - T_y) \tag{3.79}$$

which implies that $1 - \beta - T_y \leq 0$. By setting $e = 0$, $d = 0$ in equation (3.69), however, $1 - \beta - T_y \geq 0$, yielding the required result. ∎

Define $X := \bar{X} + \hat{x}I$, $Y := \bar{Y} + \hat{y}I$, $T_x := \bar{T}_x + \hat{x}M_0$.

Lemma 3.15 $Y \geq \beta^2$, $X \geq 0$, $T_x \geq 0$.

Proof (Lemma): From equation (3.69), for negative values of $\langle e, \mathbf{M}d\rangle$

$$T_x \geq \frac{-\beta^2\|e\|^2 + \langle e, Ye\rangle + \langle d, Xd\rangle}{\langle e, \mathbf{M}d\rangle} - 1. \tag{3.80}$$

If $X \not\geq 0$, one can find a sequence (d_k, e_k) such that the numerator in equation (3.80) is bounded above by some negative value while the denominator is made arbitrarily small in magnitude. This would imply that T_x is unbounded. A similar argument holds for $Y \not\geq \beta^2$.
Finally, for all $d \in \mathcal{D}$, $\langle d, Xd\rangle \leq T_x$, which by the positivity of X implies that $T_x \geq 0$. ∎

Lemma 3.16

$$\sup_{\|\bar{e}\|^2\leq 1}\sup_{d\in\mathcal{D}}\langle \bar{e}, Y^{-\frac{1}{2}}\mathbf{M}d\rangle < 1. \tag{3.81}$$

Proof of Lemma 3.16: Define $\bar{e} := Y^{\frac{1}{2}}e$. Thus for all $\|\bar{e}\|^2 = 1$

$$\langle \bar{e}, Y^{-\frac{1}{2}}\mathbf{M}d\rangle \leq 1 - \epsilon + \langle d, Xd\rangle - T_x\langle \bar{e}, Y^{-\frac{1}{2}}\mathbf{M}d\rangle, \tag{3.82}$$

where $\epsilon > 0$, and $\|e\|^2 \leq \frac{1}{\beta^2}$ and is thus allowable. It thus follows that for all $d \in \mathcal{D}$, $\|\bar{e}\|^2 = 1$,

$$\langle \bar{e}, Y^{-\frac{1}{2}}\mathbf{M}d\rangle \leq \frac{1 + T_x - \epsilon}{1 + T_x} < 1, \tag{3.83}$$

which yields the required result. ∎

Step 3: Constructing X

It has been shown that

$$\sup_{e\in\mathcal{E}}\sup_{d\in\mathcal{D}}\langle e, \mathbf{M}d\rangle < 1 \implies \sup_{\|e\|^2\le 1}\sup_{d\in\mathcal{D}}\langle e, Y^{-\frac{1}{2}}\mathbf{M}d\rangle < 1, \tag{3.84}$$

where Y satisfies equation (3.40) and associated T_y satisfies equation (3.42). Referring back to the diagram in Figure 3.4, we have shown that for all $d \in \mathcal{D}$, there exists convex region $\mathfrak{Z}_0$ defined by a hyperplane, strictly inside $\mathfrak{Z}$, such that the resulting $\Lambda(z)$ are inside this region. By defining

$$\bar{\mathcal{E}} := \left\{e \in l_2^p : \|e\|^2 \le 1\right\}, \tag{3.85}$$

the condition of Lemma 3.16 is equivalent to

$$\sup_{d\in\mathcal{D}}\sup_{\bar{e}\in\bar{\mathcal{E}}}\langle d, \mathbf{M}^* Y^{-\frac{1}{2}}\bar{e}\rangle < 1. \tag{3.86}$$

Thus by holding Y constant, replacing $\mathcal{E}$ with $\mathcal{D}$, $\mathcal{D}$ with $\bar{\mathcal{E}}$, e with d, d with $\bar{e}$, $\mathbf{M}$ with $\mathbf{M}^*Y^{-\frac{1}{2}}$, and repeating Step 1 and Step 2, scale X satisfying equation (3.39) may be constructed, with the associated T_x satisfying equation (3.41), and

$$\sup_{\|\bar{d}\|^2\le 1}\sup_{\|\bar{e}\|^2\le 1}\langle \bar{d}, X^{-\frac{1}{2}}\mathbf{M}^* Y^{-\frac{1}{2}}\bar{e}\rangle < 1, \tag{3.87}$$

which implies equation (3.38). ∎

3.4 Synthesis Condition

In this section, the full solution to the Generalized l_2 Synthesis problem is presented, which takes the form of an AMI. This is accomplished by invoking the AMI $\mathcal{H}_\infty$ solution. The following result is from [Packard, 1994]:

Theorem 3.17 *Let system* $\bar{\mathbf{G}}$ *have minimal state-space representation*

$$\left[\begin{array}{c|cc} \bar{A} & \bar{B}_1 & \bar{B}_2 \\ \hline \bar{C}_1 & \bar{D}_{11} & \bar{D}_{12} \\ \bar{C}_2 & \bar{D}_{21} & \bar{D}_{22} \end{array}\right].$$

There exists a stabilizing controller $\mathbf{K}$ *for* $\bar{\mathbf{G}}$ *such that* $\left\|\bar{\mathbf{G}} \star \mathbf{K}\right\| < 1$ *if and only if there exist positive definite matrices* S *and* T *such that*

$$\bar{V}\left(\bar{R}^*\begin{bmatrix} S & 0 \\ 0 & I \end{bmatrix}\bar{R} - \begin{bmatrix} S & 0 \\ 0 & I \end{bmatrix}\right)\bar{V}^* < 0, \tag{3.88}$$

$$\bar{U}^*\left(\bar{R}\begin{bmatrix} T & 0 \\ 0 & I \end{bmatrix}\bar{R}^* - \begin{bmatrix} T & 0 \\ 0 & I \end{bmatrix}\right)\bar{U} < 0, \tag{3.89}$$

$$\begin{bmatrix} S & I \\ I & T \end{bmatrix} \geq 0, \tag{3.90}$$

where

$$\begin{aligned} \bar{R} &= \begin{bmatrix} \bar{A} & \bar{B}_1 \\ \bar{C}_1 & \bar{D}_{11} \end{bmatrix}, \\ \bar{V} = \begin{bmatrix} \bar{V}_1 & \bar{V}_2 \end{bmatrix} &: \begin{bmatrix} \bar{C}_2 & \bar{D}_{21} \\ \bar{V}_1 & \bar{V}_2 \end{bmatrix} \text{invertible}, \quad \bar{C}_2\bar{V}_1^* + \bar{D}_{21}\bar{V}_2^* = 0, \\ \bar{U} = \begin{bmatrix} \bar{U}_1 \\ \bar{U}_2 \end{bmatrix} &: \begin{bmatrix} \bar{B}_2 & \bar{U}_1 \\ \bar{D}_{12} & \bar{U}_2 \end{bmatrix} \text{invertible}, \quad \bar{U}_1^*\bar{B}_2 + \bar{U}_2^*\bar{D}_{12} = 0. \end{aligned} \tag{3.91}$$

Remarks: As discussed in [Packard, 1994], it can be assumed without loss of generality that $\begin{bmatrix} \bar{C}_2 & \bar{D}_{21} \end{bmatrix}$ is full row rank; thus there always exists a $\bar{V}$ satisfying equation (3.91). Similarly for $\bar{U}$.

We are now in a position to state and prove the main result of this chapter:

Theorem 3.18 *Let system* **G** *have minimal state-space representation*

$$\left[\begin{array}{c|cc} A & B_1 & B_2 \\ \hline C_1 & D_{11} & D_{12} \\ C_2 & D_{21} & D_{22} \end{array}\right].$$

There exists a **K** *which solves the Generalized l_2 Synthesis problem if and only if there exist scales X and Y satisfying the conditions of Theorem 3.6, and positive definite matrices S, T, $\bar{X}$ and $\bar{Y}$, such that*

$$V\left(R^*\begin{bmatrix} S & 0 \\ 0 & \bar{Y} \end{bmatrix}R - \begin{bmatrix} S & 0 \\ 0 & X \end{bmatrix}\right)V^* < 0, \tag{3.92}$$

$$U^*\left(R\begin{bmatrix} T & 0 \\ 0 & \bar{X} \end{bmatrix}R^* - \begin{bmatrix} T & 0 \\ 0 & Y \end{bmatrix}\right)U < 0, \tag{3.93}$$

$$\begin{bmatrix} S & I \\ I & T \end{bmatrix} \geq 0, \quad \begin{bmatrix} X & I \\ I & \bar{X} \end{bmatrix} \geq 0, \quad \begin{bmatrix} Y & I \\ I & \bar{Y} \end{bmatrix} \geq 0 \tag{3.94}$$

where

$$\begin{aligned} R &= \begin{bmatrix} A & B_1 \\ C_1 & D_{11} \end{bmatrix}, \\ V = \begin{bmatrix} V_1 & V_2 \end{bmatrix} &: \begin{bmatrix} C_2 & D_{21} \\ V_1 & V_2 \end{bmatrix} \text{invertible}, \quad C_2V_1^* + D_{21}V_2^* = 0, \\ U = \begin{bmatrix} U_1 \\ U_2 \end{bmatrix} &: \begin{bmatrix} B_2 & U_1 \\ D_{12} & U_2 \end{bmatrix} \text{invertible}, \quad U_1^*B_2 + U_2^*D_{12} = 0. \end{aligned} \tag{3.95}$$

Proof: In the previous section, an analysis condition was derived which involved scales X and Y. If $\mathbf{M}$ is a bounded system and the scales X and Y are fixed, equation (3.38) reduces to a standard $\mathcal{H}_\infty$ optimization problem, and results in the following corollary to Theorem 3.6:

Corollary 3.19 *The Generalized l_2 Synthesis problem is solvable if and only if there exist scales X and Y satisfying the conditions of Theorem 3.6 and a stabilizing controller $\mathbf{K}$ for $\mathbf{G}$ such that*

$$\left\| Y^{-\frac{1}{2}} \left(\mathbf{G} \star \mathbf{K} \right) X^{-\frac{1}{2}} \right\| < 1. \tag{3.96}$$

Define

$$\bar{\mathbf{G}} := \begin{bmatrix} Y^{-\frac{1}{2}} & \\ & I \end{bmatrix} \mathbf{G} \begin{bmatrix} X^{-\frac{1}{2}} & \\ & I \end{bmatrix}. \tag{3.97}$$

Then equation (3.96) is equivalent to $\left\| \bar{\mathbf{G}} \star \mathbf{K} \right\| < 1$. Furthermore,

$$\left[\begin{array}{c|cc} \bar{A} & \bar{B}_1 & \bar{B}_2 \\ \hline \bar{C}_1 & \bar{D}_{11} & \bar{D}_{12} \\ \bar{C}_2 & \bar{D}_{21} & \bar{D}_{22} \end{array}\right] := \left[\begin{array}{c|cc} A & B_1 X^{-\frac{1}{2}} & B_2 \\ \hline Y^{-\frac{1}{2}} C_1 & Y^{-\frac{1}{2}} D_{11} X^{-\frac{1}{2}} & Y^{-\frac{1}{2}} D_{12} \\ C_2 & D_{21} X^{-\frac{1}{2}} & D_{22} \end{array}\right] \tag{3.98}$$

is a minimal state-space representation for $\bar{\mathbf{G}}$. Define

$$\tilde{X} := \begin{bmatrix} I & 0 \\ 0 & X \end{bmatrix}, \quad \tilde{Y} := \begin{bmatrix} I & 0 \\ 0 & Y \end{bmatrix}, \tag{3.99}$$

and U, V, and R as in equation (3.95). Then $\bar{R} = \tilde{Y}^{-\frac{1}{2}} R \tilde{X}^{-\frac{1}{2}}$, and $\bar{V} := V \tilde{X}^{\frac{1}{2}}$, $\bar{U} := \tilde{Y}^{-\frac{1}{2}} U$ satisfy equations (3.91). Substituting into equations (3.88) and (3.89) yields

$$V \left(R^* \begin{bmatrix} S & 0 \\ 0 & Y^{-1} \end{bmatrix} R - \begin{bmatrix} S & 0 \\ 0 & X \end{bmatrix} \right) V^* < 0, \tag{3.100}$$

$$U^* \left(R \begin{bmatrix} T & 0 \\ 0 & X^{-1} \end{bmatrix} R^* - \begin{bmatrix} T & 0 \\ 0 & Y \end{bmatrix} \right) U < 0. \tag{3.101}$$

Finally, by Schur complement arguments [Zhou et al., 1995], if $\bar{X}$ satisfies matrix inequality

$$\begin{bmatrix} \bar{X} & I \\ I & X \end{bmatrix} \geq 0,$$

then $\bar{X} \geq X^{-1}$. Furthermore, $\bar{X} = X^{-1}$ satisfies the matrix inequality. This concludes the proof. ∎

Remarks:

- A controller may be constructed as described in [Packard, 1994] using the state-space description for $\bar{\mathbf{G}}$ (which includes scales X and Y) and scales S and T. The details are omitted.
- The order of the resulting controller is less than or equal to the order of the plant. Thus the added complexity of sets $\mathcal{D}$ and $\mathcal{E}$ only manifests itself in the computation of the controller, not in the order of the controller itself. This is due to the fact that no dynamics are utilized when describing sets $\mathcal{D}$ and $\mathcal{E}$.
- $\bar{X}$ is taken to be a positive definite matrix in the above AMI. This results in an added $m(m+1)/2$ decision variables. In fact, $\bar{X}$ need only have the structure of X^{-1}; for example, if

$$X = \begin{bmatrix} x_1 & 0 \\ 0 & x_2 \end{bmatrix},$$

then it suffices to consider $\bar{X}$ with structure

$$\bar{X} = \begin{bmatrix} \bar{x}_1 & 0 \\ 0 & \bar{x}_2 \end{bmatrix},$$

eliminating one decision variable from the AMI. A similar argument holds for Y and $\bar{Y}$.

- The AMI may be solved using standard convex optimization tools, such as The LMI Control Toolbox [Gahinet et al., 1994].

3.5 Concluding Remarks

In the next two chapters, various open problems are solved using the framework developed in this chapter, justifying the results from a practical standpoint. From a purely theoretical standpoint, the result in this chapter appears to be the natural extension of $\mathcal{H}_\infty$ optimization, in the sense that arbitrary convex sets are used to describe the allowable disturbance classes and cost criteria.

A natural extension of this work is to allow dynamic constraints in the description of $\mathcal{D}$ and $\mathcal{E}$. For example, one might want to include extra terms in the description of $\mathfrak{D}$ and $\mathcal{D}$ ($\mathfrak{E}$ and $\mathcal{E}$) such as $\Lambda(d, \mathbf{\Phi}_i d)$, where the $\mathbf{\Phi}_i$ are systems (this generalization will allow one to capture general IQCs in the Generalized l_2 Synthesis framework). The results in this chapter could then be seen as a special case, with $\mathbf{\Phi} = \mathbf{I}$. In fact, the analysis condition of Section 3.3 can trivially be extended to the above case. The synthesis condition, however, cannot. A prelude to this extension is given in Chapter 5, where correlation constraints of the form $\Lambda(d, \boldsymbol{\lambda}^T d) = 0$ are imposed, which do not fit directly into the Generalized l_2 Synthesis framework.

Chapter 4

Applications of Generalized l_2 Synthesis

In this chapter, various problems are solved using the Generalized l_2 Synthesis framework developed in Chapter 3; synthesis for independently norm bounded disturbances, robust stability with "element by element" bounded structured uncertainty, and certain classes of robust performance problems. In addition, recent results on the design of gain scheduled controllers are extended to the above cases.

4.1 Square $\mathcal{H}_\infty$

In this section, a variant of $\mathcal{H}_\infty$ synthesis where norm constraints on each component of the disturbance can be imposed is posed and cast into the Generalized l_2 Synthesis framework.

The reason for the title of this section will become apparent shortly, although it is admittedly an abuse of notation. Consider the standard $\mathcal{H}_\infty$ synthesis problem depicted in Figure 4.1, where $z \in l_2^p$ and $d \in l_2^m$: it is required to find a controller $\mathbf{K}$ which minimizes the energy output of the closed loop system $\mathbf{M} := \mathbf{G} \star \mathbf{K}$ subject to all possible unit energy (by linearity) disturbance inputs.

If we consider the motivation for this problem, it seems reasonable to lump the cost as $\|z\| = \sqrt{\|z_1\|^2 + \cdots + \|z_p\|^2}$; it is required to keep the error z small in some sense, and large deviations are penalized more than smaller ones. It is not so clear,

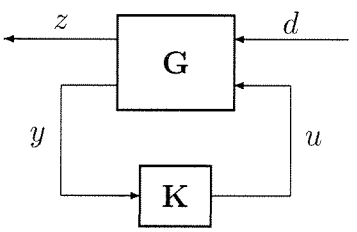

Figure 4.1: Synthesis formulation

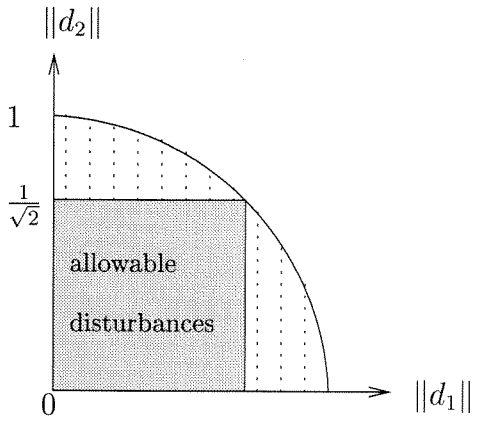

Figure 4.2: Square versus round spatial constraint

however, why the disturbance size is lumped together as $\|d\| = \sqrt{\|d_1\|^2 + \cdots + \|d_m\|^2}$; if the d_i are physically motivated, their magnitudes will, in general, be independent. One would expect specifications of the form $\|d_i\| \leq \alpha_i$ for each component (this is, incidentally, one of the arguments for l_1 design [Dahleh and Diaz-Bobillo, 1995] versus $\mathcal{H}_\infty$ design, albeit only on the spatial aspect of the norm). Assume without loss of generality that $\alpha_i = \frac{1}{\sqrt{m}}$, since these constants can be absorbed into system $\mathbf{G}$. To capture these constraints into the standard $\mathcal{H}_\infty$ setup, one would have to cover the given allowable disturbance set by the following round constraint:

$$\sum_{i=1}^{m} \|d_i\|^2 \leq 1 \tag{4.1}$$

which corresponds to the diagram of Figure 4.2 for $m = 2$.

The "square" disturbance set which we want to design for lies inside the round set. Let $\mathbf{\Phi}$ be a linear operator. Define the following induced norm:

$$\|\mathbf{\Phi}\|_{\mathbf{SQ}} := \sup_{\|d_i\| \leq \frac{1}{\sqrt{m}}} \|\mathbf{\Phi} d\|, \tag{4.2}$$

referred to as the *square* norm. The following relationship between $\|\mathbf{\Phi}\|_{\mathbf{SQ}}$ and $\|\mathbf{\Phi}\|$ follows immediately from the above definition:

$$\|\mathbf{\Phi}\|_{\mathbf{SQ}} \leq \|\mathbf{\Phi}\| \leq \sqrt{m}\, \|\mathbf{\Phi}\|_{\mathbf{SQ}}\,, \tag{4.3}$$

with the above bounds being tight for any m, i.e., one can always find $\mathbf{\Phi}$ such that $\|\mathbf{\Phi}\|_{\mathbf{SQ}} = \|\mathbf{\Phi}\|$, or such that $\|\mathbf{\Phi}\| = \sqrt{m}\, \|\mathbf{\Phi}\|_{\mathbf{SQ}}$. Thus the $\mathcal{H}_\infty$ norm of a system may be $\sqrt{m}$ times larger than the square norm, and occurs when only one disturbance has an effect on the output error.

It is straightforward to construct a simple example such that *synthesis* will give this gap. By this, it is meant that doing $\mathcal{H}_\infty$ optimization results in a square norm

which is $\sqrt{m}$ times greater than if the optimization were done directly with the square criterion:

	$\|\cdot\|_\infty$ Analysis	$\|\cdot\|_{\mathbf{SQ}}$ Analysis
$\|\cdot\|_\infty$ Synthesis	1	1
$\|\cdot\|_{\mathbf{SQ}}$ Synthesis	1	$1/\sqrt{m}$

It should be noted, however, that the simplicity of this example stems from the assumed controller structure. Consider the following *static* equations:

$$\begin{aligned} z_1 &= (1+\epsilon Q)d_1, \qquad (4.4)\\ z_i &= (1-Q)d_i, \quad 2 \le i \le m,\\ \epsilon &> 0, \qquad (4.5) \end{aligned}$$

where $Q \in \mathbb{R}$ is the design variable. The $\mathcal{H}_\infty$ design problem reduces to

$$\inf_{Q\in\mathbb{R}} \bar{\sigma} \begin{bmatrix} 1+\epsilon Q & & & \\ & 1-Q & & \\ & & \ddots & \\ & & & 1-Q \end{bmatrix}. \qquad (4.6)$$

This infimum is 1 for all $\epsilon > 0$, and is uniquely achieved at $Q = 0$. The square norm for this design is also 1.

If, however, one chooses $Q = 1$, the resulting $\mathcal{H}_\infty$ and square norms are $1+\epsilon$ and $(1+\epsilon)/\sqrt{m}$, respectively. Thus by letting ϵ go to zero, by the bounds in (4.3), one can come arbitrarily close to the optimal square norm, and a gap which approaches $\sqrt{m}$.

Thus if the size of each component of the disturbance is known, one might want to perform the design directly with the square, versus the round, spatial constraint on the disturbance (hence the name Square $\mathcal{H}_\infty$, since the signal norm is still l_2):

Square $\mathcal{H}_\infty$ Synthesis:

Given system $\mathbf{G}$, *find a stabilizing controller* K *such that* $\|\mathbf{G} \star \mathbf{K}\|_{\mathbf{SQ}} < 1$.

This may be cast into the Generalized l_2 Synthesis framework by defining

$$\begin{aligned} \mathcal{D} &:= \left\{ d \in l_2^m : \|d_k\|^2 \le 1,\ 1 \le k \le m \right\}, \qquad (4.7)\\ \mathcal{E} &:= \left\{ e \in l_2^p : \|e\|^2 \le 1 \right\}, \qquad (4.8) \end{aligned}$$

or in terms of sets $\mathfrak{D}$ and $\mathfrak{E}$,

$$D_k \in \mathbb{R}_s^{m\times m},\ D_{k[i,j]} := \begin{cases} 1 & i=j=k \\ 0 & \text{otherwise} \end{cases},\ 1 \le k \le m, \tag{4.9}$$

$$M_k := 1,\ 1 \le k \le m, \tag{4.10}$$

$$E_1 := I \in \mathbb{R}_s^{p\times p}, \tag{4.11}$$

$$P_1 := 1. \tag{4.12}$$

Note that in definition of the square norm, $d \in l_2^m$ was partitioned into m scalar valued signals. In general, one could define the square norm for any partition of d.

Remarks: It should be noted that the argument for choosing a square versus a round spatial constraint is based on a worst case design methodology; the round set must cover the square set to account for all possible disturbances. If, however, one wishes to relax the worst case assumption, the round set could be seen as a means to prevent all the components from achieving their maximum energy content (i.e., the design is performed with the round set inside the square set). In this context, the square design is the more conservative one. This, however, is simply a scaling argument ($\sqrt{m}$ to be exact); the resulting $\mathcal{H}_\infty$ design is the same whether done inside or outside the "square". Regardless of the interpretation, $\mathcal{H}_\infty$ design may not be the wisest thing to do (as illustrated by the previous example, where it is clear that the square design is better than the $\mathcal{H}_\infty$ design). This usually stems from requiring optimality, or near-optimality. This is often remedied by considering sub-optimal designs, and employing other criteria for choosing a controller (for example, maximum entropy controllers [Glover and Mustafa, 1989]). In this light, Square $\mathcal{H}_\infty$ design should be seen as an additional tool in the $\mathcal{H}_\infty$ methodology; the specific application will determine whether it yields better designs.

4.2 Robust Stability

Consider the setup of Figure 4.3; variables z and d are partitioned into C_e and C_d components (not necessarily scalar valued). This partition induces a corresponding one for $\mathbf{\Delta}$:

$$d_k = \sum_{l=1}^{C_e} \mathbf{\Delta}_{kl} z_l,\ \ 1 \le k \le C_d. \tag{4.13}$$

The set $\mathbf{U\Delta}$ (where "U" symbolizes uncertainty) is defined as follows:

$$\mathbf{U\Delta} := \{\mathbf{\Delta} : \mathbf{\Delta} \in \mathcal{L}(l_2), \|\mathbf{\Delta}_{kl}\| \le 1\}. \tag{4.14}$$

The plant uncertainty, $\mathbf{\Delta}$, is then assumed to be in set $\mathbf{U\Delta}$. Note that $\mathbf{\Delta}$ is not assumed to be causal, but as shall be argued later, all the results in this section are valid for causal perturbations as well. Analysis conditions for systems subject to this

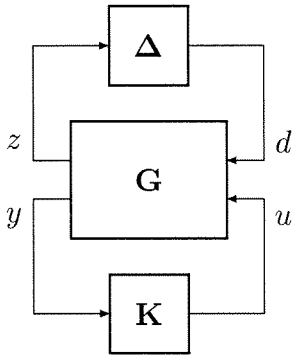

$$\mathbf{\Delta} = \begin{bmatrix} \mathbf{\Delta}_{11} & \cdots & \mathbf{\Delta}_{1,c_e} \\ & \vdots & \\ \mathbf{\Delta}_{c_d,1} & \cdots & \mathbf{\Delta}_{c_d,c_e} \end{bmatrix}$$

Figure 4.3: Synthesis for robust stability

type of structured uncertainty, typically referred to as *full-structured uncertainty*, are explored in [Kouvaritakis and Latchman, 1985] and [Young, 1996].

$\mathbf{K}$ is referred to as a *robustly stabilizing controller* for $\mathbf{G}$ and $\mathbf{U\Delta}$ if $\mathbf{K}$ is a stabilizing controller for $\mathbf{G}$ and

$$\sup_{\mathbf{\Delta} \in \mathbf{U\Delta}} \left\| (\mathbf{I} - \mathbf{M\Delta})^{-1} \right\| < \infty, \tag{4.15}$$

where $\mathbf{M} := \mathbf{G} \star \mathbf{K}$. This condition establishes the stability and well-posedness of the closed loop system for all allowable uncertainty; any l_2 signal injected in the loop will be amplified by a finite amount. If the condition above is satisfied, the closed loop system of Figure 4.3 is said to be *robustly stable.*

The following theorem establishes the equivalence of finding a robustly stabilizing controller $\mathbf{K}$ to a problem which can be cast into the Generalized l_2 Synthesis framework:

Theorem 4.1 *The following statements are equivalent:*

I. $\mathbf{K}$ *is a robustly stabilizing controller for* $\mathbf{G}$ *and* $\mathbf{U\Delta}$.

II. $\mathbf{K}$ *is a stabilizing controller for* $\mathbf{G}$ *and*

$$\sup_{\|d_k\|^2 \leq 1} \sum_{l=1}^{C_e} \|z_j\| < 1, \tag{4.16}$$

where $z = \mathbf{M}d$.

Before proving the above theorem, the following preliminary lemma is required:

Lemma 4.2 *Given* $x_j, y \in l_2$, $\|y\| \leq \sum \|x_j\|$ *if and only if there exist* $\mathbf{\Delta}_j \in \mathcal{L}(l_2)$, $\|\mathbf{\Delta}_j\| \leq 1$, *such that* $y = \sum \mathbf{\Delta}_j x_j$.

Proof of Lemma 4.2: First, assume that $y = \sum \mathbf{\Delta}_j x_j$, with $\|\mathbf{\Delta}_j\| \leq 1$. Then $\|y\| \leq \sum \|\mathbf{\Delta}_j\| \|x_j\| \leq \|x_j\|$ as required.
Assume that $\gamma := \sum \|x_j\| \geq \|y\|$. Define the following operators:

$$\mathbf{\Delta}_j(\cdot) := \begin{cases} \dfrac{y}{\gamma \|x_j\|} \langle x_j, \cdot \rangle & \text{for } \gamma \|x_j\| > 0 \\ 0 & \text{for } \gamma \|x_j\| = 0 \end{cases}. \tag{4.17}$$

By construction, $y = \sum \mathbf{\Delta}_j x_j$. Furthermore, since $\gamma \geq \|y\|$, it follows that $\|\mathbf{\Delta}_j\| \leq 1$. ■

Proof of Theorem 4.1:
II $\Rightarrow$ **I:** Assume that $\mathbf{K}$ is not a robustly stabilizing controller, violating (4.15). Thus $\forall \epsilon > 0$, $\exists n, \tilde{z} \in l_2$ and $\mathbf{\Delta} \in \mathbf{U\Delta}$ such that $\|n\| < \epsilon$, $\sum \|\tilde{z}_l\| = 1$, and $\tilde{z} = (\mathbf{I} - \mathbf{M\Delta})^{-1} n$. Setting $d = \mathbf{\Delta}\tilde{z}$ results in $z := \mathbf{M}d = \tilde{z} - n$, with $\|d_k\| \leq 1$ by Lemma 4.2. Since ϵ is arbitrary, (4.16) is contradicted.

I $\Rightarrow$ **II:** Since $\mathbf{K}$ is a robustly stabilizing controller, it immediately follows that $\mathbf{K}$ is a stabilizing controller for $\mathbf{G}$. Furthermore, by continuity, (4.15) implies that there exists $r < 1$ such that

$$\sup_{r\mathbf{\Delta} \in \mathbf{U\Delta}} \left\| (\mathbf{I} - \mathbf{M\Delta})^{-1} \right\| < \infty. \tag{4.18}$$

Assume that (4.16) is not satisfied. Then $\exists d \in l_2$, $\|d_k\| \leq 1$, such that $\sum \|z_l\| \geq r$. By Lemma 4.2, it follows that there exists $\mathbf{\Delta}$ such that $r\mathbf{\Delta} \in \mathbf{U\Delta}$ and $\mathbf{\Delta} z = d$, which contradicts equation (4.18). ■

It remains to show how statement **II** can be cast into a Generalized l_2 Synthesis problem. First, note that $\|x\| = \sup_{\|y\|^2 \leq 1} \langle y, x \rangle$; the cost criterion in equation (4.16) is therefore equivalent to

$$\sum_{l=1}^{C_{\mathbf{e}}} \|z_j\| = \sup_{\|e_l\|^2 \leq 1} \langle e, z \rangle. \tag{4.19}$$

Thus one can choose $\mathcal{E}$ and $\mathcal{D}$ to be the following sets:

$$\mathcal{D} := \left\{ d \in l_2^m : \|d_k\|^2 \leq 1,\ 1 \leq k \leq C_{\mathbf{d}} \right\}, \tag{4.20}$$

$$\mathcal{E} := \left\{ e \in l_2^p : \|e_l\|^2 \leq 1,\ 1 \leq l \leq C_{\mathbf{e}} \right\}. \tag{4.21}$$

Sets $\mathfrak{D}$ and $\mathfrak{E}$ may be constructed as in Section 4.1.

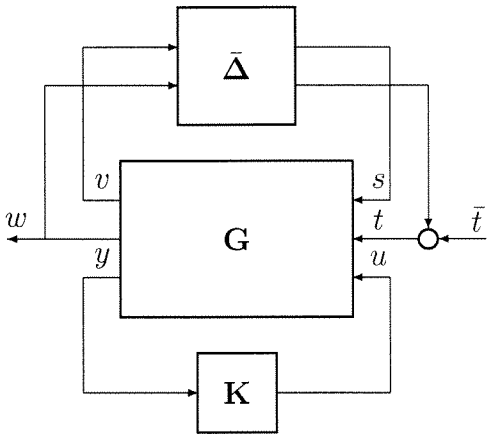

Figure 4.4: Robust performance

Remarks:

- The above is a special case of the Robust l_2 Synthesis problem formulation of Section 2.2.2; there is no performance requirement, and by rearranging the uncertainty $\mathbf{\Delta^u}$ in block diagonal form, as per equation (2.28), the above can be cast as a Robust l_2 Synthesis problem.
- It is shown in [Shamma, 1994] that for the Robust l_2 Synthesis problem with LTV uncertainty, if robust performance can be violated with a non-causal $\mathbf{\Delta}$, it will also fail for some causal $\mathbf{\Delta}$. Thus all the results in the section hold for causal $\mathbf{\Delta}$ as well.

4.3 Robust Performance

In standard μ theory [Packard and Doyle, 1993], robust performance problems may be recast as robust stability problems by introducing fictitious uncertainty blocks. In this section, this idea is used to explore the types of robust performance problems which are equivalent to the robust stability problems encountered in the previous section.

In Figure 4.3, let $z = (v, w)$ and $d = (s, t)$. Signals v, w, s, and t are themselves partitioned into $C_{\mathbf{v}}$, $C_{\mathbf{w}}$, $C_{\mathbf{s}}$, and $C_{\mathbf{t}}$ (not necessarily scalar valued) components. This induces the following partition for $\mathbf{\Delta}$

$$\mathbf{\Delta} = \begin{bmatrix} \mathbf{\Delta^{sv}} & \mathbf{\Delta^{sw}} \\ \mathbf{\Delta^{tv}} & \mathbf{\Delta^{tw}} \end{bmatrix}, \tag{4.22}$$

and results in the diagram of Figure 4.4, where $\bar{t} = \mathbf{\Delta}^{tw} w$ and

$$\bar{\mathbf{\Delta}} := \begin{bmatrix} \mathbf{\Delta^{sv}} & \mathbf{\Delta^{sw}} \\ \mathbf{\Delta^{tv}} & 0 \end{bmatrix}. \tag{4.23}$$

Allowable uncertainty set $\mathbf{U\bar{\Delta}}$ can be defined analogously to $\mathbf{U\Delta}$. A class of robust performance problems may be obtained by replacing constraint $\bar{t} = \mathbf{\Delta}^{tw} w$ with a corresponding gain constraint between $\bar{t}$ and w:

Theorem 4.3 *The following statements are equivalent:*

I. $\mathbf{K}$ *is a robustly stabilizing controller for* $\mathbf{G}$ *and* $\mathbf{U\bar{\Delta}}$, *and*

$$\sup_{\bar{\mathbf{\Delta}} \in \mathbf{U\bar{\Delta}}} \sup_{\|\bar{t}_k\| \le 1} \sum_{l=1}^{C_\mathbf{w}} \|w_l\| < 1. \tag{4.24}$$

II. $\mathbf{K}$ *is a stabilizing controller for* $\mathbf{G}$ *and*

$$\sup_{\|d_k\| \le 1} \sum_{l=1}^{C_\mathbf{e}} \|z_l\| < 1. \tag{4.25}$$

Proof:

II $\Rightarrow$ **I:** By assumption, $\exists \epsilon > 0$ such that $\sum \|z_l\| < 1 - \epsilon$ for all $d \in l_2$ with $\|d_k\| \le 1$. Assume that statement **I** is false. Since $\mathbf{U\bar{\Delta}} \subset \mathbf{U\Delta}$, if $\mathbf{K}$ is not a robustly stabilizing controller for $\mathbf{G}$ and $\mathbf{U\bar{\Delta}}$, statement **II** must be false by Theorem 4.1, a contradiction. Thus $\exists \bar{t} \in l_2$ with $\|\bar{t}_k\| \le 1$ and $\bar{\mathbf{\Delta}} \in \mathbf{U\bar{\Delta}}$ such that $1 - \epsilon < \sum \|w_l\| < 1$ (where the upper bound follows by appropriately scaling $\bar{t}$). Define $\gamma := \sum \|v_l\|$. By linearity, $\exists \bar{t} \in l_2$ with $\|\bar{t}_k\| \le 1/(1+\gamma)$ and $\bar{\mathbf{\Delta}} \in \mathbf{U\bar{\Delta}}$ such that $(1-\epsilon)/(1+\gamma) < \sum \|w_l\| < 1/(1+\gamma)$ and $\sum \|v_l\| = \gamma/(1+\gamma)$. By Lemma 4.2, it follows that $\|d_k\| \le 1$, and $\sum \|z_l\| > 1 - \epsilon$, a contradiction of statement **II**.

I $\Rightarrow$ **II:** By continuity, statement **I** is equivalent to the existence of $0 < r < 1$ such that

$$\sup_{r\bar{\mathbf{\Delta}} \in \mathbf{U\bar{\Delta}}} \left\| \left(\mathbf{I} - \mathbf{M}\bar{\mathbf{\Delta}}\right)^{-1} \right\|_\infty < \infty \tag{4.26}$$

and

$$\sup_{r\bar{\mathbf{\Delta}} \in \mathbf{U\bar{\Delta}}} \sup_{\|\bar{t}_k\| \le 1} \sum_{l=1}^{C_\mathbf{w}} \|w_l\| < r. \tag{4.27}$$

Assume that statement **II** is false. Thus $\exists d \in l_2$ with $\|d_k\| \le 1$ such that $\alpha := \sum \|z_l\| > r$. Let $\gamma := \sum \|w_l\|$. There are two cases:

$\gamma = \mathbf{0}$: Since $\sum \|v_k\| > r$, by Lemma 4.2 $\exists \mathbf{\Delta}^{\mathbf{sv}}$ and $\mathbf{\Delta}^{\mathbf{tv}}$ such that $s = \mathbf{\Delta}^{\mathbf{sv}} v$ and $t = \mathbf{\Delta}^{\mathbf{tv}} v$, with $\|r\mathbf{\Delta}^{sv}_{kl}\| \le 1$ and $\left\|r\mathbf{\Delta}^{\mathbf{tv}}_{kl}\right\| \le 1$. Thus the following equation is satisfied

$$\begin{bmatrix} v \\ 0 \end{bmatrix} - \mathbf{M} \begin{bmatrix} \mathbf{\Delta}^{\mathbf{sv}} & 0 \\ \mathbf{\Delta}^{\mathbf{tv}} & 0 \end{bmatrix} \begin{bmatrix} v \\ 0 \end{bmatrix} = 0, \tag{4.28}$$

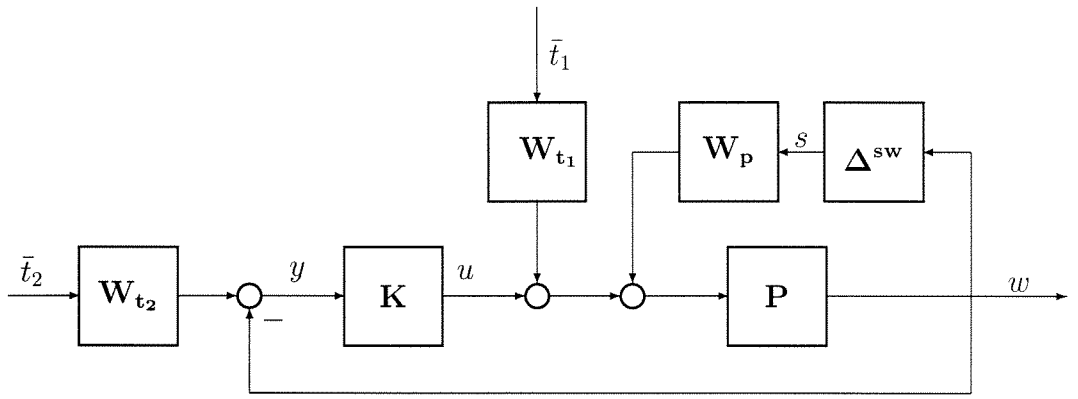

Figure 4.5: Robust disturbance rejection

which contradicts equation (4.26).

$\gamma > \mathbf{0}$: By linearity, $\exists d \in l_2$ with $\|d_k\| \leq r/\gamma$ such that $\sum \|z_l\| = \alpha r/\gamma$, $\sum \|w_l\| = r$, and $\sum \|v_l\| = r(\alpha/\gamma - 1) > r(r/\gamma - 1)$. By Lemma 4.2, there exist $\mathbf{\Delta^{sv}}$, $\mathbf{\Delta^{sw}}$ such that $s = \mathbf{\Delta^{sv}} v + \mathbf{\Delta^{sw}} w$, with $\|r\mathbf{\Delta}^{\mathbf{sv}}_{kl}\| \leq 1$ and $\|r\mathbf{\Delta}^{\mathbf{sw}}_{kl}\| \leq 1$. It remains to show the existence of $\bar{t} \in l_2$ and $\mathbf{\Delta^{tv}}$ such that $t = \mathbf{\Delta^{tv}} v + \bar{t}$, $\left\|r\mathbf{\Delta}^{\mathbf{tv}}_{kl}\right\| \leq 1$, and $\|\bar{t}_k\| \leq 1$ to contradict equation (4.27). Let $\beta_k := \|t_k\|$. Construct $\bar{t}_k$ as follows:

$$\bar{t}_k = \begin{cases} t_k & \text{for } \beta_k \leq 1 \\ \dfrac{t_k}{\beta_k} & \text{for } \beta_k > 1 \end{cases} . \tag{4.29}$$

Thus $\|t_k - \bar{t}_k\| = 0$ for $\beta_k < 1$ and $\|t_k - \bar{t}_k\| = \beta_k - 1 \leq r/\gamma - 1$ for $\beta_k \geq 1$. Since $\sum \|v_l\| > r(r/\gamma - 1)$, application of Lemma 4.2 yields the required $\mathbf{\Delta^{tv}}$, as required. ■

4.3.1 Examples

Robust Disturbance Rejection

Consider the setup of Figure 4.5. Given $\mathbf{P}$, it is required to design $\mathbf{K}$ such that disturbances $\bar{t}_1$, along with measurement errors $\bar{t}_2$, have a small effect on plant output w. The plant is subject to inverse additive unstructured uncertainty $\mathbf{\Delta^{sw}}$, with associated weight $\mathbf{W_p}$. The exact problem formulation is the following: find a controller $\mathbf{K}$ such that the closed loop system is robustly stable and

$$\sup_{\|\mathbf{\Delta^{sw}}\| \leq 1} \sup_{\|\bar{t}_1\| \leq 1} \sup_{\|\bar{t}_2\| \leq 1} \|w\| < 1. \tag{4.30}$$

This can be converted to the setup of Figure 4.4 by noting that $s = \mathbf{\Delta^{sw}} w$. Also note that if either of $\bar{t}_1$ or $\bar{t}_2$ are vector valued signals, they can further be partitioned and bounded in norm separately, as per the Square $\mathcal{H}_\infty$ problem.

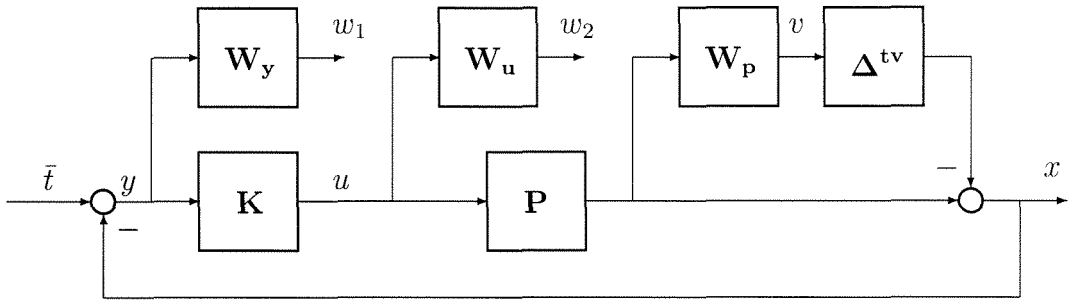

Figure 4.6: Robust tracking

Robust Tracking

Consider the setup of Figure 4.6. Given $\mathbf{P}$, it is required to design $\mathbf{K}$ such that x tracks $\bar{t}$. Equivalently, letting $\mathbf{W_y}$ be a weight which captures the range over which tracking is desired, it is required to keep w_1 small. The plant is subject to multiplicative, unstructured uncertainty $\mathbf{\Delta^{tv}}$, with associated weight $\mathbf{W_p}$. It may also be required to bound the control effort; this is done by weighting the controller output by $\mathbf{W_u}$, and requiring w_2 to be small. Formally, it is required to find $\mathbf{K}$ such that the closed loop system is robustly stable and

$$\sup_{\|\mathbf{\Delta^{tv}}\| \leq 1} \sup_{\|\bar{t}\| \leq 1} \|w\| < 1. \tag{4.31}$$

This problem can also be converted to the setup of Figure 4.4 by defining $t := \bar{t} + \mathbf{\Delta^{tv}} v$. Note that if $\bar{t}$ is vector valued, it may be partitioned and bounded in norm separately (with an appropriately defined $\mathbf{\Delta^{tv}}$).

4.4 Robust Gain Scheduling

In [Packard, 1994, Apkarian and Gahinet, 1995], the AMI approach is used to extend $\mathcal{H}_\infty$ theory to the design of parameter varying controllers for parameter varying systems; these results allow one to design gain scheduled controllers which achieve guaranteed performance and stability objectives. One of the drawbacks of the theory, however, is that plant uncertainty cannot directly be incorporated in the design process.

In this section, the results in [Packard, 1994] are extended to allow for structured uncertainty in the given system. In this formulation, the controller to be designed has access to the time varying parameters, but does not have access to the plant uncertainty. This is achieved by combining the parameter varying framework with the Generalized l_2 Synthesis framework of Chapter 3. The solution takes the form of an AMI, which is both a necessary and sufficient condition for the posed problem to have a solution.

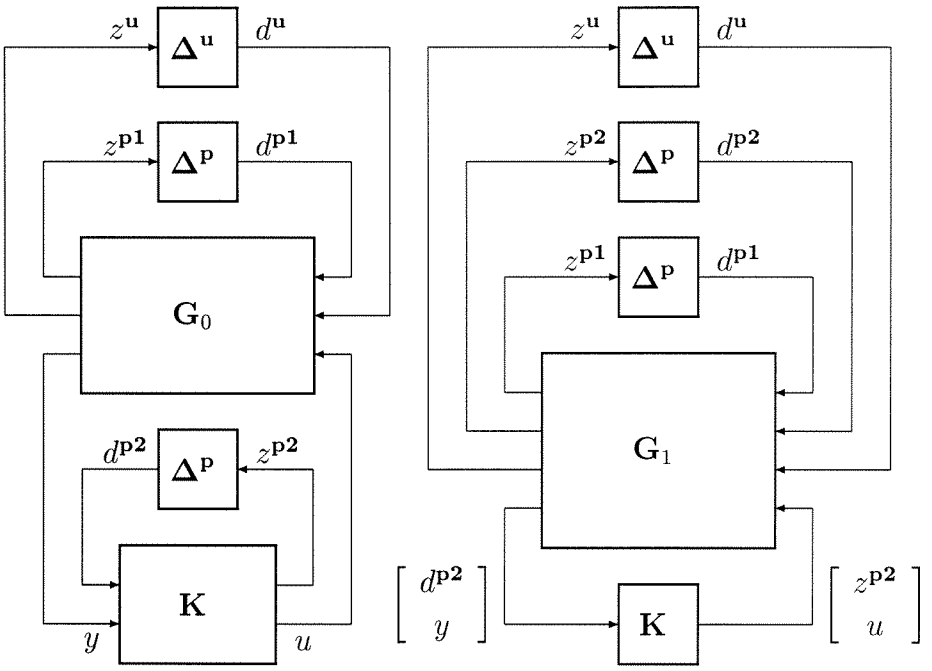

Figure 4.7: Gain scheduling design

4.4.1 Robust Gain Scheduling Problem Formulation

Consider the block diagram of Figure 4.7. $\mathbf{G}_0$ is the given system, $\mathbf{\Delta^u}$ is the plant uncertainty, and $\mathbf{\Delta^p}$ is a structured operator (to be defined) which parameterizes the plant and which the controller $\mathbf{K}$ (to be designed) has access to.

Partition variables $z^{\mathbf{u}}$ and $d^{\mathbf{u}}$ into $C_{\mathbf{e}}^{\mathbf{u}}$ and $C_{\mathbf{d}}^{\mathbf{u}}$ components (not necessarily scalar valued). This partition induces a corresponding one for $\mathbf{\Delta^u}$:

$$d_k^{\mathbf{u}} = \sum_{l=1}^{C_{\mathbf{e}}^{\mathbf{u}}} \mathbf{\Delta}_{kl}^{\mathbf{u}} z_l^{\mathbf{u}}, \quad 1 \leq k \leq C_{\mathbf{d}}^{\mathbf{u}}. \tag{4.32}$$

The set $\mathbf{U\Delta}$ is the same one encountered in Section 4.2, and is defined as follows:

$$\mathbf{U\Delta} := \{\mathbf{\Delta^u} : \mathbf{\Delta^u} \in \mathcal{L}(l_2), \|\mathbf{\Delta}_{kl}^{\mathbf{u}}\| \leq 1\}. \tag{4.33}$$

The plant uncertainty is then assumed to be in set $\mathbf{U\Delta}$. The plant parameters $\mathbf{\Delta^p}$ are assumed to be in set $\boldsymbol{P\Delta}$:

$$\boldsymbol{P\Delta} := \{\mathbf{\Delta^p} = \mathbf{diag}[\boldsymbol{\delta}_1 I, \cdots, \boldsymbol{\delta}_{C^{\mathbf{p}}} I] : \boldsymbol{\delta}_i \in \mathcal{L}(l_2), \|\boldsymbol{\delta}_i\| \leq 1\}, \tag{4.34}$$

where the identities above are of arbitrary, but fixed dimension. It is required to find system $\mathbf{K}$ such that the closed loop system is robustly stable. More precisely, construct system $\mathbf{G}_1$ from $\mathbf{G}_0$ such that the two closed loop systems in Figure 4.7 are identical, i.e.,

$$\mathbf{\Delta^u} \star (\mathbf{\Delta^p} \star \mathbf{G}_0) \star (\mathbf{\Delta^p} \star \mathbf{K}) = \mathbf{\Delta^u} \star (\mathbf{\Delta^p} \star (\mathbf{\Delta^p} \star (\mathbf{G}_1 \star \mathbf{K}))). \tag{4.35}$$

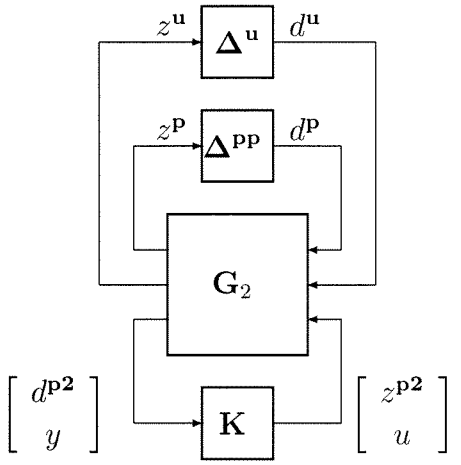

Figure 4.8: Equivalent system

Define the following uncertainty set:

$$\boldsymbol{PP\Delta} := \{\boldsymbol{\Delta}^{\mathbf{pp}} = \mathbf{diag}[\delta_1 I, \delta_1 I, \cdots, \delta_{C^{\mathbf{p}}} I, \delta_{C^{\mathbf{p}}} I] : \delta_i \in \mathcal{L}(l_2), \|\delta_i\| \leq 1\}. \tag{4.36}$$

Thus the multiplicity of each operator in $\boldsymbol{P\Delta}$ has been doubled in size. By rearranging $\mathbf{G}_1$, a new system $\mathbf{G}_2$ can be constructed such that the closed loop systems of Figure 4.7 and the one in Figure 4.8 are identical, i.e.,

$$\boldsymbol{\Delta}^{\mathbf{u}} \star (\boldsymbol{\Delta}^{\mathbf{p}} \star (\boldsymbol{\Delta}^{\mathbf{p}} \star (\mathbf{G}_1 \star \mathbf{K}))) = \boldsymbol{\Delta}^{\mathbf{u}} \star (\boldsymbol{\Delta}^{\mathbf{pp}} \star (\mathbf{G}_2 \star \mathbf{K})). \tag{4.37}$$

The problem formulation is as follows:

Robust Gain Scheduling

Find system $\mathbf{K}$ *which stabilizes* $\mathbf{G}_2$ *and satisfies*

$$\sup_{\boldsymbol{\Delta}^{\mathbf{u}} \in \mathbf{U}\boldsymbol{\Delta}} \sup_{\boldsymbol{\Delta}^{\mathbf{pp}} \in \boldsymbol{PP\Delta}} \left\| (\mathbf{I} - (\mathbf{G}_2 \star \mathbf{K})\, \boldsymbol{\Delta})^{-1} \right\| < \infty, \tag{4.38}$$

where $\boldsymbol{\Delta} := \mathbf{diag}[\boldsymbol{\Delta}^{\mathbf{pp}}, \boldsymbol{\Delta}^{\mathbf{u}}]$.

Remarks:

- In practice, the operators in set $\boldsymbol{P\Delta}$ will be time varying bounded real parameters, not arbitrary bounded operators on l_2. Thus the above condition may be conservative.
- Note that $\mathbf{G}_1$, and hence $\mathbf{G}_2$, is a highly structured system matrix; system $\mathbf{K}$ has full access to $\boldsymbol{\Delta}^{\mathbf{p}}$. This is the key fact utilized in [Packard, 1994] to solve the gain scheduling problem when $\boldsymbol{\Delta}^{\mathbf{u}}$ is unstructured, or one full block.

- Note that the multiplicity of each $\boldsymbol{\delta}_i$ in $\boldsymbol{\Delta}^{\mathbf{P}}$ which $\mathbf{K}$ has access to is assumed to be the same as that which affects system $\mathbf{G}_0$; it is conceivable that allowing more copies of each $\boldsymbol{\delta}_i$ might lead to better performance controllers. It has been shown in [Packard, 1994], however, that one can always do as well with a duplicate copy of $\boldsymbol{\Delta}^{\mathbf{P}}$ for the controller $\mathbf{K}$. This is analogous to standard $\mathcal{H}_\infty$ optimization (and is in fact intimately related), where the order of the controller can always be assumed to be equal to that of the plant.
- The above is a robust stability problem; as in Section 4.3, however, many robust performance problems may be converted to robust stability problems. This is explored in Section 4.4.3.
- As stated in the problem formulation, the $\boldsymbol{\Delta}^{\mathbf{u}}$ and $\boldsymbol{\Delta}^{\mathbf{P}}$ do not have to be causal. But as argued in Section 4.2, all the results hold for causal $\boldsymbol{\Delta}$ as well.

Given linear, time invariant bounded operator $\mathbf{M}$, define the following set in l_2:

$$\bar{\mathcal{D}} := \left\{ d \in l_2^m : D_k \textcircled{T} \Lambda(d) + \bar{D}_k \textcircled{T} \Lambda(\mathbf{M}d) - M_k \leq 0, \;\; 0 \leq k \leq C_{\mathbf{d}} \right\}. \tag{4.39}$$

Set $\bar{\mathcal{D}}$ differs from $\mathcal{D}$ in that an extra term involving $\Lambda(\mathbf{M}d)$ is included in the constraints. As in the definition of $\mathcal{D}$, it is assumed that $0 < M_0 \in \mathbb{R}$, with $D_0 = I \in \mathbb{R}^{m \times m}$, and $\bar{D}_0 = 0 \in \mathbb{R}^{m \times m}$, implying that $\|d\|^2 \leq M_0$. $\bar{\mathcal{D}}^\epsilon$ can be defined analogously to $\mathcal{D}^\epsilon$.

The following corollary is an extension of Theorem 3.6 in Chapter 3:

Corollary 4.4 *Given linear, time invariant, bounded operator* $\mathbf{M}$ *and sets* $\bar{\mathcal{D}}$ *and* $\mathcal{E}$*, the following are equivalent:*

I. *There exists* $\epsilon > 0$ *such that the following supremum is satisfied:*

$$\sup_{e \in \mathcal{E}^\epsilon} \sup_{d \in \bar{\mathcal{D}}^\epsilon} \langle e, \mathbf{M}d \rangle < 1. \tag{4.40}$$

II. *There exist* $0 < X_k \in \mathbb{R}_{\mathbf{P}}^{m_k \times m_k}, 0 \leq k \leq C_{\mathbf{d}}$ *and* $0 < Y_l \in \mathbb{R}_{\mathbf{P}}^{p_l \times p_l}, 0 \leq l \leq C_{\mathbf{e}}$ *such that*

$$\left\| Y^{-\frac{1}{2}} \mathbf{M} X^{-\frac{1}{2}} \right\| < 1, \tag{4.41}$$

$$X := \sum_{k=0}^{C_{\mathbf{d}}} \dot{D}_k \textcircled{T} X_k + \mathbf{M}^* \left(\dot{\bar{D}}_k \textcircled{T} X_k \right) \mathbf{M} > 0, \tag{4.42}$$

$$Y := \sum_{l=0}^{C_{\mathbf{e}}} \dot{E}_l \textcircled{T} Y_l > 0, \tag{4.43}$$

$$T_x := \sum_{k=0}^{C_{\mathbf{d}}} \mathbf{trace}\left(M_k X_k\right) < 1, \tag{4.44}$$

$$T_y := \sum_{l=0}^{C_{\mathbf{e}}} \mathbf{trace}\left(P_l Y_l\right) < 1. \tag{4.45}$$

Remarks:

- The proof of the above claim is essentially equivalent to that of Theorem 3.6 in Chapter 3 when $D_k \textcircled{T} \Lambda(d)$ is replaced by $D_k \textcircled{T} \Lambda(d) + \bar{D}_k \textcircled{T} \Lambda(\mathbf{M}d)$ and $\grave{D}_k \textcircled{T} X_k$ is replaced by $\grave{D}_k \textcircled{T} X_k + \mathbf{M}^*(\grave{\bar{D}}_k \textcircled{T} X_k)\mathbf{M}$. Note, however, that X is now a positive definite operator, not a constant matrix.
- Statement **I** in Corollary 4.4 is stronger than statement **I** in Theorem 3.6. This simplifies the proof that statement **I** implies statement **II** since the continuity property presented in Theorem 3.1 is not required; this continuity property has not been proved for $\bar{\mathcal{D}}$. Conversely, one can only infer from the proof of Theorem 3.6 that statement **II** implies statement **I** in Corollary 4.4 when $\epsilon = 0$; since the inequalities in statement **II** are strict, however, the result follows for some $\epsilon > 0$.
- While the analysis condition can be extended to allow constraints $\bar{\mathcal{D}}$, the synthesis condition in Chapter 3 cannot be extended, in general.

4.4.2 Converting to Generalized l_2 Synthesis Setup

The Robust Gain Scheduling problem will now be converted to the modified Generalized l_2 Synthesis setup of Corollary 4.4. This will result in a scaled $\mathcal{H}_\infty$ condition, which will later be converted to an AMI.

Define the following sets:

$$\bar{\mathcal{D}}^\epsilon := \left\{ d \in l_2 : d = (d^{\mathbf{p}}, d^{\mathbf{u}}),\ \Lambda\left(d_k^{\mathbf{p}}\right) - \Lambda\left((\mathbf{M}d)_k^{\mathbf{p}}\right) \leq \epsilon I,\ \|d_k^{\mathbf{u}}\|^2 \leq 1 + \epsilon \right\}, \tag{4.46}$$

$$\mathcal{E}^\epsilon := \left\{ e \in l_2 : e = (e^{\mathbf{p}}, e^{\mathbf{u}}), \|e^{\mathbf{p}}\|^2 \leq \epsilon,\ \|e_l^{\mathbf{u}}\|^2 \leq 1 + \epsilon \right\}, \tag{4.47}$$

which can readily be put in the form of equations (4.39) and (3.15).

Theorem 4.5 *System* $\mathbf{K}$ *solves the Robust Gain Scheduling problem if and only if* $\mathbf{K}$ *stabilizes* $\mathbf{G}_2$ *and there exists an* $\epsilon > 0$ *such that the following two conditions are satisfied:*

$$\sup_{d \in \bar{\mathcal{D}}^\epsilon} \sup_{e \in \mathcal{E}^\epsilon} \langle e, \mathbf{M}d \rangle < 1, \tag{4.48}$$

$$\bar{\mathcal{D}}^\epsilon \text{ is bounded}, \tag{4.49}$$

where $\mathbf{M} := \mathbf{G}_2 \star \mathbf{K}$.

Proof of Theorem 4.5: The following preliminary lemma is required:

Lemma 4.6 *[Paganini et al., 1994] Given* $x, y \in l_2$, *there exists a linear operator* $\boldsymbol{\delta}$, $\|\boldsymbol{\delta}\| \leq 1$, *such that* $y = \boldsymbol{\delta} I x$ *if and only if* $\Lambda(x) - \Lambda(y) \geq 0$.

Sufficiency: Assume that $\mathbf{K}$ does not solve the Robust Gain Scheduling problem. It suffices to show that either of equations (4.48) or (4.49) is not satisfied. Fix $\epsilon > 0$. By equation (4.38), there exists $n = (n^{\mathbf{p}}, n^{\mathbf{u}}) \in l_2$, $\bar{z} = (\bar{z}^{\mathbf{p}}, \bar{z}^{\mathbf{u}}) \in l_2$, such that $\bar{z} = n + M\mathbf{\Delta}\bar{z}$, $\|n\| \leq \epsilon$, and either of the following two conditions are satisfied:

$$\sum_{l=1}^{C_{\mathbf{e}}^{\mathbf{u}}} \|\bar{z}_l^{\mathbf{u}}\| = 1 \quad , \quad \|\bar{z}^{\mathbf{p}}\| \leq \frac{1}{\sqrt{\epsilon}}; \tag{4.50}$$

$$\sum_{l=1}^{C_{\mathbf{e}}^{\mathbf{u}}} \|\bar{z}_l^{\mathbf{u}}\| \leq 1 \quad , \quad \|\bar{z}^{\mathbf{p}}\| = \frac{1}{\sqrt{\epsilon}}. \tag{4.51}$$

Let $d = (d^{\mathbf{p}}, d^{\mathbf{u}}) := \mathbf{\Delta}\bar{z}$, $z = (z^{\mathbf{p}}, z^{\mathbf{u}}) := \bar{z} - n = \mathbf{M}d$. If equation (4.50) is satisfied, then by Lemmas 4.2 and 4.6 and the norm bound on n the following conditions must be satisfied:

$$\|d_k^{\mathbf{u}}\| \leq 1, \ \Lambda(d_k^{\mathbf{p}}) - \Lambda(z_k^{\mathbf{p}}) \leq \mathrm{O}\left(\sqrt{\epsilon}\right)I; \tag{4.52}$$

$$\sum_{l=1}^{C_{\mathbf{e}}^{\mathbf{u}}} \|z_l^{\mathbf{u}}\| \geq 1 - \mathrm{O}(\epsilon). \tag{4.53}$$

From equation (4.53), one can find $e \in \mathcal{E}$ such that $\langle e, \mathbf{M}d \rangle \geq 1 - \mathrm{O}(\epsilon)$.
If equation (4.51) is satisfied,

$$\|d_k^{\mathbf{u}}\| \leq 1, \ \Lambda(d_k^{\mathbf{p}}) - \Lambda(z_k^{\mathbf{p}}) \leq \mathrm{O}\left(\sqrt{\epsilon}\right)I, \ \|z^{\mathbf{p}}\| \geq \frac{1}{\sqrt{\epsilon}} - \mathrm{O}(\epsilon). \tag{4.54}$$

Since $\mathbf{M}$ is bounded, $\|d^{\mathbf{p}}\| \geq 1/\mathrm{O}\left(\sqrt{\epsilon}\right)$. Since ϵ is arbitrary, at least one of equations (4.48) and (4.49) are not satisfied.

Necessity: Assume that for all $\epsilon > 0$, equation (4.48) is not satisfied. Define $z = \mathbf{M}d$. Then

$$\|d_k^{\mathbf{u}}\|^2 \leq 1 + \epsilon, \ \Lambda(d_k^{\mathbf{p}}) - \Lambda(z_k^{\mathbf{p}}) \leq \epsilon I, \ \sum_{l=1}^{C_{\mathbf{e}}^{\mathbf{u}}} \|z_l^{\mathbf{u}}\| \geq 1 - \mathrm{O}(\epsilon). \tag{4.55}$$

It follows that there exists $\bar{z}, n \in l_2$ such that $\bar{z} = z + n$ with

$$\Lambda(d_k^{\mathbf{p}}) - \Lambda(\bar{z}_k^{\mathbf{p}}) \leq 0, \ \sum_{l=1}^{C_{\mathbf{e}}^{\mathbf{u}}} \|\bar{z}_l^{\mathbf{u}}\| \geq 1 + \epsilon, \ \|n\| \leq \mathrm{O}\left(\sqrt{\epsilon}\right). \tag{4.56}$$

By Lemmas 4.2 and 4.6, there exists $\mathbf{\Delta}$ such that $d = \mathbf{\Delta}\bar{z}$, yielding

$$\bar{z} = (\mathbf{I} - \mathbf{M}\mathbf{\Delta})^{-1} n, \ \|\bar{z}\| \geq 1, \ \|n\| \leq \mathrm{O}\left(\sqrt{\epsilon}\right). \tag{4.57}$$

Since ϵ is arbitrary, equation (4.38) is not satisfied.

Assume that for all $\epsilon > 0$, equation (4.49) is not satisfied. By appropriate scaling, the following equations are satisfied:

$$\|d_k^{\mathbf{u}}\| \leq \epsilon, \quad \Lambda\left(d_k^{\mathbf{p}}\right) - \Lambda\left(z_k^{\mathbf{p}}\right) \leq \epsilon I, \quad \|d^{\mathbf{p}}\| \geq 1. \tag{4.58}$$

It follows that there exists $\bar{z}, n \in l_2$ such that $\bar{z} = z + n$ with

$$\Lambda\left(d_k^{\mathbf{p}}\right) - \Lambda\left(\bar{z}_k^{\mathbf{p}}\right) \leq 0, \quad \sum_{l=1}^{C_{\mathbf{e}}^{\mathbf{u}}} \|\bar{z}_l^{\mathbf{u}}\| \geq \epsilon, \quad \|n\| \leq \mathrm{O}\left(\sqrt{\epsilon}\right). \tag{4.59}$$

By Lemmas 4.2 and 4.6, there exists $\mathbf{\Delta}$ such that $d = \mathbf{\Delta}\bar{z}$, yielding

$$\bar{z} = \left(\mathbf{I} - \mathbf{M}\mathbf{\Delta}\right)^{-1} n, \quad \|\bar{z}\| \geq \|d^{\mathbf{p}}\| \geq 1, \quad \|n\| \leq \mathrm{O}\left(\sqrt{\epsilon}\right). \tag{4.60}$$

Since ϵ is arbitrary, equation (4.38) is not satisfied. ■

We are now in a position to invoke Corollary 4.4:

Theorem 4.7 *System* $\mathbf{K}$ *solves the Robust Gain Scheduling problem if and only if* $\mathbf{K}$ *stabilizes* $\mathbf{G}_2$ *and there exists scales*

$$X_{\mathbf{u}} = \mathbf{diag}[x_1 I, \cdots, x_{C_{\mathbf{d}}^{\mathbf{u}}} I], \quad x_k > 0, \quad \sum_{k=1}^{C_{\mathbf{d}}^{\mathbf{u}}} x_k < 1, \tag{4.61}$$

$$Y_{\mathbf{u}} = \mathbf{diag}[y_1 I, \cdots, y_{C_{\mathbf{e}}^{\mathbf{u}}} I], \quad y_l > 0, \quad \sum_{l=1}^{C_{\mathbf{e}}^{\mathbf{u}}} y_l < 1, \tag{4.62}$$

$$X_{\mathbf{p}} = \mathbf{diag}[X_1, \cdots, X_{C^{\mathbf{p}}}], \quad X_k > 0, \tag{4.63}$$

such that

$$\left\| \begin{bmatrix} X_{\mathbf{p}}^{\frac{1}{2}} & 0 \\ 0 & Y_{\mathbf{u}}^{-\frac{1}{2}} \end{bmatrix} \mathbf{M} \begin{bmatrix} X_{\mathbf{p}}^{-\frac{1}{2}} & 0 \\ 0 & X_{\mathbf{u}}^{-\frac{1}{2}} \end{bmatrix} \right\| < 1. \tag{4.64}$$

Proof of Theorem 4.7: First, note that equation (4.64) is equivalent to

$$\mathbf{M}^* \begin{bmatrix} X_{\mathbf{p}} & 0 \\ 0 & Y_{\mathbf{u}}^{-1} \end{bmatrix} \mathbf{M} - \begin{bmatrix} X_{\mathbf{p}} & 0 \\ 0 & X_{\mathbf{u}} \end{bmatrix} < 0. \tag{4.65}$$

Sufficiency: Assume that the above scales exist, and that equation (4.65) is satisfied. It follows that there exists $Y_{\mathbf{p}} > 0$, sufficiently large, and $\delta > 0$, sufficiently small,

such that

$$\mathbf{M}^* Y^{-1} \mathbf{M} - X < 0, \tag{4.66}$$

$$Y := \begin{bmatrix} Y_{\mathbf{p}} & 0 \\ 0 & Y_{\mathbf{u}} \end{bmatrix} > 0, \tag{4.67}$$

$$X := \begin{bmatrix} X_{\mathbf{p}} & 0 \\ 0 & X_{\mathbf{u}} \end{bmatrix} - \mathbf{M}^* \begin{bmatrix} X_{\mathbf{p}} & 0 \\ 0 & 0 \end{bmatrix} \mathbf{M} > 0, \tag{4.68}$$

$$(1+\delta) \sum_{k=1}^{C_{\mathbf{d}}^{\mathbf{u}}} x_k + \delta \sum_{k=1}^{C_{\mathbf{d}}^{\mathbf{u}}} \mathbf{trace}\,(X_k^{\mathbf{p}}) < 1, \tag{4.69}$$

$$(1+\delta) \sum_{l=1}^{C_{\mathbf{e}}^{\mathbf{u}}} y_l + \delta \mathbf{trace}\,(Y^{\mathbf{p}}) < 1. \tag{4.70}$$

Since $\delta > 0$, it can readily be verified that there exists $\epsilon > 0$ such that $\langle e, Ye \rangle \leq 1 \ \forall e \in \mathcal{E}^\epsilon$ and that $\langle d, Xd \rangle \leq 1 \ \forall d \in \bar{\mathcal{D}}^\epsilon$. Since $X > 0$, this implies that $\bar{\mathcal{D}}^\epsilon$ is bounded, verifying condition (4.49). Invoking the same arguments used in the sufficiency proof of Theorem 3.6, it follows that equation (4.48) is satisfied as well.

Necessity: All the conditions of Corollary 4.4 are satisfied, with the exception of additional constraints $\|e\|^2 \leq P_0$, $\|d\|^2 \leq M_0$ for some $P_0, M_0 > 0$, which are not explicitly included in sets $\mathcal{E}$ and $\bar{\mathcal{D}}$; these constraints are necessary, since the proof of Theorem 3.6 explicitly depends on the presence of these constraints. Since $\mathcal{E}^\epsilon$ is bounded, by construction, and it is given that $\bar{\mathcal{D}}^\epsilon$ is bounded, there exist constants $P_0, M_0 > 0$, sufficiently large, such that constraints $\|e\|^2 \leq P_0$, $\|d\|^2 \leq M_0$ do not affect sets $\mathcal{E}^\epsilon$ and $\bar{\mathcal{D}}^\epsilon$. In addition, there exists $\delta > 0$ such that constraint $\|e^{\mathbf{p}}\|^2 \leq 0$ in $\mathcal{E}$ may be replaced by $\|e^{\mathbf{p}}\|^2 \leq \delta$, since $\mathbf{M}$ and $\bar{\mathcal{D}}$ are bounded. The following scales can thus be constructed, as per Corollary 4.4, such that $\mathbf{M}^* \tilde{Y}^{-1} \mathbf{M} - \tilde{X} < 0$:

$$\tilde{X} = -\mathbf{M}^* \begin{bmatrix} \tilde{X}_{\mathbf{p}} & 0 \\ 0 & 0 \end{bmatrix} \mathbf{M} + \begin{bmatrix} \tilde{X}_{\mathbf{p}} & 0 \\ 0 & \tilde{X}_{\mathbf{u}} \end{bmatrix} + \tilde{X}_0 I > 0, \tag{4.71}$$

$$\tilde{Y} = \begin{bmatrix} \tilde{Y}_{\mathbf{p}} & 0 \\ 0 & \tilde{Y}_{\mathbf{u}} \end{bmatrix} + \tilde{Y}_0 I > 0, \tag{4.72}$$

$$\tilde{X}_{\mathbf{u}} = \mathbf{diag}[\tilde{x}_1 I, \cdots, \tilde{x}_{C_{\mathbf{d}}^{\mathbf{u}}} I], \ \ \tilde{x}_k > 0, \tag{4.73}$$

$$\tilde{Y}_{\mathbf{u}} = \mathbf{diag}[\tilde{y}_1 I, \cdots, \tilde{y}_{C_{\mathbf{e}}^{\mathbf{u}}} I], \ \ \tilde{y}_l > 0, \tag{4.74}$$

$$\tilde{X}_{\mathbf{p}} = \mathbf{diag}[\tilde{X}_1, \cdots, \tilde{X}_{C^{\mathbf{p}}}], \ \ \tilde{X}_k > 0, \tag{4.75}$$

$$\tilde{Y}_{\mathbf{p}} > 0, \tag{4.76}$$

$$\sum_{k=1}^{C_{\mathbf{d}}^{\mathbf{u}}} \tilde{x}_k + M_0 \tilde{X}_0 < 1, \ \ \sum_{l=1}^{C_{\mathbf{e}}^{\mathbf{u}}} \tilde{y}_l + \tilde{Y}_0 P_0 + \delta \mathbf{trace}\left(\tilde{Y}_{\mathbf{p}}\right) < 1. \tag{4.77}$$

Define the following scales:

$$X_{\mathbf{p}} := \tilde{X}_{\mathbf{p}} + \tilde{X}_0 I, \ \ X_{\mathbf{u}} := \tilde{X}_{\mathbf{u}} + \tilde{X}_0 I, \ \ Y_{\mathbf{u}} := \tilde{Y}_{\mathbf{u}} + \tilde{Y}_0 I. \tag{4.78}$$

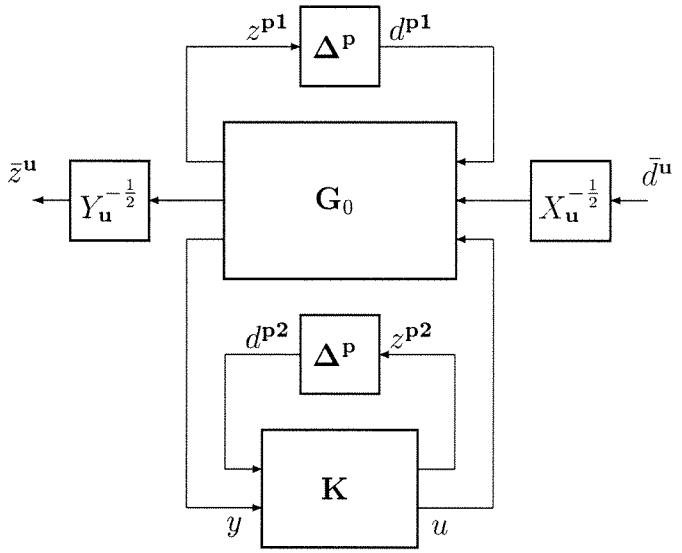

Figure 4.9: Equivalent gain scheduling problem

Since $P_0 \geq C_e^u$ and $M_0 \geq C_d^u$ for constraints $\|e\|^2 \leq P_0$ and $\|d\|^2 \leq M_0$ to be inactive, these scalings satisfy the first three conditions of Theorem 4.7. This leads to the following matrix inequality:

$$\mathbf{M}^* \begin{bmatrix} X_p + \tilde{Y}_p^{-1} - \tilde{X}_0 I & 0 \\ 0 & Y_u^{-1} \end{bmatrix} \mathbf{M} - \begin{bmatrix} X_p & 0 \\ 0 & X_u \end{bmatrix} < 0. \tag{4.79}$$

Since $\delta > 0$, $\tilde{Y}_p$ is bounded. Furthermore, $\tilde{X}_0 < M_0^{-1}$. Thus M_0 can be chosen sufficiently large such that $\tilde{Y}_p^{-1} - \tilde{X}_0 I \geq 0$. This yields equation (4.65), as required. ■

4.4.3 Synthesis Condition

The condition of Theorem 4.7 and the particular structure of $\mathbf{G}_2$ could be used to convert the Robust Gain Scheduling problem to an AMI. Much of this development, however, would duplicate the main results in [Packard, 1994]. The condition of Theorem 4.7 will instead be converted to a form for which the results in [Packard, 1994] may be applied, and an AMI constructed from the resulting conditions.

For fixed scales X_u and Y_u, the conditions of Theorem 4.7 are equivalent to the Gain Scheduling problem of [Packard, 1994] in Figure 4.9; it is required to find a nominally stabilizing controller $\mathbf{K}$ such that

$$\sup_{\Delta^p \in P\Delta} \left\| \left(\Delta^p \star \bar{G}_0\right) \star \left(\Delta^p \star \mathbf{K}\right) \right\| < 1, \tag{4.80}$$

where

$$\bar{\mathbf{G}}_0 := \begin{bmatrix} \mathbf{I} & \mathbf{0} & \mathbf{0} \\ \mathbf{0} & Y_{\mathbf{u}}^{-\frac{1}{2}} & \mathbf{0} \\ \mathbf{0} & \mathbf{0} & \mathbf{I} \end{bmatrix} \mathbf{G}_0 \begin{bmatrix} \mathbf{I} & \mathbf{0} & \mathbf{0} \\ \mathbf{0} & X_{\mathbf{u}}^{-\frac{1}{2}} & \mathbf{0} \\ \mathbf{0} & \mathbf{0} & \mathbf{I} \end{bmatrix}. \tag{4.81}$$

In [Packard, 1994], scalings which commute with $\mathbf{\Delta^P}$ are introduced to convert the above problem to a scaled $\mathcal{H}_\infty$ condition; these scales are in fact the $X_\mathbf{p}$ of the previous section, modulo the transformation from $\mathbf{G}_0$ to $\mathbf{G}_2$. The following result is from [Packard, 1994]:

Theorem 4.8 *Let*

$$\left[\begin{array}{c|ccc} \bar{A}_{11} & \bar{A}_{12} & \bar{B}_{11} & \bar{B}_{21} \\ \hline \bar{A}_{21} & \bar{A}_{22} & \bar{B}_{12} & \bar{B}_{22} \\ \bar{C}_{11} & \bar{C}_{12} & \bar{D}_{11} & \bar{D}_{12} \\ \bar{C}_{21} & \bar{C}_{22} & \bar{D}_{21} & \bar{D}_{22} \end{array}\right]$$

be a minimal state-space description for system $\bar{\mathbf{G}}_0$. There exists a nominally stabilizing controller $\mathbf{K}$ such that equation (4.80) is satisfied if there exist structured positive definite matrices X and Y satisfying an AMI (with structure and AMI outlined in [Packard, 1994]) such that

$$\bar{V}\left(\bar{R}^* \begin{bmatrix} Y & 0 \\ 0 & I \end{bmatrix} \bar{R} - \begin{bmatrix} Y & 0 \\ 0 & I \end{bmatrix}\right) \bar{V}^* < 0, \tag{4.82}$$

$$\bar{U}^*\left(\bar{R} \begin{bmatrix} X & 0 \\ 0 & I \end{bmatrix} \bar{R}^* - \begin{bmatrix} X & 0 \\ 0 & I \end{bmatrix}\right) \bar{U} < 0, \tag{4.83}$$

where

$$\begin{aligned} \bar{R} &= \begin{bmatrix} \bar{A} & \bar{B}_1 \\ \bar{C}_1 & \bar{D}_{11} \end{bmatrix}, \\ \bar{V} = \begin{bmatrix} \bar{V}_1 & \bar{V}_2 \end{bmatrix} &: \begin{bmatrix} \bar{C}_2 & \bar{D}_{21} \\ \bar{V}_1 & \bar{V}_2 \end{bmatrix} \text{invertible}, \quad \bar{C}_2\bar{V}_1^* + \bar{D}_{21}\bar{V}_2^* = 0, \\ \bar{U} = \begin{bmatrix} \bar{U}_1 \\ \bar{U}_2 \end{bmatrix} &: \begin{bmatrix} \bar{B}_2 & \bar{U}_1 \\ \bar{D}_{12} & \bar{U}_2 \end{bmatrix} \text{invertible}, \quad \bar{U}_1^*\bar{B}_2 + \bar{U}_2^*\bar{D}_{12} = 0. \end{aligned} \tag{4.84}$$

Remarks:

- As discussed in [Packard, 1994], it can be assumed without loss of generality that $\begin{bmatrix} \bar{C}_2 & \bar{D}_{21} \end{bmatrix}$ is full row rank; thus there always exists a $\bar{V}$ satisfying equation (4.84). Similarly for $\bar{U}$.

- As stated in the theorem, the above condition is only sufficient for the existence of a $\mathbf{K}$ such that equation (4.80) is satisfied. As argued in the previous section, however, the above condition is also necessary (again assuming that the $\mathbf{\Delta^P}$ are LTV operators).

We are now in a position to state and prove the main result:

Theorem 4.9 *Let*

$$\left[\begin{array}{c|ccc} A_{11} & A_{12} & B_{11} & B_{21} \\ \hline A_{21} & A_{22} & B_{12} & B_{22} \\ C_{11} & C_{12} & D_{11} & D_{12} \\ C_{21} & C_{22} & D_{21} & D_{22} \end{array}\right]$$

be a minimal state-space description for system $\mathbf{G}_0$. *There exists a* $\mathbf{K}$ *which solves the Robust Gain Scheduling problem if and only if there exist scales* $X_{\mathbf{u}}$ *and* $Y_{\mathbf{u}}$ *satisfying the conditions of Theorem 4.7, positive definite matrices* $\bar{X}_{\mathbf{u}}$ *and* $\bar{Y}_{\mathbf{u}}$, *and structured positive definite matrices* X *and* Y *satisfying an AMI (with structure and AMI outlined in [Packard, 1994]), such that*

$$V\left(R^*\begin{bmatrix} Y & 0 \\ 0 & \bar{Y}_{\mathbf{u}} \end{bmatrix} R - \begin{bmatrix} Y & 0 \\ 0 & X_{\mathbf{u}} \end{bmatrix}\right) V^* < 0, \tag{4.85}$$

$$U^*\left(R\begin{bmatrix} X & 0 \\ 0 & \bar{X}_{\mathbf{u}} \end{bmatrix} R^* - \begin{bmatrix} X & 0 \\ 0 & Y_{\mathbf{u}} \end{bmatrix}\right) U < 0, \tag{4.86}$$

$$\begin{bmatrix} X_{\mathbf{u}} & I \\ I & \bar{X}_{\mathbf{u}} \end{bmatrix} \geq 0, \quad \begin{bmatrix} Y_{\mathbf{u}} & I \\ I & \bar{Y}_{\mathbf{u}} \end{bmatrix} \geq 0, \tag{4.87}$$

where

$$\begin{aligned} R &= \begin{bmatrix} A & B_1 \\ C_1 & D_{11} \end{bmatrix}, \\ V = \begin{bmatrix} V_1 & V_2 \end{bmatrix} &: \begin{bmatrix} C_2 & D_{21} \\ V_1 & V_2 \end{bmatrix} \text{invertible}, \quad C_2 V_1^* + D_{21} V_2^* = 0, \\ U = \begin{bmatrix} U_1 \\ U_2 \end{bmatrix} &: \begin{bmatrix} B_2 & U_1 \\ D_{12} & U_2 \end{bmatrix} \text{invertible}, \quad U_1^* B_2 + U_2^* D_{12} = 0. \end{aligned} \tag{4.88}$$

Proof of Theorem 4.9: By the definition of $\bar{\mathbf{G}}_0$, defining

$$\left[\begin{array}{c|cc} \bar{A} & \bar{B}_1 & \bar{B}_2 \\ \hline \bar{C}_1 & \bar{D}_{11} & \bar{D}_{12} \\ \bar{C}_2 & \bar{D}_{21} & \bar{D}_{22} \end{array}\right] := \left[\begin{array}{c|cc} A & B_1 X_{\mathbf{u}}^{-\frac{1}{2}} & B_2 \\ \hline Y_{\mathbf{u}}^{-\frac{1}{2}} C_1 & Y_{\mathbf{u}}^{-\frac{1}{2}} D_{11} X_{\mathbf{u}}^{-\frac{1}{2}} & Y_{\mathbf{u}}^{-\frac{1}{2}} D_{12} \\ C_2 & D_{21} X_{\mathbf{u}}^{-\frac{1}{2}} & D_{22} \end{array}\right] \tag{4.89}$$

yields a minimal state-space representation for $\bar{\mathbf{G}}_0$. Define

$$\tilde{X} := \begin{bmatrix} I & 0 \\ 0 & X_{\mathbf{u}} \end{bmatrix}, \quad \tilde{Y} := \begin{bmatrix} I & 0 \\ 0 & Y_{\mathbf{u}} \end{bmatrix},$$

and U, V, and R as in equation (4.88). Then $\bar{R} = \tilde{Y}^{-\frac{1}{2}} R \tilde{X}^{-\frac{1}{2}}$, and $\bar{V} := V\tilde{X}^{\frac{1}{2}}$, $\bar{U} := \tilde{Y}^{-\frac{1}{2}} U$ satisfy equations (4.84). Substituting into equations (4.82) and (4.83) yields

$$V\left(R^* \begin{bmatrix} Y & 0 \\ 0 & Y_{\mathbf{u}}^{-1} \end{bmatrix} R - \begin{bmatrix} Y & 0 \\ 0 & X_{\mathbf{u}} \end{bmatrix}\right) V^* < 0, \tag{4.90}$$

$$U^*\left(R \begin{bmatrix} X & 0 \\ 0 & X_{\mathbf{u}}^{-1} \end{bmatrix} R^* - \begin{bmatrix} X & 0 \\ 0 & Y_{\mathbf{u}} \end{bmatrix}\right) U < 0. \tag{4.91}$$

Finally, by Schur complement arguments [Zhou et al., 1995], if $\bar{X}_{\mathbf{u}}$ satisfies matrix inequality $\begin{bmatrix} \bar{X}_{\mathbf{u}} & I \\ I & X_{\mathbf{u}} \end{bmatrix} \geq 0$, then $\bar{X}_{\mathbf{u}} \geq X_{\mathbf{u}}^{-1}$. Furthermore, $\bar{X}_{\mathbf{u}} = X_{\mathbf{u}}^{-1}$ satisfies the matrix inequality. This concludes the proof. ∎

Remarks:

- A controller may be constructed as described in [Packard, 1994] using the state-space description for $\bar{\mathbf{G}}_0$ (which includes scales $X_{\mathbf{u}}$ and $Y_{\mathbf{u}}$) and scales X and Y.
- The affine matrix inequalities may be solved using standard convex optimization tools, such as The LMI Control Toolbox [Gahinet et al., 1994].

Example

The robust performance examples of Section 4.3 can now be extended to allow for parameter varying plants. In particular, consider the setup of Figure 4.10. Given system $\mathbf{P}$, it is required to design system $\mathbf{K}$ such that disturbance $\bar{t}_1$ and measurement noise $\bar{t}_2$ have a small effect on plant output w. The plant is subject to inverse additive unstructured uncertainty $\bar{\mathbf{\Delta}}^{\mathbf{u}}$, weighted by $\mathbf{W}_p$. In addition, plant $\mathbf{P} \star \mathbf{\Delta}^{\mathbf{p}}$ is a function of time varying parameters $\mathbf{\Delta}^{\mathbf{p}}$ in set $\boldsymbol{P\Delta}$. The system to be designed, $\mathbf{K}$, has access to these parameters as well. The exact problem formulation is to find a system $\mathbf{K}$ such that the closed loop system is robustly stable and

$$\sup_{\mathbf{\Delta}^{\mathbf{p}} \in \boldsymbol{P\Delta}} \sup_{\|\bar{\mathbf{\Delta}}^{\mathbf{u}}\| \leq 1} \sup_{\|\bar{t}_1\| \leq 1} \sup_{\|\bar{t}_2\| \leq 1} \|w\| < 1. \tag{4.92}$$

Note that if either of $\bar{t}_1$ or $\bar{t}_2$ are vector valued signals, they can further be partitioned and bounded in norm separately. The above can be converted to the problem setup

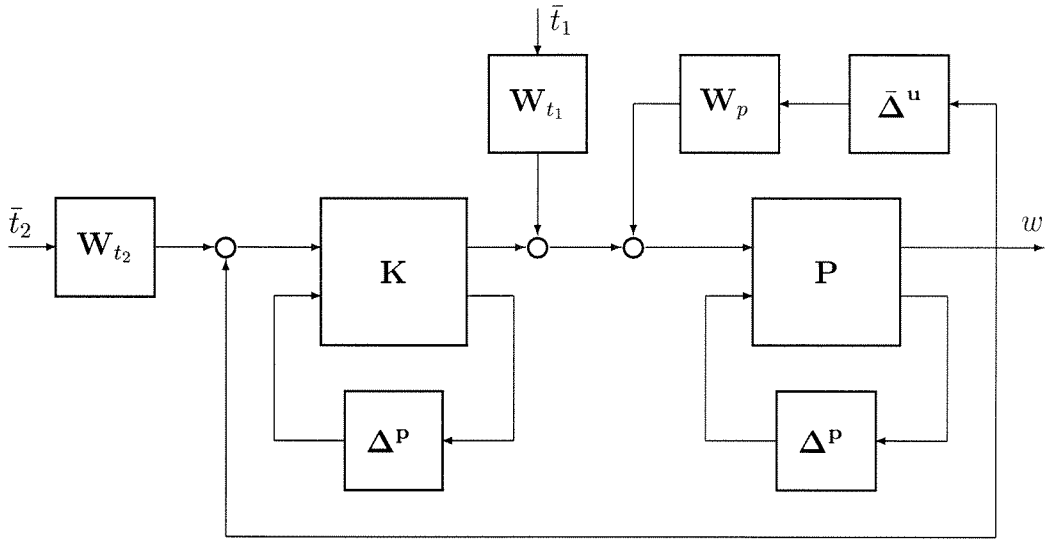

Figure 4.10: Robust gain scheduled disturbance rejection

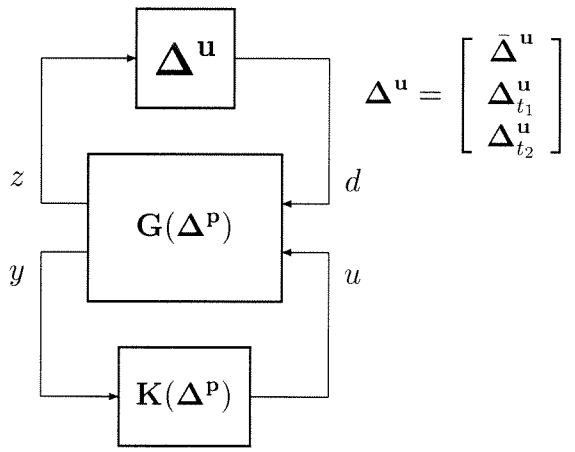

Figure 4.11: Equivalent problem

of Figure 4.7 using techniques similar to those in Section 4.3. The idea is to first apply the tools in Section 4.3, with plant $\mathbf{P} \star \mathbf{\Delta^P}$ and controller $\mathbf{K} \star \mathbf{\Delta^P}$, to convert the above robust performance problem to the robust stability problem of Figure 4.11. The $\mathbf{\Delta^P}$s can then be unwrapped from $\mathbf{G}(\mathbf{\Delta^P})$ and $\mathbf{K}(\mathbf{\Delta^P})$ to yield the block diagram in Figure 4.7.

Chapter 5

Extension to Deterministic Noise Disturbances

In the standard robust control paradigm, the signal space which characterizes performance is equivalent to that which captures a system's uncertainty. For example, $\mathcal{H}_\infty$ tools are used when dealing with bounded energy (or power) gain uncertainty [Packard and Doyle, 1993, Megretski and Treil, 1993], while when working with l_∞ disturbances, the uncertainty is assumed to be of finite amplitude gain [Khammash and Pearson, 1991].

While it is often the case that the particular characterization of the uncertainty is not critical to the design process, the signal space used to characterize the performance often is. In particular, one of the common complaints among control design engineers who use $\mathcal{H}_\infty$ methods is that the resulting designs tend to be sluggish and overly conservative. As an alternative, $\mathcal{H}_2$ designs are often employed. The attractive feature of $\mathcal{H}_2$ designs is their gain interpretation; they minimize the power output when the disturbances are assumed to be white noise or impulses. This is in contrast to $\mathcal{H}_\infty$ designs, which minimize the energy to energy (or power to power) gain; in many applications, modeling the disturbances as arbitrary signals is a poor modeling choice, and thus $\mathcal{H}_\infty$ designs may lead to low performance controllers. A potential problem with $\mathcal{H}_2$ designs, however, is that they lack robustness properties, as first outlined in [Doyle, 1978]. $\mathcal{H}_\infty$ design methods, on the other hand, can readily be extended to encompass a system's uncertainty. A desirable control design strategy would then be one which has the I/O gain interpretation of the $\mathcal{H}_2$ norm, but can readily accommodate $\mathcal{H}_\infty$ bounds on the uncertainty.

In [Paganini, 1993], a framework is developed whereby white noise signals are captured in a deterministic setting. The main motivation behind this approach was the reconciling of the worst case setting, natural when considering robustness issues, with the stochastic setting. This framework proved very natural when addressing the so-called *Robust $\mathcal{H}_2$ Analysis* problem, which was solved in [Paganini et al., 1994] and [Paganini, 1995a]. The elements of this framework relevant to the material presented in this chapter are outlined in Section 2.2.3.

In this chapter, the Generalized l_2 Synthesis results of Chapters 3 and 4 are extended to allow deterministic noise disturbances. In particular, the Square $\mathcal{H}_\infty$

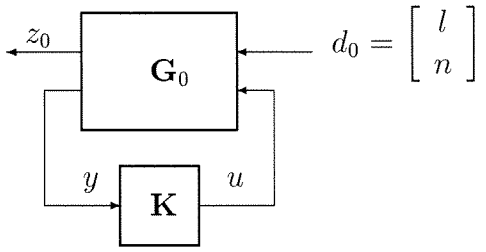

Figure 5.1: Problem Formulation

problem can be extended to provide a solution to the so called mixed $\mathcal{H}_2 - \mathcal{H}_\infty$ problem, and the robust performance problems of Chapter 4 can be extended to allow noise disturbances as well as arbitrary l_2 bounded disturbances.

The chapter is organized as follows: The problem formulation is first outlined in Section 5.1. The solution is obtained by transforming the problem to a Generalized l_2 Synthesis problem in Sections 5.2 through 5.4. Various synthesis problems are solved in Sections 5.5 and 5.6, followed by a simple numerical example which illustrates the tools developed and their numerical properties in Section 5.7. The extension to general Robust $\mathcal{H}_2$ Synthesis is discussed in Section 5.8.

5.1 Problem Formulation

Consider the feedback interconnection of systems $\mathbf{G}_0$ and $\mathbf{K}$ in Figure 5.1, and denote the closed loop system as $\mathbf{M}_0 := \mathbf{G}_0 \star \mathbf{K}$. The problem formulation is as follows:

Generalized l_2 Synthesis with Correlation Constraints

Given system $\mathbf{G}_0$ *and sets* $\mathcal{D}_0$, $\mathcal{E}_0$, *and* $\mathcal{W}_N^m$, *find a stabilizing controller* $\mathbf{K}$ *such that*

$$\sup_{l \in \mathcal{D}_0} \sup_{n \in \mathcal{W}_N^m} \sup_{e_0 \in \mathcal{E}_0} \langle e_0, \mathbf{M}_0 d_0 \rangle < 1. \tag{5.1}$$

Set $\mathcal{D}_0$ and $\mathcal{E}_0$ are of the same form as equation (3.14) and equation (3.15) in Chapter 3. Set $\mathcal{W}_N^m$ is the noise set of Section 2.2.3. Standard $\mathcal{H}_\infty$ and $\mathcal{H}_2$ synthesis can be recast in the above setup. For example, by considering only signals l with constraint $\|l\|^2 \leq 1$ and cost criterion $\|z_0\|^2 < 1$ (implementable by $\|e_0\|^2 \leq 1$), the result is $\mathcal{H}_\infty$ optimization. By considering only signals n with constraint $n \in \mathcal{W}_N^m$ and cost criterion $\|z_0\|^2 < 1$, the resulting design approaches the optimal $\mathcal{H}_2$ design exponentially in N from above, as per Lemma 2.1.

5.2 Image Representation for $\mathcal{W}_N^m$

In this section, an alternate characterization of $\mathcal{W}_N^m$ is presented which is compatible with the Generalized l_2 Synthesis problem formulation. In particular, the Generalized l_2 Synthesis setup does not allow constraints of the form $\Lambda(n, \boldsymbol{\lambda}^\tau n) = 0$ to be imposed. These are exactly the types of constraints required to capture $\mathcal{W}_N^m$.

What will be done instead is to construct a system $\mathbf{V}$, let $n = \mathbf{V}\tilde{n}$, and impose constraints on $\tilde{n}$ which are compatible with the Generalized l_2 Synthesis setup. It is shown that these constraints, plus an additional norm constraint on n, result in $n \in \mathcal{W}_N^m$.

Let N and m be given. Define

$$\mathbf{U}_k := \frac{1+\boldsymbol{\lambda}^k}{\sqrt{8N}}, \qquad \bar{\mathbf{U}}_k := \frac{1-\boldsymbol{\lambda}^k}{\sqrt{8N}} \quad 1 \le k \le N, \tag{5.2}$$

$$\mathbf{U} := \left[\mathbf{U}_1 \ \bar{\mathbf{U}}_1 \ \ldots \ \mathbf{U}_N \ \bar{\mathbf{U}}_N\right], \tag{5.3}$$

$$\mathbf{V} := \mathbf{diag}\left[\mathbf{U}, \mathbf{U}, \cdots, \mathbf{U}\right]. \tag{5.4}$$

Thus $\mathbf{V}$ is an m output, $2mN$ input block diagonal stable system, with m copies of $\mathbf{U}$ on the block diagonal. In can readily be verified that $\mathbf{U}$ and $\mathbf{V}$ are co-inner systems:

$$\mathbf{V}\mathbf{V}^* = \frac{1}{2N}\mathbf{I}, \tag{5.5}$$

and furthermore, $\|\mathbf{V}\| = \|\mathbf{U}\| = \frac{1}{\sqrt{2N}}$.

Define $\tilde{n} \in l_2^{2mN}$ as follows:

$$\begin{aligned} \tilde{n} &:= (\tilde{n}_1, \ \ldots, \ \tilde{n}_m), \\ \tilde{n}_i &:= (n_{i,1}, \ \bar{n}_{i,1}, \ \ldots, \ n_{i,N}, \ \bar{n}_{i,N}), \end{aligned} \tag{5.6}$$

and the following set of constraints:

$$\begin{array}{lllll} \mathbf{C_1}: & \|n_{i,k}\|^2 \le 1, \ \|\bar{n}_{i,k}\|^2 \le 1 & 1 \le i \le m, & 1 \le k \le N \\ \mathbf{C_2}: & \langle n_{i,k}, n_{j,k}\rangle - \langle \bar{n}_{i,k}, \bar{n}_{j,k}\rangle = 0 & 1 \le i < j \le m, & 1 \le k \le N \\ \mathbf{C_3}: & \langle n_{i,k}, \bar{n}_{j,k}\rangle - \langle \bar{n}_{i,k}, n_{j,k}\rangle = 0 & 1 \le i < j \le m, & 1 \le k \le N \\ \mathbf{C_4}: & \langle n_{i,k}, n_{j,k}\rangle + \langle \bar{n}_{i,k}, \bar{n}_{j,k}\rangle = 0 & 1 \le i < j \le m, & k = 1. \end{array} \tag{5.7}$$

The constraint set $\mathcal{N}$ is then defined as:

$$\mathcal{N} := \left\{\tilde{n} \in l_2^{2mN} : \mathbf{C_1}, \ \mathbf{C_2}, \ \mathbf{C_3}, \ \mathbf{C_4} \text{ are satisfied}\right\}. \tag{5.8}$$

The *image set* $\tilde{\mathcal{W}}_{N,\gamma}^m$ may now be defined:

$$\tilde{\mathcal{W}}_{N,\gamma}^m := \left\{n \in l_2^m : n = \mathbf{V}\tilde{n}, \tilde{n} \in \mathcal{N}, \|n_i\| \ge 1 - \gamma\right\}. \tag{5.9}$$

For $\gamma = 1$, define

$$\tilde{\mathcal{W}}_N^m := \tilde{\mathcal{W}}_{N,1}^m, \tag{5.10}$$

which corresponds to no explicit norm constraint on n_i, and can thus be captured with the type of constraints in the Generalized l_2 Synthesis setup, i.e., $\mathcal{N}$ can be captured in the form of equation (3.14), and $\mathcal{N}^\epsilon$ defined analogously. The following theorem outlines how $\mathcal{W}_N^m$ and $\tilde{\mathcal{W}}_{N,\gamma}^m$ are related, and is crucial to the synthesis results which follow:

Theorem 5.1

I. $\tilde{\mathcal{W}}_{N,0}^m = \mathcal{W}_N^m$.

II. $\mathcal{W}_N^m \subset \tilde{\mathcal{W}}_{N,\gamma}^m$ *for* $\gamma \geq 0$.

III. $\mathrm{d}\left(\tilde{\mathcal{W}}_{N,\gamma}^m, \mathcal{W}_N^m\right)$ *is upper semi-continuous as a function of* γ *at* $\gamma = 0$, *where the maximum distance function* $\mathrm{d}(\cdot,\cdot)$ *is defined in equation (2.8).*

The above theorem states that one may replace the constraint $n \in \mathcal{W}_N^m$ by $n = \mathbf{V}\tilde{n}$, $\tilde{n} \in \mathcal{N}$ provided that the norm of each component of n is close to 1. Before proving Theorem 5.1, the following two preliminary lemmas are required:

Lemma 5.2

$$S := \{n \in l_2^m : 2N\mathbf{V}^* n \in \mathcal{N}, \|n_i\| = 1\} = \tilde{\mathcal{W}}_{N,0}^m. \tag{5.11}$$

Proof of Lemma 5.2: Since $\mathbf{V}$ is co-inner, it is clear that by setting $\tilde{n} = 2NV^*n$, $S \subset \tilde{\mathcal{W}}_{N,0}^m$. To show that $\tilde{\mathcal{W}}_{N,0}^m \subset S$, let $n \in \tilde{\mathcal{W}}_{N,0}^m$, where $n = \mathbf{V}\tilde{n}$, $\tilde{n} \in \mathcal{N}$. For each component of n, by constraints $\mathbf{C_1}$, $\|\tilde{n}_i\|^2 \leq 2N$, which implies $\|n_i\|^2 \leq 1$. Thus $\|n_i\|^2 = 1$, $\|\tilde{n}_i\|^2 = 2N$. Since $\mathbf{U}$ is co-inner, there exists stable system $\mathbf{U}_\perp$ such that $\sqrt{2N}\begin{bmatrix} \mathbf{U} \\ \mathbf{U}_\perp \end{bmatrix}$ is unitary. Thus for each i, $\tilde{n}_i$ can be uniquely decomposed as

$$\tilde{n}_i = \mathbf{U}^* v_i + \mathbf{U}_\perp^* w_i, \tag{5.12}$$

where $v_i \in l_2$, $w_i \in l_2^{2N-1}$. Furthermore, $\|\tilde{n}_i\|^2 = \|\mathbf{U}^* v_i\|^2 + \|\mathbf{U}_\perp^* w_i\|^2$. Since $n_i = \mathbf{U}\tilde{n}_i$, it follows that $v_i = 2Nn_i$, and that $\|v_i\| = \|\mathbf{U}^* v_i\|^2 = \|\tilde{n}_i\|^2 = 2N$; thus $w_i = 0$, and $\tilde{n}_i = 2N\mathbf{U}^* n_i$. This implies that $\tilde{n} = 2N\mathbf{V}^* n$, as required. ∎

Lemma 5.3 *Given* $R \in \mathcal{R}_{N,\gamma}^m$, *where* $\gamma < \frac{1}{m(N+1)^2}$, *there exists a signal* $x \in l_2^+$ *such that* $R_x(\tau) = R(\tau)$ *for* $\tau \in [-N, N]$.

The proof of Lemma 5.3 may be found in the appendix at the end of this chapter. We are now in a position to prove Theorem 5.1:

Proof of Theorem 5.1: We begin by showing how n is constrained when $2N\mathbf{V}^*n \in \mathcal{N}$. Let $\tilde{n} = 2N\mathbf{V}^*n$. Thus

$$n_{i,k} = 2N\mathbf{U}_k^* n_i,\ \bar{n}_{i,k} = 2N\bar{\mathbf{U}}_k^* n_i,\ \ 1 \le i \le m,\ 1 \le k \le N. \tag{5.13}$$

By substitution, constraints $\mathbf{C_1}$ to $\mathbf{C_4}$ are equivalent to :

$$\begin{array}{lllll}
\mathbf{C_1}: & \|n_i\|^2 + \langle n_i, \boldsymbol{\lambda}^k n_i\rangle \le 1 & 1 \le i \le m, & 1 \le k \le N & \\
& \|n_i\|^2 - \langle n_i, \boldsymbol{\lambda}^k n_i\rangle \le 1 & 1 \le i \le m, & 1 \le k \le N & \\
\mathbf{C_2}: & \langle n_i, \boldsymbol{\lambda}^k n_j\rangle + \langle n_i, \boldsymbol{\lambda}^{-k} n_j\rangle = 0 & 1 \le i < j \le m, & 1 \le k \le N & \\
\mathbf{C_3}: & \langle n_i, \boldsymbol{\lambda}^k n_j\rangle - \langle n_i, \boldsymbol{\lambda}^{-k} n_j\rangle = 0 & 1 \le i < j \le m, & 1 \le k \le N & (5.14)\\
\mathbf{C_4}: & \langle n_i, n_j\rangle = 0 & 1 \le i < j \le m, & &
\end{array}$$

where $\boldsymbol{\lambda}$ is the unit delay operator defined in equation (2.15).
Proof of I: Let $n \in \mathcal{W}_N^m$. The above constraints are then trivially satisfied, proving $n \in S$ since $\|n_i\|^2 = 1$; thus by Lemma 5.2, $n \in \tilde{\mathcal{W}}_{N,0}^m$. Now let $n \in \tilde{\mathcal{W}}_{N,0}^m$, or equivalently, $n \in S$ by Lemma 5.2. It is then straightforward to show that the above constraints imply that $n \in \mathcal{W}_N^m$, as required.

Proof of II: This follows from **I** and $\tilde{\mathcal{W}}_{N,\gamma}^m \subset \tilde{\mathcal{W}}_{N,\gamma_0}^m$ for $0 \le \gamma \le \gamma_0$.

Proof of III: Let $\epsilon > 0$ be given. It will be shown that there exists a $\gamma_0 > 0$ such that for all $0 \le \gamma \le \gamma_0$, $\mathrm{d}\left(\tilde{\mathcal{W}}_{N,\gamma}^m, \mathcal{W}_N^m\right) < \epsilon$. Let $\gamma_0 > 0$ be fixed. For any $0 \le \gamma \le \gamma_0$, $n \in \tilde{\mathcal{W}}_{N,\gamma}^m$ and corresponding $\tilde{n}$, we may decompose $\tilde{n}$ as in equation (5.12) yielding:

$$\tilde{n}_i = 2N\mathbf{U}^* n_i + \mathbf{U}_\perp^* w_i. \tag{5.15}$$

Since $\|\tilde{n}_i\| \le \sqrt{2N}$ and $\|n_i\| \ge 1 - \gamma_0$, it follows that $\|w_i\| \le 2N\sqrt{2\gamma_0}$. Applying constraints $\mathbf{C_1}$ through $\mathbf{C_4}$ to equation (5.15) results in

$$\begin{array}{lllll}
\mathbf{C_1}: & \|n_i\|^2 + \langle n_i, \boldsymbol{\lambda}^k n_i\rangle \le 1 + O(\|w_i\|) & 1 \le i \le m, & 1 \le k \le N & \\
& \|n_i\|^2 - \langle n_i, \boldsymbol{\lambda}^k n_i\rangle \le 1 + O(\|w_i\|) & 1 \le i \le m, & 1 \le k \le N & \\
\mathbf{C_2}: & |\langle n_i, \boldsymbol{\lambda}^k n_j\rangle + \langle n_i, \boldsymbol{\lambda}^{-k} n_j\rangle| \le O(\|w_i\|) & 1 \le i < j \le m, & 1 \le k \le N & \\
\mathbf{C_3}: & |\langle n_i, \boldsymbol{\lambda}^k n_j\rangle - \langle n_i, \boldsymbol{\lambda}^{-k} n_j\rangle| \le O(\|w_i\|) & 1 \le i < j \le m, & 1 \le k \le N & (5.16)\\
\mathbf{C_4}: & |\langle n_i, n_j\rangle| \le O(\|w_i\|) & 1 \le i < j \le m. & &
\end{array}$$

It follows that there exists a constant C, independent of γ_0, such that $n \in \mathcal{W}_{N,C\sqrt{\gamma_0}}$. Since $n \in l_2$, there exists a $T \in \mathbb{Z}^+$ such that $\left\| n_i - \frac{\boldsymbol{P_T} n_i}{\|\boldsymbol{P_T} n_i\|} \right\| \le 2\gamma_0$. Define

$$\hat{n} := (\hat{n}_1, \ldots, \hat{n}_m), \tag{5.17}$$

$$\hat{n}_i := (1 - \frac{\epsilon}{6\sqrt{m}}) \frac{\boldsymbol{P_T} n_i}{\|\boldsymbol{P_T} n_i\|}. \tag{5.18}$$

It can be shown that for $\gamma_0 \leq \frac{1}{2C}$, $\hat{n} \in \mathcal{W}_{N,2C\sqrt{\gamma_0}}$. Furthermore, $\|n - \hat{n}\| \leq \frac{\epsilon}{6} + 2\sqrt{m}\gamma_0$. Define

$$C_1 := 1 - \left(1 - \frac{\epsilon}{6\sqrt{m}}\right)^2, \tag{5.19}$$

$$R(\tau) := -C_1^{-1} R_{\hat{n}}(\tau), \qquad 1 \leq |\tau| \leq N, \tag{5.20}$$

$$R(0) = C_1^{-1}\left(I - R_{\hat{n}}(0)\right). \tag{5.21}$$

It can be verified that $R \in \mathcal{R}^m_{N,2C\sqrt{\gamma_0}C_1^{-1}}$. By Lemma 5.3, for $\gamma_0 \leq \frac{C_1^2}{8C^2m^2(N+1)^4}$, there exists signal $x \in l_2^+$ such that $R_x(\tau) = R(\tau)$ for $\tau \in [-N, N]$.
Define

$$d := \hat{n} + C_1 \boldsymbol{\lambda}^{N+T+1} x. \tag{5.22}$$

Then

$$\begin{aligned} R_d(\tau) &= R_{\hat{n}}(\tau) + C_1 R_x(\tau) \\ &= 0 \qquad\qquad \tau \neq 0, \\ &= I \qquad\qquad \tau = 0. \end{aligned} \tag{5.23}$$

Thus $d \in \mathcal{W}_N^m$. Furthermore,

$$\begin{aligned} \|n - d\| &\leq \|n - \hat{n}\| + \|\hat{n} - d\| \\ &\leq \frac{\epsilon}{6} + 2\sqrt{m}\gamma_0 + \frac{\epsilon}{3}. \end{aligned} \tag{5.24}$$

Choosing

$$\gamma_0 = \min\left\{\frac{1}{2C}, \frac{C_1^2}{8C^2m^2(N+1)^4}, \frac{\epsilon}{6\sqrt{m}}\right\} \tag{5.25}$$

gives the required result. ∎

5.3 Converting to Generalized l_2 Synthesis Setup

Referring back to Figure 5.1, it is required to find a stabilizing controller $\mathbf{K}$ such that

$$\sup_{l \in \mathcal{D}_0} \sup_{n \in \mathcal{W}_N^m} \sup_{e_0 \in \mathcal{E}_0} \langle e_0, \mathbf{M}_0 d_0 \rangle < 1, \tag{5.26}$$

where $\mathbf{M}_0 := \mathbf{G}_0 \star \mathbf{K}$ and $d_0 = (l, n)$.

The diagram of Figure 5.2 can be used to gain intuition into how the above problem may be converted to a Generalized l_2 Synthesis problem. By the results in the previous section, one can impose the constraint $n \in \mathcal{W}_N^m$ by setting $n = \mathbf{V}\tilde{n}$ and imposing Generalized l_2 Synthesis type of constraints on $\tilde{n}$, along with norm

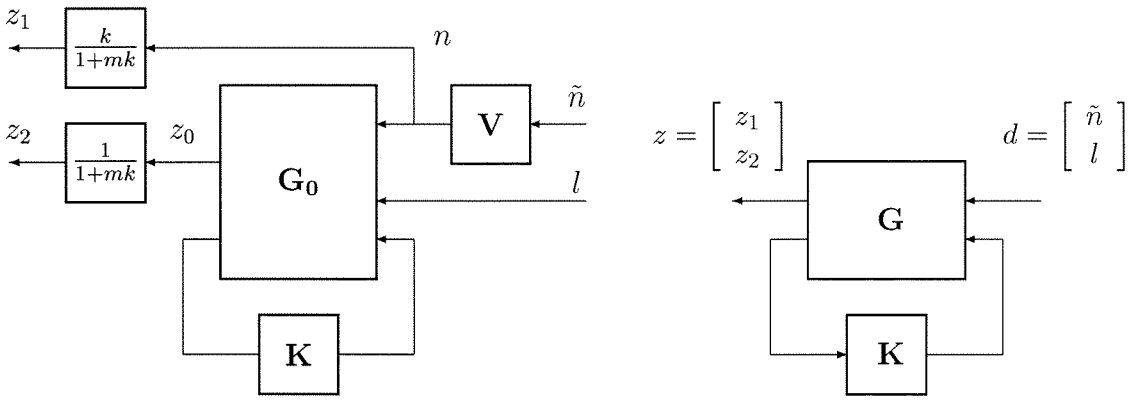

Figure 5.2: Converting to Generalized l_2 Synthesis problem

constraints $\|n_i\| = 1$. There is no direct way to impose this norm constraint on n, so it will be done indirectly. By choosing a large value for k in Figure 5.2, error signal z_1 will dominate error signal z_2; thus the worst case signal is one which makes z_1 as large as possible. But making z_1 as large as possible is equivalent to forcing n to have maximum norm, and thus to be in set $\mathcal{W}_N^m$. We make this more precise as follows:

For fixed k, define

$$\alpha := \frac{1}{1+mk} \tag{5.27}$$

$$\mathbf{G} := \begin{bmatrix} \alpha\mathbf{G}_{11}^l & \alpha\mathbf{G}_{11}^n\mathbf{V} & \alpha\mathbf{G}_{12} \\ 0 & k\alpha\mathbf{V} & 0 \\ \mathbf{G}_{21}^l & \mathbf{G}_{21}^n\mathbf{V} & \mathbf{G}_{22} \end{bmatrix}, \tag{5.28}$$

$$\mathcal{E}^{\mathbf{n}} := \left\{\tilde{e} \in l_2^m : \|\tilde{e}_i\|^2 \leq 1,\ 1 \leq i \leq m\right\}, \tag{5.29}$$

$$\mathcal{D} := \left\{d = (l, \tilde{n}) \in l_2 : l \in \mathcal{D}_0,\ \tilde{n} \in \mathcal{N}\right\}, \tag{5.30}$$

$$\mathcal{E} := \left\{e = (e_0, \tilde{e}) : e_0 \in \mathcal{E}_0,\ \tilde{e} \in \mathcal{E}^{\mathbf{n}}\right\}. \tag{5.31}$$

The following theorem establishes the equivalence of the Generalized l_2 Synthesis with Correlation Constraints problem to an augmented Generalized l_2 Synthesis problem:

Theorem 5.4 *The following two statements are equivalent:*

I. $\mathbf{K}$ *is a stabilizing controller for* $\mathbf{G_0}$ *and*

$$\sup_{l \in \mathcal{D}_0} \sup_{n \in \mathcal{W}_N^m} \sup_{e_0 \in \mathcal{E}_0} \langle e_0, \mathbf{M}_0 d_0 \rangle < 1. \tag{5.32}$$

II. $\mathbf{K}$ *is a stabilizing controller for* $\mathbf{G}$ *and there exists constant* k_0 *such that* $\forall k \geq k_0$,

$$\sup_{d \in \mathcal{D}} \sup_{e \in \mathcal{E}} \langle e, \mathbf{M}d \rangle < 1 \tag{5.33}$$

where $\mathbf{M} := \mathbf{G} \star \mathbf{K}$.

Proof: First note that $\mathbf{K}$ stabilizes $\mathbf{G}_0$ if and only if $\mathbf{K}$ stabilizes $\mathbf{G}$.

II $\Longrightarrow$ **I** : Assume statement **II**. Then by straight substitution

$$\sup_{l\in\mathcal{D}_0}\sup_{\tilde{n}\in\mathcal{N}}\sup_{e_0\in\mathcal{E}_0}\sup_{\tilde{e}\in\mathcal{E}^{\mathbf{n}}}\alpha\left(\langle e_0,\mathbf{M}_0\begin{bmatrix} l \\ \mathbf{V}\tilde{n}\end{bmatrix}\rangle + k\langle\tilde{e},\mathbf{V}\tilde{n}\rangle\right) < 1. \tag{5.34}$$

Since $\mathcal{W}_N^m \subset \tilde{\mathcal{W}}_N^m$ and $\sup_{\|\tilde{e}_i\|^2\leq 1}\langle\tilde{e}_i,(\mathbf{V}\tilde{n})_i\rangle = \|(\mathbf{V}\tilde{n})_i\|$, it follows that

$$\sup_{l\in\mathcal{D}_0}\sup_{n\in\mathcal{W}_N^m}\sup_{e_0\in\mathcal{E}_0}\left(\langle e_0,\mathbf{M}_0 d_0\rangle + k\sum_{i=1}^{m}\|n_i\|\right) < 1+km. \tag{5.35}$$

Since $\|n_i\| = 1$, the result follows.

I $\Longrightarrow$ **II** : Assume statement **I**. By continuity of $\mathrm{d}\left(\tilde{\mathcal{W}}_{N,\gamma}^m, \mathcal{W}_N^m\right)$ at $\gamma = 0$, there exists $\gamma_0 > 0$, constant C_0, and controller $\mathbf{K}$ such that

$$\sup_{l\in\mathcal{D}_0}\sup_{n\in\tilde{\mathcal{W}}_{N,\gamma_0}^m}\sup_{e_0\in\mathcal{E}_0}\langle e_0,\mathbf{M}_0 d_0\rangle \leq C_0 < 1. \tag{5.36}$$

Furthermore, since $\mathbf{M}_0$ is a stable system and $\mathcal{D}_0$, $\tilde{\mathcal{W}}_{N,\gamma_0}^m$, and $\mathcal{E}_0$ are bounded, there exists constant C_1 such that

$$C_1 := \sup_{l\in\mathcal{D}_0}\sup_{n\in\tilde{\mathcal{W}}_N^m}\sup_{e_0\in\mathcal{E}_0}\langle e_0,\mathbf{M}_0 d_0\rangle < \infty. \tag{5.37}$$

If statement **II** is false, for all $\mathbf{K}$ and k there exists l, $\tilde{n}$, e_0, $\tilde{e}$ in their respective sets such that

$$\langle e_0,\mathbf{M}_0\begin{bmatrix} l \\ \mathbf{V}\tilde{n}\end{bmatrix}\rangle + k\langle\tilde{e},\mathbf{V}\tilde{n}\rangle \geq 1+km, \tag{5.38}$$

or equivalently,

$$\sum_{i=1}^{m}\|(\mathbf{V}\tilde{n})_i\| \geq m + \frac{1}{k}\left(\frac{C_0+1}{2} - \langle e_0,\mathbf{M}_0\begin{bmatrix} l \\ \mathbf{V}\tilde{n}\end{bmatrix}\rangle\right). \tag{5.39}$$

In particular, let $k = C_1/\gamma_0$. Then $\|(\mathbf{V}\tilde{n})_i\| \geq 1-\gamma_0$ and thus $n := \mathbf{V}\tilde{n} \in \tilde{\mathcal{W}}_{N,\gamma_0}^m$. Furthermore,

$$\frac{C_0+1}{2} - \langle e_0,\mathbf{M}_0\begin{bmatrix} l \\ \mathbf{V}\tilde{n}\end{bmatrix}\rangle = \frac{C_0+1}{2} - \langle e_0,\mathbf{M}_0 d_0\rangle \leq 0, \tag{5.40}$$

a contradiction of equation (5.36). ∎

Note that $\mathcal{D}$ is consistent with the Generalized l_2 Synthesis formulation of Chapter 3. The solution in Chapter 3 can thus be invoked and provide a solution to the Generalized l_2 Synthesis with Correlation Constraints problem.

	COST
$\mathbf{C_1}$	$2mN$
$\mathbf{C_2}$	$\frac{1}{2}m(m-1)N$
$\mathbf{C_3}$	$\frac{1}{2}m(m-1)N$
$\mathbf{C_4}$	$\frac{1}{2}m(m-1)$
TOTAL	$m\left(2N+(m-1)(N+\frac{1}{2})\right)$

Table 5.1: Cost of constraints

5.4 Computation

A controller $\mathbf{K}$ may be found which satisfies equation (5.33) using the Generalized l_2 Synthesis solution in Chapter 3 for a given k; thus one would choose k, and synthesize a controller. In order to solve the original problem of equation (5.32), however, we need to ensure that $k > k_0$. It is possible to find a lower bound for k_0 given the open loop system $\mathbf{G}$, the number of correlation constraints N, and how closely we want to approximate the optimal solution. In practice, however, k should be chosen as large as the numerical algorithm allows, and the resulting closed loop system analyzed to determine what performance level was achieved.

For a given N and m, it is also worth noting how much constraints $\mathbf{C_1}$ through $\mathbf{C_4}$ cost, in terms of the number of constraints (which is linearly related to the number of decision variables required). This is outlined in Table 5.1; thus the growth is linear in N and quadratic in m. In order to keep the computational complexity down, constraints $\mathbf{C_2}$ through $\mathbf{C_4}$ may be omitted, with the result being that each component of n will tend to be a white noise signal, but may be correlated to other components. The particular nature of the problem will dictate how conservative this omission will be.

In addition, $\mathbf{G}$ consists of an augmented version of $\mathbf{G}_0$. In particular, $\mathbf{V}$ results in an extra mN number of states. Since the number of decision variables grows as the *square* of the number of states of the plant, quadratic growth is unavoidable, both in N and in m.

5.5 Mixed $\mathcal{H}_2 - \mathcal{H}_\infty$ Synthesis

In this section, the problem of synthesizing controllers when the disturbance class consists of a mix of arbitrary l_2 bounded signals and deterministic noise signals is addressed. This in effect provides a solution to the so called mixed $\mathcal{H}_2 - \mathcal{H}_\infty$ problem formulated in [Doyle et al., 1994b], variations of which have been the focus of much research activity this last decade [D'Andrea, 1996b], [D'Andrea and Paganini, 1994], [Stoorvogel, 1993], [Petersen et al., 1993], [Khargonekar and Rotea, 1991], [Bernstein and Haddad, 1989].

Consider the feedback interconnection of Figure 5.1, and denote the closed loop system as $\mathbf{M}_0 := \mathbf{G}_0 \star \mathbf{K}$. Define set $\mathcal{D}_0$ as follows:

$$\mathcal{D}_0 := \left\{ l \in l_2 : \|l_i\|^2 \leq 1 \right\}, \tag{5.41}$$

for some partition of l. The problem formulation is the following:

Mixed $\mathcal{H}_2 - \mathcal{H}_\infty$ Synthesis

Given system $\mathbf{G}_0$ *and set* $\mathcal{D}_0$, *find a stabilizing controller* $\mathbf{K}$ *such that*

$$\lim_{N \to \infty} \sup_{l \in \mathcal{D}_0} \sup_{n \in \mathcal{W}_N^m} \|\mathbf{M}_0 d_0\| < 1, \tag{5.42}$$

where $d_0 := (l, n)$.

The above problem formulation is intimately related to the Square $\mathcal{H}_\infty$ problem of Chapter 4; the only difference is that some of the disturbances are required to satisfy correlation constraints. A specific example of where this problem formulation may arise is tracking a reference signal l (which may be weighted to restrict tracking over a certain frequency range), in the presence of sensor noise or other random disturbance n.

Defining $\mathcal{E}_0 := \left\{ e_0 \in l_2 : \|e_0\|^2 \leq 1 \right\}$, Theorem 5.4 may be applied to convert the Mixed $\mathcal{H}_2 - \mathcal{H}_\infty$ problem to a Generalized l_2 Synthesis problem for fixed N, for which a solution may be found in Chapter 3.

Remarks:

- In order to solve the Mixed $\mathcal{H}_2 - \mathcal{H}_\infty$ Synthesis problem as stated, one might have to choose an arbitrarily large N. As discussed in Section 5.4, however, the computational cost grows substantially as N is increased, as is the order of the resulting controller. One would thus choose an N which gives the required tradeoff between controller/computational complexity and performance improvement. This issue is explored in Section 5.7.
- It is not readily apparent whether a controller which solves the Mixed $\mathcal{H}_2 - \mathcal{H}_\infty$ Synthesis problem can be taken to be of fixed and bounded order. For example, when there is no signal l, the problem reduces to an $\mathcal{H}_2$ synthesis problem, for which the order of the controller has to be no larger than the order of the plant. Similarly, if there is no signal n, the problem reduces to an $\mathcal{H}_\infty$ synthesis problem, where again the order of the controller needs to be no larger than that of the plant. The solution provided in this chapter will yield controllers of arbitrarily large order as N goes to infinity. It remains to be shown whether this is an inherent property of the problem formulation or of the approach taken to solve the problem. Even if a condition for which the order of the controller is bounded exists, it may not be convex in the design parameters (analogous to the Robust l_2 Synthesis problem for LTV uncertainty).

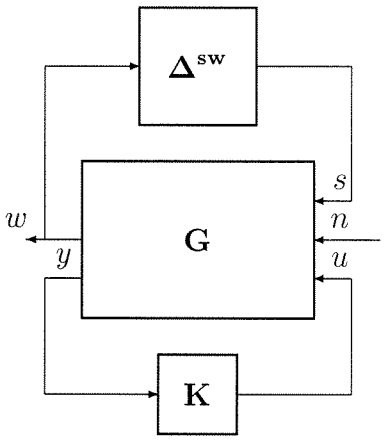

Figure 5.3: Robust $\mathcal{H}_2$ performance

5.6 Synthesis for Robust $\mathcal{H}_2$ Performance

The robust performance results of Chapter 4 may be extended to include deterministic noise disturbances as in the Square $\mathcal{H}_\infty$ problem. Consider the setup of Figure 5.3. The allowable uncertainty set $\mathbf{U}\bar{\mathbf{\Delta}}$ is defined as

$$\mathbf{U}\bar{\mathbf{\Delta}} := \{\mathbf{\Delta}^{\mathbf{sw}} : \mathbf{\Delta}^{\mathbf{sw}} \in \mathcal{L}(l_2), \|\mathbf{\Delta}^{\mathbf{sw}}_{kl}\| \leq 1\}, \tag{5.43}$$

consistent with the following partition of s and w:

$$s_k = \sum_l \mathbf{\Delta}^{\mathbf{sw}}_{kl} w_l. \tag{5.44}$$

The problem is to design a robustly stabilizing controller $\mathbf{K}$ such that the worst case gain from $n \in \mathcal{W}_N^m$ to w is minimized for all allowable uncertainty $\mathbf{\Delta}^{\mathbf{sw}}$. The following corollary is an extension of Theorem 4.3:

Corollary 5.5 *The following statements are equivalent:*

I. $\mathbf{K}$ *is a robustly stabilizing controller for* $\mathbf{G}$ *and* $\mathbf{U}\bar{\mathbf{\Delta}}$*, and*

$$\sup_{\bar{\mathbf{\Delta}} \in \mathbf{U}\bar{\mathbf{\Delta}}} \sup_{n \in \mathcal{W}_N^m} \sum_l \|w_l\| < 1. \tag{5.45}$$

II. $\mathbf{K}$ *is a stabilizing controller for* $\mathbf{G}$ *and*

$$\sup_{\|s_k\| \leq 1} \sup_{n \in \mathcal{W}_N^m} \sum_l \|w_l\| < 1. \tag{5.46}$$

	$\mathcal{H}_\infty$ Analysis	$\mathcal{H}_2$ Analysis	Optimal Controller
$\mathcal{H}_\infty$ Synthesis	1.1429	1.1429	$K = \frac{5}{12}$
$\mathcal{H}_2$ Synthesis	1.7143	0.9897	$K = 1 + 0.3889\lambda$

Table 5.2: Exact synthesis results

Remarks:

- Theorem 5.4 may be applied to statement **II** and thus solve the posed robust performance problem.
- Note that the allowable uncertainty set is a subset of that considered in the robust performance problem of Chapter 4; if signal v were present in the problem formulation, as in Figure 4.4, the proof of Theorem 4.3 could not be extended to Corollary 5.5.
- The types of problems which may be cast into the above setup include the Robust Disturbance Rejection problem of Figure 4.5, where now correlation constraints can be imposed on $\bar{t}_1$ and/or $\bar{t}_2$, forcing them to be white noise signals.
- The Robust Tracking problem of Figure 4.6 cannot be generalized to restrict $\bar{t}$ to be in set $\mathcal{W}_N^m$, since it does not fit into the above framework.

5.7 Numerical Example

A simple example for which the exact solution is known is presented in this section. In particular, the machinery developed in this chapter is used to synthesize an optimal $\mathcal{H}_2$ controller for a given plant. This is not being proposed as a general means to synthesize optimal $\mathcal{H}_2$ controllers, since exact solutions exist; knowing the solution, however, allows us to explore the properties of the algorithm on a simple example.

Consider the following unstable, non-minimum phase, single input, single output plant:

$$\mathbf{P} = \frac{-\boldsymbol{\lambda} + \frac{1}{2}}{\boldsymbol{\lambda} + \frac{2}{3}}. \tag{5.47}$$

The goal is to minimize the $\mathcal{H}_2$ norm of the sensitivity function, $\mathbf{S} = (\mathbf{1} + \mathbf{PK})^{-\mathbf{1}}$. The generalized plant $\mathbf{G}_0$ for this problem is

$$\mathbf{G}_0 = \begin{bmatrix} \mathbf{1} & -\mathbf{P} \\ \mathbf{1} & -\mathbf{P} \end{bmatrix}. \tag{5.48}$$

Table 5.2 summarizes the results obtained using standard synthesis methods, as described in [Dahleh and Diaz-Bobillo, 1995]. The design was then repeated for

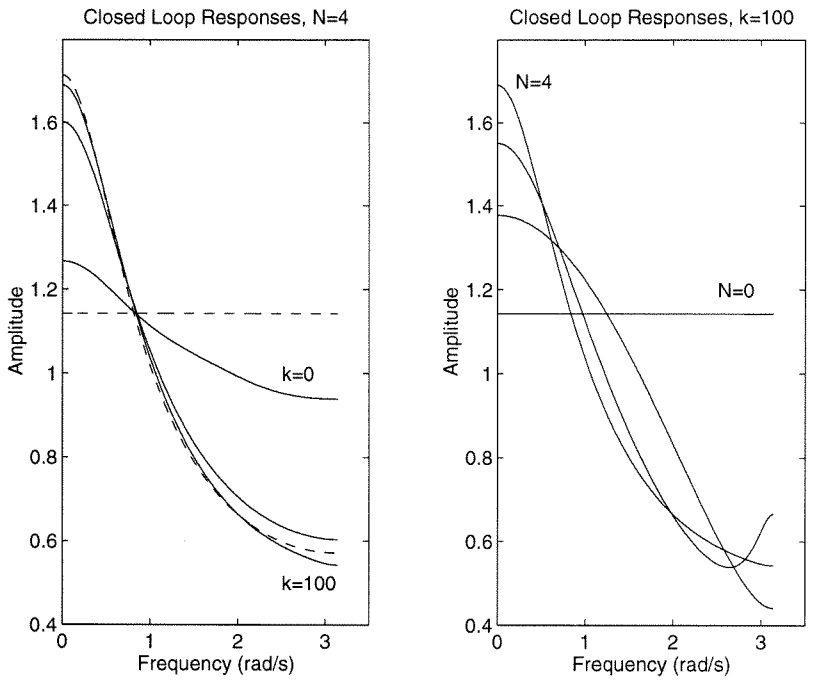

Figure 5.4: Synthesis with constraints

$k = 0, 10, 100$ with N fixed at 4, and for $N = 0, 1, 2, 4$ with k fixed at 100. The resulting closed loop responses (shown as solid lines) are depicted in Figure 5.4, along with the optimal $\mathcal{H}_2$ and $\mathcal{H}_\infty$ results (shown as dashed lines) for comparison purposes.

In the first plot, the flat response is that of the optimal $\mathcal{H}_\infty$ closed loop, while the response with the highest peak is that of the optimal $\mathcal{H}_2$ closed loop. The three intermediate curves correspond to different values of k, ascending values of k corresponding to ascending values of the $\mathcal{H}_\infty$ norm (i.e., the peak at 0 frequency).

In the second plot, ascending values of N correspond to ascending values of the $\mathcal{H}_\infty$ norm. Note that the $N = 0$, $k = 100$ design is identical to the $\mathcal{H}_\infty$ design, as expected.

The $N = 4$, $k = 100$ controller is

$$\mathbf{K} = \frac{1.0079 + 0.3953\boldsymbol{\lambda}}{1 + 0.0306\boldsymbol{\lambda}} \tag{5.49}$$

which is very close to the optimal $\mathcal{H}_2$ controller. Furthermore, the closed loop $\mathcal{H}_2$ norm for this design is 0.9899, and the $\mathcal{H}_\infty$ norm is 1.690, again extremely close to the optimal $\mathcal{H}_2$ design. Note that the $N = 4$ design is not necessarily the "best" one. For example, the $N = 1$ design has a closed loop $\mathcal{H}_2$ norm of 1.021 and $\mathcal{H}_\infty$ norm of 1.377; As a percentage, the $N = 1$ design has $\mathcal{H}_2$ norm which is approximately 3% larger than the $N = 4$ design, but $\mathcal{H}_\infty$ norm which is 23% smaller. The point is that most of the reduction in the $\mathcal{H}_2$ norm occurred with only one constraint; pushing harder to reduce the $\mathcal{H}_2$ norm only serves to increase the $\mathcal{H}_\infty$ norm.

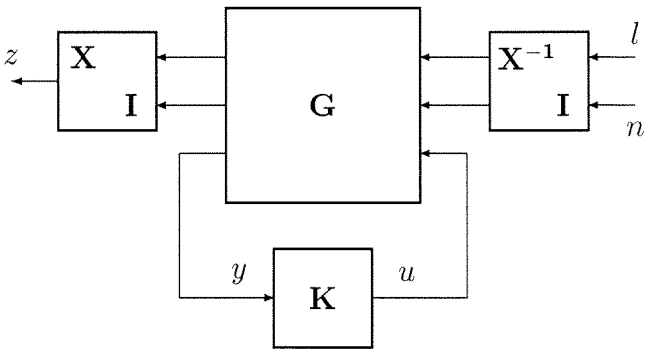

Figure 5.5: Equivalent mixed problem

5.8 Robust $\mathcal{H}_2$ Synthesis

Recall the Robust $\mathcal{H}_2$ Synthesis problem of Section 2.2.4:

Robust $\mathcal{H}_2$ Synthesis

Given system $\mathbf{G}$ *and uncertainty class* $\mathbf{\Delta}$, *find system* $\mathbf{K}$ *such that*

- $\mathbf{\Delta} \star \mathbf{G} \star \mathbf{K}$ *is internally stable for all* $\mathbf{\Delta} \in \mathbf{B\Delta}$.
- $\lim_{N\to\infty} \|\mathbf{\Delta} \star \mathbf{G} \star \mathbf{K}\|_{\mathcal{W}_N^m} < 1$ *for all* $\mathbf{\Delta} \in \mathbf{B\Delta}$.

A scaling $\mathbf{X}$ was introduced to account for the uncertainty $\mathbf{\Delta}$, while a scaling $\mathbf{Y}$ was introduced to account for the input noise disturbance, which led to an iterative synthesis/analysis scheme similar to that of the Robust l_2 Synthesis case. This is shown in Figure 2.7. Scaling $\mathbf{Y}$ was introduced to convert the synthesis step to an $\mathcal{H}_\infty$ optimization; this, in fact, is not necessary. An equivalent condition is the following:

$$\lim_{N\to\infty} \sup_{\frac{\sqrt{m}}{\|n\|} n \in \mathcal{W}_N^m,\ \frac{\|n\|^2}{m} + \|l\|^2 \le 1} \|z\|^2 < 1, \tag{5.50}$$

as depicted in Figure 5.5.

For fixed $\mathbf{X}$, the above reduces to a variant of the Mixed $\mathcal{H}_2 - \mathcal{H}_\infty$ problem presented in Section 5.5 (the difference being that the norms of n and l are coupled); the results in that section can be generalized to include this case. The following iterative procedure can thus be used for controller synthesis for fixed N:

Synthesis: For fixed scales $\mathbf{X}$, find $\mathbf{K}$ which minimizes the closed loop output error in the Mixed $\mathcal{H}_2 - \mathcal{H}_\infty$ problem of Figure 5.5.

Analysis: For fixed $\mathbf{K}$, obtain new scales $\mathbf{X}$ and $\mathbf{Y}$ which minimize the closed loop $\mathcal{H}_\infty$ norm of the system in Figure 2.7 with input $(d_\mathbf{u}, d)$ and output $(z_\mathbf{u}, z)$. This problem may be approximated by an AMI [Paganini, 1995b].

This iterative scheme differs from the one presented in Section 2.2.4 in that scales $\mathbf{Y}$ are not assumed to be fixed during the synthesis iteration (solving the mixed problem is equivalent to solving for the optimal $\mathbf{K}$ *and* for the optimal $\mathbf{Y}$ in the scaled $\mathcal{H}_\infty$ problem). Thus scales $\mathbf{Y}$ are allowed to vary over both the synthesis *and* analysis iterations. This alleviates the first concern outlined in Section 2.2.4, since no new local minima are introduced when considering $\mathcal{H}_2$ performance instead of $\mathcal{H}_\infty$ performance.

Appendix

Proof of Lemma 5.3: Let

$$Q = \begin{bmatrix} \frac{1}{N+1}R(0) & \frac{1}{N}R(1) & \cdots & R(N) \\ \frac{1}{N}R(-1) & \frac{1}{N+1}R(0) & \cdots & \frac{1}{2}R(N-1) \\ \vdots & \ddots & & \vdots \\ R(-N) & \frac{1}{2}R(-N+1) & \cdots & \frac{1}{N+1}R(0) \end{bmatrix} \in \mathbb{R}^{m(N+1)\times m(N+1)}. \tag{5.51}$$

By Gergorshin's Circle Theorem [Strang, 1988], we may bound each eigenvalue of Q from below by

$$\frac{1-m\gamma}{N+1} - \sum_{k=1}^{N} m\gamma > \frac{1-\gamma m(N+1)^2}{N+1}. \tag{5.52}$$

Since $\gamma < \frac{1}{m(N+1)^2}$, $Q > 0$. Thus there exists $P > 0$ such that $P^2 = Q$. Let

$$\bar{P} := \begin{bmatrix} P \\ 0 \end{bmatrix} \in \mathbb{R}^{2m(N+1)\times m(N+1)}, \tag{5.53}$$

i.e., we have added $m(N+1)$ rows of zeros to P. Now define $x(t)$ as follows

$$\begin{bmatrix} x(0) \\ \vdots \\ x\left(2m(N+1)^2\right) \end{bmatrix} := \mathbf{vec}\ (\bar{P},) \tag{5.54}$$

i.e., formed by stacking the columns of $\bar{P}$ into one long vector. We claim that $R_x(\tau) = R(\tau)$ for $|\tau| \leq N$. Partition P as

$$P = \begin{bmatrix} P_{00} & \cdots & P_{0N} \\ \vdots & \ddots & \vdots \\ P_{N0} & \cdots & P_{NN} \end{bmatrix} \tag{5.55}$$

which implies

$$R(\tau) = (N + 1 - |\tau|) \sum_{k=0}^{N} P_{ik} P_{kj}, \quad j = i + \tau. \tag{5.56}$$

Further partitioning each P_{ik} as

$$P_{ik} = \begin{bmatrix} (P_{ik})_1 & \cdots & (P_{ik})_m \end{bmatrix} \tag{5.57}$$

and using the fact that $P_{kj} = P_{jk}^{\mathrm{T}}$, we have

$$R(\tau) = (N + 1 - |\tau|) \sum_{k=0}^{N} \sum_{l=1}^{m} (P_{ik})_l (P_{jk})_l^{\mathrm{T}}, \quad j = i + \tau. \tag{5.58}$$

It thus follows from the definition of $x(t)$ in (5.54), for $0 \leq \tau \leq N$,

$$\begin{aligned} R_x(\tau) &= \sum_{j=0}^{N} \sum_{l=1}^{m} \sum_{i=0}^{N-\tau} (P_{ij})_l (P_{i+\tau,j})_l^{\mathrm{T}} \\ &= \sum_{i=0}^{N-\tau} \sum_{j=0}^{N} \sum_{l=1}^{m} (P_{ij})_l (P_{i+\tau,j})_l^{\mathrm{T}} \\ &= \sum_{i=0}^{N-\tau} \frac{1}{N+1-\tau} R(\tau) \\ &= R(\tau). \end{aligned} \tag{5.59}$$

A similar argument holds for negative τ. ■

Chapter 6

State-Space Manipulations for Behavioral Representations

In this chapter, state-space descriptions are used to represent the behavioral systems introduced in Section 2.3, and various tools to manipulate these representations are developed. The reasons for adopting a state-space framework are twofold: the first is that it provides a convenient method for generalizing the behavioral framework to include uncertainty; this is discussed in Section 6.7. The second is that the $\mathcal{H}_\infty$ Optimal Interconnections problem of Chapter 7 is solved using state-space techniques.

6.1 Output Nulling Representations

Output Nulling (ON) representations are a state-space method of capturing the behavior of a system. In this section, ON representations for systems are introduced, and various tools for manipulating and analyzing systems in this form are developed. These first-order representations are extensively described in [Weiland, 1991]. Some of the results in this section and related algorithms first appeared in [D'Andrea and Paganini, 1993]. Related results on first-order representations and various construction algorithms can be found in [Kuijper, 1992].

Given the following set of equations,

$$\begin{bmatrix} \dot{x} \\ 0 \end{bmatrix} = \begin{bmatrix} A & B \\ C & D \end{bmatrix} \begin{bmatrix} x \\ w \end{bmatrix} =: M \begin{bmatrix} x \\ w \end{bmatrix} \tag{6.1}$$

where $A \in \mathbb{R}^{n\times n}$, $B \in \mathbb{R}^{n\times q}$, $C \in \mathbb{R}^{r\times n}$, $D \in \mathbb{R}^{r\times q}$, and $M \in \mathbb{R}^{(n+q)\times(n+r)}$, the behavior of a system $\Sigma = \{\mathbb{R}, \mathbb{R}^q, \mathcal{B}\}$ is defined to be

$$\mathcal{B} := \{w \in C^\infty : (6.1) \text{ is satisfied for some } x \in C^\infty\}. \tag{6.2}$$

Note that C^∞ functions are considered. This is done to streamline the development and avoid working with distributions. Some of the issues associated with $\mathcal{L}_1^{loc}$ functions are explored in Section 6.5.1. Matrix M is referred to as as a *representation matrix* for Σ. Matrices A, B, C, and D are uniquely specified for a given M and

q; since q will usually be known from context and be constant, M contains all the information required to characterize $\mathcal{B}$.

Since there are many representations which yield the same behavior, it will be useful to define the following equivalence relation: given $M \in \mathbb{R}^{(n+r)\times(n+q)}$ and $\hat{M} \in \mathbb{R}^{(\hat{n}+\hat{r})\times(\hat{n}+q)}$, $M \sim \hat{M}$ if M and $\hat{M}$ yield the same behavior.

Representation matrix M is termed *observable* if (C, A) is an observable pair. Given M, one can always construct observable $\hat{M} \sim M$ by eliminating the unobservable portion of x in (6.1).

M is termed *dependent* if there exists $\hat{M} \sim M$ such that $\hat{r} < r$. Thus a dependent representation has redundant equations.

M is termed *minimal* if $\hat{M} \sim M \Rightarrow \hat{n} \geq n,\ \hat{r} \geq r$. The following lemma establishes a condition for minimality:

Lemma 6.1 *([Weiland, 1991]) Representation matrix M is minimal if and only if it is observable and D is full row rank.*

The following lemma outlines the transformations which may be performed on M to yield equivalent representations:

Lemma 6.2 *([Weiland, 1991]) Given a (minimal) representation matrix M, $\hat{M}$ is an equivalent representation matrix if (and only if)*

$$\hat{M} = \begin{bmatrix} T^{-1}(A+LC)T & T^{-1}(B+LD) \\ PCT & PD \end{bmatrix}, \tag{6.3}$$

where L is any matrix, P and T are any square, invertible matrices.

6.1.1 Constructing ON Representations from AR Representations

The following procedure yields an observable, but not necessarily minimal, ON representation given an AR representation. The reduction procedure of Section 6.1.2 can be used to make the resulting representation minimal.

Given the following set of AR equations

$$R_L \frac{d^L w}{dt^L} + \cdots + R_0 w = 0, \tag{6.4}$$

consider the following set of equations:

$$\begin{aligned} \dot{x}_1 &= R_0 w, \\ &\vdots \\ \dot{x}_L &= x_{L-1} + R_{L-1} w, \end{aligned} \tag{6.5}$$

$$0 = x_L + R_L w, \tag{6.6}$$

which can be captured in ON form by setting M equal to

$$M := \begin{bmatrix} 0 & R_0 \\ I & \hat{R} \end{bmatrix}, \text{ with } \hat{R} := \begin{bmatrix} R_1 \\ \vdots \\ R_L \end{bmatrix}. \tag{6.7}$$

Note that the above partition for M *does not* correspond to the partition of equation (6.1). By repeated differentiation of equation (6.6) and substituting for the x_l, it immediately follows that any w which satisfies the ON equations must also satisfy the AR equations. To show the converse, let w satisfy the AR equations. By integrating (6.4) L times, it follows that

$$R_L w(t) + x_L(t) = 0, \tag{6.8}$$

where

$$x_l(t) := \int_0^t (x_{l-1}(\tau) + R_{L-1} w(\tau))\, d\tau + c_l, \quad c_l \in \mathbb{R} \tag{6.9}$$

for $1 \leq l \leq L$. These x_l and w also satisfy the ON equations.

Note that M in (6.7) is not necessarily minimal, since R_L need not be full row rank. The total number of states in this representation are rL. By building an ON representation for each AR equation, and interconnecting them as described in Section 6.4, a lower state dimension representation can be constructed, with the total number of states equal to $\sum d_l(R(\xi))$, with $d_l(R(\xi))$:= the degree of the l-th row of $R(\xi)$. The resulting representation is minimal if and only if the *leading coefficient matrix* of $R(\xi)$ is of full row rank; equivalently, if $R(\xi)$ is *row proper* [Willems, 1992].

6.1.2 Constructing Minimal ON Representations

Let M be an observable representation matrix. Let P_1^* be a basis for Im $(\begin{bmatrix} C & D \end{bmatrix})$, P_2^* a basis for Im $(P_1 D)$, and T_1 a basis for Ker $(P_2^{\perp} P_1 C)$. Define

$$P := \begin{bmatrix} P_2 P_1 \\ P_2^{\perp} P_1 \\ P_1^{\perp} \end{bmatrix}, \quad T := \begin{bmatrix} T_1 & T_1^{\perp} \end{bmatrix}. \tag{6.10}$$

Applying the behavior preserving transformations of Lemma 6.2 results in the following equivalent representation

$$\begin{bmatrix} A_{11} & A_{12} & B_1 \\ A_{21} & A_{22} & B_2 \\ C_1 & C_2 & D_1 \\ 0 & C_4 & 0 \\ 0 & 0 & 0 \end{bmatrix}, \tag{6.11}$$

where C_4 is an invertible, square matrix. Partitioning x into x_1 and x_2, consistent with the partition in (6.11), the second to last equation implies that $x_2 = 0$, and hence $\dot{x}_2 = 0$. It follows that that following is an equivalent, observable representation:

$$\begin{bmatrix} A_{11} & B_1 \\ C_1 & D_1 \\ A_{21} & B_2 \end{bmatrix}. \tag{6.12}$$

The above procedure can be repeated until the resulting D matrix has full row rank. Note that the above procedure yields an equivalent representation with less number of states n, or less number of equations r (or both), if the original representation was not minimal.

6.2 I/O Maps

Given a minimal representation matrix $M \in \mathbb{R}^{(n+r)\times(n+q)}$, it is a straightforward matter to construct a proper, I/O parameterization of the behavior $\mathcal{B}$. Since D is full row rank, there exists a re-ordering of variables $w = (y, u)$ such that $D = \begin{bmatrix} D_y & D_u \end{bmatrix}$ with D_y square and invertible, and $B = \begin{bmatrix} B_y & B_u \end{bmatrix}$. By the transformations of Lemma 6.2 ($P = D_y^{-1}$, $L = -B_y D_y^{-1}$), it follows that the following is an equivalent parameterization of $\mathcal{B}$:

$$\begin{bmatrix} \dot{x} \\ y \end{bmatrix} = \begin{bmatrix} A - B_y D_y^{-1} C & B_u - B_y D_y^{-1} D_u \\ -D_y^{-1} C & -D_y^{-1} D_u \end{bmatrix} \begin{bmatrix} x \\ u \end{bmatrix}. \tag{6.13}$$

It can be shown that all proper I/O maps may be generated in this fashion [Willems, 1991]. Note that the number of outputs is equal to r, and the number of inputs $q - r$. As shown in [Willems, 1991], these are integer invariants, thus all I/O maps (proper or not) must have r outputs and $q - r$ inputs.

A variable w_i is said to be *free* if it can take on all values in C^∞ and still be consistent with the behavior $\mathcal{B}$. Equivalently, the system description provides no information on the properties of variable w_i. It is shown in [Willems, 1991] that the maximum number of free variables must be equal to the number of input variables, $q - r$, and leads to the following corollary:

Corollary 6.3 *Given that a representation matrix M is not dependent, the number of outputs in any I/O map is r, and the number of free variables is at most $q - r$.*

6.3 Stability

A system Σ with variables w is said to be *stable* if $w \in \mathcal{B} \Rightarrow w(t) \longrightarrow 0$ as $t \longrightarrow \infty$. Let M be an observable representation matrix for Σ. The following is a characterization of stability:

Lemma 6.4 *Given an observable representation matrix M, Σ is stable if and only if*

$$\begin{bmatrix} A - sI & B \\ C & D \end{bmatrix} \quad \textit{is full column rank } \forall s \in \mathbb{C}^+. \tag{6.14}$$

Proof: Assume that (6.14) is not full column rank for some $s_0 \in \mathbb{C}^+$. Then there exist complex vectors v_1 and v_2 such that $x(t) = v_1 e^{s_0 t}$ and $w(t) = v_2 e^{s_0 t}$ satisfy the ON equations. Note that by observability, $v_2 \neq 0$. Furthermore, since Re $(s_0) \geq 0$, $w(t)$ does not decay to zero. If s_0 is purely real, v_1 and v_2 can be taken to be real, implying that $w(t)$ is real; note that if s_0 has an imaginary component, the real parts of $x(t)$ and $w(t)$ are non-zero and will also satisfy the ON equations.
Now assume that (6.14) is full column rank. D is not necessarily full row rank, but by applying the reduction procedure of Section 6.1.2, it can be shown that the resulting minimal representation will also satisfy the rank condition of (6.14). This implies that the resulting D matrix is square and invertible. Setting $P = D^{-1}$, $L = -BD^{-1}$, and applying the transformations of Lemma 6.2, the following is an equivalent representation matrix for Σ:

$$\begin{bmatrix} A - BD^{-1}C & 0 \\ D^{-1}C & I \end{bmatrix} =: \begin{bmatrix} \hat{A} & 0 \\ \hat{C} & I \end{bmatrix}, \tag{6.15}$$

where the rank condition implies that $\hat{A}$ is Hurwitz. The only solutions to these equations are $w(t) = \hat{C}e^{\hat{A}t}x_0$, which decay to zero. ∎

6.4 Interconnection

If Σ_1 and Σ_2 are two dynamical systems, their interconnection can simply be considered as imposing the laws of both Σ_1 and Σ_2. Formally the *interconnection* of $\Sigma_1 = (\mathbb{R}, \mathbb{R}^q, \mathcal{B}_1)$ and $\Sigma_2 = (\mathbb{R}, \mathbb{R}^q, \mathcal{B}_2)$ is denoted by $\Sigma_1 \wedge \Sigma_2$ and defined as

$$\Sigma_1 \wedge \Sigma_2 := \{\mathbb{R}, \mathbb{R}^q, \mathcal{B}_1 \cap \mathcal{B}_2\}. \tag{6.16}$$

Thus interconnection can be interpreted as the intersection of behaviors, or as combining constraint equations. Thus an allowable trajectory must satisfy the governing equations of both systems.

There are several integer invariants associated with a system Σ [Willems, 1991]. One is $p^*(\Sigma)$, the number of outputs in any I/O map; given a representation which is not dependent, this invariant is equal to r. Another is the minimum number of states required to describe Σ in ON form, $n^*(\Sigma)$; given a minimal representation, this invariant is equal to n.

As defined in [Willems, 1992], $\Sigma_1 \wedge \Sigma_2$ is termed a *feedback interconnection* if

$$p^*(\Sigma_1 \wedge \Sigma_2) = p^*(\Sigma_1) + p^*(\Sigma_2). \tag{6.17}$$

An interpretation of the above is that the laws of the systems can be viewed as independent. A feedback interconnection is termed *regular* if

$$n^*(\Sigma_1 \wedge \Sigma_2) = n^*(\Sigma_1) + n^*(\Sigma_2). \tag{6.18}$$

If $n^*(\Sigma_1 \wedge \Sigma_2) < n^*(\Sigma_1) + n^*(\Sigma_2)$, the interconnection is termed *singular*. Regular feedback interconnections are the standard ones considered in feedback control. Singular feedback interconnections differ in that the interconnection results in algebraic constraints on the states; thus the states of the individual systems must be matched before interconnection can take place.

Perhaps the simplest example of a singular interconnection is connecting two capacitors in parallel; the voltages across each capacitor must be the same before interconnection, else an infinite (in practice, "large") current will flow between the two components. In terms of the invariant n, one state (the voltage across the capacitor) is required to describe each component, but only one state is required to describe the two capacitors in parallel, not two, since the voltages across each capacitor are required to be the same.

One may think of interconnection in two contexts. First, when interconnection is simply an artifice of the modeling process, where the system has been broken into subsystems. Second, when a physical interconnection is established at a particular time. When interconnecting for modeling, a singular interconnection is simply a flag that the states are constrained and therefore one might want to simplify the model. When connecting two systems at a particular instant in time, however, a singular interconnection would require that the states be matched in advance, otherwise a transient phenomenon will occur which is not modeled and is potentially damaging; in the simple parallel capacitors example, the residual charges on the two capacitors must be compatible, otherwise a large current may flow at the time of contact.

The following lemma can be used to construct a representation matrix for the interconnection of two systems:

Lemma 6.5 *Given minimal representations matrices M_1 and M_2 for systems Σ_1 and Σ_2,*

$$M := \begin{bmatrix} A_1 & 0 & B_1 \\ 0 & A_2 & B_2 \\ C_1 & 0 & D_1 \\ 0 & C_2 & D_2 \end{bmatrix} \tag{6.19}$$

is a representation matrix for $\Sigma = \Sigma_1 \wedge \Sigma_2$. The interconnection is a feedback interconnection if and only if M is not dependent; the feedback interconnection is regular if and only if M is minimal.

Proof: The definition of interconnection immediately implies that M is a representation matrix for Σ. The equivalence between the interconnection being a feedback interconnection and M not being dependent is a direct consequence of Corollary 6.3. The equivalence between regularity and minimality of M is a direct consequence of (C, A) being an observable pair. ∎

6.5 Latent Variable Elimination

Given a system Σ, with behavior $\mathcal{B}$ and variables $w = (v, l)$, it is required to construct a representation for system $\Sigma_{\mathbf{v}}$ with behavior $\mathcal{B}_{\mathbf{v}}$ defined by:

$$\mathcal{B}_{\mathbf{v}} := \{v \in C^\infty : (v, l) \in \mathcal{B} \text{ for some } l \in C^\infty\}\,. \tag{6.20}$$

In the terminology of [Willems, 1991], variables l are the *latent* variables, while variables v are the *manifest* variables. The latent variables are thus seen as auxiliary variables used to describe the system, while the manifest variables are presumably the variables of interest. Let M be a minimal representation matrix for Σ:

$$M = \begin{bmatrix} A & B_v & B_l \\ C & D_v & D_l \end{bmatrix}. \tag{6.21}$$

Let V_3 be a basis for $\mathrm{Ker}\left(\begin{bmatrix} B_l \\ D_l \end{bmatrix}\right)$, and V_2 a basis for $\left(\mathrm{Ker}\begin{bmatrix} B_l \\ D_l \end{bmatrix}\right)^\perp \cap \mathrm{Ker}(D_l)$. Let $V_1 = \begin{bmatrix} V_2 & V_3 \end{bmatrix}^\perp$. Since $D_l V_1$ is full column rank, there exists L such that $(B_l + LD_l)V_1 = 0$. Define $P := \begin{bmatrix} V_1^* D_l^* \\ (V_1^* D_l^*)^\perp \end{bmatrix}$ and $T := \begin{bmatrix} V_2^* B_l^* \\ (V_2^* B_l^*)^\perp \end{bmatrix}^{-1}$. Defining $l =: V_1 l_1 + V_2 l_2 + V_3 l_3$ and applying the behavior preserving transformations of Lemma 6.2 results in the following representation which does not change behavior $\mathcal{B}_{\mathbf{v}}$ (since V is square and invertible):

$$\begin{bmatrix} A_{11} & A_{12} & B_{v,1} & 0 & B_{l_2} & 0 \\ A_{21} & A_{22} & B_{v,2} & 0 & 0 & 0 \\ C_{11} & C_{12} & D_{v,1} & D_{l_1} & 0 & 0 \\ C_{21} & C_{22} & D_{v,2} & 0 & 0 & 0 \end{bmatrix}, \tag{6.22}$$

where B_{l_2} and D_{l_1} are square and invertible. Let state x be partitioned into x_1 and x_2, consistent with the above partition.

Proposition 6.6 *The following ON representation, with x_1 a latent variable, captures behavior $\mathcal{B}_{\mathbf{v}}$:*

$$\begin{bmatrix} A_{22} & B_{v,2} & A_{21} \\ C_{22} & D_{v,2} & C_{21} \end{bmatrix}. \tag{6.23}$$

Proof: If v satisfies (6.22), it must also satisfy (6.23); if v satisfies (6.23) for some x_1, it also satisfies (6.22) by appropriately defining l_1 and l_2. ∎

The above procedure can be repeated until there are no more latent variables left. Note that the minimality of the representation is not necessarily preserved, since (C_{22}, A_{22}) need not be an observable pair; in that case, however, the unobservable modes can be truncated to yield a minimal representation.

6.5.1 Proper Elimination

The elimination procedure just outlined is valid as long as the behavior consists of C^∞ trajectories. Problems arise, however, if the larger class of locally absolutely integrable trajectories, $\mathcal{L}_1^{loc}$, are considered. In particular, such an elimination also captures the closure of $\mathcal{B}_{\mathbf{v}}$ in the topology of $\mathcal{L}_1^{loc}$, denoted $\overline{\mathcal{B}}_{\mathbf{v}}$, as discussed in [Rapisarda and Willems, 1996]. A simple example is presented shortly to illustrate this fact.

There are several reasons why one might want to consider $\mathcal{L}_1^{loc}$ trajectories. The most compelling one, from an aesthetic point of view, is that functions such as steps and ramps should not be excluded from the allowable behavior. From a practical point of view, this may be dismissed as irrelevant since one can argue that all "real signals" are C^∞, and that discontinuities are a human abstraction. While this may very well be the case, it is useful to consider what effects steps and ramps have on a system; one would be reluctant to construct an amplifier which results in unbounded outputs for step-like inputs.

In terms of latent variable elimination, one might want to know if the removed latent variables are well behaved for all possible manifest trajectories, including steps and ramps, consistent with the manifest behavior. As a simple example, consider the following equation:

$$\dot{v} = l, \tag{6.24}$$

where the solutions are taken to be in $\mathcal{L}_1^{loc}$. In terms of the manifest behavior $\mathcal{B}_{\mathbf{v}}$, this system is equivalent to

$$0v = 0 \tag{6.25}$$

with the *additional* smoothness constraint that v be absolutely continuous. By considering $\overline{\mathcal{B}}_{\mathbf{v}}$, this constraint is eliminated and v can be any $\mathcal{L}_1^{loc}$ trajectory.

It may be desirable to know when these smoothness constraints on v exist, however, as previously argued:

Theorem 6.7 *Let M, as per equation (6.21), be a minimal representation matrix for Σ. $\mathcal{B}_{\mathbf{v}} = \overline{\mathcal{B}}_{\mathbf{v}}$ if and only if rank$(D_l) = p^*(\Sigma) - p^*(\Sigma_v)$.*

Proof:

$\Longleftarrow$: Assume that the rank condition is satisfied. Since M is a minimal representation matrix, rank$(\begin{bmatrix} D_v & D_l \end{bmatrix}) = p^*(\Sigma)$. By assumption, there exists a partition of latent variables l into l_1 and l_2 with the size of l_1 equal to rank(D_l), and a partition of the manifest variables v into y and u with the size of y equal to $p^*(\Sigma_v)$, such that $\begin{bmatrix} D_{l_1} & D_y \end{bmatrix}$ is invertible (after allowing for re-ordering of variables l and v). As per Section 6.2, construct the following I/O representation of Σ from representation matrix M:

$$\begin{aligned} \dot{x} &= \tilde{A}x + \tilde{B}_1 u + \tilde{B}_2 l_2, \\ y &= \tilde{C}_1 x + \tilde{D}_{11} u + \tilde{D}_{12} l_2, \\ l_1 &= \tilde{C}_2 x + \tilde{D}_{21} u + \tilde{D}_{22} l_2. \end{aligned} \tag{6.26}$$

First, note that variables u are free in C^∞ (and $\mathcal{L}_1^{loc}$ as well), and are thus legitimate input variables for both $\mathcal{B}$ and $\mathcal{B}_\mathbf{v}$. By the rank assumption and Corollary 6.3, however, the size of u constitutes the maximum number of free variables for $\mathcal{B}_\mathbf{v}$. From this it can be concluded that the transfer function from l_2 to y must be zero; if this were not the case, there would exist at least one component of y which is free in C^∞ for $u \equiv 0$. Thus

$$\begin{aligned} \dot{x} &= \tilde{A}x + \tilde{B}_1 u, \\ y &= \tilde{C}_1 x + \tilde{D}_{11} u, \end{aligned} \tag{6.27}$$

is a valid parameterization of $\overline{\mathcal{B}}_\mathbf{v}$. Note, however, that for all $(y, u) \in \mathcal{L}_1^{loc}$ satisfying equations (6.27), $(l_1, l_2) = (\tilde{C}_2 x + \tilde{D}_{21} u, 0) \in \mathcal{L}_1^{loc}$ satisfies equations (6.26) as well, proving that $\mathcal{B}_\mathbf{v} = \overline{\mathcal{B}}_\mathbf{v}$.

$\Longrightarrow$: Assume that the rank condition is not satisfied. If $\text{rank}(D_l) > p^*(\Sigma) - p^*(\Sigma_v)$, form an I/O representation for Σ as in the previous construction with the size of y *less* than $p^*(\Sigma)$; this implies that $p^*(\Sigma_\mathbf{v}) < p^*(\Sigma_\mathbf{v})$, obviously a contradiction. Thus the assumption implies that $\text{rank}\,(D_l) < p^*(\Sigma) - p^*(\Sigma_v)$. For any I/O partition of manifest variables v into y and u:

$$\begin{aligned} \text{rank}\left(\begin{bmatrix} D_l & D_y \end{bmatrix}\right) &\leq \text{rank}(D_l) + \text{rank}(D_y) \\ &< p^*(\Sigma) - p^*(\Sigma_\mathbf{v}) + \text{rank}(D_y) \\ &\leq p^*(\Sigma). \end{aligned} \tag{6.28}$$

Thus for all I/O partitions of manifest variables v into y and u, there exists a column of D_u which is not in the column space of $\begin{bmatrix} D_l & D_y \end{bmatrix}$. For any given partition, let j^* be such a column. Let $u(t)$ be the following $\mathcal{L}_1^{loc}$ time trajectory:

$$\begin{aligned} u(t) &= 0 \text{ for } t < 0, \\ u_j(t) &= 0 \text{ for } t \geq 0, \quad j \neq j^*, \\ u_{j^*}(t) &= 1 \text{ for } t \geq 0, \end{aligned} \tag{6.29}$$

resulting in the following equation,

$$D_{u_{j^*}} = C\left(x(0^-) - x(0^+)\right) + D_l\left(l(0^-) - l(0^+)\right) + D_y\left(y(0^-) - y(0^+)\right). \tag{6.30}$$

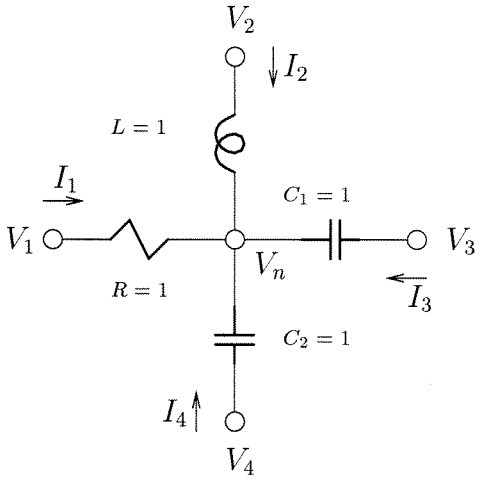

Figure 6.1: Circuit example

This implies that $x(0^-) - x(0^+) \neq 0$, contradicting the fact that x must be absolutely continuous for all l and v in $\mathcal{L}_1^{loc}$. Thus trajectory u above is not an allowable trajectory, which implies that u is not free in $\mathcal{L}_1^{loc}$. This proves that $\mathcal{B}_{\mathbf{v}} \neq \overline{\mathcal{B}}_{\mathbf{v}}$, as required. ■

The following corollary follows immediately, independently proved in [Polderman, 1993]:

Corollary 6.8 *$\mathcal{B}_{\mathbf{v}} = \overline{\mathcal{B}}_{\mathbf{v}}$ if and only if there exists a partition of v into y and u with the size of y equal to $p^*(\Sigma)$, and a partition of l into l_1 and l_2 with the size of l_1 equal to $p^*(\Sigma) - p^*(\Sigma_{\mathbf{v}})$, such that $l_2 = 0$ defines a proper I/O map from u to y and l_1.*

6.6 Example

In this section, a simple example is used to illustrate some of the machinery developed in this chapter. Consider the circuit diagram of Figure 6.1. The various currents and voltages satisfy the following equations:

$$V_1 - V_n = I_1, \tag{6.31}$$
$$V_2 - V_n = \dot{I}_2, \tag{6.32}$$
$$\dot{V}_3 - \dot{V}_n = I_3, \tag{6.33}$$
$$\dot{V}_4 - \dot{V}_n = I_4, \tag{6.34}$$
$$I_1 + I_2 + I_3 + I_4 = 0, \tag{6.35}$$

which can be put in ON form by the procedure outlined in Section 6.1.1:

$$\begin{bmatrix} \dot{x}_1 \\ \dot{x}_2 \\ \dot{x}_3 \\ 0 \\ 0 \\ 0 \\ 0 \\ 0 \end{bmatrix} = \left[\begin{array}{ccc||ccccccccc} 0 & 0 & 0 & 0 & 1 & 0 & 0 & -1 & 0 & 0 & 0 & 0 \\ 0 & 0 & 0 & 0 & 0 & 0 & 0 & 0 & 0 & 0 & 1 & 0 \\ 0 & 0 & 0 & 0 & 0 & 0 & 0 & 0 & 0 & 0 & 0 & 1 \\ \hline\hline 0 & 0 & 0 & 1 & 0 & 0 & 0 & -1 & -1 & 0 & 0 & 0 \\ 1 & 0 & 0 & 0 & 0 & 0 & 0 & 0 & 0 & -1 & 0 & 0 \\ 0 & 1 & 0 & 0 & 0 & -1 & 0 & 1 & 0 & 0 & 0 & 0 \\ 0 & 0 & 1 & 0 & 0 & 0 & -1 & 1 & 0 & 0 & 0 & 0 \\ 0 & 0 & 0 & 0 & 0 & 0 & 1 & 0 & 1 & 1 & 1 & 1 \end{array}\right] \begin{bmatrix} x_1 \\ x_2 \\ x_3 \\ V_1 \\ V_2 \\ V_3 \\ V_4 \\ V_n \\ I_1 \\ I_2 \\ I_3 \\ I_4 \end{bmatrix}. \tag{6.36}$$

The double lines in the representation matrix are used to highlight the partition into matrices A, B, C and D. By Lemma 6.1, the above is a minimal representation since (C, A) is an observable pair and D is full row rank. Note that the use of variable V_n greatly simplified the description of the equations governing the system, but is not necessary when describing the terminal behavior of the network. It can thus be seen as a latent variable, and removed by invoking the procedure of Section 6.5:

$$\begin{bmatrix} \dot{x}_1 \\ \dot{x}_2 \\ \dot{x}_3 \\ 0 \\ 0 \\ 0 \\ 0 \end{bmatrix} = \left[\begin{array}{ccc||cccccccc} 0 & 0 & 0 & -1 & 1 & 0 & 0 & 1 & 0 & 0 & 0 \\ 0 & 0 & 0 & 0 & 0 & 0 & 0 & 0 & 0 & 1 & 0 \\ 0 & 0 & 0 & 0 & 0 & 0 & 0 & 0 & 0 & 0 & 1 \\ \hline\hline -1 & 0 & 0 & 0 & 0 & 0 & 0 & 0 & 1 & 0 & 0 \\ 0 & -1 & 0 & -1 & 0 & 1 & 0 & 1 & 0 & 0 & 0 \\ 0 & 0 & -1 & -1 & 0 & 0 & 1 & 1 & 0 & 0 & 0 \\ 0 & 0 & 0 & 0 & 0 & 0 & 1 & 1 & 1 & 1 & 1 \end{array}\right] \begin{bmatrix} x_1 \\ x_2 \\ x_3 \\ V_1 \\ V_2 \\ V_3 \\ V_4 \\ I_1 \\ I_2 \\ I_3 \\ I_4 \end{bmatrix}. \tag{6.37}$$

Note that the above representation is still minimal. Also note that V_n was properly eliminable; this implies that no voltage spikes can occur at node n.

Assume that V_2, V_3 and V_4 are grounded. Equivalently, interconnect the circuit with $V_2 = V_3 = V_4 = 0$, and eliminate these variables:

$$\begin{bmatrix} \dot{x}_1 \\ \dot{x}_2 \\ \dot{x}_3 \\ 0 \\ 0 \\ 0 \\ 0 \end{bmatrix} = \left[\begin{array}{ccc||ccccc} 0 & 0 & 0 & -1 & 1 & 0 & 0 & 0 \\ 0 & 0 & 0 & 0 & 0 & 0 & 1 & 0 \\ 0 & 0 & 0 & 0 & 0 & 0 & 0 & 1 \\ \hline\hline -1 & 0 & 0 & 0 & 0 & 1 & 0 & 0 \\ 0 & -1 & 0 & -1 & 1 & 0 & 0 & 0 \\ 0 & 0 & -1 & -1 & 1 & 0 & 0 & 0 \\ 0 & 0 & 0 & 0 & 1 & 1 & 1 & 1 \end{array}\right] \begin{bmatrix} x_1 \\ x_2 \\ x_3 \\ V_1 \\ I_1 \\ I_2 \\ I_3 \\ I_4 \end{bmatrix}. \tag{6.38}$$

Note that the resulting D matrix is not full row rank; by Lemma 6.5, a singular interconnection has occurred. This captures the fact that the voltage across the two capacitors, which are also states, must be equal ($x_2 = x_3$).

Construct a minimal representation as per Section 6.1.2:

$$\begin{bmatrix} \dot{x}_1 \\ \dot{x}_2 \\ 0 \\ 0 \\ 0 \\ 0 \end{bmatrix} = \left[\begin{array}{cc||ccccc} 0 & 0 & -1 & 1 & 0 & 0 & 0 \\ 0 & 0 & 0 & 0 & 0 & 1 & 0 \\ \hline\hline -1 & 0 & 0 & 0 & 1 & 0 & 0 \\ 0 & -1 & -1 & 1 & 0 & 0 & 0 \\ 0 & 0 & 0 & 0 & 0 & 1 & -1 \\ 0 & 0 & 0 & 1 & 1 & 1 & 1 \end{array}\right] \begin{bmatrix} x_1 \\ x_2 \\ V_1 \\ I_1 \\ I_2 \\ I_3 \\ I_4 \end{bmatrix}, \tag{6.39}$$

and eliminate I_2, I_3, and I_4:

$$\begin{bmatrix} \dot{x}_1 \\ \dot{x}_2 \\ 0 \end{bmatrix} = \left[\begin{array}{cc||cc} 0 & 0 & -1 & 1 \\ -0.5 & 0 & 0 & -0.5 \\ \hline\hline 0 & -1 & -1 & 1 \end{array}\right] \begin{bmatrix} x_1 \\ x_2 \\ V_1 \\ I_1 \end{bmatrix}. \tag{6.40}$$

Again, it can be verified that I_2, I_3, and I_4 are properly eliminable. Create I/O map from I_1 to V_1, as per Section 6.2:

$$\begin{bmatrix} \dot{x}_1 \\ \dot{x}_2 \\ V_1 \end{bmatrix} = \left[\begin{array}{cc||c} 0 & 1 & 0 \\ -0.5 & 0 & -0.5 \\ \hline\hline 0 & -1 & 1 \end{array}\right] \begin{bmatrix} x_1 \\ x_2 \\ I_1 \end{bmatrix}. \tag{6.41}$$

Note that V_1 could have been chosen as the input. The resulting transfer function is the impedance at node 1:

$$Z(s) = \frac{s^2 + 0.5s + 0.5}{s^2 + 0.5}. \tag{6.42}$$

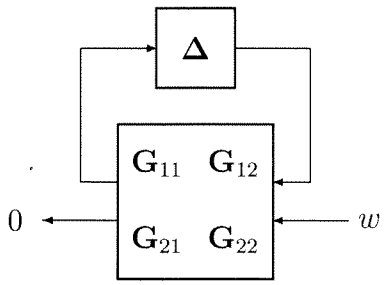

Figure 6.2: Extension to uncertain systems

6.7 Extension to Uncertain Systems

As argued in Section 2.3, in many instances it is more natural to model a system in implicit, or behavioral form, as opposed to an I/O relation between signals. In addition, it was argued in Section 2.2 that the likelihood of success of model based control designs is vastly increased when the discrepancies between a model and the behavior of the system it is trying to capture are taken into account. In this section, these two ideas are merged, and a method for incorporating uncertainty into the description of behavioral systems is proposed based on the LFT framework.

The behavior captured by an ON representation is simply the set of w which satisfy $\mathbf{G}w = 0$, where system $\mathbf{G}$ has state-space representation

$$\mathbf{G} := \left[\begin{array}{c|c} A & B \\ \hline C & D \end{array}\right]. \tag{6.43}$$

In order to incorporate uncertainty in the description of a system, one can consider trajectories which satisfy

$$(\boldsymbol{\Delta} \star \mathbf{G})\, w = 0, \tag{6.44}$$

where $\boldsymbol{\Delta}$ has the following spatial structure:

$$\boldsymbol{\Delta} = \mathbf{diag}\left[\delta_1 I_{k_1}, \ldots, \delta_L I_{k_L}, \boldsymbol{\Delta}_{L+1}, \ldots, \boldsymbol{\Delta}_{L+F}\right]. \tag{6.45}$$

This is depicted in Figure 6.2. Thus $\mathbf{G}_{22}w = 0$ captures the "nominal" behavior which occurs when $\boldsymbol{\Delta} = 0$.

A potential problem with this parametrization is that one has to ensure the well posedness of the above LFT (i.e., the existence of $(\mathbf{I} - \mathbf{G}_{11}\boldsymbol{\Delta})^{-1}$). A way to study this well posedness simultaneously with the parametrized behavior is to introduce latent variables l and to consider the following set of equations:

$$\left[\begin{array}{cc} I - \boldsymbol{\Delta}\mathbf{G}_{11} & -\boldsymbol{\Delta}\mathbf{G}_{12} \\ \mathbf{G}_{21} & \mathbf{G}_{22} \end{array}\right] \left[\begin{array}{c} l \\ w \end{array}\right] = 0. \tag{6.46}$$

System $\mathbf{G}$ can in turn be expressed as an LFT on the differentiation operator $\frac{d}{dt}$ (or the delay operator $\boldsymbol{\lambda}$ in discrete time). With this modification, $\boldsymbol{\Delta}$ can be augmented to include a block $\frac{d}{dt}I$, which is consistent with the structure of equation (6.45).

We formalize this as follows: the allowable class of uncertainty, $\boldsymbol{\Theta}$, is taken to be an (L+F)-tuple of operators, $\boldsymbol{\delta}_1$ through $\boldsymbol{\delta}_N$ and $\boldsymbol{\Delta}_{L+1}$ through $\boldsymbol{\Delta}_{L+F}$. Each $\boldsymbol{\delta}_i$ and $\boldsymbol{\Delta}_j$ is restricted to be a certain type of operator: LTV, LTI, a real parameter, or the operator $\frac{d}{dt}$. For example, a particular choice for $\boldsymbol{\Theta}$ is the following:

$$\boldsymbol{\Theta} := \{\boldsymbol{\theta} = (\boldsymbol{\delta}_1, \cdots, \boldsymbol{\delta}_L) : \boldsymbol{\delta}_i \in \mathcal{L}(l_2), \|\boldsymbol{\delta}_i\| \leq 1\}; \tag{6.47}$$

in this example, $\boldsymbol{\Theta}$ consists of arbitrary (equivalently LTV) contractive operators from $\mathcal{L}_2$ to $\mathcal{L}_2$. Another choice could be some of the $\boldsymbol{\delta}_i$ being real parameters with size restriction $|\boldsymbol{\delta}_i| \leq 1$. Associated with $\boldsymbol{\Theta}$ is an L-tuple of integers $\mathbf{k}$, which establishes the multiplicity of each $\boldsymbol{\delta}_i$, and is used to define the uncertainty:

$$\mathbf{k} := (k_1, \cdots, k_L), \tag{6.48}$$

$$\boldsymbol{\Delta}(\mathbf{k}, \boldsymbol{\theta}) := \mathbf{diag}\left[\boldsymbol{\delta}_1 I_{k_1}, \cdots, \boldsymbol{\delta}_L I_{k_L}, \boldsymbol{\Delta}_{L+1}, \cdots, \boldsymbol{\Delta}_{L+F}\right]. \tag{6.49}$$

Let matrix M (referred to as the *representation matrix*) with the following structure be given

$$M = \begin{bmatrix} A & B \\ C & D \end{bmatrix}, \tag{6.50}$$

where $A \in \mathbb{R}^{n\times n}$, $B \in \mathbb{R}^{n\times q}$, $C \in \mathbb{R}^{r\times n}$, and $D \in \mathbb{R}^{r\times q}$, and let $\mathbf{k}$ be given. For a fixed $\boldsymbol{\theta}$, and hence $\boldsymbol{\Delta}(\mathbf{k}, \boldsymbol{\theta})$, denote $\mathcal{B}_{\boldsymbol{\theta}}$ as the following set of time trajectories:

$$\mathcal{B}_{\boldsymbol{\theta}} := \left\{w \in \mathcal{L}_1^{loc} : \exists\, l \in \mathcal{L}_1^{loc} \text{ s.t. equation (6.51) is satisfied}\right\} :$$

$$\begin{bmatrix} I - \boldsymbol{\Delta}A & -\boldsymbol{\Delta}B \\ C & D \end{bmatrix} \begin{bmatrix} l \\ w \end{bmatrix} = 0. \tag{6.51}$$

The behavior $\mathcal{B}$ of system Σ is then defined as follows:

$$\mathcal{B} := \bigcup_{\boldsymbol{\theta}\in\boldsymbol{\Theta}} \mathcal{B}_{\boldsymbol{\theta}}. \tag{6.52}$$

The triple $(M, \mathbf{k}, \boldsymbol{\Theta})$ is referred to as a *representation* for system Σ.

Example

Consider Newton's famous law

$$F = \frac{d}{dt}\left(m\frac{dy}{dt}\right) \tag{6.53}$$

where F is the force acting on a particle of mass m at position y. This relation can be captured by the following set of equations:

$$\begin{aligned} l_1 &= \frac{dy}{dt}, && (6.54)\\ l_3 &= ml_1, && (6.55)\\ l_2 &= \frac{dl_3}{dt}, && (6.56)\\ 0 &= F - l_2. && (6.57) \end{aligned}$$

This can be put in the form of equation (6.51) by defining $w = (F, y)$,

$$\mathbf{\Delta} = \mathbf{diag}\left[\frac{d}{dt}I_2, m\right], \tag{6.58}$$

and a suitable choice for M. Assume that the mass m is known to be in the range $0.8 \leq m \leq 1.2$. Then the behavior $\mathcal{B}$, consisting of all possible trajectories consistent with equation (6.53), can be captured as per equation (6.52) by defining

$$\begin{aligned} \mathbf{\Theta} &:= \left\{(\frac{d}{dt}, m) : 0.8 \leq m \leq 1.2\right\}; && (6.59)\\ \mathbf{k} &:= (2, 1). && (6.60) \end{aligned}$$

□

Remarks: Note that when $\mathbf{\Theta} = \{\frac{d}{dt}\}$, equation (6.51) *does not* reduce to an ON representation. In fact, the following equations are obtained:

$$\begin{bmatrix} x \\ 0 \end{bmatrix} = \begin{bmatrix} A & B \\ C & D \end{bmatrix} \begin{bmatrix} \dot{x} \\ w \end{bmatrix}. \tag{6.61}$$

It is a straight forward matter to convert the above equations to ON form; this is discussed in Section 7.4. One could capture ON representations directly by setting $\mathbf{\Theta} = \{\int_{-\infty}^{t}\}$ and imposing an additional constraint on $x(-\infty)$; it seems more natural, however, to work with the differentiation operator since most dynamic equations are in differential (as opposed to integral) form.

Given a method of parametrizing the behavior of a system, it is natural to ask when two representations yield the same behavior, and when a representation is minimal. This is explored next.

6.7.1 Weak and Strong Equivalence

Let the uncertainty class $\mathbf{\Theta}$ be given. $(M, \mathbf{k}, \mathbf{\Theta})$ and $(\hat{M}, \hat{\mathbf{k}}, \mathbf{\Theta})$ are said to be *weakly equivalent* representations if they parametrize the same behavior:

$$\mathcal{B} = \hat{\mathcal{B}}. \tag{6.62}$$

$(M, \mathbf{k}, \boldsymbol{\Theta})$ and $(\hat{M}, \hat{\mathbf{k}}, \boldsymbol{\Theta})$ are said to be *strongly equivalent* if

$$\mathcal{B}_{\boldsymbol{\theta}} = \hat{\mathcal{B}}_{\boldsymbol{\theta}} \quad \forall \boldsymbol{\theta} \in \boldsymbol{\Theta}. \tag{6.63}$$

It is clear that strong equivalence implies weak equivalence; the converse, however, is typically not true. To illustrate the difference between these two notions of equivalence, let $\boldsymbol{\Theta}$ consist of the uncertainty structure defined in equation (6.47) and consider the three following system equations:

$$v_1 = \boldsymbol{\delta}_1 v_2; \tag{6.64}$$

$$v_1 = -\boldsymbol{\delta}_1 v_2; \tag{6.65}$$

$$v_1 = \boldsymbol{\delta}_1 \boldsymbol{\delta}_2 v_2. \tag{6.66}$$

All of the above systems capture the same behavior; it thus follows that all representations for these systems will be weakly equivalent. For different values of $\boldsymbol{\delta}_i$, however, the behaviors of the above systems are all different, and are thus not strongly equivalent.

A class of strongly equivalent representations for a given $(M, \mathbf{k}, \boldsymbol{\Theta})$ is of the form $(\hat{M}, \mathbf{k}, \boldsymbol{\Theta})$, where $\hat{M}$ is defined as

$$\hat{M} := \begin{bmatrix} T^{-1}(A + LC)T & T^{-1}(B + LD) \\ PCT & PD \end{bmatrix}, \tag{6.67}$$

where T is an invertible matrix such that $T\boldsymbol{\Delta}(\mathbf{k}, \boldsymbol{\theta}) = \boldsymbol{\Delta}(\mathbf{k}, \boldsymbol{\theta})T$ for all $\boldsymbol{\theta} \in \boldsymbol{\Theta}$, L is any matrix of compatible dimension, and P is any invertible matrix of compatible dimension. The above does not parametrize all strongly (and thus weakly) equivalent representations; for example, there might exist a representation with fewer latent variables n or fewer equations r, or both. For the special case where $\boldsymbol{\Theta} = \{\frac{d}{dt}\}$, (C, A) is an observable pair, and M is full row rank, it can be shown that the above captures all equivalent representations [D'Andrea, 1994], [Weiland, 1991] (note that when $\boldsymbol{\Theta}$ consists of a single operator, the notions of strong and weak equivalence are the same).

Let the uncertainty structure $\boldsymbol{\Theta}$ be fixed, and let representation $(M, \mathbf{k}, \boldsymbol{\Theta})$ be given. If for all other weakly (strongly) equivalent representations $(\hat{M}, \hat{\mathbf{k}}, \boldsymbol{\Theta})$, $\hat{r} \geq r$ and $\hat{n} \geq n$, then $(M, \mathbf{k}, \boldsymbol{\Theta})$ is said to be a weakly (strongly) *minimal* representation (note that it is not readily apparent whether a minimal representation exists or not). Returning to the special case of $\boldsymbol{\Theta} = \{\frac{d}{dt}\}$ (for which strong and weak equivalence are the same), it can be shown that a representation is minimal if and only if (C, A) is an observable pair and M is full row rank. Thus equation (6.67) parametrizes all equivalent minimal representations when $\boldsymbol{\Theta} = \{\frac{d}{dt}\}$, similar to the result of Lemma 6.2.

A natural question arises as to when a representation is minimal for a given $\boldsymbol{\Theta}$, and how to construct minimal representations. This appears to be a difficult problem; to date, only when special cases for $\boldsymbol{\Theta}$ are considered (LTV operators) and an I/O notion of strong equivalence is adopted (discussed in the next section) have computationally tractable methods for constructing minimal representations been obtained.

6.7.2 I/O Equivalence

When the B and D matrices in representation matrix M are restricted to be of the form

$$\begin{bmatrix} B \\ D \end{bmatrix} = \begin{bmatrix} 0 & B_u \\ -I & D_u \end{bmatrix} \tag{6.68}$$

and the manifest variables are partitioned into $w = (y, u)$, the following I/O equations are obtained:

$$l = \mathbf{\Delta}(\mathbf{k}, \boldsymbol{\theta})(Al + B_u u), \tag{6.69}$$

$$y = Cl + D_u u. \tag{6.70}$$

Define

$$M_{io} := \begin{bmatrix} A & B_u \\ C & D_u \end{bmatrix}, \; \hat{M}_{io} := \begin{bmatrix} \hat{A} & \hat{B}_u \\ \hat{C} & \hat{D}_u \end{bmatrix}, \tag{6.71}$$

which are obtained from the corresponding representation matrices M and $\hat{M}$. Representations $(M, \mathbf{k}, \mathbf{\Theta})$ and $(\hat{M}, \hat{\mathbf{k}}, \mathbf{\Theta})$ are said to be *weakly I/O equivalent* if

$$\begin{aligned} \forall \boldsymbol{\theta} \in \mathbf{\Theta}, \exists \hat{\boldsymbol{\theta}} \in \mathbf{\Theta} \text{ s.t. } \mathbf{\Delta}(\mathbf{k}, \boldsymbol{\theta}) \star M_{io} &= \mathbf{\Delta}(\hat{\mathbf{k}}, \hat{\boldsymbol{\theta}}) \star \hat{M}_{io}, \\ \forall \hat{\boldsymbol{\theta}} \in \mathbf{\Theta}, \exists \boldsymbol{\theta} \in \mathbf{\Theta} \text{ s.t. } \mathbf{\Delta}(\mathbf{k}, \boldsymbol{\theta}) \star M_{io} &= \mathbf{\Delta}(\hat{\mathbf{k}}, \hat{\boldsymbol{\theta}}) \star \hat{M}_{io}. \end{aligned}$$

$(M, \mathbf{k}, \mathbf{\Theta})$ and $(\hat{M}, \hat{\mathbf{k}}, \mathbf{\Theta})$ are said to be *strongly I/O equivalent* if

$$\mathbf{\Delta}(\mathbf{k}, \boldsymbol{\theta}) \star M_{io} = \mathbf{\Delta}(\hat{\mathbf{k}}, \boldsymbol{\theta}) \star \hat{M}_{io} \;\; \forall \boldsymbol{\theta} \in \mathbf{\Theta}. \tag{6.72}$$

In general, I/O equivalence is a more restrictive notion of equivalence; the I/O equivalence of two representations does not imply that they parametrize the same behavior. For example, the following two sets of equations are I/O equivalent, but capture different behaviors:

$$\dot{l} = 0u, \; y = l; \qquad\qquad y = 0u. \tag{6.73}$$

6.7.3 Concluding Remarks

All the notions of equivalence are related as per the following diagram:

$$\begin{array}{ccc} \text{weak} & \Longleftarrow & \text{strong} \\ \text{equivalence} & & \text{equivalence} \\ \Downarrow & & \Downarrow \\ \text{weak} & & \text{strong} \\ \text{I/O} & \Longleftarrow & \text{I/O} \\ \text{equivalence} & & \text{equivalence} \end{array}$$

One can also ask the question of how equivalence is related for different types of uncertainty class $\mathbf{\Theta}$. It is clear that the following relation holds:

$$\begin{array}{ccccc} \text{LTV} & & \text{LTI} & & \text{parametric} \\ \text{equivalence} & \Longrightarrow & \text{equivalence} & \Longrightarrow & \text{equivalence} \end{array}$$

Thus a strong case can be made for considering strongly equivalent representations for LTV uncertainty: if given a representation one substitutes for it a strongly equivalent representation for LTV $\mathbf{\Theta}$, it will also be equivalent irrespective of what kind of equivalence or what type of uncertainty is desired at some later stage. Thus if one does not know a priori how the model will be used or whether the uncertainty is LTV, LTI, or parametric, the right equivalence class to consider is that induced by strongly equivalent representations and LTV uncertainty.

Another reason for considering strong equivalence and LTV $\mathbf{\Theta}$ is that strong equivalence is much easier to check for than weak equivalence, and that working with LTV uncertainty typically leads to more tractable conditions than when working with LTI or parametric uncertainty; to date, the only type of equivalence which has yielded computationally tractable methods for determining whether two realizations are equivalent and for constructing minimal representations is strong I/O equivalence for LTV $\mathbf{\Theta}$ [Beck, 1995], [D'Andrea, 1997]. Current research includes extending these techniques and the earlier algorithms presented in this chapter, such as latent variable elimination, to the more general case of strong equivalence for LTV $\mathbf{\Theta}$. It is conjectured that for uncertainty other than LTV $\mathbf{\Theta}$ or when the notion of weak equivalence is adopted, the question of equivalence and the characterization of minimality are NP-Hard in the number of elements in $\mathbf{\Theta}$, $L + F$.

The concepts introduced in this section have been used in other seemingly unrelated areas of research: in [Paganini et al., 1994], the analysis conditions in [Megretski and Treil, 1993] were extended to the above types of uncertain systems; by incorporating the set descriptions of white noise in [Paganini, 1993] with these analysis results, an analysis condition for robust $\mathcal{H}_2$ performance was derived. These results were expanded to the general case of implicitly defined systems in [Paganini, 1995b]. How model validation and system identification can be unified using these representations is outlined in [Newlin, 1996], [Paganini, 1995b] and [Doyle et al., 1994a].

Chapter 7
$\mathcal{H}_\infty$ Optimal Interconnections

In this chapter, an optimal control problem for continuous time, linear time invariant systems is formulated and solved in a behavioral framework. This general formulation, which includes standard $\mathcal{H}_\infty$ optimization as a special case, provides added freedom in the design of sub-optimal compensators, and can in fact be viewed as a means of designing optimal systems. In particular, the formulation presented allows for singular interconnections, which naturally occur when interconnecting first principles models.

7.1 Introduction

Invariably, most of the tools developed in the field of optimal control have relegated the control design process to a secondary role in the design of systems: a control algorithm is only sought after the system to be controlled has already been designed, and the type and location of the actuators and sensors has been determined; equivalently, given both sensor variables and actuator variables, a viable control strategy consists of an algorithm which produces actuators signals from the measured variables, and results in a closed loop system which achieves certain performance objectives. These objectives may be I/O in nature (such as $\mathcal{H}_\infty$, $\mathcal{H}_2$, or $\mathcal{L}_\infty$), or transient oriented (such as LQR).

For most applications, however, the level of performance which can be attained by *any* control strategy is dictated by the dynamics of the plant [Doyle et al., 1992]. Thus from a system level, the above standard approaches are not optimal, since the control design process is decoupled from the design of the rest of the system. The result is that the control engineer is left with little freedom in how to control the system, or an iteration must take place between the design of the system and the design of the controller. Clearly, the optimal strategy would be to design the system *and* controller at the same time, or in other words, to view the design of the controller as part of the system design process.

In this chapter, a general optimization problem is posed where the objective is of finding optimal relations between a system's variables. This type of formulation is very closely related to the behavioral framework for describing systems, outlined in Chapter 6. The design process in this framework takes the form of finding additional

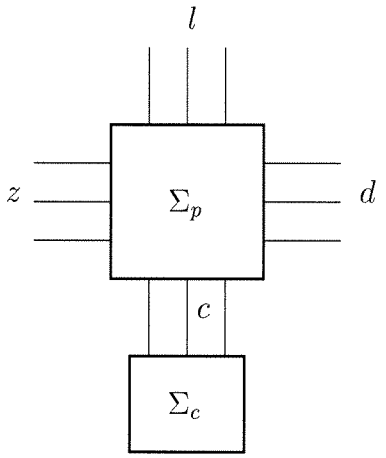

Figure 7.1: Problem formulation

constraints on a system's behavior such that the remaining allowable trajectories satisfy given a priori requirements. The optimization criterion adopted in this chapter is the rejection of $\mathcal{L}_2$ bounded disturbances, which leads to a general version of the $\mathcal{H}_\infty$ design problem for continuous time, linear time invariant systems described by implicit equations.

Other research in this area includes [Trentelman and Willems, 1995], where a similar type of problem formulation from a polynomial representation standpoint is addressed. The problem of integrated system and controller design using a successive covariance approximation approach is addressed in [Skelton, 1995], and includes a summary of the key issues which will drive future research into integrated system design.

The chapter is organized as follows: The problem formulation is outlined in Section 7.2, followed by a simple example in Section 7.3 which is cast in this framework. The problem is solved in Sections 7.4, 7.5 and 7.6. In Section 7.7, the example problem of Section 7.3 is solved. In Section 7.8, the concepts of Full Information and Full Control are introduced, followed by an example in Section 7.9.

7.2 Problem Formulation

Let system $\Sigma_p = \{\mathbb{R}, \mathbb{R}^{q_z+q_d+q_c+q_l}, \mathcal{B}_p\}$ be given, i.e., w is partitioned into four parts, $w = (z, d, c, l)$:

- **z**: error signals which are required to be small;
- **d**: exogenous disturbances, unexplained by the given model;
- **c**: variables which are accessible for control purposes;
- **l**: latent variables, auxiliary variables used when constructing Σ_p.

The objective is to find system $\Sigma_c = \{\mathbb{R}, \mathbb{R}^{q_c}, \mathcal{B}_c\}$, acting on the variables c, such

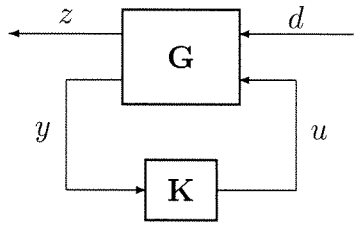

Figure 7.2: Standard I/O $\mathcal{H}_\infty$ formulation

that $\Sigma := \Sigma_p \wedge \Sigma_c = \{\mathbb{R}, \mathbb{R}^{q_z+q_d+q_c+q_l}, \mathcal{B}\}$ satisfies the following:

(P1) **Unrestricted Disturbance:** For the interconnected system, d is free:

$$\forall d \in C^\infty, \ \exists\, z, c, l \in C^\infty s.t.\ w \in \mathcal{B}. \tag{7.1}$$

Equivalently, system Σ_c does not provide any additional information about the disturbance.

(P2) **Stability:**

$$d = 0, w \in \mathcal{B} \Longrightarrow \lim_{t\to\infty} z(t), c(t) = 0. \tag{7.2}$$

Thus if one stops exciting the system, the error and control signals decay to 0. Note that there is no such restriction on latent variables l; this will be motivated by the simple example in Section 7.3.

(P3) **Performance:**

$$\sup_{d\in(C^\infty\cap\mathcal{L}_2),\, \|d\|\leq 1, w\in\mathcal{B}} \|z\| < 1. \tag{7.3}$$

Note that the general performance specification $\|z\| < \gamma$ can be imposed by appropriately scaling z.

In general, a system Σ_c which only has access to variables c will be referred to as a *compensator*. If in addition Σ satisfies constraints P1, P2, and P3, Σ_c will be referred to as an *allowable* compensator.

It is useful to compare the above problem formulation to the standard, I/O $\mathcal{H}_\infty$ formulation of Figure 7.2. Variables z and d have the same interpretation, c is a priori partitioned into y and u, and there are no latent variables l. In terms of P1 through P3, P1 is automatically satisfied by the imposed structure on $\mathbf{K}$, P2 is typically replaced by the requirement that the closed loop system be internally stable, a more stringent requirement as shall be demonstrated later, and P3 reduces to $\|\mathbf{G} \star \mathbf{K}\| < 1$.

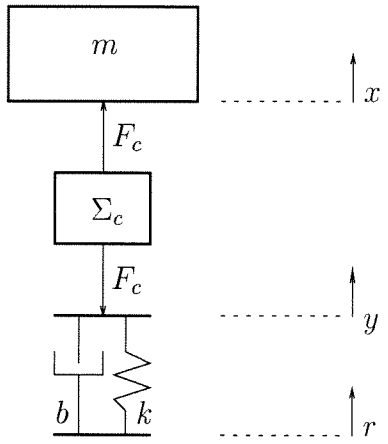

Figure 7.3: Suspension design

7.3 Example

The following simple example can be used to illustrate the main differences between the problem formulation outlined above and standard $\mathcal{H}_\infty$ design. It consists of a one degree of freedom suspension design; an explicit solution to this problem is provided in Section 7.7. Consider the setup of Figure 7.3. The goal is to design system Σ_c, the suspension, in order to achieve certain performance objectives which will be described shortly. Variable m denotes the sprung mass, or the mass of the cab where the passengers will ride. Σ_c is the mechanism which is to be designed; it is restricted to be a relation between F_c and $x - y$. The spring and the damper model a tire, which is in contact with the road.

The equations describing the system and the performance objectives are as follows:

$$\begin{aligned} 0 &= F_c - m\ddot{x} \\ 0 &= F_c + b(\dot{y} - \dot{r}) + k(y - r) \\ c_1 &= F_c \\ c_2 &= x - y \\ z_1 &= x - r \quad \text{(tracking)} \\ z_2 &= \dddot{x} \qquad \text{(comfort)} \\ d &= \ddot{r}. \end{aligned} \tag{7.4}$$

The first two equations are the equations of motion about an equilibrium point. The second two equations dictate which variables system Σ_c has access to. The next two equations describe the performance objectives; the sprung mass is required to track the road, while simultaneously be subjected to small values of jerk (the jerk, or third derivative of position, is to a first approximation a good measure of passenger discomfort, and is in general a quantity which should be kept small in the design of mechanical systems [Shigley and Uicker, 1980]). The last equation models

the allowable road disturbances; restricting d to be an $\mathcal{L}_2$ disturbance of unit norm restricts r to be small at high frequencies and allows r to be large at low frequencies. This corresponds to restricting large amplitude road disturbances to be gradual (hills), while allowing smaller amplitude disturbances to be sharper (potholes and speed bumps). Also note that when $d = 0$, $r(t) = C_0 + C_1 t$ for some constants C_0 and C_1; this corresponds to a constant climb, which should be allowed in the equations of motion.

It is clear from this example why the definition of stability should not encompass the latent variables: r should not be restricted to decay to 0 when $d = 0$. In general, if one is concerned about the size of a latent variable, it could be penalized and be made a part of z.

There are several reasons why standard $\mathcal{H}_\infty$ design cannot directly handle this problem. The first is that there is no way to manipulate the above system into the form of Figure 7.2 with $\mathbf{G}$ proper. This precludes the use of standard state-space methods for solving the problem. A further constraint is that the resulting design must result in a singular interconnection with the plant; equivalently, the interconnection must impose algebraic constraints on the states (this is demonstrated in Section 7.7). This is not allowed in standard feedback control. It should be noted that by choosing appropriate weights for the various signals (for example, by first constructing a non-proper $\mathbf{G}$, and then low-pass filtering all transfer functions which are not proper by a sufficient amount), one can approximate the problem with one which fits the setup of Figure 7.2. It is very unnatural to do so, however, and as shall be demonstrated, unnecessary as well.

7.4 Dual Representations

It will be useful to introduce the notion of a dual ON representation for a system Σ. Given an observable representation M, where it can be assumed without loss of generality that the A matrix is invertible by Lemma 6.2, the following equations capture the behavior $\mathcal{B}$:

$$\begin{bmatrix} x \\ 0 \end{bmatrix} = \begin{bmatrix} A^{-1} & -A^{-1}B \\ CA^{-1} & D - CA^{-1}B \end{bmatrix} \begin{bmatrix} \dot{x} \\ w \end{bmatrix} =: \begin{bmatrix} \tilde{A} & \tilde{B} \\ \tilde{C} & \tilde{D} \end{bmatrix} \begin{bmatrix} \dot{x} \\ w \end{bmatrix} =: \tilde{M} \begin{bmatrix} \dot{x} \\ w \end{bmatrix}. \tag{7.5}$$

It can be verified that the behavior preserving transformations of Lemma 6.2 apply to dual ON representations as well. The definitions of observable, dependent, and minimal can be applied to dual ON representations; it can be shown that these definitions are satisfied for an ON representation if and only if they are satisfied for its dual.

7.4.1 Stability Conditions

By the following identities:

$$\begin{bmatrix} A-sI & B \\ C & D \end{bmatrix} = \begin{bmatrix} sI & 0 \\ 0 & I \end{bmatrix} \begin{bmatrix} \tilde{A}-s^{-1}I & \tilde{B} \\ \tilde{C} & \tilde{D} \end{bmatrix} \begin{bmatrix} A & B \\ 0 & I \end{bmatrix}, \quad s \neq 0, \tag{7.6}$$

$$\begin{bmatrix} A & B \\ C & D \end{bmatrix} = \begin{bmatrix} I & 0 \\ \tilde{C} & \tilde{D} \end{bmatrix} \begin{bmatrix} A & B \\ 0 & I \end{bmatrix}, \tag{7.7}$$

and Lemma 6.4, the following corollary may be used to characterize stability:

Corollary 7.1 *Given observable dual representation matrix* $\tilde{M}$, Σ *is stable if and only if* $\begin{bmatrix} \tilde{A}-sI & \tilde{B} \\ \tilde{C} & \tilde{D} \end{bmatrix}$ *is full column rank* $\forall s \in \mathbb{C}^+/\{0\}$ *and* $\tilde{D}$ *is full column rank.*

7.4.2 Constructing AR Representations from Dual ON Representations

When the problem formulation of Section 7.2 is solved in Section 7.5, the resulting Σ_c will be in dual ON form. The following procedure may be used to construct an AR representation given a dual ON representation.

Let $\mathcal{B}$ be captured by the following observable dual ON equations:

$$\begin{aligned} x &= A\dot{x} + Bw, \\ 0 &= C\dot{x} + Dw. \end{aligned} \tag{7.8}$$

Let matrix F be such that $A+FC$ is nilpotent. The following equations capture the same behavior as (7.8):

$$x = \bar{A}\dot{x} + \bar{B}w = (A+FC)\dot{x} + (B+FD)w, \tag{7.9}$$

$$0 = C\dot{x} + Dw. \tag{7.10}$$

Let L be the dimension of the largest Jordan block of $\bar{A}$. Define the following:

$$R_0 := D, \tag{7.11}$$

$$R_l := C\bar{A}^{l-1}\bar{B}, \quad 1 \leq l \leq L. \tag{7.12}$$

Proposition 7.2 $R(\frac{d}{dt})w = 0$ *is an AR representation for* Σ.

Proof: If w satisfies (7.9) and (7.10), repeated differentiation of (7.9), substitution into (7.10), and the fact that $\bar{A}^L = 0$, implies that w satisfies $R(\frac{d}{dt})w = 0$. Now assume that w satisfies $R(\frac{d}{dt})w = 0$. Define

$$x := \bar{A}^{L-1}\bar{B}\frac{dw^{L-1}}{dt^{L-1}} + \cdots + \bar{B}w. \tag{7.13}$$

It follows that (7.10) is satisfied. Furthermore, since $\bar{A}^L = 0$, (7.9) is satisfied as well. ■

7.5 Problem Conversion

A solution to the problem of Section 7.2 is presented with the assumption that the compensator Σ_c forms a feedback interconnection with Σ_p. It is shown below, however, that a pre-compensating system can be first interconnected with Σ_p to make this assumption unrestrictive.

Theorem 7.3 *Let Σ_c be an allowable compensator. There exist systems $\bar{\Sigma}_c$ and $\hat{\Sigma}_c$ such that*

1. *$\bar{\Sigma}_c \wedge \Sigma_c$ is an allowable compensator.*
2. *$\hat{\Sigma}_c$ and $\Sigma_p \wedge \bar{\Sigma}_c$ form a feedback interconnection.*
3. *$\Sigma_p \wedge \bar{\Sigma}_c \wedge \Sigma_c = \Sigma_p \wedge \bar{\Sigma}_c \wedge \hat{\Sigma}_c$.*

Proof: Let $R_p(\xi) = [\ R_p^z(\xi)\ \ R_p^d(\xi)\ \ R_p^l(\xi)\ \ R_p^c(\xi)\ ]$ be an AR representation for Σ_p. Using the Smith form decomposition for polynomial matrices (see Section 2.1.4) and the equivalence of AR representations under left multiplication by unimodular matrices [Willems, 1991], it follows that $R_p(\xi)$ can be assumed to have the form

$$R_p(\xi) = \begin{bmatrix} R_{p1}^z(\xi) & R_{p1}^d(\xi) & R_{p1}^l(\xi) & R_{p1}^c(\xi) \\ 0 & 0 & 0 & D(\xi)R_{p2}^c(\xi) \end{bmatrix}, \tag{7.14}$$

where $[\ R_{p1}^z(\xi)\ \ R_{p1}^d(\xi)\ \ R_{p1}^l(\xi)\ ]$ is full normal row rank, $R_{p2}^c(\xi)$ is right invertible, and $D(\xi)$ is square and full normal rank.
Define $\bar{\Sigma}_c$ by AR representation R_{p2}^c. Interconnecting Σ_p with $\bar{\Sigma}_c$ results in the following AR representation for the interconnected system:

$$\begin{bmatrix} R_{p1}^z(\xi) & R_{p1}^d(\xi) & R_{p1}^l(\xi) & R_{p1}^c(\xi) \\ 0 & 0 & 0 & R_{p2}^c(\xi) \end{bmatrix}. \tag{7.15}$$

In the language of [Willems, 1991], this pre-compensator has the effect of removing the finite dimensional *uncontrollable behavior* which involves only variables c. Since the behavior of $\Sigma_p \wedge \bar{\Sigma}_c \wedge \Sigma_c$ is a subset of the behavior of $\Sigma_p \wedge \Sigma_c$, it follows that requirements P2 and P3 are satisfied for compensator $\bar{\Sigma}_c \wedge \Sigma_c$. Furthermore, since the two closed loop behaviors differ only by a finite dimensional subspace, requirement P1 must be satisfied as well. This proves part 1.
Let $R_c(\xi)$ be an AR representation for Σ_c. An AR representation for $\Sigma_p \wedge \bar{\Sigma}_c \wedge \Sigma_c$ is

$$\begin{bmatrix} R_{p1}^z(\xi) & R_{p1}^d(\xi) & R_{p1}^l(\xi) & R_{p1}^c(\xi) \\ 0 & 0 & 0 & R_{p2}^c(\xi) \\ 0 & 0 & 0 & R_c(\xi) \end{bmatrix}. \tag{7.16}$$

By the rank conditions on $[\ R^z_{p1}(\xi)\quad R^d_{p1}(\xi)\quad R^l_{p1}(\xi)\ ]$ and R^c_{p2}, there must exist polynomial matrices $U_1(\xi)$ and $U_2(\xi)$ such that

$$\begin{bmatrix} I & 0 \\ U_1(\xi) & U_2(\xi) \end{bmatrix} \begin{bmatrix} R^c_{p2}(\xi) \\ R_c(\xi) \end{bmatrix} = \begin{bmatrix} R^c_{p2}(\xi) \\ \hat{R}_c(\xi) \\ 0 \end{bmatrix}, \tag{7.17}$$

where $U_2(\xi)$ is a unimodular matrix and

$$\begin{bmatrix} R^c_{p2}(\xi) \\ \hat{R}_c(\xi) \end{bmatrix} \tag{7.18}$$

is full normal row rank. Thus system $\hat{\Sigma}_c$ defined by AR representation $\hat{R}_c(\xi)$ forms a feedback interconnection with $\Sigma_p \wedge \bar{\Sigma}_c$, and $\Sigma_p \wedge \bar{\Sigma}_c \wedge \Sigma_c = \Sigma_p \wedge \bar{\Sigma}_c \wedge \hat{\Sigma}_c$, proving parts 2 and 3. ■

Thus by first interconnecting the given system Σ_p with pre-compensator $\bar{\Sigma}_c$ and forming $\hat{\Sigma}_p := \Sigma_p \wedge \bar{\Sigma}_c$, one need only consider compensators $\hat{\Sigma}_c$ which form feedback interconnections with $\hat{\Sigma}_p$. Furthermore, if $\hat{\Sigma}_c$ is an allowable compensator for $\hat{\Sigma}_p$, $\bar{\Sigma}_c \wedge \hat{\Sigma}_c$ is an allowable compensator for Σ_p.

One of the major complications which arises in the problem formulation of Section 7.2 is allowing singular interconnections, since they result in algebraic constraints on the states. This problem is circumvented by working with dual representations; as will be shown, algebraic constraints take the form of uncontrollable modes at $s = 0$ for a related I/O state-space representation. This characterization of singular interconnections vastly simplifies the problem at hand, and allows one to convert it to an almost standard $\mathcal{H}_\infty$ problem with minor modifications. The solution to this associated $\mathcal{H}_\infty$ problem may be found in Section 7.6.

It will be assumed that pre-compensator $\bar{\Sigma}_c$ has already been applied to the given system, as per Theorem 7.3. The reader is referred to [Kailath, 1980] for details on how to construct an AR representation for $\bar{\Sigma}_c$ as per equation (7.14). It will also be assumed that Σ_p has no latent variables. The removal of these variables may be accomplished with the algorithm in Section 6.5.

Let $\tilde{M}_p \in \mathbb{R}^{(n_p+r_p)\times(n_p+q_z+q_d+q_c)}$ be a minimal dual representation matrix for Σ_p and $\tilde{M}_c \in \mathbb{R}^{(n_c+r_c)\times(n_c+q_c)}$ be a dual representation matrix for the candidate compensator Σ_c. Let $\Sigma = \Sigma_p \wedge \Sigma_c$ be the resulting feedback interconnection. By Lemma 6.5 and equation (7.5), the following is a dual representation matrix for Σ:

$$\tilde{M} = \begin{bmatrix} \tilde{A}_p & 0 & \tilde{B}^z_p & \tilde{B}^d_p & \tilde{B}^c_p \\ 0 & \tilde{A}_c & 0 & 0 & \tilde{B}_c \\ \tilde{C}_p & 0 & \tilde{D}^z_p & \tilde{D}^d_p & \tilde{D}^c_p \\ 0 & \tilde{C}_c & 0 & 0 & \tilde{D}_c \end{bmatrix}. \tag{7.19}$$

The following lemma is central to converting the problem data to a more usable form:

Lemma 7.4 *If an an allowable compensator Σ_c exists, there exists invertible matrix W such that the behavior of Σ_p can be captured by the following equations:*

$$\begin{bmatrix} x_p \\ z \\ y \end{bmatrix} = M_p^{IO} \begin{bmatrix} \dot{x}_p \\ d \\ u \end{bmatrix}, \quad M_p^{IO} := \begin{bmatrix} A & B_1 & B_2 \\ C_1 & D_{11} & D_{12} \\ C_2 & D_{21} & 0 \end{bmatrix}, \quad c = W^{-1} \begin{bmatrix} y \\ u \end{bmatrix}. \tag{7.20}$$

Furthermore, one need only consider compensators Σ_c which are captured by the following equations:

$$\begin{bmatrix} x_c \\ u \end{bmatrix} = M_c^{IO} \begin{bmatrix} \dot{x}_c \\ y \end{bmatrix}, \quad M_c^{IO} := \begin{bmatrix} \bar{A} & \bar{B} \\ \bar{C} & \bar{D} \end{bmatrix} \tag{7.21}$$

Proof: By Lemma 6.5, $\tilde{M}$ is not a dependent representation. By requirement P1, the number of free variables must be at least q_d; by Corollary 6.3 this implies that $r_p + r_c \leq q_z + q_c$. Stability requirement P2, on the other hand, implies that $r_p + r_c \geq q_z + q_c$ by the rank condition of Corollary 7.1. Thus $r_c = q_z + q_c - r_p$, and by Corollary 7.1, the following matrix must be square and invertible:

$$\begin{bmatrix} \tilde{D}_p^z & \tilde{D}_p^c \\ 0 & \tilde{D}_c \end{bmatrix}. \tag{7.22}$$

Since $\tilde{D}_p^z$ must have full column rank, by the behavior preserving transformations of Lemma 6.2, it can be assumed that

$$\tilde{D}_p^z = \begin{bmatrix} I \\ 0 \end{bmatrix}, \quad \tilde{D}_p^c = \begin{bmatrix} \tilde{D}_{p_1}^c \\ \tilde{D}_{p_2}^c \end{bmatrix}, \tag{7.23}$$

where $\tilde{D}_{p_2}^c$ must be full row rank. There exists, therefore, invertible matrix W such that $\tilde{D}_{p_2}^c W^{-1} = \begin{bmatrix} I & 0 \end{bmatrix}$. Define the following change of co-ordinates for variables c:

$$\begin{bmatrix} y \\ u \end{bmatrix} = \bar{c} := Wc =: \begin{bmatrix} W_1 \\ W_2 \end{bmatrix} c, \tag{7.24}$$

where the size of variable y is equal to the number of rows of $\tilde{D}_{p_2}^c$. Finally, partition $\tilde{D}_{p_2}^{\bar{c}} = \begin{bmatrix} I & 0 \end{bmatrix}$ induces partition $\tilde{D}_{\bar{c}} = \begin{bmatrix} \tilde{D}_{\bar{c}}^y & \tilde{D}_{\bar{c}}^u \end{bmatrix}$, where $\tilde{D}_{\bar{c}}^u$ must be square and invertible. It now follows that by applying the behavior preserving transformations of Lemma 6.2 as in Section 6.2, Σ_p can now be captured in dual I/O form with y and z as outputs and d and u as inputs, and $\Sigma_{\bar{c}}$ can be captured in dual I/O form with u an output and y an input, as stated in the lemma. Matrices M_p^{IO} and M_c^{IO} can readily be determined from $\tilde{M}_p$ and $\tilde{M}_c$; the details are omitted. ∎

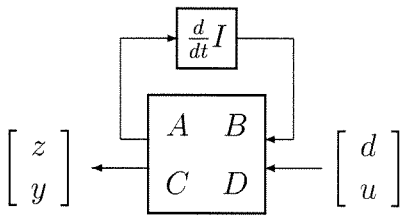

Figure 7.4: I/O representation

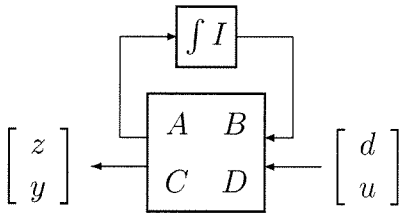

Figure 7.5: Dual problem

Lemma 7.4 has a simple interpretation: for there to be a solution to the $\mathcal{H}_\infty$ Optimal Interconnection problem, there must exist a partition of control variables c into y and u such that the behavior of Σ_p can be captured by the possibly non-proper, non-standard I/O map of Figure 7.4.

Given this representation, a solution to the $\mathcal{H}_\infty$ Optimal Interconnection problem may be obtained by applying a slightly modified version of the standard $\mathcal{H}_\infty$ solution in [Glover and Doyle, 1989] to the system of Figure 7.5. Note that the system of Figure 7.5 is constructed purely for technical reasons; there is no natural physical interpretation for it.

Theorem 7.5 *Let* $\mathbf{G}$ *be the system corresponding to state space representation*

$$\left[\begin{array}{c|cc} A & B_1 & B_2 \\ \hline C_1 & D_{11} & D_{12} \\ C_2 & D_{21} & 0 \end{array}\right],$$

as per Figure 7.5. There exists an allowable compensator Σ_c *if and only if there exists system* $\mathbf{K}$ *with state space representation*

$$\left[\begin{array}{c|c} \bar{A} & \bar{B} \\ \hline \bar{C} & \bar{D} \end{array}\right]$$

such that

I. $\mathbf{K}$ *internally stabilizes* $\mathbf{G}$ *except for possible modes at* 0*;*

II. $\|\mathbf{G} \star \mathbf{K}\| < 1.$

If such a $\mathbf{K}$ *exists, a dual representation matrix for an allowable* Σ_c *is*

$$\begin{bmatrix} x \\ 0 \end{bmatrix} = \begin{bmatrix} \bar{A} & \bar{B}W_1 \\ \bar{C} & (\bar{D}W_1 - W_2) \end{bmatrix} \begin{bmatrix} \dot{x} \\ c \end{bmatrix}. \tag{7.25}$$

Proof: Let Σ_c be an allowable compensator. By Lemma 7.4 and equation (7.20), the following dual I/O representation for Σ may be constructed:

$$\begin{bmatrix} x \\ z \\ c \end{bmatrix} = \begin{bmatrix} \hat{A} & \hat{B} \\ \hat{C}^z & \hat{D}^z \\ \hat{C}^c & \hat{D}^c \end{bmatrix} \begin{bmatrix} \dot{x} \\ d \end{bmatrix}, \tag{7.26}$$

where the above matrices can be determined from the matrices in Lemma 7.4; the details are omitted. By Corollary 7.1, the eigenvalues of $\hat{A}$ must be in $\mathbb{C}^- \cup \{0\}$ since $(\hat{C}, \hat{A})$ is an observable pair; this proves part **I**. There exists, therefore, a state transformation which yields the following equations:

$$\begin{bmatrix} x_s \\ x_{0_1} \\ x_{0_2} \\ x_{0_3} \\ z \end{bmatrix} = \begin{bmatrix} \hat{A}_s & 0 & 0 & 0 & \hat{B}_s \\ 0 & \hat{A}_{0_{11}} & 0 & \hat{A}_{0_{13}} & \hat{B}_{0_1} \\ 0 & \hat{A}_{0_{21}} & \hat{A}_{0_{22}} & \hat{A}_{0_{23}} & \hat{B}_{0_2} \\ 0 & 0 & 0 & \hat{A}_{0_{33}} & 0 \\ \hat{C}_s^z & \hat{C}_{0_1}^z & 0 & \hat{C}_{0_3}^z & \hat{D}^z \end{bmatrix} \begin{bmatrix} \dot{x}_s \\ \dot{x}_{0_1} \\ \dot{x}_{0_2} \\ \dot{x}_{0_3} \\ d \end{bmatrix}, \tag{7.27}$$

where $\hat{A}_s$ is Hurwitz and $\hat{A}_{0_{11}}, \hat{A}_{0_{22}}, \hat{A}_{0_{33}}$ are nilpotent. Equation $x_{0_3} = \hat{A}_{0_{33}}\dot{x}_{0_3}$ implies that $x_{0_3} = 0$; these are the algebraic constraints which result from a singular interconnection. Thus singularity is equivalent to uncontrollable modes at 0. States x_{0_2} are controllable from d, but unobservable from z; they are, however, observable from y and/or u; these states correspond to derivatives of d appearing in the closed loop expressions for y and u (note that this does not violate the stability requirement). The x_{0_1} states are controllable from d and observable from z. If any of these states are present, derivatives of d will appear in the closed loop expression for z, violating performance requirement P3.

Given that there are no x_{0_1} states, and since $\hat{A}_s$ is invertible, the following state-space I/O map from d to z may be written:

$$\begin{bmatrix} \dot{x}_s \\ z \end{bmatrix} = \begin{bmatrix} \hat{A}_s^{-1} & -\hat{A}_s^{-1}\hat{B}_s \\ \hat{C}_s^z\hat{A}_s^{-1} & \hat{D}^z - \hat{C}_s^z\hat{A}_s^{-1}\hat{B}_s \end{bmatrix} \begin{bmatrix} x_s \\ d \end{bmatrix}. \tag{7.28}$$

Furthermore, P3 is satisfied if and only if there are no x_{0_1} states and

$$\begin{aligned} &\sup_{w\in\mathbb{R}} \quad \bar{\sigma}\left(\hat{D}^z - \hat{C}_s^z\hat{A}_s^{-1}\hat{B}_s - \hat{C}_s^z\hat{A}_s^{-1}\left(jwI - \hat{A}_s^{-1}\right)^{-1}\hat{A}_s^{-1}\hat{B}_s\right) = \\ &\sup_{\bar{w}\in\mathbb{R}} \quad \bar{\sigma}\left(\hat{D}^z - \hat{C}_s^z\hat{A}_s^{-1}\hat{B}_s - j\bar{w}\hat{C}_s^z\hat{A}_s^{-1}\left(I - j\bar{w}\hat{A}_s^{-1}\right)^{-1}\hat{A}_s^{-1}\hat{B}_s\right) = \\ &\sup_{\bar{w}\in\mathbb{R}} \quad \bar{\sigma}\left(\hat{D}^z + \hat{C}_s^z\left(j\bar{w}I - \hat{A}\right)^{-1}\hat{B}_s\right) < 1. \end{aligned} \tag{7.29}$$

This proves part **II**. The sufficiency of conditions **I** and **II**, and the given representation for an allowable Σ_c, follow directly from the previous arguments and Lemma 7.4. ■

Under some mild assumptions, the solution to the $\mathcal{H}_\infty$ synthesis problem of Theorem 7.5 is presented next.

7.6 $\mathcal{H}_\infty$ Solution

A Riccati based solution to the synthesis problem of Theorem 7.5 is presented in this section, in the style of [Doyle et al., 1989]. The development will closely parallel that in [Glover and Doyle, 1989], and specific references to this work will be made to streamline the proofs and arguments.

The techniques used to solve this problem are very similar to those in [Mita et al., 1993] where an $\mathcal{H}_\infty$ control problem with unstable weighting functions is solved. In fact, the derived conditions in [Mita et al., 1993] are equivalent to those presented in this section, even though extra assumptions on their problem data are made. Similarly, in [Copeland and Safonov, 1995], a general synthesis procedure is outlined where pre-compensators are used to cancel zeros on the $j\omega$ axis; this approach, however, cannot be applied in general to the problem of Theorem 7.5.

In the setup of Theorem 7.5, a controller which internally stabilizes the system with the exception of possible modes at $s = 0$ will be termed an *admissible* controller. Note that the state-space equations for the closed loop system $\mathbf{G} \star \mathbf{K}$ are:

$$\left[\begin{array}{cc|c} A + B_2\bar{D}C_2 & B_2\bar{C} & B_1 + B_2\bar{D}D_{21} \\ \bar{B}C_2 & \bar{A} & \bar{B}D_{21} \\ \hline C_1 + D_{12}\bar{D}C_2 & D_{12}\bar{C} & D_{11} + D_{12}\hat{D}D_{21} \end{array}\right]. \tag{7.30}$$

For $\mathbf{K}$ to be admissible, any modes at $s = 0$ must be either unobservable or uncontrollable (or both). As is shown in [Zhou et al., 1995], the unobservable modes at $s = 0$ of (7.30) must correspond to the invariant zeros at $s = 0$ of $\mathbf{G}_{12}$, and the uncontrollable modes at $s = 0$ must correspond to the invariant zeros at $s = 0$ of $\mathbf{G}_{21}$, where

$$\mathbf{G}_{12} := \left[\begin{array}{c|c} A & B_2 \\ \hline C_1 & D_{12} \end{array}\right], \quad \mathbf{G}_{21} := \left[\begin{array}{c|c} A & B_1 \\ \hline C_2 & D_{21} \end{array}\right]. \tag{7.31}$$

These violate the invariant zero assumptions in [Glover and Doyle, 1989], as will be discussed next.

7.6.1 Assumptions

The following assumptions are made on the problem data:

(A2) D_{12} full column rank with $\begin{bmatrix} D_{12} & D_\perp \end{bmatrix}$ unitary, D_{21} full row rank with $\begin{bmatrix} D_{21} \\ \tilde{D}_\perp \end{bmatrix}$ unitary.

(A3) $\begin{bmatrix} A - j\omega & B_2 \\ C_1 & D_{12} \end{bmatrix}$ full column rank $\forall \omega \neq 0$.

(A4) $\begin{bmatrix} A - j\omega & B_1 \\ C_2 & D_{21} \end{bmatrix}$ full row rank $\forall \omega \neq 0$.

Condition (A3) is equivalent to $(D_\perp^* C_1, A - B_2 D_{12}^* C_1)$ having no purely imaginary unobservable modes, except possibly at $s = 0$. A Kalman decomposition induces the following state transformation S:

$$\begin{aligned} A^{FI} &= \begin{bmatrix} A_{11}^{FI} & A_{12}^{FI} \\ A_{21}^{FI} & A_{22}^{FI} \end{bmatrix} := S^{-1} A S, \\ \begin{bmatrix} B_1^{FI} & B_2^{FI} \end{bmatrix} &= \begin{bmatrix} B_{11}^{FI} & B_{21}^{FI} \\ B_{12}^{FI} & B_{22}^{FI} \end{bmatrix} := S^{-1} \begin{bmatrix} B_1 & B_2 \end{bmatrix}, \\ \begin{bmatrix} C_1^{FI} \\ C_2^{FI} \end{bmatrix} &= \begin{bmatrix} C_{11}^{FI} & C_{12}^{FI} \\ C_{21}^{FI} & C_{22}^{FI} \end{bmatrix} := \begin{bmatrix} C_1 \\ C_2 \end{bmatrix} S. \end{aligned} \tag{7.32}$$

In this co-ordinate system,

$$D_\perp^* C_1^{FI} = \begin{bmatrix} \bar{C}^{FI} & 0 \end{bmatrix}, \; (A^{FI} - B_2^{FI} D_{12}^* C_1^{FI}) = \begin{bmatrix} \bar{A}^{FI} & 0 \\ * & \Sigma^{FI} \end{bmatrix}, \tag{7.33}$$

where Σ^{FI} is nilpotent, and $(\bar{C}^{FI}, \bar{A}^{FI})$ has no purely imaginary unobservable modes.

Similarly, condition (A4) is equivalent to $(A - B_1 D_{21}^* C_2, B_1 \tilde{D}_\perp^*)$ having no purely imaginary uncontrollable modes, except possibly at $s = 0$. State transformation T is defined analogously to S.

The final assumption on the problem data follows, presented last since it is more natural to do so in the appropriate co-ordinate system:

(A1) $(A_{11}^{FI}, B_{21}^{FI})$ stabilizable, $(C_{21}^{FC}, A_{11}^{FC})$ detectable.

Assumption (A2) is equivalent to requiring that D_{12} and D_{21} be full column rank and full row rank, respectively, by the freedom in the change of co-ordinates of equation (7.24). In general, assumptions (A2), (A3), and (A4) are not necessary for a solution to exist, but they allow the Riccati based approach in [Glover and Doyle, 1989] to be used. (A1), however, is necessary for a solution to exist. If not satisfied, it can be shown that all closed loop maps will have unstable modes, with any modes

at $s = 0$ appearing in the map from d to z. The simplest method of relaxing assumptions (A2), (A3), and (A4) is to modify the various $\mathcal{H}_\infty$ LMI solutions in [Gahinet and Apkarian, 1994] and [Packard, 1994]. This is a topic of future research.

The only differences between the above assumptions and those in [Glover and Doyle, 1989] are the relaxation on the invariant zeros at $s = 0$ of $\mathbf{G}_{12}$ and $\mathbf{G}_{21}$; this is done to allow the closed loop system to have unobservable and/or uncontrollable modes at $s = 0$, as previously discussed.

7.6.2 Equivalence of Special Problems

Most of the complications which arise from relaxing the invariant zero at $s = 0$ assumption can be eliminated by showing the equivalence between two Full Information problems:

(FI) Given $\mathbf{G} = \left[\begin{array}{c|cc} A & B_1 & B_2 \\ \hline C_1 & D_{11} & D_{12} \\ \begin{bmatrix} I \\ 0 \end{bmatrix} & \begin{bmatrix} 0 \\ I \end{bmatrix} & \begin{bmatrix} 0 \\ 0 \end{bmatrix} \end{array}\right]$, find an admissible $\mathbf{K}$ such that $\|\mathbf{G} \star \mathbf{K}\| < 1$.

($\overline{\text{FI}}$) Given $\overline{\mathbf{G}} = \left[\begin{array}{c|cc} A_{11}^{FI} & B_{11}^{FI} & B_{21}^{FI} \\ \hline C_{11}^{FI} & D_{11} & D_{12} \\ \begin{bmatrix} I \\ 0 \end{bmatrix} & \begin{bmatrix} 0 \\ I \end{bmatrix} & \begin{bmatrix} 0 \\ 0 \end{bmatrix} \end{array}\right]$, find a stabilizing $\overline{\mathbf{K}}$ such that $\|\overline{\mathbf{G}} \star \overline{\mathbf{K}}\| < 1$.

Associated with problems FI and $\overline{\text{FI}}$ are Hamiltonians H_∞ and $\overline{H}_\infty$, respectively; their definitions may be found in [Glover and Doyle, 1989], equation (3.1). If $\overline{H}_\infty \in dom(Ric)$, we will denote $\overline{X}_\infty := Ric(\overline{H}_\infty)$, and

$$X_\infty := S^{-*} \begin{bmatrix} \overline{X}_\infty & 0 \\ 0 & 0 \end{bmatrix} S^{-1}.$$

Note that X_∞ is not defined in terms of $Ric(H_\infty)$; when $H_\infty \in dom(Ric)$, however, it can be shown that $X_\infty = Ric(H_\infty)$.

The following lemma outlines the equivalence of the two problems:

Lemma 7.6 FI *has a solution if and only if* $\overline{\text{FI}}$ *has a solution. Furthermore, all admissible* K *such that* $\|\mathbf{G} \star \mathbf{K}\| < 1$ *are given by the formulas in [Glover and Doyle, 1989], Theorem 3.1 (c).*

Proof: Assume, without loss of generality, that the state-space data for FI is in the same co-ordinates as $\overline{\text{FI}}$, i.e., $S = I$. The superscript ^{FI} will thus be dropped to simplify the notation. Let

$$\mathbf{K} = \left[\begin{array}{c|c} \hat{A} & \hat{B} \\ \hline \hat{C} & \hat{D} \end{array}\right]$$

be a candidate controller for FI, resulting in the following equations:

$$\begin{aligned} \dot{x}_1 &= A_{11}x_1 + B_{11}d + B_{21}(D_{12}^* C_{12}x_2 + u), \\ z &= C_{11}x_1 + D_{11}d + D_{12}(D_{12}^* C_{12}x_2 + u), \\ \dot{x}_2 &= A_{21}x_1 + A_{22}x_2 + B_{12}d + B_{22}u, \\ \dot{\hat{x}} &= \hat{A}\hat{x} + \hat{B}_1 x_1 + \hat{B}_2 x_2 + \hat{B}_3 d, \\ u + D_{12}^* C_{12}x_2 &= \hat{C}\hat{x} + \hat{D}_1 x_1 + \hat{D}_2 x_2 + \hat{D}_3 d + D_{12}^* C_{12}. \end{aligned} \tag{7.34}$$

Assume $\mathbf{K}$ solves FI. Then defining $\overline{\mathbf{K}}$ by the last three equations of (7.34) results in $\|\overline{\mathbf{G}} \star \overline{\mathbf{K}}\| < 1$. Note that it isn't clear whether $\overline{\mathbf{K}}$ is an internally stabilizing controller, since there could be closed loop modes at $s = 0$. By construction, the following matrix is full column rank

$$\left[\begin{array}{cc} A_{11} & B_{21} \\ C_{11} & D_{12} \end{array}\right];$$

it follows that $(u + D_{12}^* C_{12}x_2) \in \mathcal{L}_2^+ \; \forall d \in \mathcal{L}_2^+$. Thus a minimal realization for $\overline{\mathbf{K}}$ will internally stabilize $\overline{\mathbf{G}}$.
Conversely, if $\overline{\mathbf{K}} = \left[\begin{array}{cc} \mathbf{K}_1 & \mathbf{K}_d \end{array}\right]$ solves $\overline{\text{FI}}$, it follows that

$$\mathbf{K} := \left[\begin{array}{ccc} \mathbf{K}_1 & -D_{12}^* C_{12} & \mathbf{K}_d \end{array}\right] \tag{7.35}$$

is admissible since $(A_{22} - B_{22}D_{12}^* C_{12})$ is nilpotent, and the x_2 states are unobservable. Furthermore, $\|\mathbf{G} \star \mathbf{K}\| < 1$.
By equations (7.34) and the above arguments, it is clear that any $\mathbf{K}$ which solves FI can be decomposed into the form of (7.35), where $\overline{\mathbf{K}} = \left[\begin{array}{cc} \mathbf{K}_1 & \mathbf{K}_d \end{array}\right]$ solves $\overline{\text{FI}}$. It thus follows that if one could generate all $\overline{\mathbf{K}}$ which solve $\overline{\text{FI}}$, all $\mathbf{K}$ which solve FI could be generated as well. It can readily be verified that the equations in [Glover and Doyle, 1989] Theorem 3.1 (c) give this parameterization. ■

Full Control problems FC and $\overline{\text{FC}}$, the duals of the Full Information problems FI and $\overline{\text{FI}}$, can be defined analogously, along with J_∞, $\overline{J}_\infty$, and $\overline{Y}_\infty$. It can be shown that if $\overline{J}_\infty \in dom(Ric)$ and $\overline{Y}_\infty = Ric(\overline{J}_\infty)$, the corresponding definition for Y_∞ is $Y_\infty := T \left[\begin{array}{cc} \overline{Y}_\infty & 0 \\ 0 & 0 \end{array}\right] T^*$.

The equivalence of the FC and $\overline{\text{FC}}$ problems follow by duality.

7.6.3 Output Feedback

The formulas for all admissible controllers and the conditions for their existence are virtually identical to those in [Glover and Doyle, 1989], Theorem 4.1. In the interest of clarity, the formulas and conditions for $D_{11} = 0$ are given, although the proofs presented hold for $D_{11} \neq 0$. The formulas for the $D_{11} \neq 0$ case may be generalized as in [Glover and Doyle, 1989], Theorem 4.1.

Theorem 7.7 *Suppose* $\mathbf{G}$ *satisfies assumptions (A1) through (A4).*

1. *There exists an admissible* $\mathbf{K}$ *such that* $\|\mathbf{G} \star \mathbf{K}\| < 1$ *if and only if*
   (a) $\overline{H}_\infty \in dom(Ric)$, *with* $\overline{X}_\infty = Ric(\overline{H}_\infty) \geq 0$;
   (b) $\overline{J}_\infty \in dom(Ric)$, *with* $\overline{Y}_\infty = Ric(\overline{J}_\infty) \geq 0$;
   (c) $\rho(X_\infty Y_\infty) < 1$.
2. *Given that the conditions of part 1 are satisfied, then all rational admissible controllers* $\mathbf{K}$ *satisfying* $\|\mathbf{G} \star \mathbf{K}\| < 1$ *are given by* $\mathbf{K} = (\mathbf{K}_a \star \mathbf{\Phi})$ *for arbitrary* $\Phi \in \mathcal{RH}_\infty$ *such that* $\|\mathbf{\Phi}\| < 1$ *where*

$$
\begin{aligned}
\mathbf{K}_a &= \left[\begin{array}{c|cc} \hat{A} & \hat{B}_1 & \hat{B}_2 \\ \hline \hat{C}_1 & 0 & I \\ \hat{C}_2 & I & 0 \end{array}\right] := \left[\begin{array}{c|cc} A + BF + \hat{B}_1\hat{C}_2 & -Z_\infty^{-1}L_2 & Z_\infty^{-1}(B_2 + L_{12}) \\ \hline F_2 & 0 & I \\ -(C_2 + F_{12}) & I & 0 \end{array}\right], \\
Z_\infty &:= (I - Y_\infty X_\infty), \qquad (7.36) \\
F &:= \left[\begin{array}{c} B_1^* X_\infty \\ -(D_{12}^* C_1 + B_2^* X_\infty) \end{array}\right], \\
L &:= \left[\begin{array}{cc} Y_\infty C_1^* & -(B_1 D_{21}^* + Y_\infty C_2^*) \end{array}\right].
\end{aligned}
$$

Note, in fact, that the only difference between Theorem 7.7 and Theorem 4.1 in [Glover and Doyle, 1989] is that only Hamiltonians $\overline{H}_\infty$ and $\overline{Y}_\infty$ are required to be in $dom(Ric)$, not H_∞ and Y_∞. Also note that the coupling condition is on X_∞ and Y_∞, not on $\overline{X}_\infty$ and $\overline{Y}_\infty$. X_∞ and Y_∞ can be constructed from $\overline{X}_\infty$ and $\overline{Y}_\infty$, as outlined earlier.

Proof: The main idea in [Glover and Doyle, 1989] is to convert the output feedback problem to an output estimation problem, given that the Full Information problem has a solution. The solution to the output estimation problem, in turn, can be derived from the Full Control problem. This approach can also be used to prove Theorem 7.7; the only technical difficulty is allowing modes at $s = 0$, which must be uncontrollable and/or unobservable throughout the development. Thus one needs to ensure that the arguments used throughout the proofs in [Glover and Doyle, 1989] carry over when internal stability is relaxed to allowing modes at $s = 0$. This has already been done for the Full Information problem in Lemma 7.6, and the Full Control problem by duality.

It can be verified that the results on the disturbance feedforward and output estimation problems carry through once the results for the Full Information and Full Control problems are established; the main observation is that Lemma 3.4 in [Glover and Doyle, 1989] is still valid, since the modes at $s = 0$ of A_F are unobservable ([Glover and Doyle, 1989], equation (3.22)). The conversion from an output feedback problem to an output estimation problem follows immediately as well. The last step is then to solve the resulting output estimation problem, and establish the coupling condition and formulas.
The generalized plant for the derived output estimation problem is the following:

$$\mathbf{G}_{tmp} := \left[\begin{array}{c|cc} A + B_1F_1 & B_1 & B_2 \\ \hline -D_{12}F_2 & D_{11} & D_{12} \\ C_2 + D_{21}F_1 & D_{21} & 0 \end{array}\right]. \tag{7.37}$$

As shown in [Glover and Doyle, 1989], it is required to solve the corresponding Full Control problem. Assume, without loss of generality, that we are in the $\overline{\text{FC}}$ co-ordinate system. $\mathbf{G}_{tmp}$ then has the following form:

$$\mathbf{G}_{tmp} := \left[\begin{array}{cc|cc} A_{11} + B_{11}F_{11} & A_{12} + B_{11}F_{12} & B_{11} & B_{21} \\ A_{21} + B_{12}F_{11} & A_{22} + B_{12}F_{12} & B_{12} & B_{22} \\ \hline -D_{12}F_{21} & -D_{12}F_{22} & D_{11} & D_{12} \\ C_{21} + D_{21}F_{11} & C_{22} + D_{21}F_{12} & D_{21} & 0 \end{array}\right]. \tag{7.38}$$

It follows that $(\mathbf{G}_{tmp})_{21}$ inherits the same invariant zeros of $\mathbf{G}_{21}$. The corresponding Full Control problem to be solved (by Lemma 7.6 and duality) is therefore

$$\overline{\mathbf{G}}^{FC}_{tmp} := \left[\begin{array}{c|c|c} A_{11} + B_{11}F_{11} & B_{11} & \begin{bmatrix} I & 0 \end{bmatrix} \\ \hline -D_{12}F_{21} & D_{11} & \begin{bmatrix} 0 & I \end{bmatrix} \\ \hline C_{21} + D_{21}F_{11} & D_{21} & \begin{bmatrix} 0 & 0 \end{bmatrix} \end{array}\right], \tag{7.39}$$

with corresponding Hamiltonian $\overline{J}_{tmp}$. We thus need to establish that $\overline{J}_{tmp} \in dom(Ric)$ and that $\overline{Y}_{tmp} = Ric(\overline{J}_{tmp}) \geq 0$. In [Glover and Doyle, 1989], the following condition is derived:

$$J_{tmp} \begin{bmatrix} I - X_\infty Y_\infty \\ Y_\infty \end{bmatrix} = \begin{bmatrix} I - X_\infty Y_\infty \\ Y_\infty \end{bmatrix} (A + LC)^*, \tag{7.40}$$

where J_{tmp} is the Hamiltonian associated with the Full Control problem of (7.38). Because of the co-ordinate system chosen, this condition implies that

$$\overline{J}_{tmp} \begin{bmatrix} I - (\overline{X}_\infty)_{11}\overline{Y}_\infty \\ \overline{Y}_\infty \end{bmatrix} = \begin{bmatrix} I - (\overline{X}_\infty)_{11}\overline{Y}_\infty \\ \overline{Y}_\infty \end{bmatrix} \Lambda^*, \tag{7.41}$$

where Λ is associated with the $\overline{\text{FC}}$ problem, and is Hurwitz. It then follows that $\overline{Y}_{tmp} := \overline{Y}_\infty \left(I - (\overline{X}_\infty)_{11}\overline{Y}_\infty\right)^{-1} \geq 0 \iff \rho\left((\overline{X}_\infty)_{11}\overline{Y}_\infty\right) < 1 \iff \rho(X_\infty Y_\infty) < 1$. Furthermore, defining $Y_{tmp} := \begin{bmatrix} \overline{Y}_{tmp} & 0 \\ 0 & 0 \end{bmatrix}$, yields the required formulas, as per [Glover and Doyle, 1989]. ■

7.7 Example Revisited

We return to the example first outlined in Section 7.3. The following values for the system parameters are chosen:

$$m = 1,\ b = 20,\ k = 100.$$

Furthermore, z_1 is scaled by a factor of 100 relative to z_2.

Equations (7.4) are in AR form. Using the procedure of Section 6.1.1 to construct an ON representation, the procedure of Section 6.1.2 to make it minimal, and finally the procedure of Section 6.5 to eliminate latent variables F_c, x, y and r (which are properly eliminable), results in a representation matrix with the following D matrix

$$D = \begin{bmatrix} 0 & -0.0082 & 0 & 0 & -0.0001 \\ 0 & 0.0100 & 0 & 0.0087 & -0.9998 \\ 0 & 0.0002 & 0 & -0.5773 & -0.0151 \end{bmatrix} \tag{7.42}$$

and variables z_1, z_2, d, c_1 and c_2. It follows from Section 6.2 that the only one way to write the above as a proper I/O map is with z_1 and d as inputs. Furthermore, since the allowable control strategies must only involve c_1 and c_2, it follows that all interconnections must be singular. Thus standard $\mathcal{H}_\infty$ tools cannot be applied to this problem.

By next constructing a dual representation matrix as in Section 7.4, applying the procedure of Section 7.5 to convert it to the form of Theorem 7.5, using the $\mathcal{H}_\infty$ solution of Section 7.6, and constructing an AR representation from the resulting dual ON representation for Σ_c via Section 7.4.2, the following form for the optimal system Σ_c is obtained:

$$1.3379(\ddot{x} - \ddot{y}) + 10.1164(\dot{x} - \dot{y}) + 17.1342(x - y) + 0.1623\dot{F}_c + F_c = 0, \tag{7.43}$$

with the corresponding optimal performance level of $\gamma = 5.84$. Defining $k_{opt} := 17.1342$, $b_{opt} := 8.2417$, and I/O map $\mathbf{F}$ by transfer function $\frac{5.5861s}{s+6.1601}$, the following is an equivalent expression for (7.43):

$$F_c = -k_{opt}(x - y) - b_{opt}(\dot{x} - \dot{y}) + \mathbf{F}(x - y). \tag{7.44}$$

Thus the optimal system may be implemented as a spring with coefficient k_{opt}, a damper with coefficient b_{opt}, and an active component $\mathbf{F}$ (note that this parameterization is not unique. The criterion used to extract k_{opt} and b_{opt} was that the resulting

Synthesis	k	b	active component	γ achieved
$\mathcal{H}_\infty$ optimal	17.13	8.24	YES	5.84
$\mathcal{H}_\infty$ optimal	17.13	8.24	set to 0	6.11
Search	16.70	7.55	NO	6.00
$\mathcal{H}_\infty$, no tire	16.06	6.23	NO	6.23

Table 7.1: Comparison of various designs

transfer function be proper with a DC gain of 0). For comparison purposes, the resulting performance level without $\mathbf{F}$ is $\gamma = 6.11$.

In order to determine how close the above design comes to predicting what the optimal values of spring and damper coefficients are in the absence of $\mathbf{F}$, a search was performed by gridding the space of spring and damper coefficients, and determining the $\mathcal{H}_\infty$ norm for the resulting designs. The optimal design was a spring coefficient $k_{search} = 16.70$ and a damper coefficient $b_{search} = 7.55$, with a resulting performance level of $\gamma = 6.00$.

For this simple example, the optimal $\mathcal{H}_\infty$ design essentially gives the parallel interconnection of a spring and a damper as the optimal compensator Σ_c, the suspension. The difference between this design and that obtained by searching for optimal spring and damper values was less than 3%. This is mainly due to the simple performance specifications and road disturbance profile, which result in a relation between F_c and $x - y$ which can be approximated very well by a spring and a damper. In fact, by residualizing the tire dynamics (equivalently, by setting $y = r$), the optimal $\mathcal{H}_\infty$ design results in a performance level of $\gamma = 6.23$ a value of 16.06 for k_{opt}, a value of 6.23 for b_{opt}, and a value of 0 for $\mathbf{F}$. The various results are tabulated in Table 7.1.

7.8 Full Information and Full Control in a Behavioral Context

In the previous sections, a solution to the $\mathcal{H}_\infty$ Optimal Interconnection problem was presented which consisted of two Riccati equations and a coupling condition. Associated with each Riccati equation was a special problem from standard $\mathcal{H}_\infty$ theory: Full Information and Full Control . Since the original problem data was converted to a form for which the standard $\mathcal{H}_\infty$ tools could be applied, the physical meaning of these special problems is not readily apparent. In this section, the concepts of Full Information and Full Control are extended to the behavioral framework, and the implications of these definitions are explored. It is shown that these definitions are more fundamental than those given for the standard I/O case; in particular, the concept of state is not required and no a priori partition of the system variables into inputs and outputs needs to be performed.

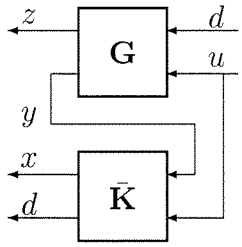

Figure 7.6: Full Information observer

7.8.1 Full Information and Full Control in the I/O Setting

In the Full Information problem, it is assumed that the controller has full access to the system state (denoted x) and the disturbances d. In the Full Control problem, it is assumed that the controller can influence the state equations (the ones involving $\dot{x}$) and the output error equations (the ones involving z) independently.

Given a system **G**, it can readily be shown that if the controller has access to x and d, the associated Full Control problem has a trivial solution; similarly, if the controller can influence the state and output error equations independently, the associated Full Information problem has a trivial solution. In each of the above two cases, only one Riccati equation needs to be solved, and the coupling condition is trivially satisfied.

In the behavioral framework, there is no distinction between inputs and outputs, and the concept of state is not an inherent property of the system. Thus one may ask the following question; is there a natural notion of Full Information and Full Control in the behavioral framework? If such a notion exists, it must not depend on I/O partitions, and be state-space independent. We motivate below how the concept of state may be removed from the Full Information problem in the I/O setting, as a prelude to the results of Section 7.8.2.

Stateless Full Information

A standard $\mathcal{H}_\infty$ problem reduces to a Full Information problem if an observer can be constructed which yields x and d, as shown in Figure 7.6. In this case, only one Riccati equation needs to be solved, since the associated Full Control problem is trivially satisfied, as previously discussed. As will be shown, the following is an equivalent condition: can an observer be constructed which yields d and z? We have the following proposition:

Proposition 7.8 *An observer can be constructed which yields x and d if and only if an observer (possibly improper) can be constructed which yields z and d.*

Proof: Let

$$\left[\begin{array}{c|cc} A & B_1 & B_2 \\ \hline C_1 & D_{11} & D_{12} \\ C_2 & D_{21} & D_{22} \end{array}\right]$$

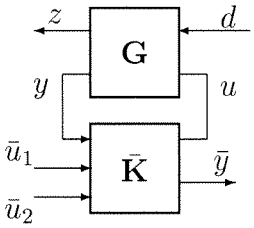

Figure 7.7: Full Control pre-compensator

be a minimal state space representation for **G**, with inputs d and u, and outputs z and y. Let an observer which yields x and d exist. Since $z = C_1 x + D_{11} d + D_{12} u$, one can recover z as well. Now assume that an observer which yields z and d exists. Note that

$$Cx = \begin{bmatrix} z \\ y \end{bmatrix} - D \begin{bmatrix} d \\ u \end{bmatrix}, \tag{7.45}$$

where all the variables on the right hand side are know. Thus by repeatedly differentiating the above equation and substituting for $\dot{x}$, and since (C, A) is an observable pair, one may recover state x. ■

Full Control

A problem reduces to a Full Control problem if a pre-compensator can be constructed such that u_1 can be injected into the state equations and u_2 can be injected into the output error equations, as shown in Figure 7.7. Unlike the Full Information problem, however, there is no simple definition of Full Control which does not involve the state; this is a shortcoming of the I/O framework, as shown below.

7.8.2 Full Information and Full Control in the Behavioral Setting

We proceed to define Full Information and Full Control in a behavioral context. Let Σ_p be given, and define $v := (z, d)$. The starting point is a minimal AR representation for the behavior $\mathcal{B}_p$:

$$R^v(\frac{d}{dt})v = R^c(\frac{d}{dt})c \tag{7.46}$$

Note that all the latent variables in Σ_p have been removed (see Section 6.5). We have the following definitions:

Definition 1 *The $\mathcal{H}_\infty$ Optimal Interconnection problem is a Full Information problem if $R^v(s)$ is full column rank $\forall s \in \mathbb{C}^+$.*

Definition 2 *The $\mathcal{H}_\infty$ Optimal Interconnection problem is a Full Control problem if $R^c(s)$ is full row rank $\forall s \in \mathbb{C}^+$.*

We now discuss the ramifications of these definitions:

Full Information

Assume that $R^v(s)$ satisfies the Full Information rank condition. By Smith decomposing $R^v(s)$ and left multiplication by a unimodular matrix (which does not change the behavior, see [Willems, 1991]), it can be assumed that

$$R^v(s) = \begin{bmatrix} \Delta(s) \\ 0 \end{bmatrix} V(s), \tag{7.47}$$

$$R^c(s) = \begin{bmatrix} R_1^c(s) \\ R_2^c(s) \end{bmatrix}, \tag{7.48}$$

where $\Delta(s)$ is square and invertible for all s in $\mathbb{C}^+$, $V(s)$ is unimodular, and $R_2^c(s)$ is full normal row rank. $R_2^c(s)$, in turn, can be decomposed as

$$R_2^c(s) = \begin{bmatrix} \Delta_2(s) & 0 \end{bmatrix} V_2(s) \tag{7.49}$$

where $\Delta_2(s)$ is square and of full normal rank, and $V_2(s)$ is unimodular. Define $\bar{c} := V_2(\frac{d}{dt})c =: (c_1, c_2)$. Thus $R_2^c(\frac{d}{dt})c = 0$ is equivalent to $\Delta_p(\frac{d}{dt})c_1 = 0$. Note that this change of co-ordinates in no way affects the feasibility of finding a solution; if $R_c^c(\frac{d}{dt})\bar{c} = 0$ is an allowable compensator in the new set of compensator co-ordinates, then $R_c^c(\frac{d}{dt})V_2(\frac{d}{dt})c = 0$ is an allowable compensator in the original compensator co-ordinates. Similarly if $R_c^c(\frac{d}{dt})c = 0$ is allowable in the original co-ordinates, then $R_c^c(\frac{d}{dt})V_c^{-1}(\frac{d}{dt})\bar{c} = 0$ is allowable in the new co-ordinates. As is argued in Section 7.5, a pre-compensator of the form $c_1 = 0$ can be applied to the system without changing the feasibility of finding an allowable compensator. Thus a Full Information problem can always be converted to the following form:

$$\Delta(\frac{d}{dt})V(\frac{d}{dt})v = R^c(\frac{d}{dt})c \tag{7.50}$$

after a possible change of compensator co-ordinates and applying an appropriate pre-compensator.

Given c, let $\tilde{v}$ solve the following system of equations

$$\Delta(\frac{d}{dt})V(\frac{d}{dt})\tilde{v} = R^c(\frac{d}{dt})c. \tag{7.51}$$

Thus

$$\Delta(\frac{d}{dt})\left(V(\frac{d}{dt})(v - \tilde{v})\right) = 0, \tag{7.52}$$

and by the assumed structure of $\Delta(s)$, $V(\frac{d}{dt})\tilde{v} \overset{t\longrightarrow\infty}{\longrightarrow} V(\frac{d}{dt})v$. Since $V(s)$ is unimodular, this implies that $\tilde{v} \overset{t\longrightarrow\infty}{\longrightarrow} v$. Thus by having access to control variables c, one may infer what variables v are, resulting in knowledge of all the system variables. Note that this is exactly the interpretation given in Section 7.8.1.

There is a connection between the Full Information problem discussed here and the behavioral version of $\mathcal{H}_\infty$ explored in [Trentelman and Willems, 1995]; in their formulation, $R^v(s)$ is assumed to be the identity, which is a special case of the Full Information rank condition.

Full Control

Assume that $R^c(s)$ satisfies the Full Control rank condition. Using a Smith decomposition, it can be assumed that

$$R^c(s) = \begin{bmatrix} \Delta(s) & 0 \end{bmatrix} V(s) \tag{7.53}$$

where $\Delta(s)$ is square and invertible for all s in $\mathbb{C}^+$, and $V(s)$ is unimodular. Define $\bar{c} := V(\frac{d}{dt})c =: (c_1, c_2)$. Thus

$$R^v(\frac{d}{dt})v = \Delta(\frac{d}{dt})c_1 \tag{7.54}$$

and c_2 does not affect v.

Given $\tilde{c}_1$, let c_1 solve the following system of equations

$$\Delta(\frac{d}{dt})c_1 = \tilde{c}_1. \tag{7.55}$$

Thus

$$R^v(\frac{d}{dt})v = \tilde{c}_1, \tag{7.56}$$

and by the assumed structure of $\Delta(s)$, $\tilde{c}_1 \overset{t\longrightarrow\infty}{\longrightarrow} 0 \Rightarrow c_1 \overset{t\longrightarrow\infty}{\longrightarrow} 0$. Thus one can fully control all the equations which involve variables v, and control variables c_1 approach the desired values $\tilde{c}_1$. It is clear why there is no simple I/O interpretation of the above result, as mentioned in Section 7.8.1; controlling the equations involving d and z has no simple counterpart in the I/O framework. The duality is apparent, however; in the I/O Full Information problem, it was shown that estimating x and d is equivalent to estimating z and d. For the Full Control problem, controlling x and z is equivalent to controlling the equations involving d and z.

7.8.3 Connections with Riccati Solution

We show in this section that if the Full Information rank condition of Definition 1 is satisfied, the I/O Full Control problem $\overline{\text{FC}}$ of Section 7.6.2 has a trivial solution and only the Riccati equation associated with the I/O Full Information problem $\overline{\text{FI}}$ needs to be solved. Similarly, if the Full Control rank condition of Definition 2 is satisfied, the I/O Full Information problem $\overline{\text{FI}}$ has a trivial solution and only the Riccati equation associated with the I/O Full Control problem $\overline{\text{FC}}$ needs to be solved.

Full Information

Let equation (7.50) be given, where $\Delta(s)$ is square and invertible for all s in $\mathbb{C}^+$ and $V(s)$ is unimodular. By Lemma 7.4, there exists a dual representation for the behavior $\mathcal{B}_p$ of the following form:

$$\begin{bmatrix} x \\ 0 \\ 0 \end{bmatrix} = \begin{bmatrix} A & 0 & B_1 & B_2W_2 \\ C_1 & -I & D_{11} & D_{12}W_2 \\ C_2 & 0 & D_{21} & -W_1 \end{bmatrix} \begin{bmatrix} \dot{x} \\ z \\ d \\ c \end{bmatrix}, \tag{7.57}$$

We have the following Theorem:

Theorem 7.9 *D_{21} is square and invertible, and the eigenvalues of $(A - B_1D_{21}^{-1}C_2)$ have negative real part or are zero. Furthermore, the I/O Full Control problem $\overline{FC}$ of Section 7.6.2 has a trivial solution.*

Proof: That D_{21} is square follows directly by setting $c = 0$ in equation (7.57) and by noting that $\Delta(s)V(s)$ is square. First assume that D_{21} is not invertible. Then there exists vector d_0 such that $D_{21}d_0 = 0$; then $(x, z, d, c) := (B_1d_0, D_{11}d_0, d_0, 0)$ satisfies equation (7.57), and thus

$$\Delta(0)V(0) \begin{bmatrix} D_{11}d_0 \\ d_0 \end{bmatrix} = 0,$$

a contradiction. Now let $s_0 \neq 0$ be an eigenvalue of $(A - B_1D_{21}^{-1}C_2)$ with positive or zero real part. By Schur complement arguments, this implies that there exist vectors x_0 and d_0 such that

$$\begin{bmatrix} A - s_0I & B_1 \\ C_2 & D_{21} \end{bmatrix} \begin{bmatrix} x_0 \\ d_0 \end{bmatrix} = 0.$$

Thus $(x, z, d, c) = (s_0x_0, C_1x_0 + D_{11}d_0, d_0, 0)\exp(s_0^{-1}t)$ satisfies equation (7.57). Note that if $d_0 = 0$, then $C_1x_0 \neq 0$ by the minimality of the dual representation in equation (7.57); thus

$$\Delta(s_0^{-1})V(s_0^{-1}) \begin{bmatrix} C_1x_0 + D_{11}d_0 \\ d_0 \end{bmatrix} = 0,$$

a contradiction.

Note that since D_{21} is invertible, it can be assumed to be unitary without loss of generality (pre-multiply the last row of equation (7.57) by D_{21}^{-1}, for example). The detectability assumption in (A1) and the rank condition in (A4) are satisfied as well. Since the eigenvalues of $(A - B_1D_{21}^{-1}C_2)$ have negative real part or are zero, it follows that the eigenvalues of $(A_{11}^{FC} - B_{11}^{FC}D_{21}^*C_{21}^{FC})$ must have negative real part. Applying the following control strategy to the I/O Full Control problem

$$\tilde{u}_1 = -B_{11}D_{21}^*\tilde{y}, \tag{7.58}$$

$$\tilde{u}_2 = -D_{11}D_{21}^*\tilde{y} \tag{7.59}$$

results in the following closed loop equations:

$$\dot{\tilde{x}} = (A_{11}^{FC} - B_{11}^{FC} D_{21}^{*} C_{21}^{FC})\tilde{x}, \tag{7.60}$$

$$\tilde{z} = (C_{11}^{FC} - D_{11}^{FC} D_{21}^{*} C_{21}^{FC})\tilde{x}. \tag{7.61}$$

Since the closed loop eigenvalues have negative real part, the above constant feedback law solves the I/O Full Control problem, and results in perfect disturbance attenuation. ■

Note that the Riccati equation associated with the above I/O Full Control problem has zero as a solution (all the closed loop modes are stable and uncontrollable); thus only the I/O Full Information problem needs to be solved, and the coupling condition between the two Riccati solutions is trivially satisfied.

Full Control

Let equation (7.54) be given, where $\Delta(s)$ is square and invertible for all s in $\mathbb{C}^+$. To avoid extra notation, replace c_1 by c. By Lemma 7.4, there exists a dual representation for the behavior $\mathcal{B}_p$ as in equation (7.57). We have the following Theorem:

Theorem 7.10 *D_{12} is square and invertible, and the eigenvalues of $(A - B_2 D_{12}^{-1} C_1)$ have negative real part or are zero. Furthermore, the I/O Full Information problem $\overline{FI}$ has a trivial solution.*

Proof: The proof is essentially the dual of the Full Information case and follows by setting $(d, z) = 0$ in equation (7.57); the details are omitted. ■

Analogous to the previous case, the Riccati equation associated with the associated I/O Full Information problem has zero as a solution (all the closed loop modes are stable and unobservable); thus only the I/O Full Control problem needs to be solved, and the coupling condition between the two Riccati solutions is trivially satisfied.

Example

We return to the example of Section 7.3. For positive values of b and k, this is a Full Information problem; the solution in Section 7.7 reduces to one Riccati equation. This may also be verified by expressing variables z and d as functions of c:

$$b\dot{z}_1 + kz_1 = b\dot{c}_2 + kc_2 - c_1 \tag{7.62}$$

$$z_2 = \frac{1}{m}\dot{c}_1 \tag{7.63}$$

$$d = \frac{1}{m}c_1 - \ddot{z}_1 \tag{7.64}$$

Thus z_1 can be recovered using the first equation, z_2 from the second equation, and since z_1 is now known, d can be recovered from the third equation.

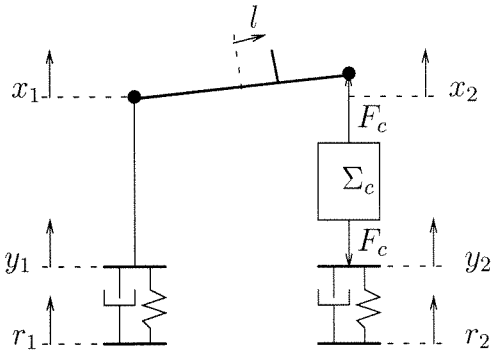

Figure 7.8: Suspension with two disturbances

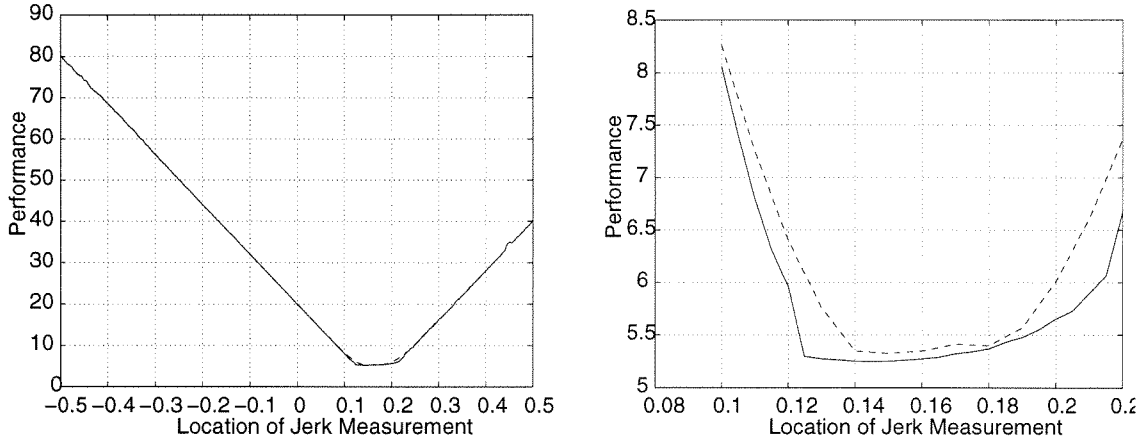

Figure 7.9: Suspension design as a function of l. The solid curve corresponds to the optimal design, while the dashed curve corresponds to a search for the optimal spring and damper values for the suspension.

7.9 Another Example

A slightly different example is the suspension design for a bicycle, depicted in Figure 7.8. The rider is situated at point l relative to the center of mass of the "frame," modeled as a rigid bar. The disturbances are $d_1 := \ddot{r}_1$ and $d_2 := \ddot{r}_2$, the control variables F_c and $x_2 - y_2$, and the output errors $x_2 - r_2$ and the jerk at point l. It can readily be verified that once the above system is written in the form of equation (7.46), the corresponding $R^v(s)$ is a three by four matrix, which cannot have full column rank for any value of s. By adding control variable $c_3 = d_1$, however, the above may be converted to a Full Information problem.

It is desired to design the suspension as a function of l. As in Section 7.7, the sprung mass has mass 1, the damper coefficient is 20, and the spring coefficient is 100. The tracking error is scaled by a factor of 100 relative to the jerk at point

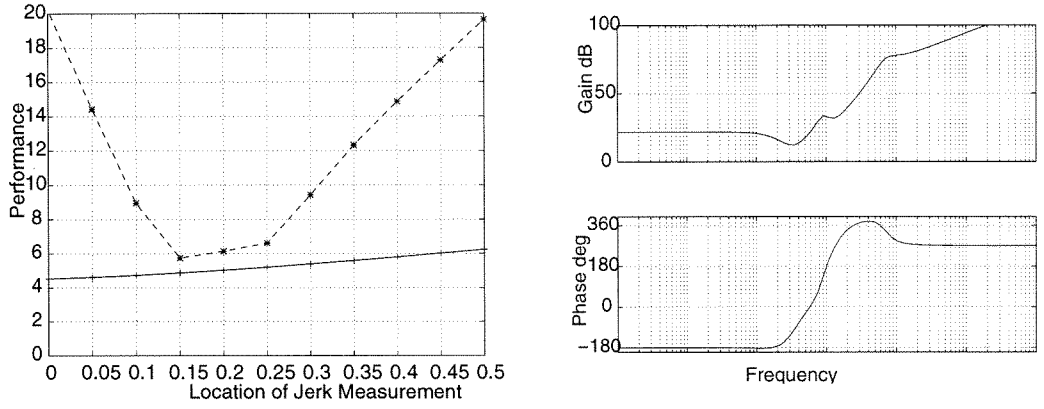

Figure 7.10: Suspension design as a function of l, $d_1(t) = d_2(t-1)$. In the left plot, the solid curve corresponds to the optimal design, while the dashed curve corresponds to a search for the optimal spring and damper values for the suspension. A bode plot for the optimal compensator (with the displacement an input and the force an output) at $l = 0.05$ is shown in the right plot.

l. The resulting designs are depicted in Figure 7.9. The solid curve corresponds to the optimal design, while the dashed curve corresponds to a search for the optimal spring and damper values for the suspension. For this simple case, the optimal design essentially resulted in a spring and a damper as the optimal components for the suspension.

A more interesting example is obtained by letting d_1 be a delayed version of d_2, $d_1(t) = d_2(t-1)$ (this is implemented as a first-order Pade approximation); this corresponds to the rear tire being subject to the same disturbance as the front tire, consistent with the bicycle moving forwards at a fixed speed. The resulting designs are depicted in Figure 7.10.

Note that the optimal compensator may be implemented as a spring, a damper, and an active component. Also note that unlike the previous examples, the active component is substantial and improves the design by over a factor of three (at $l = 0.05$).

Two interesting points may be concluded from this example. The first is that a substantial increase in performance may be achieved by using an active suspension. The second is that the optimal location for the rider depends on whether an active component is used or not.

7.10 Concluding Remarks

The results in this chapter extend the $\mathcal{H}_\infty$ framework to allow for singular interconnections. These types of interconnections occur naturally when interconnecting first principle models; for example, the simple suspension design presented in Sec-

tion 7.7 resulted in three algebraic constraints on the states.

A desirable feature of this design methodology is also demonstrated by this simple example; the optimal design consists of a part which can be implemented with passive components, and an active part. Typically, these designs are not performed simultaneously; i.e., the choice of which spring and damper values to use would not typically be made at the same time that an active suspension design was being performed. The problem formulation in this chapter makes no distinction between these two phases, and views the design process as determining the optimal relation between a given set of variables.

There are several logical continuations to this work. On the technical side, assumptions A_2, A_3, and A_4 in Theorem 7.5 need to be relaxed to provide a purely general solution. While issues of optimality have been explored in this chapter, the important issue of implementability has not been addressed. In many cases, the optimal relation between a system's variables may not be physically realizable; for example, how would one implement relation $F_c = \ddot{x} - \ddot{y}$ in the suspension design of Section 7.7? More generally, designs of real systems must take into account numerous other types of constraints, such as mass and size limitations, and other properties of a model, such as non-linearities, distributed effects, and model uncertainty, which make the design techniques presented in this chapter not directly applicable. The results in this chapter should thus be seen as providing bounds on the best achievable performance, and provide guidelines on how to proceed with the design of the overall system.

Part II

Rotating Stall Control of an Axial Flow Compressor using Pulsed Air Injection

Chapter 8
Preliminaries

In the next two chapters, a control strategy aimed at eliminating the hysteresis region normally associated with rotating stall is presented. This objective is a worthwhile pursuit in that it would allow operation closer to the stall line of a compressor. From a practical point of view, the elimination of the hysteresis region is a more realistic design objective than stabilizing the unstable branch of the compressor characteristic; this latter objective is typically only viable for systems with well defined stall precursors, not a justifiable assumption for many high speed systems.

We depart from previous studies in the sense that we make use of a small number of pulsed air injectors (three) as our means of actuation, and that the orientation of the injected air relative to the rotor face is not restricted to be in the axial direction. The motivation for using pulsed air injection is that they are a potentially practical technology for implementation on real engines. For similar reasons, we have concentrated on the use of wall mounted static pressure sensors for detecting stall rather than using hot wire anemometers. Indeed, one of the goals of this work is to indicate to what extent air injection is a viable actuation technology for stabilization of rotating stall, as initially explored in [Khalak and Murray, 1995].

In addition to providing detailed experimental results on the use of pulsed air injection for stabilization of rotating stall, an analysis of this approach is presented which uses the Moore-Greitzer formulation to construct a low-order nonlinear model of the dynamics in the presence of the controls. A shifted compressor characteristic is used to model the effect of the actuators, in a manner similar to that presented in [Gysling, 1993]. The analysis supports the experimental results obtained on the Caltech compressor and gives further insight into the role of pulsed air injection in the stabilization process.

This chapter serves as the background material for the results presented in Chapter 9. In Section 8.1, the phenomenon of rotating stall is briefly reviewed and the motivation for eliminating rotating stall in compression systems is presented. In Section 8.2, previous work aimed at tackling some of the issues which surfaced in the previous section is outlined. The experimental setup is described in Section 8.3; the relevant characteristics of the compressor system are described, including the steady-state performance characteristic of the compressor and the effects of continuous air injection on the steady-state performance characteristic. The Moore-Greitzer three-

state model, which is used extensively in the analyses of Chapter 9, is reviewed in Section 8.4.

8.1 Introduction and Motivation

As gas turbine engines have become better understood and better designed, substantial performance increases in engine designs have become harder to achieve, especially with passive control methods. The presence of full authority digital engine controllers (FADECs) on modern gas turbines has enabled the use of active control to achieve additional performance enhancements. Virtually all modern aircraft engines rely on the use of FADECs for controlling engine operation, although the use of dynamic feedback to modify engine operation is relatively rudimentary.

One example of the use of active control to improve engine performance is the Performance Seeking Control (PSC) program at NASA Dryden Flight Research Center. The basic idea behind performance seeking control is to modulate the engine parameters to achieve optimal performance based on the current operating conditions. In simulation studies [Smith et al., 1991] a 15% increase in thrust and a 3% decrease in fuel consumption have been obtained by the use of a controller which scheduled engine parameters for improved steady-state operation. Subsonic flight tests at NASA Dryden Flight Research Center [Gilyard and Orme, 1992] validated the technique and showed a 1–2% decrease in fuel consumption during minimum fuel mode operation and measured thrust increases of up to 15% during maximum thrust mode.

Future applications of active control to jet engines will increasingly rely on the use of dynamic feedback to modify the dynamics of the engine and provide enhanced stability which is currently unachievable with passive methods. The development of so-called smart engines [Paduano et al., 1993b] is an area of intense research activity, both in academia and in industry. A major goal is the use of feedback controllers to reduce the effects of performance limiting instabilities that currently constrain the available power and efficiency of jet engines. In addition to technological advances, success in this area requires new techniques for modelling of jet engine dynamics for the purposes of control, as well as development and application of advanced control techniques capable of taking into account the high noise levels and nonlinear operating characteristics of aeroengines.

An initial step in the development of active control techniques for gas turbine engines is active control of the compressor core of the engine. Two of the main limiting factors in the performance of compression systems are rotating stall and surge. Rotating stall refers to a dynamic instability that occurs when a non-axisymmetric flow pattern develops in the blade passages of a compressor stage and forces a drastic reduction in the performance of the compressor. This degradation in performance is usually unacceptable and must be avoided.

The Emmons stall model [Emmons et al., 1955] provides an intuitive, if somewhat simplistic, explanation of the stall phenomenon. Consider Figure 8.1. The right diagram represents a cross-section of a high hub-to-tip ratio compressor, typical of

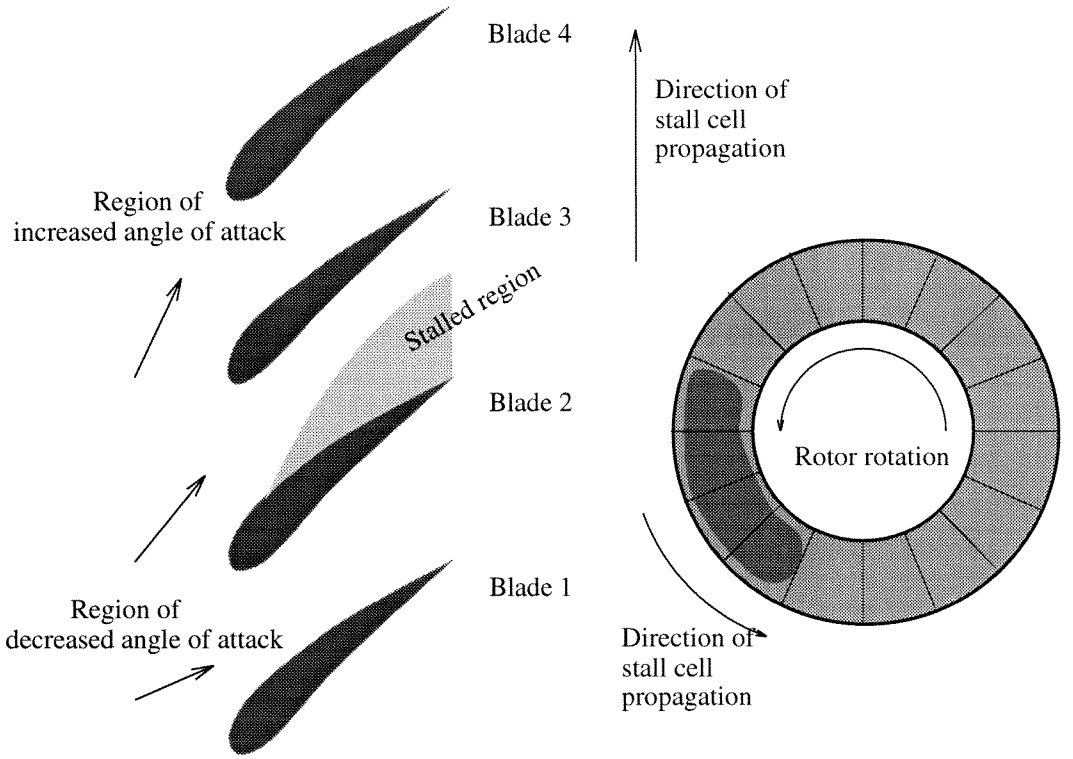

Figure 8.1: Emmons model of stall

axial flow systems. Assuming that the flow is essentially two-dimensional in nature (stemming from the high hub-to-tip ratio assumption), the rotor blades can be "unwrapped" in the circumferential direction and yield the diagram on the left. Each rotor blade is assumed to be a small airfoil. In a fixed rotor frame of reference, the free-stream incident angle can be broken down into two orthogonal components, the first due to the rotor rotation, the second due to the axial flow through the compressor. As the flow through the compressor is reduced, the angle of attack on each blade is increased (assuming that the rotation rate of rotor is kept constant). When the angle of attack exceeds the stall angle of a blade, the flow about that blade separates. The effect is to divert the flow about this reduced flow blade, increasing the local angle of attack of the blade immediately above it and decreasing the angle of attack of the blade immediately below it, as depicted in the figure. This has the effect of stalling the blade above, and unstalling the blade below. Thus the stalled region moves up the row of rotor blades, resulting in a region of reduced flow rotating around the circumference of the compressor, as depicted on the right in Figure 8.1. The rate of rotation of the stalled region is typically a fraction of the rotation rate of the rotor. It has experimentally been observed that more than one such stalled region may be present, with all the stalled regions rotating at the same rate. The overall effect of this rotating stalled region is a reduced average pressure and average flow operating condition. Furthermore, the flow typically has to be increased a substantial amount before all the blades unstall.

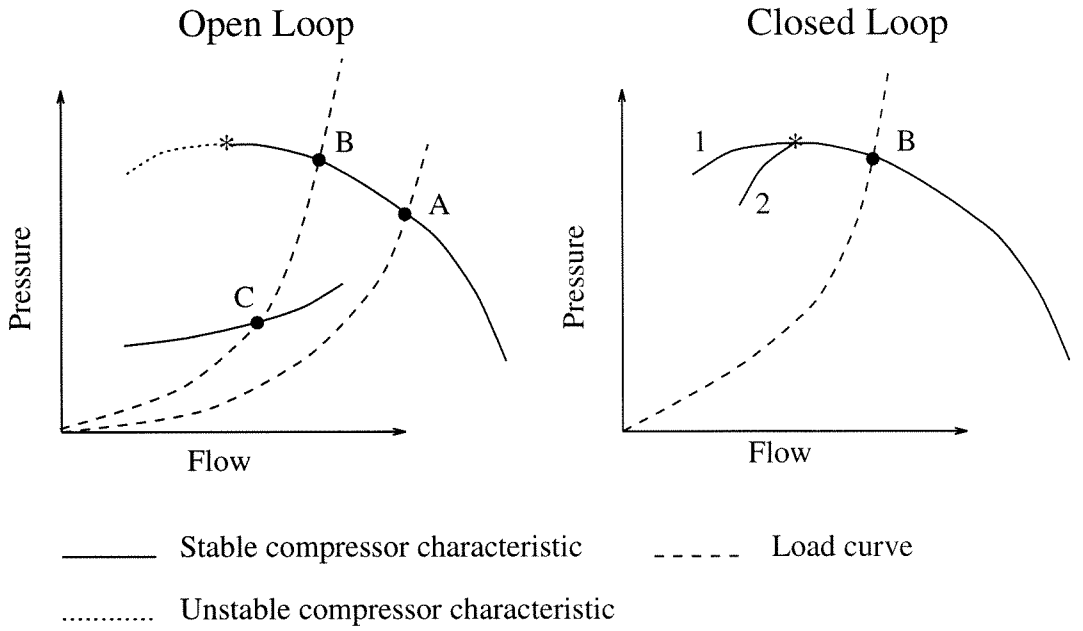

Figure 8.2: The solid curve corresponds to stable operating points for the compressor, the dotted curve unstable operating points. The actual operating point is the intersection of the compressor characteristic with the dashed load curve. The asterisk corresponds to the peak of the compressor characteristic, the transition between stable and unstable open loop operation. In the Closed Loop plot, curve 1 corresponds to a control strategy which stabilizes the unstable portion of the compressor characteristic with no rotating stall component, while curve 2 corresponds to a control strategy which stabilizes the unstable portion of the compressor characteristic with varying degrees of rotating stall.

Surge is a large amplitude, axisymmetric oscillation in the compressor which results from exciting unstable dynamics in the overall pumping system. While surge and stall are separate phenomenon, the presence of stall is a precursor to the onset of surge in many compressor systems. A more detailed description of these phenomena and their effects on overall performance can be found in the survey paper [Greitzer, 1981].

The goal of active control of stall and surge is to improve *operability* of the engine by allowing operation closer to the current stall line of the compressor. One of the significant features of high-performance axial-flow compressors is hysteresis in the performance of the compressor before and after rotating stall. As a consequence, if the operating point of a compressor momentarily crosses over the stall line due to a transient effect, the operating point of the compressor does not return to its original value, but rather to a much lower pressure/flow point.

This is depicted in the left diagram of Figure 8.2. If the compressor is operated at point B (the intersection of the steady-state compressor curve and the load curve),

another stable operating point, C, exists on the lower branch of the compressor characteristic. This operating point corresponds to the lower average pressure and average flow conditions which exist during rotating stall. The basin of attraction of operating points on the lower branch is typically much larger than that of points on the upper branch, especially when point B is near the top of the compressor characteristic; thus small disturbances and transient effects can lead to a jump from operating point B to operating point C. In order to avoid this jump, the compressor is operated at point A, where the load curve only intersects the compressor at one point.

Using active control methods it is possible to modify the dynamics of the system such that hysteresis effects are either delayed or eliminated (depending on the approach used). This is depicted in the diagram on the right-hand side of Figure 8.2. Either the unstable portion of the compressor characteristic can be stabilized (no rotating stall), or operating points which exhibit varying degrees of rotating stall can be created. In either case, the lower branch of the compressor characteristic disappears (in the region of interest), and the hysteresis region normally associated with rotating stall is eliminated.

8.2 Previous Work

Early work on rotating stall and surge concentrated on developing theoretical models which captured the main features of the two effects. In [Greitzer, 1976], a 1D (axial) model was presented which predicted the onset of surge using a single parameter, B. For large values of B the pumping system exhibits surge while for small values it operates in rotating stall. More recent work [Moore and Greitzer, 1986] gives a refined model of rotating stall and surge which uses three coupled, nonlinear, partial differential equations to model the pressure and flow in a compressor system. The Moore-Greitzer model is the starting point for many of the current models used for rotating stall. In additional to fundamental modeling issues, there has also been work in studying the details of how stall occurs in experimental systems [Day, 1993b]. The detailed dynamics of stall and surge are not yet understood, but the basic mechanisms of stall and surge are fairly well classified and models which capture the main features of these instabilities are currently available in the literature.

There have been some recent papers which give a good overview of the basic analysis techniques which can be brought to bear [Abed et al., 1993, McCaughan, 1989, McCaughan, 1990]. These papers analyze the global bifurcation behavior of the uncontrolled system and illuminate the nonlinear characteristics of the system which lead to instability as well as hysteresis. These techniques are particularly important in understanding the difference between improving operability of the engine and stabilization of the unstable dynamics.

Despite of the complexity of the dynamics of the system, experimental work has demonstrated that active control can be used to extend the operating point of the compressor past the normal stall limit. In [Paduano et al., 1993a], for example, a 20% decrease in mass flow for stall inception using actuated inlet guide vanes which

generated an upstream vortical distortion was reported; circumferential modes were used to model the compressor, actuators, and sensors, and a decoupled, linear model for the evolution of the modal coefficients was assumed. In [Day, 1993a], a similar technique with air injection as the actuation scheme was used, and an extension of approximately 5% in the stall point was achieved. Day also explored the use of air injection for destabilizing finite stall cells by injecting air in the jet nearest the stall cell. The control design was ad hoc, but gave good performance and did not rely on modal behavior. Active stabilization using aero-mechanical feedback has been reported in [Gysling, 1993, Gysling and Greitzer, 1995], where an array of twelve small reed valves upstream of the rotor which injected air based on the unsteady pressure exerted on the reed valve in the presence of rotating stall was used. By properly tuning the mechanical properties of the reed valve mechanism, rotating stall was stabilized past the normal stall point of the compressor. A modal analysis (in the circumferential variable) of the controller was used to validate the experimental results on an analytical model.

A somewhat different approach is the use of 1D actuation via bleed valves for control of rotating stall and surge. The controllers are based on a relatively complex 1D model of the compressor which captures the hysteresis and global dynamics of the system. The controllers change the nonlinear characteristics of the system so that surge does not occur and the change in operating point due to rotating stall is minimized. The approach used in [Badmus et al., 1995] used axisymmetric actuation (an outlet bleed valve) to eliminate the hysteresis effects of stall and also prevent surge without eliminating the stall cells *per se*. A theoretical description of this approach has been given in [Liaw and Abed, 1996]. Recent experimental and numerical investigations of this technique can be found in [Eveker et al., 1995].

8.3 Experimental Setup

In order to test the effects of air injection for stabilization of rotating stall, a low-speed, axial flow compressor facility designed for use in validation of active control techniques has been constructed at Caltech. While this compressor is substantially simpler than a typical compressor in a gas turbine engine, it has many of the essential operating characteristics of high-speed compressors and is ideally suited for implementation of active control techniques due to its size and ease of use.

The entire experimental setup is shown in Figure 8.3 and was designed and constructed in accordance with AMCA/ASHRE standards for measurement and calibration of compressors of this type [AMCA/ASHRAE, 1985]. The compressor is a 17 cm diameter, single stage, axial flow compressor with 14 blades, a hub to tip ratio of 0.7, and a blade chord of 3.75 cm. In addition to the compressor unit, the system consists of an inlet nozzle, adjustable downstream throttle, and an optional plenum. Sensors include a pair of static pressure rings on the inlet and outlet sides, a pitot measuring plane near the outlet, and an array of six static pressure transducers located in front of the compressor face. Actuation is achieved with a low-speed, electrically driven

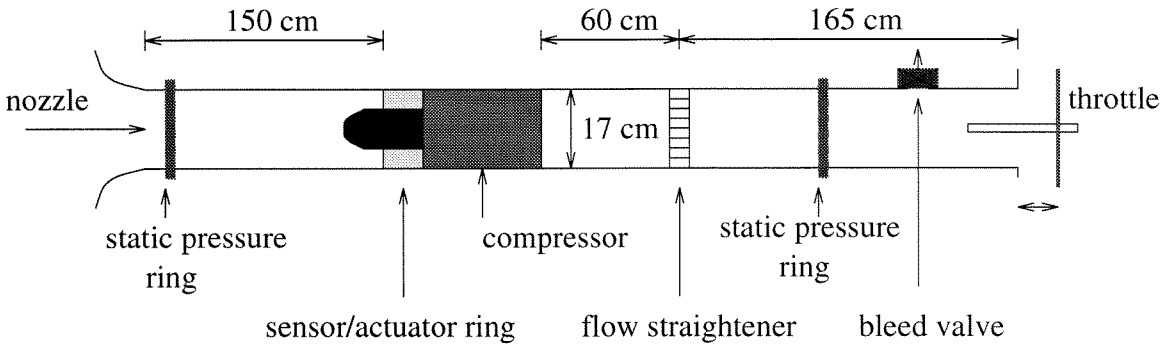

Figure 8.3: Caltech compressor rig

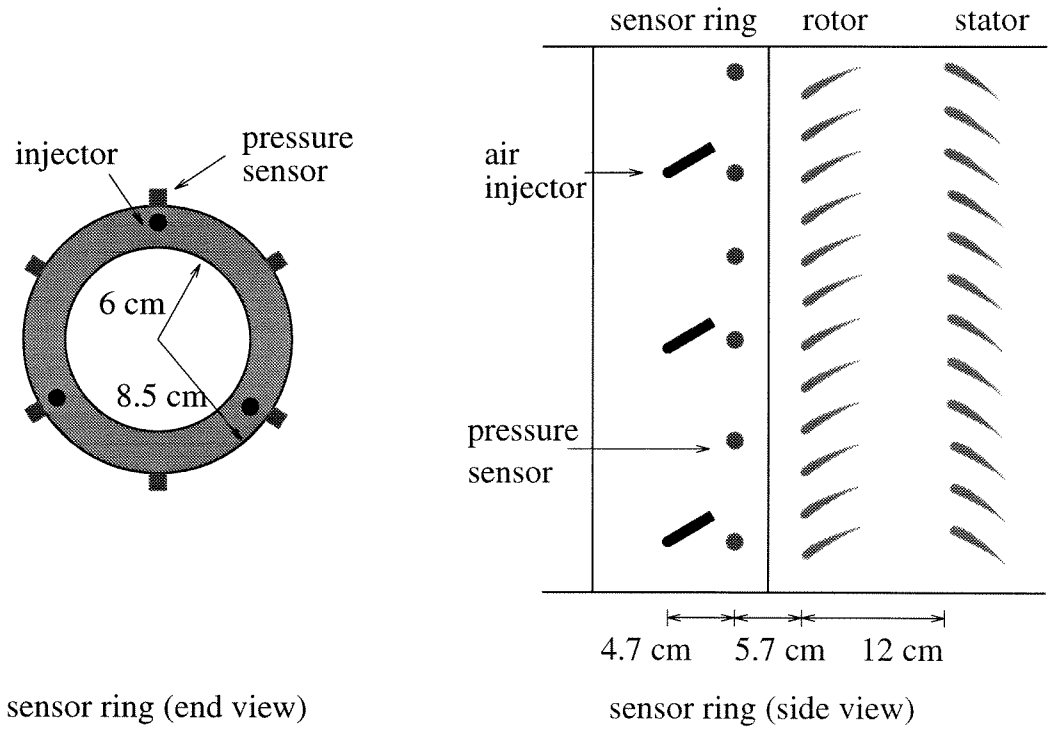

Figure 8.4: Sensor ring

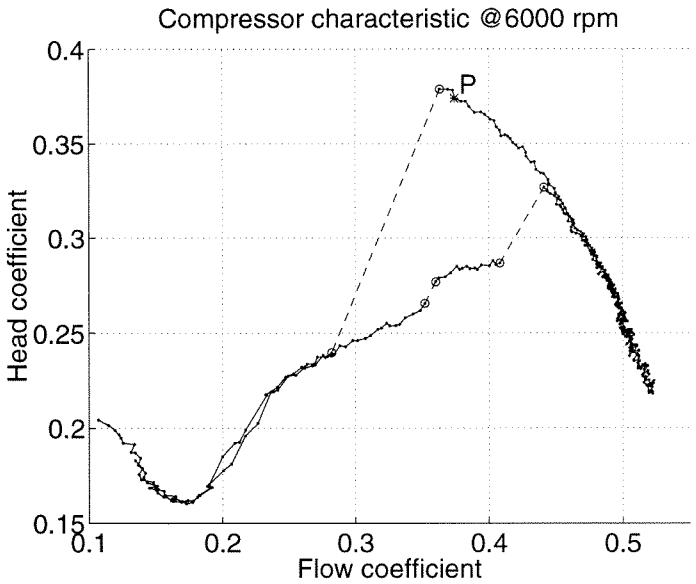

Figure 8.5: Fan characteristic for Able 29680 compressor at 6000 RPM. The flow coefficient is is defined to be $\frac{\dot{m}}{\rho A_a U_r}$, where m is the mass flow through the compressor, ρ is the density of air, A_a is the cross-sectional area of the annulus, and U_r is the rotor blade speed at mid-span. The head coefficient is defined to be $\frac{\Delta P}{\rho U_r^2}$, where ΔP is the pressure rise across the compressor. Dark lines indicate continuous changes in the operating point while lighter lines represent discontinuous changes. The circles mark the points of discontinuity. 'P' is the operating point for the parametric studies outlined in Section 9.2.

throttle at the outlet as well as a high response bleed which can be located either before or after the plenum and a set of three air injectors at the compressor face (described in more detail below).

For all the experimental results presented, the compressor was run at 6000 RPM, giving a peak head coefficient of 0.38 at a flow coefficient of 0.37, as shown in Figure 8.5. In physical units, this corresponds to 940 Pa at 0.19 m^3/s . The high response bleed valve was only used to generate disturbances, and the optional plenum was only used in the experiments of Section 9.2.3. All sensors and actuators are interfaced to a PC-based real-time control computer running at a servo rate of 2000 iterations per second.

The sensor ring shown in Figure 8.4 is located at the compressor inlet and used to measure the unsteady pressures upstream of the rotor. The ring has six pressure transducers equally spaced around the compressor circumference, approximately 5 cm (0.7 mean rotor radii) upstream of the rotor. These transducers have a resolution of approximately 1.2 Pa and a bandwidth of 1 kHz, and are low-pass filtered at 500 Hz prior to sampling by a 12 bit A/D converter. The inlet and outlet static pressure rings shown in Figure 8.3 are instrumented with similar transducers, but are not filtered

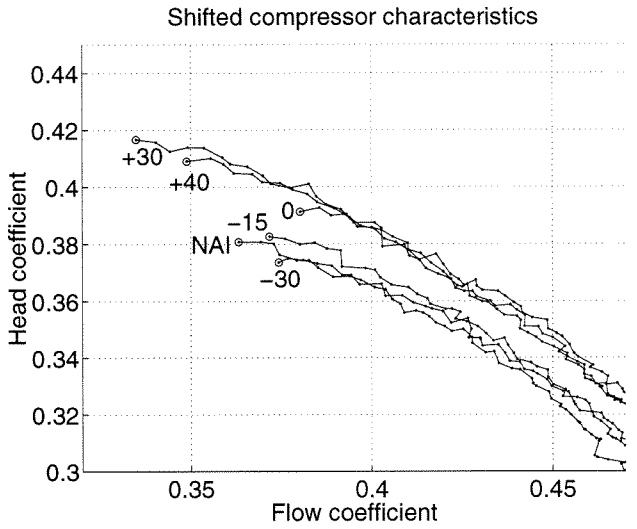

Figure 8.6: Compressor characteristics for various air injection angles. The flow coefficient calculation is based on the total flow through the compressor (i.e., it includes the contribution from the air injectors). 'NAI' corresponds to the unactuated case (no air injection). The circles mark the peak operating point for each compressor characteristic.

prior to sampling.

Three air injection actuators are also located on the sensor ring shown in Figure 8.4. The injectors are controlled by on/off solenoid valves which can be placed at a variety of (static) locations and orientations. The valves are actuated via custom overdriving circuitry interfaced directly to the computer, and are capable of a 50% duty cycle at up to 200 Hz. Hot-wire measurements were performed to determine the velocity profile of the air injection at the compressor face for the active control experiments outlined in Section 9.2. The injected air was found to disperse from 3 mm at the exit of the injector to approximately 20 mm at the compressor face; this dispersion occurred over a distance of 9 cm (the distance between the exit of the air injector and the rotor face).

Three measures of control authority were calculated to characterize the air injectors; the mass flux, the momentum flux, and the energy flux. As a percentage of the mean values for the compressor operating at the peak of the compressor characteristic, the flow through each air injector on continuously contributed to 1.7% of the mass flux, 2.4% of the momentum flux, and 1.3% of the energy flux . Each of the control authority measures is thus small compared to the corresponding values for the compressor.

The dynamic behavior of the compressor system has many of the basic properties of high performance, axial flow compressors. The measured compressor characteristic is shown in Figure 8.5. The effect of rotating stall is clearly seen in the measured compressor characteristic. If the flow is decreased beyond the value at which the characteristic reaches its peak, the compressor enters rotating stall and operates at

a much lower average pressure. Once in rotating stall the flow must be increased substantially before the system returns to the unstalled portion of the compressor characteristic.

The effects of the air injectors can be roughly characterized by their effect on the static compressor map. In [D'Andrea et al., 1995], the effect of continuous air injection into the rotor face at different incident angles was investigated. The experimental results indicated that the compressor characteristic could be altered by air injection. In Figure 8.6, the shifted compressor characteristics are plotted for various incident angles. In these plots, the flow coefficient corresponds to the mass flow through the compressor (sum of the inlet mass flow plus the injected mass flow). Note that for positive angles (air injected into the blade rotation), the shifting of the characteristic is approximately the same, with the only difference being the stall inception point (as marked by circles).

8.4 Moore-Greitzer Three-State Model

In this section, a three state model for a compression system based on a single mode Galerkin projection [Moore and Greitzer, 1986] is presented. This model is too simple to be able to reproduce in detail the operation of a compressor. It does, however, capture the essential dynamics of a compression system and allows one to perform symbolic analysis of the model.

The Moore-Greitzer three-state model is essentially a relation between the following dimensionless variables:

ξ	time
θ	circumferential position about annulus
$\Phi(\xi)$	annulus averaged flow through compressor
$A(\xi)$	amplitude of sinusoidal flow component through compressor
$\Psi(\xi)$	instantaneous annulus averaged pressure rise across compressor
γ	throttle position (the load)

The compressor is assumed to be of high hub-to-tip ratio, thus the flow at the rotor face is restricted to an annulus, and is essentially two-dimensional; θ corresponds to the angular position about this annulus. The flow through the compressor at the rotor face is assumed to be of the form $\Phi(\xi)+A(\xi)\sin(\theta+\omega\xi)$, where ω is the angular rate of rotation of the flow disturbance.

The Moore-Greitzer equations (see [Moore and Greitzer, 1986]) are:

$$\begin{aligned}
\frac{d\Psi(\xi)}{d\xi} &= \frac{1}{4l_cB^2}\left(\Phi(\xi)-\gamma\sqrt{\Psi(\xi)}\right), \\
\Psi(\xi)+l_c\frac{d\Phi(\xi)}{d\xi} &= \frac{1}{2\pi}\int_0^{2\pi}\boldsymbol{\Psi}_c(\Phi(\xi)+A(\xi)\sin\zeta),d\zeta \qquad (8.1)\\
\left(m+\frac{1}{a}\right)\frac{dA(\xi)}{d\xi} &= \frac{1}{\pi}\int_0^{2\pi}\boldsymbol{\Psi}_c(\Phi(\xi)+A(\xi)\sin\zeta)\sin\zeta d\zeta.
\end{aligned}$$

In the equations, Ψ_c is the steady-state compressor characteristic, and the quantities l_c, B, a, and m are parameters which depend on the compression system. The basic assumptions which are inherent in the above model are the following:

- Potential flow upstream of the compressor. This assumes a low-speed system and clean inlet conditions.
- Two-dimensional flow. This assumes a high hub-to-tip ratio compressor.
- The pressure rise across the compressor is small compared to the ambient level.
- The compressor characteristic is a memoryless nonlinearity operating on the local flow coefficient.
- The first modal component of the non-axis symmetric portion of the disturbance is dominant.

The reader is referred to [Moore and Greitzer, 1986] for an in-depth discussion on the above assumptions. The essential feature of the three-state model is that the complex fluid dynamic interactions in the compressor are captured by a nonlinear map (the compressor characteristic) and by first-order lags which capture the inertia of the fluid through the compressor. This apparently simple model and its extensions have been remarkably successful at capturing the essential dynamics of compression systems.

With the assumption that the nonlinearity which captures the compressor characteristic is a polynomial of order no higher than three, the previous integrals may be performed to yield the following set of ODEs:

$$\begin{aligned} \dot{\Psi} &= \frac{1}{4l_cB^2}\left(\Phi - \gamma\sqrt{\Psi}\right), \\ \dot{\Phi} &= \frac{1}{l_c}\left(\Psi_c(\Phi) - \Psi + \frac{J}{4}\frac{\partial^2\Psi_c(\Phi)}{\partial\Phi^2}\right), \\ \dot{J} &= \frac{2a}{1+ma}J\left(\frac{\partial\Psi_c(\Phi)}{\partial\Phi} + \frac{J}{8}\frac{\partial^3\Psi_c(\Phi)}{\partial\Phi^3}\right), \end{aligned} \tag{8.2}$$

where $J := A^2$.

The bifurcation properties of the above system of equations were initially studied in [McCaughan, 1989, McCaughan, 1990], where the bifurcations for the pure rotating stall case, the pure surge case, and combination stall/surge case were thoroughly investigated. Only the analysis for the pure rotating stall case is discussed here.

The bifurcation diagram for a representative compressor characteristic is known to have a transcritical bifurcation (for the choice of coordinates chosen) at the point which corresponds to operating at the peak of the steady-state compressor characteristic (see Figure 8.7). This throttle setting, which corresponds to the peak of the characteristic $(\partial\Psi_c(\Phi)/\partial\Phi) = 0$, is denoted by γ^*. This operating point corresponds

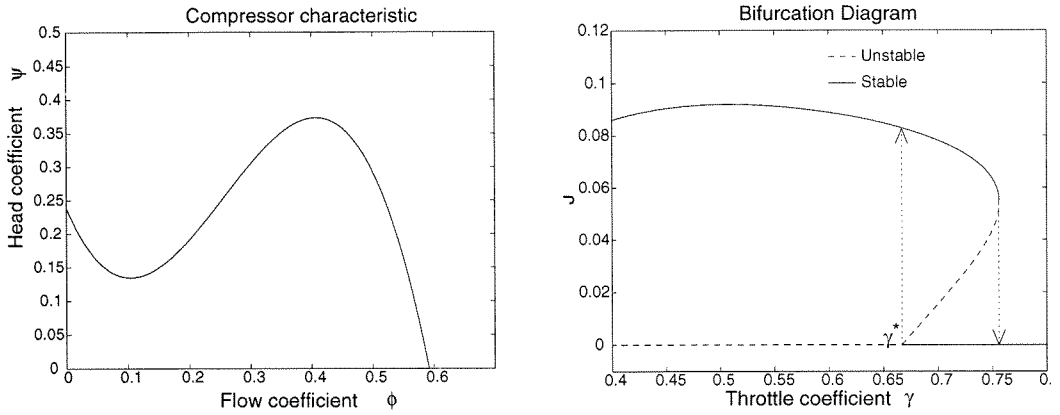

Figure 8.7: Bifurcation diagram showing jumps associated with the hysteresis loop for the compressor characteristic shown on the left. The numerical values were determined by fitting the various model parameters in equations (8.2) to the Caltech rig.

to where the stalled branch intersects the horizontal axis in the bifurcation diagram shown in Figure 8.7.

The unstable sections of the bifurcation diagram in Figure 8.7 are shown as dashed lines, and the stable sections are shown as solid lines. This diagram suggests a hysteresis region since as the throttle is closed (γ is decreased) $J = 0$ is a stable solution until γ^* is reached, at which point the stable solution for J is non-zero (which corresponds to a jump to rotating stall). As γ continues to decrease, the stable solution for J continues to be non-zero. If the throttle is then opened, beginning at $\gamma < \gamma^*$, the system continues to evolve along the stalled branch until γ is increased to a value substantially greater than γ^* before returning to the $J = 0$ branch. The system has substantially different solutions depending on the path that γ follows.

Chapter 9
Control of Rotating Stall

In this chapter, results on the use of pulsed air injection to control rotating stall in the Caltech compressor are presented. In Section 9.1, the injection of air is modeled as an unsteady shift in the compressor characteristic, and incorporated into the Moore-Greitzer three-state model of the compressor. By observing the change in the bifurcation behavior of this model subject to nonlinear feedback, the viability of various air injection orientations are established. An orientation consistent with this analysis is then used for feedback control in Section 9.2. By measuring the unsteady pressures near the rotor face, a control algorithm determines the magnitude and phase of the first mode of rotating stall and controls the injection of air in the front of the rotor face. Experimental results show that this technique eliminates the hysteresis loop normally associated with rotating stall. A parametric study is used to determine the optimal control parameters for suppression of stall. The resulting control strategy is also shown to suppress surge when a plenum is present. A simulation study in Section 9.3 using the higher fidelity distributed model in [Mansoux et al., 1994] is then presented, which yields results similar to those obtained experimentally and confirms the legitimacy of modeling the air injection as a local shift of the compressor characteristic.

9.1 Characteristic Shifting

Based on the open loop results in Figure 8.6, the air injectors are modeled as direct actuators of the steady state compressor characteristic. The effects of feedback control can then be explored when the amount of shifting is proportional to $J = A^2$, where A is the magnitude of the first Fourier coefficient of the of the stall disturbance. It should be stressed that this cannot be duplicated experimentally, since the air injectors can only be either on or off, and the air injection is not distributed evenly about the circumference of the compressor. Furthermore, this feedback strategy does not exploit the ability to actuate each air injector independently. The benefits of this simplified analysis will, however, become apparent shortly.

The controlled compressor characteristic is taken to be

$$\Psi_c = \Psi_{cnom} + KJ\Psi_{cu}, \tag{9.1}$$

where

$$\Psi_{cnom}(\Phi) = a_0 + a_1\Phi + a_2\Phi^2 + a_3\Phi^3, \qquad \Psi_{cu}(\Phi) = c_0 + c_1\Phi. \tag{9.2}$$

The bifurcation analysis in Section 8.4 can be performed with the above form for the compressor characteristic. In particular, the effects of such a control strategy on the hysteresis region can be analyzed. On the stalled branch of the bifurcation diagram, the following algebraic equations must hold:

$$\Phi^2 = \gamma^2\Psi, \tag{9.3}$$

$$\Psi_c(\Phi) = \Psi - \frac{J}{4}\frac{\partial^2\Psi_c(\Phi)}{\partial\Phi^2}, \tag{9.4}$$

$$\frac{\partial\Psi_c(\Phi)}{\partial\Phi} = -\frac{J}{8}\frac{\partial^3\Psi_c(\Phi)}{\partial\Phi^3}. \tag{9.5}$$

Since Φ, Ψ, and γ may be determined from J for each equilibrium solution on the stalled branch of the bifurcation diagram, we may differentiate equation (9.3) with respect to J to obtain

$$2\Phi\frac{d\Phi}{dJ} = 2\gamma\frac{d\gamma}{dJ}\Psi + \gamma^2\frac{d\Psi}{dJ}. \tag{9.6}$$

Differentiating equation (9.4) with respect to J and evaluating $(d\Psi/dJ)$ at the peak of the compressor characteristic yields

$$\left.\frac{d\Psi}{dJ}\right|_{\gamma=\gamma^*} = K\Psi_{cu}(\Phi) + \frac{1}{4}\frac{\partial^2\Psi_{cnom}(\Phi)}{\partial\Phi^2}. \tag{9.7}$$

Similarly, differentiating equation (9.5) with respect to J yields

$$\left.\frac{d\Phi}{dJ}\right|_{\gamma=\gamma^*} = \frac{K\dfrac{\partial\Psi_{cu}(\Phi)}{\partial\Phi} + \dfrac{1}{8}\dfrac{\partial^3\Psi_{cnom}(\Phi)}{\partial\Phi^3}}{-\dfrac{\partial^2\Psi_{cnom}(\Phi)}{\partial\Phi^2}}. \tag{9.8}$$

Substituting equations (9.7) and (9.8) into equation (9.6) and solving for $(dJ/d\gamma)$, the slope of the bifurcation diagram at the equilibrium point associated with γ^* is:

$$\left.\frac{dJ}{d\gamma}\right|_{\gamma=\gamma^*} = \frac{\sqrt{\Psi}}{\dfrac{K\dfrac{\partial \Psi_{cu}(\Phi)}{\partial \Phi} + \dfrac{1}{8}\dfrac{\partial^3 \Psi_{cnom}(\Phi)}{\partial \Phi^3}}{-\dfrac{\partial^2 \Psi_{cnom}(\Phi)}{\partial \Phi^2}} - \dfrac{\Phi}{2\Psi}\left(K\Psi_{cu}(\Phi) + \dfrac{1}{4}\dfrac{\partial^2 \Psi_{cnom}(\Phi)}{\partial \Phi^2}\right)}, \tag{9.9}$$

where all expressions in the right hand side of equation (9.9) are evaluated at the equilibrium point at the peak of the compressor characteristic.

Without feedback ($K = 0$), the denominator in equation (9.9) must be positive and greater than 0 to yield the hysteresis region in Figure 8.7. In order to eliminate this hysteresis region, the denominator must be made 0 or negative. The term associated with $-K$ is the following:

$$\frac{\dfrac{\partial \Psi_{cu}(\Phi)}{\partial \Phi}}{\dfrac{\partial^2 \Psi_{cnom}(\Phi)}{\partial \Phi^2}} + \frac{\Phi \Psi_{cu}(\Phi)}{2\Psi} \tag{9.10}$$

Thus in order to make the denominator as negative as possible for a fixed K, the above quantity needs to be made as large as possible. Since the second partial derivative of $\Psi_{cnom}(\Phi)$ with respect to Φ is negative at the stall inception point, this suggests that the most beneficial shift is one which has the largest positive offset and the largest negative slope. Referring back to the steady state shifts of Figure 8.6, this analysis suggests that the +30 and +40 characteristics are good candidates for feedback control.

9.2 Experimental Results Using Pulsed Air Injection

In this section, we present the experimental results on the use of air injection to control rotating stall. The effects of this control strategy on the surge dynamics are also explored. In Figure 9.1, the altered characteristic is plotted for an incident angle of 40 degrees, along with the unactuated characteristic for comparison purposes. This orientation was used for all the active control experiments in this section.

9.2.1 Description of Control Algorithm

The basic strategy of the control algorithm is to sense the location and magnitude of the peak of the first mode component of a circumferential pressure disturbance and apply pulses of air based on the size and location of this first mode relative to the air injectors, essentially the same strategy presented in [Day, 1993a].

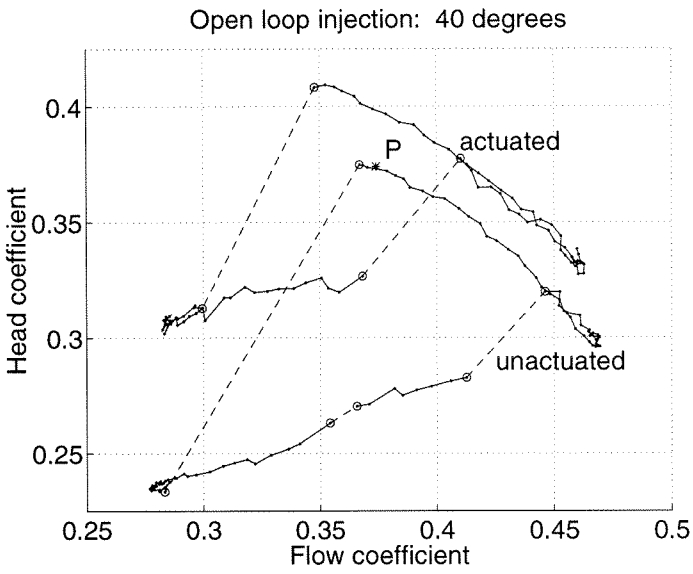

Figure 9.1: Compressor characteristic at air injection angle of 40 degrees. 'P' is the operating point for the parametric studies outlined in Section 9.2.

The plots in Figure 9.2 show the spatial Fourier modal components of the pressure disturbance when a transition from unstalled to stalled behavior occurs. Since six equally spaced pressure transducers were used to measure the pressure disturbance, only the first two modes could be determined. As can be seen, the dominant mode is the first one. From the slope of the phase plots one can conclude that both the first and second mode disturbances are rotating at a rate of approximately 65 Hz.

To ascertain that no significant aliasing was taking place due to the use of only six pressure transducers, time domain measurements were analyzed for each pressure transducer and the power spectrum determined. It was found that most of the signal power was contained in two bands centered around 65 Hz and 130 Hz, as shown in Figure 9.3. Assuming that the pressure disturbance is a traveling wave about the circumference of the compressor, this would indicate that the third mode component is also negligible spatially about the circumference of the compressor.

The parameters used in the control algorithm are:

`jeton`	injector pulse width
`threshold`	threshold for stall detection
`window`	angle window for stall detection
`angle1`	threshold angle for injector 1
`angle2`	threshold angle for injector 2
`angle3`	threshold angle for injector 3

The algorithm is illustrated in Figure 9.4, and behaves as follows: Each air injector is activated when the magnitude of the first mode is greater than `threshold` and the

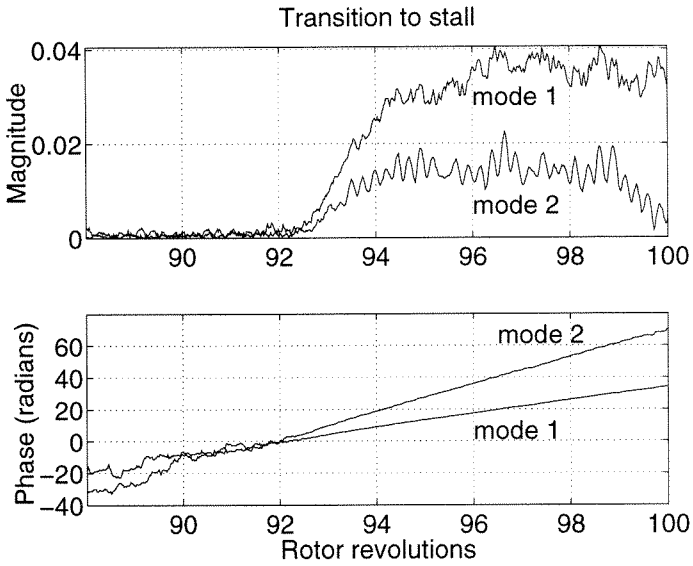

Figure 9.2: Transition to stall

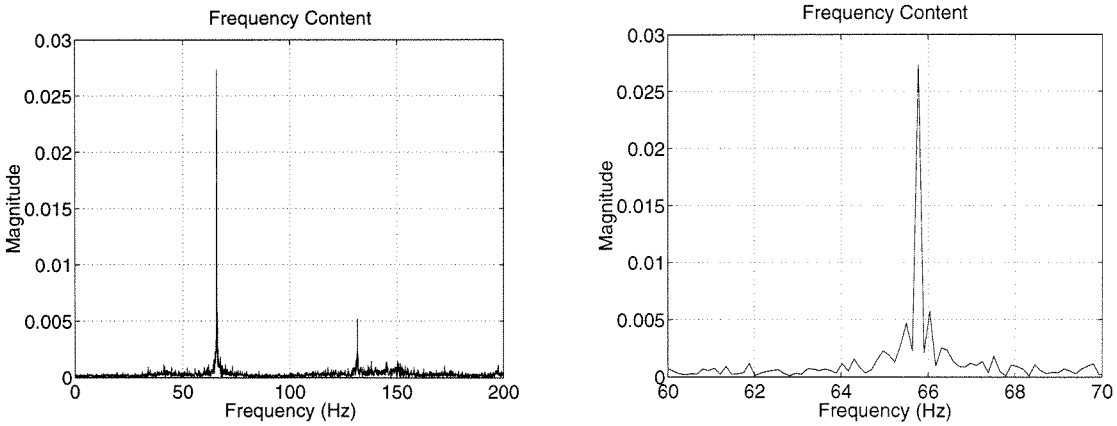

Figure 9.3: Frequency content of stall disturbance

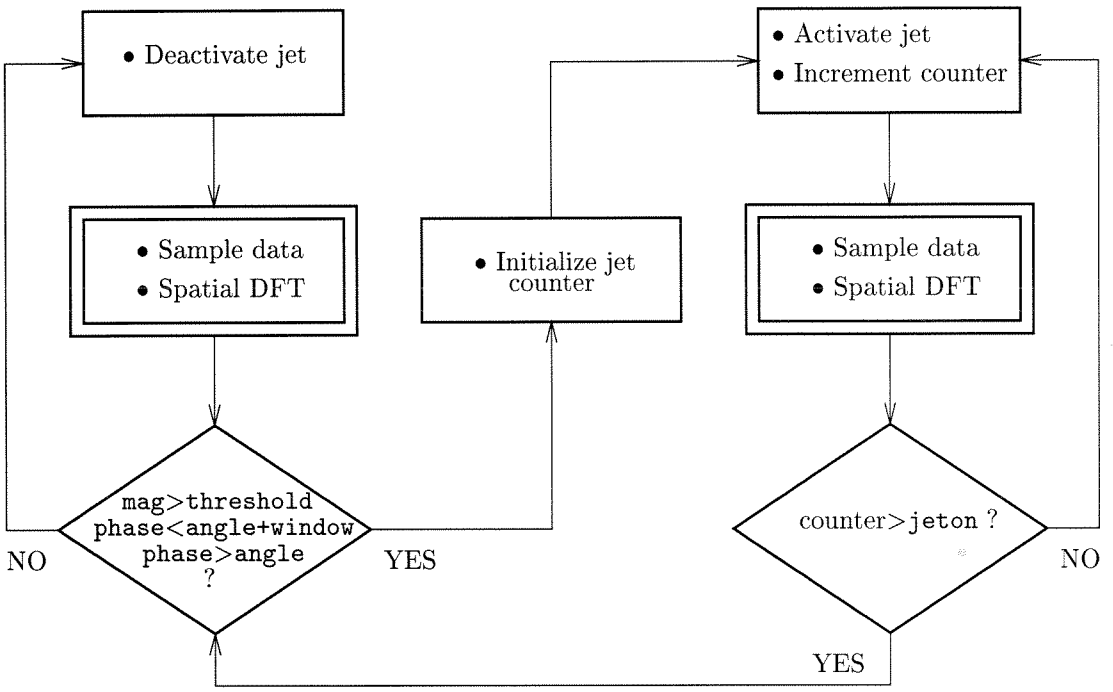

Figure 9.4: Control Algorithm. The above logic is repeated for each air injector. The double rectangle corresponds to the beginning of a servo loop, which occurs at a rate of 2000 iterations per second.

location of the peak of the first mode is within a pre-specified window (as determined by `angle` and `window`); once an air injector is activated, it remains activated for `jeton` number of servo-loops, irrespective of the magnitude `mag` and location `phase` of the first mode. Note that `phase` and `mag` refer to the phase and magnitude of the first Fourier coefficient, not the physical location and value of the peak pressure disturbance at the compressor face. In the case that the pressure disturbance is sinusoidal (which is a good approximation when fully stalled), `phase` and the physical location of the peak pressure disturbance differ by a constant, due to delays in the data acquisition stage. This delay was calculated to be 1.5 ms.

9.2.2 Parametric study

The controller parameters were varied in order to determine the optimal operating conditions for the controller, and to determine the effects on the closed loop behavior. The parameters varied were `jeton` and `angle1`, `angle2` and `angle3`. For this parametric study, the value of `threshold` was set to correspond to a head coefficient of 0.004 (10 Pa), and `window` was set to correspond to 25 degrees. The chosen value of `threshold` was slightly above that of the noise level, and thus allowed the control algorithm to sense a stall cell forming as quickly as possible. Assuming that the first mode rotates at a constant rate of 65 Hz, one servo period corresponds to a rotation of 12 degrees. By setting `window` larger than this value, we are ensured that the peak of the stall cell disturbance will not be missed. On the other hand, the window should not be too large, to ensure that we do not have double activations (this is guaranteed by setting `window` $< 12*$`jeton`), and to ensure that an air injector activates at the same time relative to the stall location (this might be a problem if the magnitude of the stall cell becomes greater than `threshold` near the end of an air injector's window). It was found experimentally that the value of `window` could be set in the range of 15 degrees to 90 degrees without changing the performance of the controller.

Effect of activation angles

For a fixed value of `jeton`, a search was performed over the activation angle for each air injector to determine the optimal strategy. The compressor was operated at point P in Figures 8.5 and 9.1. Parameters `angle1`, `angle2`, and `angle3` were each varied in 30 degree increments, from 0 to 330 degrees. Thus a total of 1,728 different controllers were tested for each value of `jeton`. For each of these settings, the control algorithm was operated for 16 seconds, and the average size of the stall cell and amount of time each air injector was on was recorded. A 0.1 second disturbance was generated every second via the high speed bleed valve to ensure that the compressor would stall.

The criterion used to determine the optimal setting for `angle1`, `angle2`, and `angle3` for a fixed `jeton` was the setting which yielded the lowest value for the average magnitude of the first mode (other criteria were also investigated, such as the total time that air injectors were on and the average pressure rise across the

jeton	angle1	angle2	angle3
11	120	270	0
13	120	240	330
15	90	210	330
17	60	180	300
19	60	180	300

Table 9.1: Optimal setting for different values of `jeton`

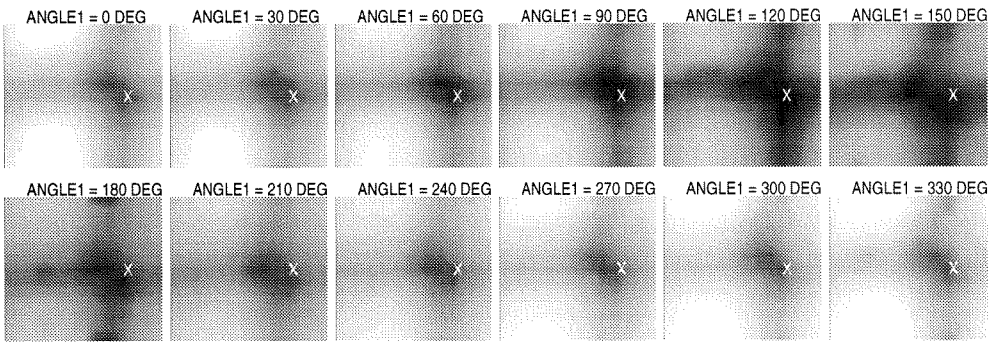

Figure 9.5: Parametric study, `jeton` = 11. Dark areas correspond to low average values for the first mode disturbance, light areas correspond to large average values. The horizontal axis for each plot corresponds to `angle2`, $0 - 360$ degrees; the vertical axis corresponds to `angle3`, $180 - 540$ degrees, shifted to center the dark areas. The white 'X' corresponds to the optimal setting for `angle2` and `angle3`

compressor, producing roughly the same results).

The results of this parametric study for `jeton` = 11, 13, 15, 17 and 19 may be found in Figures 9.5, 9.6, 9.7, 9.8, and 9.9. In each of the figures, there are twelve separate plots, one for each setting of `angle1`. Dark areas correspond to low average values for the first mode disturbance, while light areas correspond to large average values. Referring to the plots corresponding to `jeton`=15, Figure 9.7, one may conclude that the optimal setting for `angle1`, `angle2`, and `angle3` is roughly $(90, 210, 330)$; the performance of the control algorithm was insensitive to simultaneous parameter deviations of up to 30 degrees from this optimal setting. The optimal setting for the other values of `jeton` may be found in Table 9.1; The 'X' in the plots corresponds to the optimal setting for `angle2` and `angle3`.

Effect of time delays

To fully understand the operation of the controller and properly interpret the experimental results, one must take into account the activation and deactivation delays of the air injectors. Using hot-wire measurements, the average activation

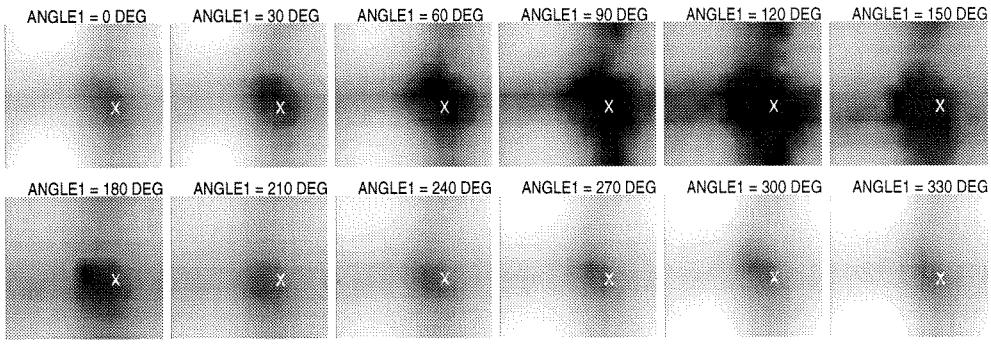

Figure 9.6: Parametric study, `jeton` = 13

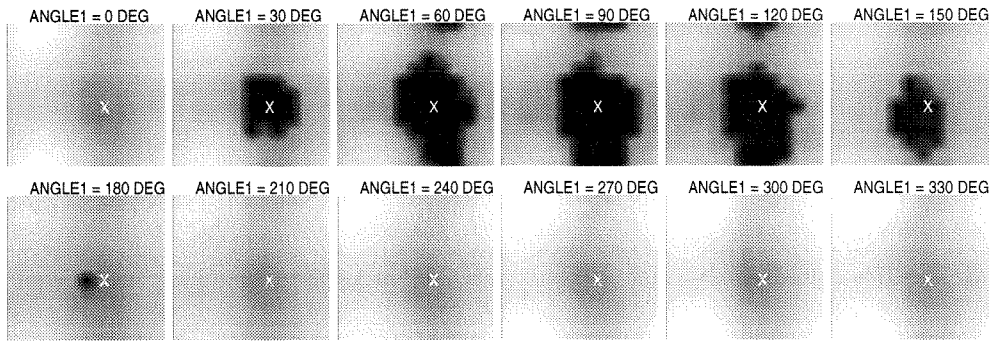

Figure 9.7: Parametric study, `jeton` = 15

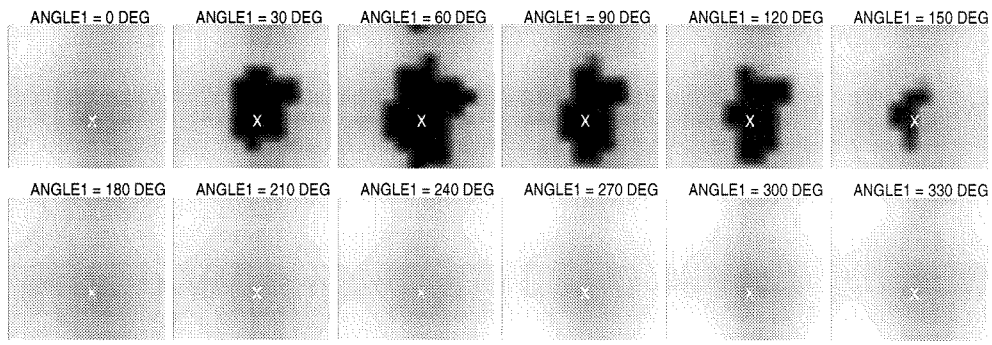

Figure 9.8: Parametric study, `jeton` = 17

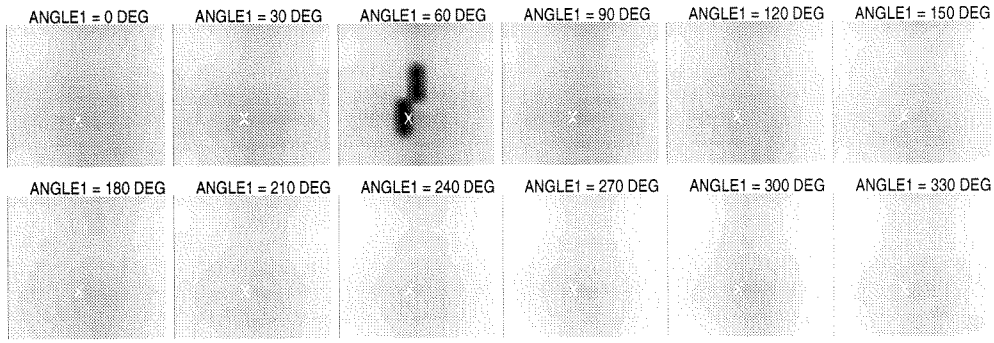

Figure 9.9: Parametric study, `jeton` = 19

delay for each injector was calculated to be 6.5 ms, while the deactivation delay was 4.5 ms. The activation delay corresponds to the total time it takes for the power of the injected air to reach 50% of its steady state value (at a distance of approximately 9 cm from the exit of the injector) from the time the injector was ordered to turn on; this delay takes into account the time required to open the solenoid valve and any delays in the air flow. Similarly for the deactivation delay.

Assuming a constant rotational speed of 65 Hz, it is possible to determine what the relative position of the peak of the first mode disturbance is relative to the activation of each air injector. This is depicted in Figure 9.10 for `jeton` = 15 and air injector 1. The 90 degree rotation corresponds to the experimentally determined optimal lag, as explained in the previous section; the 185 degree lag corresponds to the delay from sensing to actuation (1.5 ms + 6.5 ms); similarly, the de-activation lag is approximately 315 degrees (1.5 ms + 7.5 ms + 4.5 ms); the −30 degree rotation corresponds to the measured physical location where the injected air strikes the rotor face (recall that the air injectors were angled into the blade rotation). Thus air injector 1 activates approximately 55 degrees before the peak of the pressure disturbance and deactivates 75 degrees after the peak. Since the air injectors were physically spaced 120 degrees apart and the experimentally determined lags for `angle1`, `angle2`, and `angle3` were also spaced 120 degrees apart, the above argument holds for air injectors 2 and 3 as well. Thus the optimal setting for `angle1`, `angle2`, and `angle3` corresponds to a very intuitive control strategy: activate each air injector when the pressure is high and the flow is low. The above analysis can be performed for the other values of `jeton`, yielding similar results.

The experimentally determined optimal controller can easily be visualized in Figure 9.11. The light region corresponds to an area of higher pressure (stalled region), the boxes represent the position of the injected air, and the stall cell is rotating counter-clockwise. The stall cell position relative to the actuator when the injector opens is shown on the left and the stall cell position at the last instant that the injector is open is shown on the right. Intuitively, the controller attempts to increase the flow in the regions of the rotor which are stalled. The illustrations in Figure 9.11 correspond to actual data with `jeton` = 13.

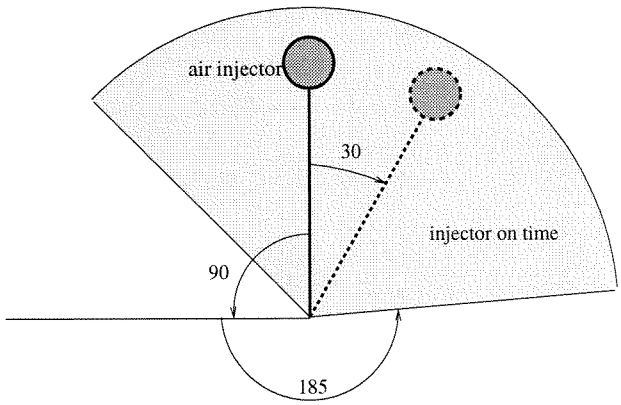

Figure 9.10: On-time for air injector 1, `jeton` = 15. The shaded region corresponds to the location of the peak of the first Fourier component of the disturbance for which an air injector is on, assuming a constant rotational rate of 65 Hz.

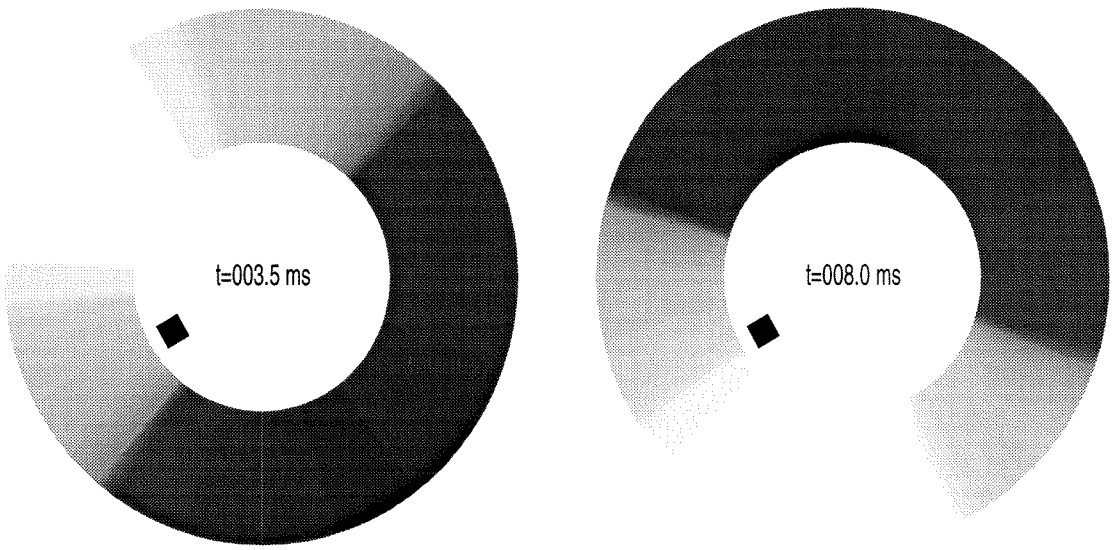

Figure 9.11: Visualization of optimal controller found via experimental search. The rotor rotation and stall cell rotation are in the counter-clockwise direction.

Effect of pulse width

It was found that for values of `jeton` less than or equal to 9 and greater than or equal to 22 the compressor remained stalled all the time. Taking the activation and deactivation delays into account, a value of 9 corresponds to approximately 2.5 ms of on-time for each injector, or about 60 degrees when the disturbance rotates at 65 Hz. This amount of time apparently was not enough to bring the compressor out of stall.

A value of 22 for `jeton` corresponds to approximately 9 ms of on-time for each injector, or about 210 degrees at a rotation rate of 65 Hz. Thus for this value, an air injectors remain active even when the local flow is above the spatially averaged value through the compressor.

One can understand why there should exist an upper and a lower bound for values of `jeton` which eliminate stall through limiting arguments. Clearly for `jeton` $= 0$ (no control), the compressor will transition into stall. To understand what happens when `jeton` $= \infty$, one need only look at the plot of Figure 9.1; when operating near the stall point of the compressor, there are two possible operating points which the compressor may reach when all the air injectors are turned on. One is the unstalled branch, while the other is the stalled branch. If the compressor is unstalled when the air injectors are activated, the operating point will shift to the upper branch; if the compressor is stalled, the operating point will shift to the lower branch (this was verified experimentally). Furthermore, phase information is lost when activating the air injectors for long periods of time. Thus one cannot eliminate the rotating stall condition by simply turning all the air injectors on. Since there exists a value of `jeton` for which stall is eliminated, it follows that a lower and upper bound exist as well.

Closed Loop Performance

A typical operation of the controller may be found in Figure 9.12. The closed loop compressor performance curve is shown in Figure 9.13 for the optimal choice of injector phasing for `jeton` $= 15$. The results shown to the left of the peak of the characteristic are time averaged values, since in this region a steady state stall disturbance is present. Error bars are included to show the variation from the mean at these operating points. In general, it was determined that operating points to the left of the peak were not dependent on the initial conditions of the system, i.e., the hysteresis region usually associated with stall was eliminated.

9.2.3 Effects of control algorithm on surge dynamics

Several experiments were performed to determine the effect of the control algorithm when the optional plenum was attached to the compressor. The results may be found in Figure 9.14. At operating point P (see Figure 8.5), a disturbance lasting 20 rotor revolutions (0.2 seconds) was generated via the high speed bleed valve (the time for which the bleed valve was closed is represented by a horizontal line in the upper left plots in Figure 9.14).

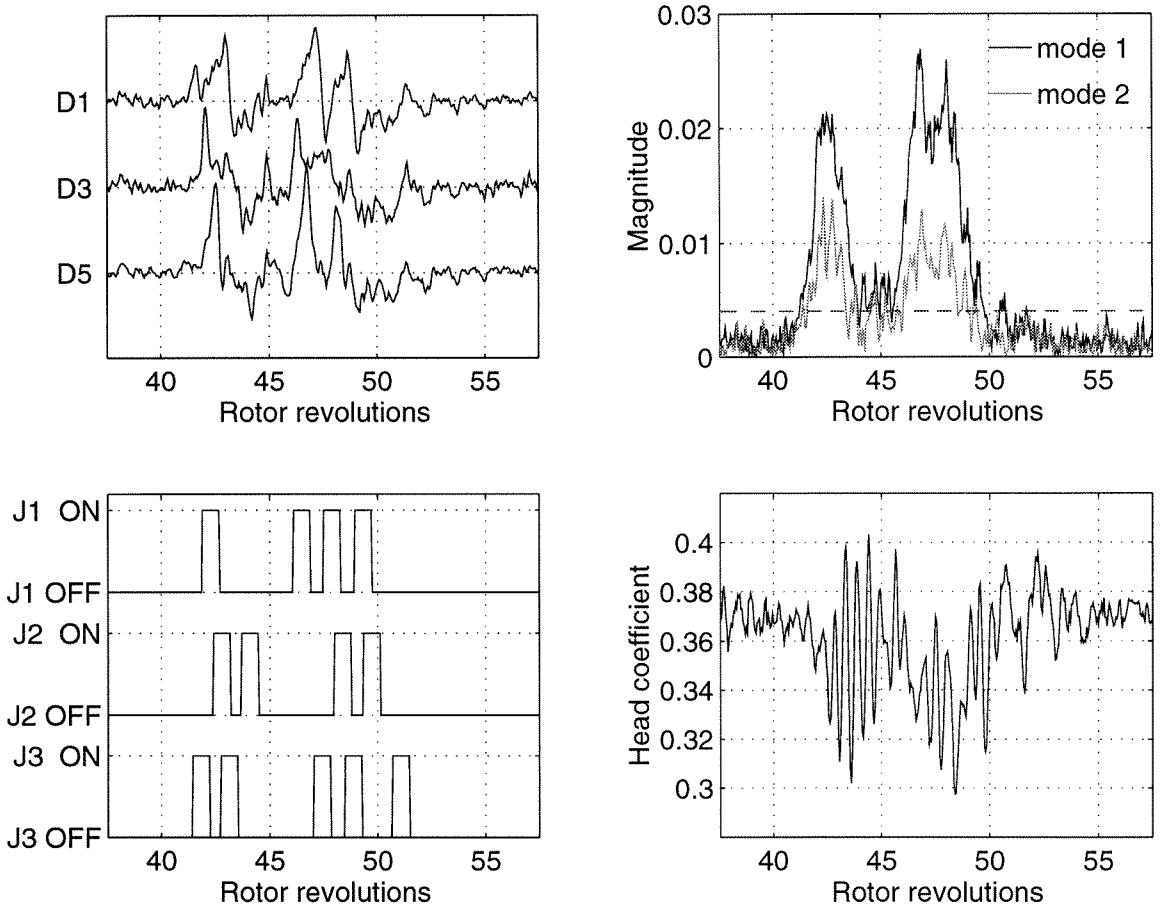

Figure 9.12: Closed loop operation. The upper left plot consists of the pressure data for transducers 1, 3, and 5. The lower left plot consists of the control signals applied to the air injectors. The upper right plot consists of the calculated first and second mode magnitudes; the dashed line corresponds to the setting for `threshold`. The lower right plot consists of the variation in the head coefficient.

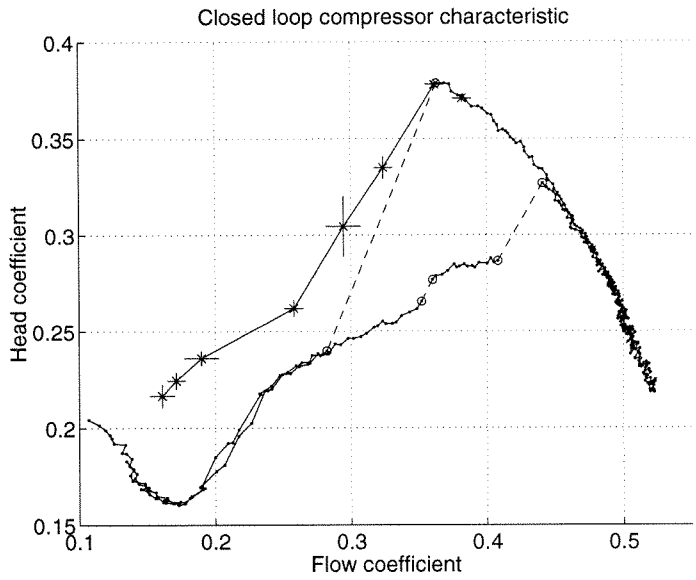

Figure 9.13: Closed loop compressor characteristic for `jeton` = 15, optimal controller. The asterisks correspond to time averaged data, while the solid lines interpolate these points. The pressure and flow variance are included for each data point as error bars. The open loop compressor characteristic is included for comparison purposes.

Referring to the uncontrolled data, the system promptly went into surge. As can be seen from the plots, there were two different surge modes, one at 1.4 Hz and the other at 1.8 Hz. The compressor was stalled during the low pressure rise intervals, and unstalled during the high pressure rise intervals. The pressure versus flow plot clearly illustrates the surge limit cycle; starting at point P (the asterisk), the graph is traversed in a counter-clockwise direction. The two different surge modes appear as two different closed circuits in this plot, which share a substantial part of the trajectory. Note that there exists a hysteresis region associated with the surge dynamics; the system did not exit surge when the disturbance was removed. This is due to the strong coupling between stall and surge. Also note that the duration of the disturbance corresponded approximately to the time it took for the pressure and flow to reach their minimum value; this observation is important in the analysis of the closed loop behavior given below.

Two pressure disturbances were generated approximately 2.5 seconds apart with the controller activated. As before, each pressure disturbance destabilized the system. Note that the controller had virtually no effect on the surge trajectory during the time the disturbance was present (in this 20 revolution time period, the trajectory is virtually the same as the one in the previous experiment). On the subsequent cycle, however, the pressure and flow variations were substantially decreased, and were completely eliminated by the end of the third cycle. It was determined that by shortening the time duration of the pressure disturbance (while still keeping it large enough to cause the open loop system to go into surge), the pressure and flow

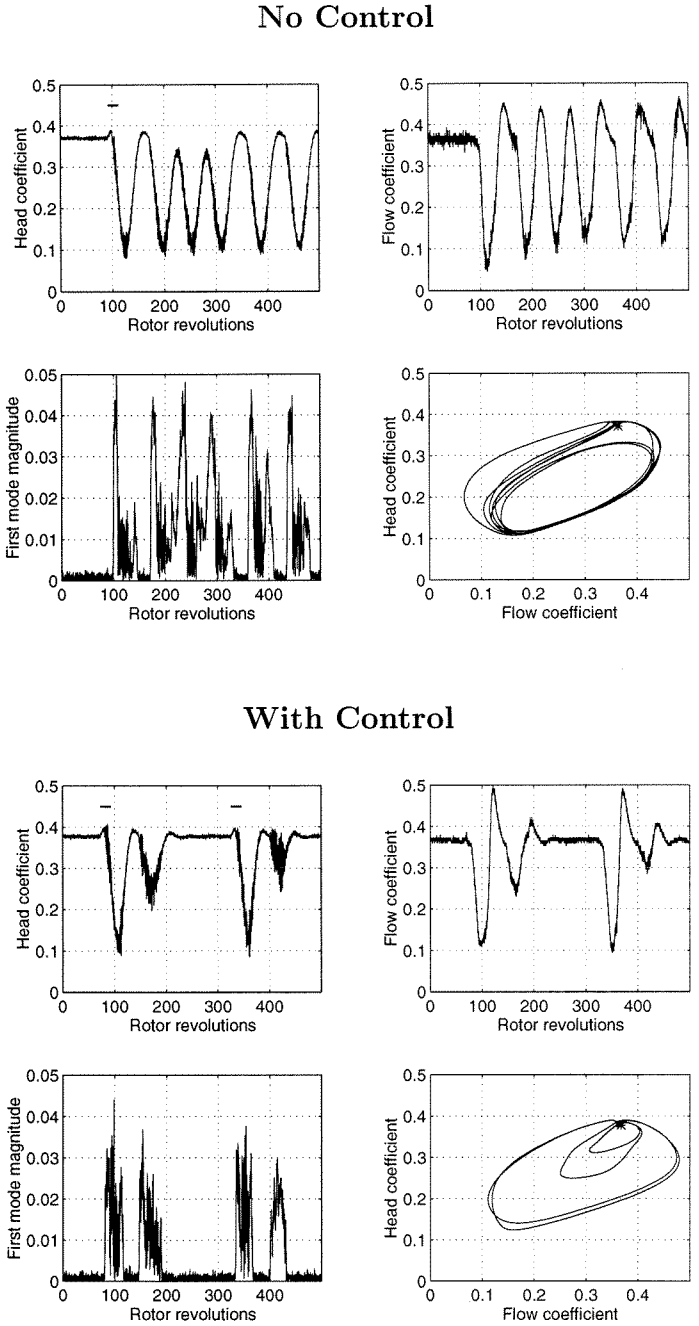

Figure 9.14: Compressor dynamics with plenum: the top set of plots correspond to data taken without the controller, the bottom set of plots with the controller. In each of the top left plots, a solid line is used to indicate the length of time for which the high speed bleed valve was activated. All data was low-pass filtered at 150 Hz, except for the pressure versus flow plots (the lower right plots), where the data was filtered at 10 Hz; the asterisk in these plots corresponds to operating point P, as per Figure 8.5.

variations during the first cycle were reduced, with the limiting behavior approaching the trajectories commencing from the second cycle in the plots. Thus if the duration of the disturbance was short enough, the magnitude of the pressure and flow disturbances could be kept to within 30% of the operating pressure and flow.

A possible explanation of why the control algorithm is successful at eliminating stall and surge is the strong coupling between the surge and stall dynamics; the compressor is stalled when the head coefficient is decreasing. The control algorithm at this point activates, and tries to eliminate the stalled condition. This has the effect of increasing the net pressure rise across the compressor during the periods of decreasing head coefficient. Thus the control algorithm is in effect providing positive damping to the surge dynamics. This is a topic for future research.

Note that the above control strategy does not displace the steady state surge line. What it does do is make the system less susceptible to disturbances by taking advantage of the strong coupling between stall and surge. This is further explored in [Behnken, 1996], where the bleed valve is used to directly control the surge instability, and the air injectors are used to control rotating stall.

9.3 Simulations

In this section, simulations using a high fidelity model are presented. The main motivation for performing the simulations was to demonstrate the validity of modeling the air injection actuation as a local shift of the compressor characteristic. This relatively simple approach to modeling the aggregate effects of injecting air into the rotor blades is very attractive from a computational (and thus control) perspective; the eventual goal is to provide a low-order mechanism which captures the essential features of air injection, analogous to capturing the dominant dynamics of a compression system via the Moore-Greitzer equations, and thus facilitate subsequent analyses and control designs which make use of air injectors. Another function of the simulations is to corroborate the experimental results and thus to give confidence in the control strategy of Section 9.2. The details on how the parameters used in the simulations were chosen and how the simulations were carried out are found in [Behnken, 1996]; only the aspects which directly relate to the experimental results in this chapter are presented here.

The compressor model used throughout the simulations is the distributed model in [Mansoux et al., 1994], a system of equations describing the dynamics of the flow coefficient Φ at discrete points around the compressor annulus. The simulations also include additional effects such as time lags associated with the change in the pressure rise delivered (Ψ_c has dynamics associated with it) and the mass/momentum effects associated with air injection. The model is attractive because the steady state compressor characteristic shifting can be included as a local effect instead of as an axially averaged shift, as was done for the Moore-Greitzer model.

9.3.1 Distributed Model

The full details of the distributed model presented in [Mansoux et al., 1994] should be obtained from that reference; only the details required to explain how the compressor characteristic shifting was included in the model will be presented here. The final equations (equations (20) in [Mansoux et al., 1994]) which make up the distributed model for a compression system are given by:

$$\dot{\Psi} = \frac{1}{4l_c B^2}\left(S\Phi - \gamma\sqrt{\Psi}\right) \tag{9.11}$$

and

$$G^{-1}D_E G\dot{\Phi} = -G^{-1}D_A G\Phi + \boldsymbol{\Psi}_{\mathrm{c}}(\Phi) - T\Psi, \tag{9.12}$$

where Ψ is the annulus averaged pressure rise coefficient, Φ is the vector of flow coefficients at discrete points around the compressor annulus, γ is the throttle position, and D_A, D_E, T, S, B and l_c are constants which depend on the compressor rig (see [Mansoux et al., 1994]). G is the discrete Fourier transform matrix, i.e.

$$\Phi = \begin{bmatrix} \Phi_1 \\ \Phi_2 \\ \vdots \\ \Phi_{2n+1} \end{bmatrix} \qquad G : \Phi \mapsto \begin{bmatrix} \tilde{\Phi}_0 \\ \mathrm{Re}\ \tilde{\Phi}_1 \\ \mathrm{Im}\ \tilde{\Phi}_1 \\ \vdots \\ \mathrm{Re}\ \tilde{\Phi}_n \\ \mathrm{Im}\ \tilde{\Phi}_n \end{bmatrix},$$

where $\tilde{\Phi}_i$ is the Fourier coefficient associated with mode i, and n is the number of modes included in the model. Seven modes were used for the results presented. Two additional effects not included in the above equations but included in the simulations are the effects of unsteady flow on the pressure rise delivered by the compressor and the mass/momentum addition terms associated with air injection.

The Caltech compressor rig has three air injectors placed 120 degrees apart around the compressor annulus (as in Figure 8.4), and each injector has an effect on a small region of the compressor rotor. In the distributed model, the vector of pressure rise coefficients around the compressor annulus is given by $\boldsymbol{\Psi}_{\mathrm{c}}(\Phi)$. In order to include the compressor characteristic shifting as a local effect, the shift is included as

$$\boldsymbol{\Psi}_{\mathrm{c}}(\Phi_i) = \boldsymbol{\Psi}_{\mathrm{cnom}}(\Phi_i) + \left(\boldsymbol{\Psi}_{\mathrm{cu}}(\Phi_i) - \boldsymbol{\Psi}_{\mathrm{cnom}}(\Phi_i)\right)\mathbf{L}(u_i) \tag{9.13}$$

at the three points around the annulus which have injectors associated with them and as

$$\boldsymbol{\Psi}_{\mathrm{c}}(\Phi_i) = \boldsymbol{\Psi}_{\mathrm{cnom}}(\Phi_i) \tag{9.14}$$

for the remaining positions. Here $\boldsymbol{\Psi}_{\mathrm{cnom}}$ is the nominal compressor characteristic, while $\boldsymbol{\Psi}_{\mathrm{cu}}$ is the locally shifted characteristic. The control variables are the u_i, which

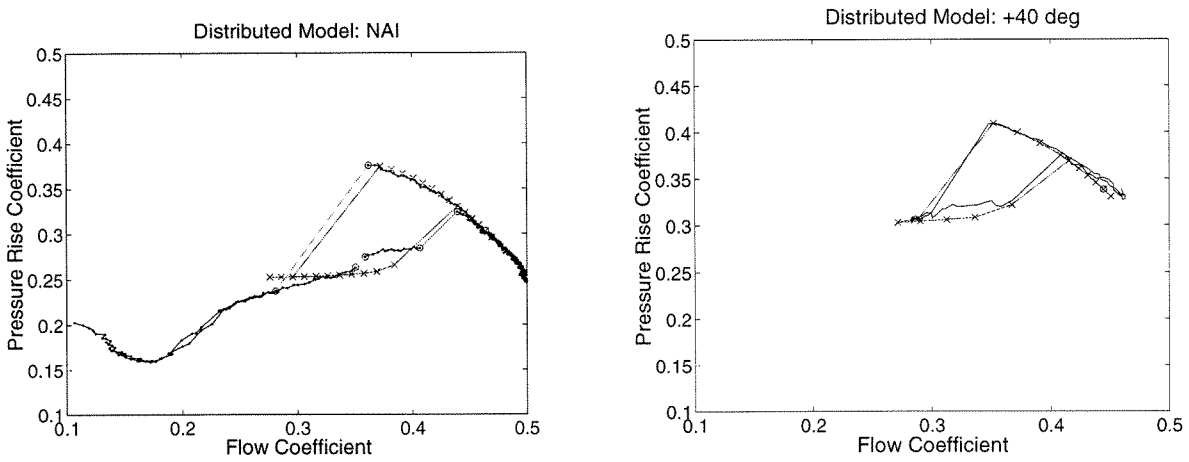

Figure 9.15: Hysteresis loops for simulation compressor characteristics. The left plot corresponds to the fit for the No Air Injection (NAI) case, the right plot corresponds to the fit for the +40 degrees case. Simulation data points are denoted with an `x`.

take the values of 0 or 1 if the air injector is off or on, respectively. The transient effect of the air injection on the compressor characteristic shift is modeled as a delay followed by a first order lag; this is captured by operator **L**. The values for the delay and lag were chosen to correspond to the values observed in the experiment.

The results of the simulations corresponding to no air injection and continuous air injection may be found in Figure 9.15. In these plots, the experimentally determined characteristics (see Figure 9.1) are included for comparison purposes.

9.3.2 Parametric Study

The goal of the simulation based parametric study was to determine the optimal control strategy based on a model for the compressor. In particular, a search for the optimal phasing for the activation of each air injector relative to the measured position of the peak of the first mode stall disturbance was performed.

The control algorithm was essentially the same as the one described in Figure 9.4 in Section 9.2. The major difference was in the implementation of what corresponded to activating the air injectors for `jeton` number of servo iterations in the experimental study. This was accomplished by activating each air injector when the magnitude of the first mode disturbance became greater than some threshold magnitude and the phase of the first mode disturbance was within a pre-specified window. The threshold magnitude was based on the noise level in the experimental determination of the magnitude of the first Fourier mode.

In terms of the logic of Figure 9.4, this corresponds to setting `jeton` to 0 and `window` to 120 degrees, and running the servo loop at an infinitely high rate. This is roughly how the control algorithm behaved in the experimental studies for `jeton` = 15. This algorithm was used to simplify the simulation code and vastly decrease its running time.

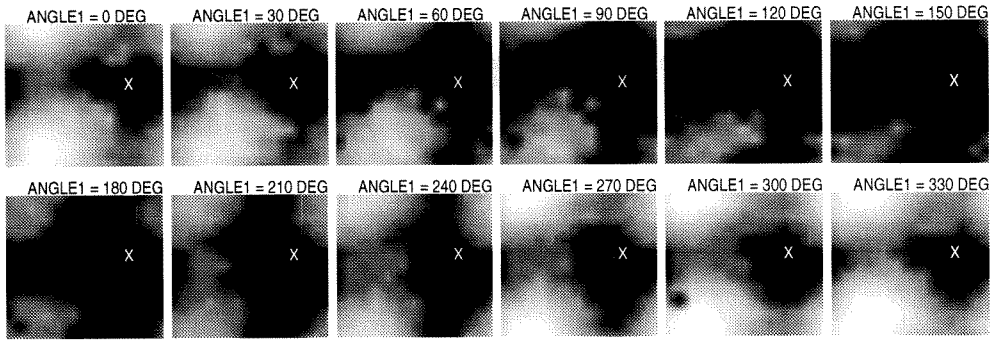

Figure 9.16: Simulation parametric study. Dark areas correspond to low average values for the first mode disturbance, light areas correspond to large average values. The horizontal axis for each plot corresponds to `angle2`, $0 - 360$ degrees; the vertical axis corresponds to `angle3`, $180 - 540$ degrees, shifted to center the dark areas. The white 'X' corresponds to the optimal setting for `angle2` and `angle3`

As in the experimental study, the phasing of each air injector was independently varied in 30 degree increments. For each controller tested, the average amplitude of the first mode stall cell was recorded. In all the simulations, the same initial stall cell disturbance (both in magnitude and phase) was used. Analogous to the experimental results of Section 9.2, the simulation results are shown in Figure 9.16. The simulation study predicts the same periodic trends for the optimal phasing observed in the experimental data.

The optimal phase setting for the simulation parametric study is approximately (150, 270, 30). The activation, de-activation, and transport delays were implemented by a Pade approximation. In the experimental setup, the air injectors were not symmetric with respect to the turn on and turn off times; it was found that the air injectors would take approximately 2 ms longer to turn on than to turn off (this was taken into account in the analysis of Figure 9.10), which corresponds to roughly 50 degree of stall rotation. This asymmetry was not implemented in the simulation. When this 50 degree phase lead is subtracted from the above optimal setting, a value consistent with the optimal setting obtained experimentally is obtained.

9.3.3 Closed Loop Simulations

The closed loop characteristic for the optimal controller obtained via simulation is shown in Figure 9.17. The hysteresis region has essentially been eliminated, as was observed in the experiments. The transition to rotating stall is also gradual, i.e. there is no jump from zero stall to fully developed stall. These two results, along with the matching of the trends between the experimental and simulation parametric studies strongly support the air injection model presented here. Further work on refining the model will focus on using numerical techniques to determine the bifurcation characteristics, and coupling surge controllers with the pulsed air injection controller for

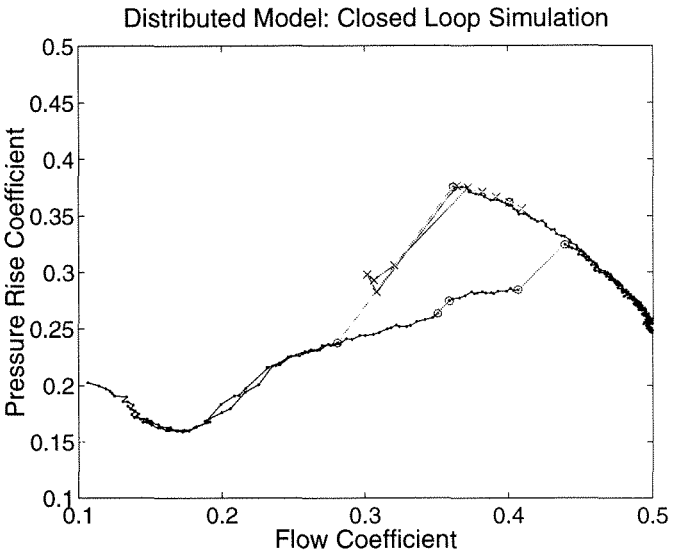

Figure 9.17: Simulated closed loop compressor characteristic. Simulation data points are denoted with an x; the experimentally obtained open loop compressor characteristic is included for comparison purposes.

rotating stall.

9.4 Conclusions and Future Work

The active control techniques presented in this chapter proved to be simple, easy to implement, yet at the same time extremely effective in eliminating the hysteresis region normally associated with rotating stall. The following procedure is suggested by the results in this chapter:

1. Experimentally determine the air injector orientation that results in a shifted compressor characteristic Ψ_{cu} maximizing the following quantity

$$\frac{\dfrac{\partial \Psi_{\mathrm{cu}}(\Phi)}{\partial \Phi}}{\dfrac{\partial^2 \Psi_{\mathrm{cnom}}(\Phi)}{\partial \Phi^2}} + \frac{\Phi \Psi_{\mathrm{cu}}(\Phi)}{2\Psi}, \tag{9.15}$$

   evaluated at the peak of the compressor characteristic. This is suggested by the bifurcation analysis of Section 9.1; maximizing the above amount tends to bend back the unstable bifurcation branch by the largest amount for a fixed amount of proportional feedback.

2. Pulse air onto the rotor face based on the strategy outlined in the flow chart of Figure 9.4; center each pulse about the peak of the first mode disturbance, and activate each air injector for the amount of time which yields the best performance.

The simulation studies performed with a high fidelity model were in agreement with the experimental results; furthermore, they justified the modeling of air injection as a localized shift in the compressor characteristic.

It should be emphasized that the above strategy for controlling rotating stall is not based on precursors; for our system, the time scale associated with the growth of the stall disturbance is comparable to the bandwidth of our actuators (see Figure 9.2), rendering control strategies based on small signal behavior ineffective. Our control scheme beats down stall after it starts to develop, but before it grows to full size. In fact, this control scheme can eliminate rotating stall starting from a fully stalled condition.

The main physical phenomenon which was utilized in the experimental work and the ensuing analysis was that the steady state compressor characteristic could be shifted by injecting air at the face of the compressor. While it has been previously shown that by introducing pre-swirl at the inlet and by the use of inlet guide vanes the compressor characteristic can be altered for many compressors [Longley, 1994], the extent to which this effect can be achieved using air injection is an open research topic. The impact of the results presented thus hinge on demonstrating the genericness of shifting the compressor characteristic using localized air injection.

The experiments were performed with three air injectors at a fixed flow rate and distance from the compressor face. It is important to characterize how the performance of the control design varies by varying these parameters. For example, given an upper limit on the total flow which can be introduced by the air injectors, what is the optimal number of air injectors which should be used for feedback control? How should they be oriented relative to the compressor face? What is the tradeoff between the velocity of injected air and the performance of the compressor? These same questions can be asked for a fixed power limit on the actuation, or velocity limit, or combinations thereof. In order to answer these questions, more parametric studies need to be performed, and a more detailed model which captures the fluid dynamical interactions needs to be developed and studied.

While it is important to determine how the closed loop performance varies as a function of these parameters, it is equally important to determine the regions of implementability for these parameters. For example, injecting air at a velocity which is much greater than the mean velocity through the compressor would not be feasible for high speed systems. It is also desirable to use re-circulation as the means to provide the needed flow for air injection [Gysling and Greitzer, 1995], which will restrict the velocity at which air can be injected. Another issue is the effect of pulsing high momentum flow onto the rotor blades; this should be studied to determine what the detrimental effects are, and see if they are offset by the resulting benefits.

The control effort required to eliminate the hysteresis region is approximately 1.3% in terms of power and 1.7% in terms of flow of the compressor operating near the peak of the compressor characteristic. In a jet engine, however, these figures are large in an absolute sense. Subsequent to the experimental results presented in this chapter, these figures were drastically reduced by moving the air injectors closer to the rotor face. In particular, the power figure was reduced to approximately 0.15% and the

flow figure to 0.35%. Furthermore, the time each air injector was on (as determined by `jeton`) was reduced to approximately 45 degrees of a stall disturbance revolution; this is consistent with hot wire measurements near the rotor face, which show that the stall disturbance is localized to less than two rotor blades, or approximately 50 degrees.

Even though controlling stall was the main purpose of the work presented in this chapter, the elimination of surge is also an important aspect of extending the operability of a compressor. We have demonstrated that the controller designed to control stall can also have positive effects in eliminating surge. This is mainly due to the strong coupling between surge and stall, although a more detailed analysis needs to be performed to fully determine this interaction. Furthermore, the transients which occur when stabilizing surge need to be made as small as possible in order to prevent the compression system from being damaged.

Chapter 10
Conclusions

In this chapter the main contributions of this dissertation are summarized and future avenues of related research are investigated.

10.1 Summary

- A general optimization problem in the l_2 framework, Generalized l_2 Synthesis, was formulated and solved. This framework appears to be the natural extension of $\mathcal{H}_\infty$ optimization, in the sense that arbitrary convex sets are used to describe the allowable disturbances and the performance criterion. The associated feasibility condition is an AMI, which is both a necessary and sufficient condition for the problem to have a solution, and is computationally tractable.

- Using the Generalized l_2 Synthesis framework several open problems in robust and optimal control were solved. These included synthesis for independently norm bounded disturbances, robust stability with "element by element" bounded structured uncertainty, and certain classes of robust performance problems. The gain scheduling results in [Packard, 1994] were extended to the Generalized l_2 Synthesis framework.

- By extending the Generalized l_2 Synthesis framework to allow for the deterministic noise disturbances of [Paganini, 1993], a solution to the mixed $\mathcal{H}_2 - \mathcal{H}_\infty$ problem was presented. This solution can, in turn, be used as one of the two iterative steps for Robust $\mathcal{H}_2$ Synthesis, truly putting Robust $\mathcal{H}_2$ Synthesis on the same par as Robust $\mathcal{H}_\infty$ Synthesis in terms of computational complexity.

- The behavioral framework for system representation was invoked to pose and solve a variant of $\mathcal{H}_\infty$ optimization where no distinction between inputs and outputs is made. This formulation allows for singular interconnections, which arise naturally when interconnecting first principle models.

- A simple control scheme which has the potential of greatly increasing the operability of compressors was outlined. By measuring the unsteady pressures near

the rotor face of the compressor, the control algorithm determines the magnitude and phase of the first mode of rotating stall and controls the injection of air in the front of the rotor face. Experimental results showed that this technique eliminates the hysteresis loop normally associated with rotating stall.

10.2 Future Research Directions

- The constraints which can be imposed using the Generalized l_2 Synthesis framework do not include dynamics. This was alleviated in Chapter 5 for the special case of correlation constraints. The theory needs to be extended to allow for general convex constraints which include dynamics. Furthermore, the boundary between problems which are computationally tractable and NP-Hard needs to be delineated. Achieving this goal will result in a truly general and complete framework for l_2 synthesis.

- While the problems solved in Chapters 3, 4, and 5 have been present in the control community for quite some time, the theory needs to be tried out on actual experimental problems to determine what the benefits are of this more general, but computationally more demanding, synthesis framework.

- The results on optimal interconnections and behavioral systems are very preliminary. A much more thorough investigation needs to be conducted in order to make the theory applicable to real systems. For example, the $\mathcal{H}_\infty$ Optimal Interconnections results could be extended to the uncertain behavioral representations introduced in Chapter 6, and combined with the Generalized l_2 Synthesis framework.

- From a practical point of view, many issues need to be resolved before the pulsed air injection control scheme can be implemented on a full scale system. From a theoretical standpoint, a more systematic means of characterizing the effects of pulsed air injection needs to be developed.

The two parts of this dissertation are, in a sense, at the two extremes of control theory. In the first part, general tools were developed for model based control design which can be used to achieve very well defined performance objectives. In the second part, the control design was not model based, and the role of mathematics was to provide guidelines on the choice of various physical parameters and to corroborate the experimental results (and thus show that results are in some sense generic to a wider class of systems). For a given problem, the particular application being considered will dictate which of the two above strategies should be adopted; if the design is to be successful, it will in all probability be a combination of both.

Bibliography

[Abed et al., 1993] Abed, E. H., Houpt, P. K., and Hosny, W. M. (1993). Bifurcation analysis of surge and rotating stall in axial flow compressors. *Journal of Turbomachinery*, 115:817–824.

[AMCA/ASHRAE, 1985] AMCA/ASHRAE (1985). Laboratory methods of testing fans for rating. Technical Report ANSI/AMCA Standard 210-85, Air Movement and Control Association.

[Anderson and Moore, 1990] Anderson, B. D. O. and Moore, J. B. (1990). *Optimal Control: Linear Quadratic Methods.* Prentice Hall.

[Apkarian and Gahinet, 1995] Apkarian, P. and Gahinet, P. (1995). A convex characterization of gain-scheduled H-infinity controllers. *IEEE Transactions on Automatic Control*, 40(5):853–864.

[Badmus et al., 1995] Badmus, O. O., Chowdhury, S., Eveker, K. M., and Nett, C. N. (1995). Control-oriented high-frequency turbomachinery modeling - single-stage compression system one-dimensional model. *Journal of Turbomachinery*, 117:47–61.

[Balakrishnan et al., 1994] Balakrishnan, V., Huang, Y., Packard, A., and Doyle, J. C. (1994). Linear matrix inequalities in analysis with multipliers. In *Proc. American Control Conference*, pages 1228–1232.

[Beck, 1995] Beck, C. (1995). *Model Reduction for Multi-Dimensional and Uncertain Systems.* PhD thesis, California Institute of Technology.

[Behnken, 1996] Behnken, R. L. (1996). *Nonlinear control of an axial flow compressor.* PhD thesis, California Institute of Technology.

[Behnken et al., 1995] Behnken, R. L., D'Andrea, R., and Murray, R. M. (1995). Control of rotating stall in a low-speed axial flow compressor using pulsed air injection: Modeling, simulations, and experimental validation. In *Proc. IEEE Conference on Decision and Control*, pages 3056–3061.

[Bernstein and Haddad, 1989] Bernstein, D. S. and Haddad, W. H. (1989). Lqg control with an H-infinity performance bound: A ricatti equation approach. *IEEE Transactions on Automatic Control*, 34(3):293–305.

[Boyd et al., 1994] Boyd, S. P., Ghaoui, L. E., Feron, E., and Balakrishnan, V. (1994). *Linear Matrix Inequalities in System and Control Theory.* SIAM studies in applied mathematics. Philadelphia : Society for Industrial and Applied Mathematics.

[Braatz et al., 1994] Braatz, R., Young, P., Doyle, J. C., and Morari, M. (1994). Computational complexity of *mu* calculation. *IEEE Transactions on Automatic Control*, 39:1000–1002.

[Copeland and Safonov, 1995] Copeland, B. R. and Safonov, M. G. (1995). A zero compensation approach to singular H-2 and H-infinity problems. *International Journal of Robust and Nonlinear Control*, 5(2):71–106.

[Dahleh and Diaz-Bobillo, 1995] Dahleh, M. A. and Diaz-Bobillo, I. J. (1995). *Control of Uncertain Systems.* Prentice Hall.

[D'Andrea, 1994] D'Andrea, R. (1994). H-infinity optimal interconnections and system design. In *Proc. IEEE Conference on Decision and Control*, pages 3701–3706.

[D'Andrea, 1995] D'Andrea, R. (1995). H-infinity optimal interconnections. Technical Report 95-030, Caltech. http://avalon.caltech.edu/cds/.

[D'Andrea, 1996a] D'Andrea, R. (1996a). Generalized l-2 synthesis: A new framework for control design. In *Proc. IEEE Conference on Decision and Control.*

[D'Andrea, 1996b] D'Andrea, R. (1996b). LMI approach to mixed H-2 and H-infinity performance objective controller design. In *Proc. IFAC World Congress.*

[D'Andrea, 1996c] D'Andrea, R. (1996c). Necessary and sufficient conditions for gain scheduling subject to full-structured uncertainty. In *Proc. IEEE Conference on Decision and Control.*

[D'Andrea, 1997] D'Andrea, R. (1997). Kalman decomposition of multi-D systems and minimality. Manuscript in preparation.

[D'Andrea et al., 1995] D'Andrea, R., Behnken, R. L., and Murray, R. M. (1995). Active control of rotating stall using pulsed air injection: A parametric study on a low-speed, axial flow compressor. In *Sensing, Actuation, and Control in Aeropropulsion; SPIE International Symposium on Aerospace/Defense Sensing and Dual-Use Photonics*, pages 152–165.

[D'Andrea et al., 1997] D'Andrea, R., Behnken, R. L., and Murray, R. M. (1997). Rotating stall control of an axial flow compressor using pulsed air injection. *Journal of Turbomachinery.* To appear.

[D'Andrea and Doyle, 1996] D'Andrea, R. and Doyle, J. C. (1996). Full information and full control in a behavioral context. In *Proc. IEEE Conference on Decision and Control.*

[D'Andrea and Paganini, 1993] D'Andrea, R. and Paganini, F. (1993). Interconnection of uncertain behavioral systems for robust control. In *Proc. IEEE Conference on Decision and Control*, pages 3642–3647.

[D'Andrea and Paganini, 1994] D'Andrea, R. and Paganini, F. (1994). Controller synthesis for implicitly defined uncertain systems. In *Proc. IEEE Conference on Decision and Control*, pages 3679–3684.

[D'Andrea et al., 1993] D'Andrea, R., Paganini, F., and Doyle, J. C. (1993). Uncertain behavior. In *Proc. IEEE Conference on Decision and Control*, pages 3891–3896.

[Day, 1993a] Day, I. J. (1993a). Active supression of rotating stall and surge in axial compressors. *Journal of Turbomachinery*, 115:40–47.

[Day, 1993b] Day, I. J. (1993b). Stall inception in axial flow compressors. *Journal of Turbomachinery*, 115:1–9.

[Doyle, 1978] Doyle, J. C. (1978). Guaranteed margins for LQG regulators. *IEEE Transactions on Automatic Control*, 23:756–757.

[Doyle et al., 1992] Doyle, J. C., Francis, B. A., and Tannenbaum, A. R. (1992). *Feedback Control Theory*. McMillan.

[Doyle et al., 1989] Doyle, J. C., Glover, K., Khargonekar, P., and Francis, B. A. (1989). State-Space solutions to standard H2 and H-infinity control problems. *IEEE Transactions on Automatic Control*, 34(8):831–847.

[Doyle et al., 1994a] Doyle, J. C., Newlin, M., Paganini, F., and Tierno, J. (1994a). Unifying robustness analysis and system ID. In *Proc. IEEE Conference on Decision and Control*, pages 3667–3672.

[Doyle et al., 1994b] Doyle, J. C., Zhou, K. M., Glover, K., and Bodenheimer, B. (1994b). Mixed H2 and H-infinity performance objectives II: Optimal control. *IEEE Transactions on Automatic Control*, 39(8):1575–1587.

[Emmons et al., 1955] Emmons, H. W., Pearson, C. E., and Grant, H. P. (1955). Compressor surge and stall propagation. *ASME Transactions*, 6.

[Eveker et al., 1995] Eveker, K. M., Gysling, D. L., Nett, C. N., and Sharma, O. P. (1995). Integrated control of rotating stall and surge in aeroengines. In *Sensing, Actuation, and Control in Aeropropulsion; SPIE 1995 International Symposium on Aerospace/Defense Sensing and Dual-Use Photonics*, pages 21–35.

[Fan et al., 1991] Fan, M., Tits, A., and Doyle, J. C. (1991). Robustness in the presence of mixed parametric uncertainty and unmodeled dynamics. *IEEE Transactions on Automatic Control*, 36:25–38.

[Gahinet and Apkarian, 1994] Gahinet, P. and Apkarian, P. (1994). A linear matrix inequality approach to H-infinity control. *IJRNC*, 4:421–448.

[Gahinet et al., 1994] Gahinet, P., Nemirovskii, A., Laub, A., and Chilali, M. (1994). *The LMI Control Toolbox.* The MathWorks Inc., beta-release edition.

[Garey and Johnson, 1979] Garey, M. R. and Johnson, D. S. (1979). *Computers and Intractability: A Guide to the Theory of NP Completeness.* W. H. Freeman.

[Gilyard and Orme, 1992] Gilyard, G. B. and Orme, J. S. (1992). Subsonic flight test evaluation of a performance seeking control algorithm on an F-15 airplane. In *Joint Propulsion Conference and Exhibit.* AIAA paper 92-3743.

[Glover and Doyle, 1989] Glover, K. and Doyle, J. C. (1989). A State Space approach to H-infinity optimal control. *Springer Verlag Lecture Notes*, 135.

[Glover and Mustafa, 1989] Glover, K. and Mustafa, D. (1989). Derivation of the maximum entropy H-infinity controller and a state space formula for its entropy. *IJC*, 50:899–916.

[Greitzer, 1976] Greitzer, E. M. (1976). Surge and rotating stall in axial flow compressors—Part I: Theoretical compression system model. *Journal of Engineering for Power*, pages 190–198.

[Greitzer, 1981] Greitzer, E. M. (1981). The stability of pumping systems—The 1980 Freeman scholar lecture. *ASME Journal of Fluids Engineering*, 103:193–242.

[Gysling, 1993] Gysling, D. L. (1993). *Dynamic Control of Rotating Stall in Axial Flow Compressors Using Aeromechanical Feedback.* PhD thesis, Department of Aeronautics and Astronautics, Massachusetts Institute of Technology, Cambridge, Massachusetts.

[Gysling and Greitzer, 1995] Gysling, D. L. and Greitzer, E. M. (1995). Dynamic control of rotating stall in axial-flow compressors using aeromechanical feedback. *Journal of Turbomachinery*, 117(3):307–319.

[Kailath, 1980] Kailath, T. (1980). *Linear Systems.* Prentice Hall.

[Khalak and Murray, 1995] Khalak, A. and Murray, R. M. (1995). Experimental evaluation of air injection for actuation of rotating stall in a low speed, axial fan. In *Proc. ASME Turbo Expo.*

[Khammash and Pearson, 1991] Khammash, M. and Pearson, J. B. (1991). Performance robustness of discrete-time systems with structured uncertainty. *IEEE Transactions on Automatic Control*, 36(4):398–412.

[Khargonekar and Rotea, 1991] Khargonekar, P. and Rotea, M. (1991). Mixed H2 and H-infinity control: A convex optimization approach. *IEEE Transactions on Automatic Control*, 36(7):824–837.

[Kouvaritakis and Latchman, 1985] Kouvaritakis, B. and Latchman, H. (1985). Necessary and sufficient stability criterion for systems with structured uncertainty: the major principle direction alignment principle. *International Journal of Control*, 42:575–598.

[Kuijper, 1992] Kuijper, M. (1992). *First-Order Representations of Linear Systems.* PhD thesis, University of Brabant.

[Liaw and Abed, 1996] Liaw, D. C. and Abed, E. H. (1996). Control of compressor stall inception - a bifurcation-theoretic approach. *Automatica*, 32(1):109–115.

[Ljung, 1987] Ljung, L. (1987). *System Identification.* Prentice Hall.

[Longley, 1994] Longley, J. P. (1994). A review of nonsteady flow models for compressor stability. *Journal of Turbomachinery*, 116:202–215.

[Mansoux et al., 1994] Mansoux, C. A., Gysling, D. L., Setiawan, J. D., and Paduano, J. D. (1994). Distributed nonlinear modeling and stability analysis of axial compressor stall and surge. In *Proc. American Control Conference*, pages 2305–2316.

[McCaughan, 1989] McCaughan, F. E. (1989). Application of bifurcation theory to axial flow compressor instability. *Journal of Turbomachinery*, 111:426–433.

[McCaughan, 1990] McCaughan, F. E. (1990). Bifurcation analysis of axial flow compressor stability. *SIAM Journal of Applied Mathematics*, 20(5):1232–1253.

[Megretski and Treil, 1993] Megretski, A. and Treil, S. (1993). Power distribution inequalities in optimization and robustness of uncertain systems. *JMSEC*, 3(3):301–319.

[Mita et al., 1993] Mita, T., Kuriyama, K., and Liu, K. (1993). H-infinity control with unstable weighting functions. In *Proc. IEEE Conference on Decision and Control*, pages 650–655.

[Moore and Greitzer, 1986] Moore, F. K. and Greitzer, E. M. (1986). A theory of post-stall transients in axial compression systems—Part I: Development of equations. *Journal of Turbomachinery*, 108:68–76.

[Nesterov and Nemirovsky, 1994] Nesterov, Y. and Nemirovsky, A. (1994). *Interior-Point Polynomial Methods in Convex Programming.* SIAM studies in applied mathematics. Philadelphia : Society for Industrial and Applied Mathematics.

[Newlin, 1996] Newlin, M. (1996). *Model Validation, Control, and Computation.* PhD thesis, California Institute of Technology.

[Packard, 1994] Packard, A. (1994). Gain scheduling via linear fractional transformations. *Systems and Control Letters*, 22(2):79–92.

[Packard and Doyle, 1993] Packard, A. and Doyle, J. C. (1993). The complex structured singular value. *Automatica*, 29(1):71–109.

[Paduano et al., 1993a] Paduano, J. D., Epstein, A. H., Valavani, L., Longley, J. P., Greitzer, E. M., and Guenette, G. R. (1993a). Active control of rotating stall in a low-speed axial compressor. *Journal of Turbomachinery*, 115:48–56.

[Paduano et al., 1993b] Paduano, J. D., Greitzer, E. M., Epstein, A. H., Guenette, G. R., Gysling, D. L., Haynes, J., Hendricks, G. J., Simon, J. S., and Valavani, L. (1993b). Smart engines: Concept and application. *Integrated Computer-Aided Engineering*, 1(1):3–28.

[Paganini, 1993] Paganini, F. (1993). Descriptions of white noise and worst case induced norms. In *32nd IEEE CDC*, pages 3658–3663.

[Paganini, 1995a] Paganini, F. (1995a). Necessary and sufficient conditions for robust H-2 performance. In *Proc. IEEE Conference on Decision and Control*, pages 1970–1975.

[Paganini, 1995b] Paganini, F. (1995b). *Sets and Constraints in the Analysis of Uncertain Systems.* PhD thesis, California Institute of Technology.

[Paganini et al., 1994] Paganini, F., D'Andrea, R., and Doyle, J. C. (1994). Behavioral approach to robustness analysis. In *Proc. American Control Conference*, pages 2782–2786.

[Petersen et al., 1993] Petersen, I., McFarlane, D., and Rotea, M. (1993). Optimal guaranteed cost control of discrete-time uncertain linear systems. In *Proc. IFAC World Congress*, pages 407–410.

[Polderman, 1993] Polderman, J. W. (1993). Proper elimination of latent variables. In *Proc. IFAC World Congress*, pages 73–76.

[Rapisarda and Willems, 1996] Rapisarda, P. and Willems, J. C. (1996). State maps for linear systems. *SIAM Journal of Control and Optimization.*

[Rockafellar, 1970] Rockafellar, R. T. (1970). *Convex Analysis.* Princeton University Press.

[Safonov et al., 1994] Safonov, M. G., Goh, K. C., and Ly, J. H. (1994). Controller synthesis via bilinear matrix inequalities. In *Proc. American Control Conference*, pages 45–49.

[Shames, 1992] Shames, I. H. (1992). *Mechanics of Fluids.* McGraw-Hill.

[Shamma, 1994] Shamma, J. (1994). Robust stability with time varying structured uncertainty. *IEEE Transactions on Automatic Control*, 39(4):714–724.

[Shigley and Uicker, 1980] Shigley, L. E. and Uicker, J. J. (1980). *Theory of Machines and Mechanisms.* McGraw-Hill.

[Skelton, 1995] Skelton, R. E. (1995). Integrated structure and controller design. In *Proc. American Control Conference*, pages 39–43.

[Smith et al., 1991] Smith, R. H., Chisholm, J. D., and Stewart, J. F. (1991). Optimizing aircraft performance with adaptive, integrated flight/propulsion control. *Journal of Engineering for Gas Turbines and Power*, 113:87–94.

[Stein and Doyle, 1991] Stein, G. and Doyle, J. C. (1991). Beyond singular values and loopshapes. *AIAA Journal of Guidance and Control*, 14(1):5–16.

[Stoorvogel, 1993] Stoorvogel, A. A. (1993). The robust H2 control problem: A worst-case design. *IEEE Transactions on Automatic Control*, 38(9):1358–1370.

[Strang, 1988] Strang, G. (1988). *Linear Algebra and its Applications.* Harcourt Brace Jovanovich.

[Tierno, 1995] Tierno, J. (1995). *Numerically Efficient Robustness Analysis of Trajectory Tracking for Nonlinear Systems.* PhD thesis, California Institute of Technology.

[Toker and Ozbay, 1995a] Toker, O. and Ozbay, H. (1995a). On the NP-hardness of solving bilinear matrix inequalities and the simultaneous stabilization with static output feedback. In *Proc. American Control Conference*, pages 2525–2526.

[Toker and Ozbay, 1995b] Toker, O. and Ozbay, H. (1995b). On the NP-hardness of the purely complex mu computation, analysis/synthesis, and some related problems in multidimensional systems. In *Proc. American Control Conference*, pages 447–451.

[Trentelman and Willems, 1995] Trentelman, H. L. and Willems, J. C. (1995). A behavioral perspective to H-infinity control. In *Proc. European Control Conference*, pages 2232–2237.

[Weiland, 1991] Weiland, S. (1991). *Theory of Approximation and Disturbance Attenuation for Linear Systems.* PhD thesis, University of Groningen.

[Willems, 1991] Willems, J. C. (1991). Paradigms and puzzles in the theory of dynamical systems. *IEEE Transactions on Automatic Control*, 36:259–294.

[Willems, 1992] Willems, J. C. (1992). Feedback in a behavioral setting. *Systems, Models and Feedback: Theory and Applications*, pages 179–191.

[Yakubovich, 1971] Yakubovich, V. A. (1971). S-procedure in nonlinear control theory. *Vestnik Leningrad University:Mathematics*, pages 62–77. In Russian.

[Young, 1993] Young, P. M. (1993). *Robustness with Parametric and Dynamic Uncertainty.* PhD thesis, California Institute of Technology.

[Young, 1996] Young, P. M. (1996). Robustness analysis with full-structured uncertainties. In *35th IEEE CDC, to appear.*

[Zames, 1966] Zames, G. (1966). On the input-output stability of time varying nonlinear feedback systems. Part I: Conditions derived using concepts of loop gain, conicity, and positivity. *IEEE Transactions on Automatic Control*, 11(2):228–238.

[Zhou et al., 1995] Zhou, K., Doyle, J. C., and Glover, K. (1995). *Robust and Optimal Control.* Prentice Hall.